SAND REPORT

SAND2005-0480
Unlimited Release
Printed February 2005

Calculation Set for Design and Optimization of Vegetative Soil Covers Sandia National Laboratories, Albuquerque, New Mexico

Jerry L. Peace and Timothy J. Goering

Prepared by
Sandia National Laboratories
Albuquerque, New Mexico 87185 and Livermore, California 94550

Sandia is a multiprogram laboratory operated by Sandia Corporation, a Lockheed Martin Company, for the U.S. Department of Energy under Contract DE-AC04-94AL85000.

Issued by Sandia National Laboratories, operated for the U.S. Department of Energy by Sandia Corporation.

Available to DOE and DOE contractors from
U.S. Department of Energy
Office of Scientific and Technical Information
P.O. Box 62
Oak Ridge, TN 37831

Telephone: (865)576-8401
Facsimile: (865)576-5728
E-Mail: reports@adonis.osti.gov
Online ordering: http://www.doe.gov/bridge

Available to the public from
U.S. Department of Commerce
National Technical Information Service
5285 Port Royal Rd
Springfield, VA 22161

Telephone: (800)553-6847
Facsimile: (703)605-6900
E-Mail: orders@ntis.fedworld.gov
Online order: http://www.ntis.gov/help/ordermethods.asp?loc=7-4-0#online

SAND2005-0480
Unlimited Release
Printed February 2005

Calculation Set for Design and Optimization of Vegetative Soil Covers Sandia National Laboratories, Albuquerque, New Mexico

Jerry L. Peace
Geophysics Department
Sandia National Laboratories
P.O. Box 5800
Albuquerque, New Mexico 87185-0750

Timothy J. Goering
GRAM, Inc.
8500 Menaul Blvd., Suite B-370
Albuquerque, New Mexico 87112

Abstract

This study demonstrates that containment of municipal and hazardous waste in arid and semiarid environments can be accomplished effectively without traditional, synthetic materials and complex, multi-layer systems. This research demonstrates that closure covers combining layers of natural soil, native plant species, and climatic conditions to form a sustainable, functioning ecosystem will meet the technical equivalency criteria prescribed by the U. S. Environmental Protection Agency.

In this study, percolation through a natural analogue and an engineered cover is simulated using the one-dimensional, numerical code UNSAT-H. UNSAT-H is a Richards' equation-based model that simulates soil water infiltration, unsaturated flow, redistribution, evaporation, plant transpiration, and deep percolation. This study incorporates conservative, site-specific soil hydraulic and vegetation parameters. Historical meteorological data are used to simulate percolation through the natural analogue and an engineered cover, with and without vegetation.

This study indicates that a 3-foot (ft) cover in arid and semiarid environments is the minimum design thickness necessary to meet the U. S. Environmental Protection Agency-prescribed technical equivalency criteria of 31.5 millimeters/year and 1×10^{-7} centimeters/second for net annual percolation and average flux, respectively. Increasing cover thickness to 4 or 5 ft results in limited additional improvement in cover performance.

This page intentionally left blank

Contents

Figures

Tables

Acronyms and Abbreviations

°C	Celsius
°F	Fahrenheit
ACAP	Alternative Cover Assessment Program
ASTM	American Society for Testing and Materials
atm	atmosphere
bgs	below ground surface
CFR	Code of Federal Regulations
cm	centimeter
cm^3	cubic centimeter
DOE	U.S. Department of Energy
DRI	Desert Research Institute
E_p	potential evaporation
EPA	U.S. Environmental Protection Agency
EPIC	The Erosion Productivity Impact Calculator
ft	foot (feet)
g	gram
HDPE	high-density polyethylene
HELP	Hydrologic Evaluation of Landfill Performance
hr	hour
in.	inch
IP	instantaneous profile
KAFB	Kirtland Air Force Base
LAI	leaf area index
lb/ft^3	pounds per cubic foot
m	meter
m^2	square meter
mi	mile
mm	millimeter
mph	miles per hour
NMED	New Mexico Environment Department
OTDR	optical time-domain reflectometry
PBA	percent bare area
PET	potential evapotranspiration
PNNL	Pacific Northwest National Laboratory
PVC	polyvinyl chloride
RCRA	Resource Conservation and Recovery Act
RETC	Retention Curve
RLD	root length density
s	second
SM	silty sand
SNL/NM	Sandia National Laboratories/New Mexico
TA-3	Technical Area 3
TDR	time domain reflectometry
T_p	potential transpiration

UMTRA	Uranium Mill Tailings Remediation Action
UNSAT-H	Unsaturated Water and Heat Flow
USCS	Unified Soil Classification System
USDA	U.S. Department of Agriculture
UV	ultraviolet
yr	year

1. Introduction

Shallow land burial has been the preferred method for disposing of municipal and hazardous waste in the United States because it is the simplest, cheapest, and most cost-effective method of disposal. Although waste minimization and recycling will reduce waste volume in the future, landfills will still be required to manage the remaining volume of waste and will be the major repositories for disposal. In recent decades, it has been found that the traditional engineering practices employed to contain waste are inadequate to isolate waste from the hydrologic processes that operate in the shallow vadose zone. These hydrologic processes account for a majority of landfill problems and failures. The most significant factor contributing to landfill problems and failures is percolation through final closure covers. To be more effective, landfill management practices should take into consideration the natural hydrological properties of final closure covers and the shallow vadose zone to isolate waste from the environment.

1.1 Waste Management Research and Development

Shallow land burial is an important element of solid waste management. Equally important is the ability to conduct landfill operations without adversely impacting human health and the environment. Government, university, and private sector scientists and engineers have been researching and developing strategies for managing the nation's waste for several decades (Reith and Thomson 1992, Winograd 1981, DOE 1988, Anderson 1997). Much of this work has been related to radioactive and mixed waste derived from nuclear weapons research and development during the cold war. This research has produced an increased understanding of containment methods and materials that will help address issues related to the protection of surface water, groundwater, and the environment. Containment of radioactive and mixed waste is viewed as an acceptable strategy for controlling risk to environmental receptors. Relatively new to the study of containment methods and materials research, scientists and engineers have been evaluating the ecological aspects of waste management practices (Waugh 1997, Waugh and Richardson 1997). Ecological processes can have either beneficial or deleterious effects on long-term performance. The conventional engineering approach fails to fully consider the ecology of cover environments. The objective is to combine regulatory and technical drivers with beneficial ecological processes to design a cover that improves rather than degrades over the long term as inevitable natural processes act on the system (Waugh 1997). Engineering designs and solutions may fail but natural systems have persisted for millennia in the form of natural analogues (Markham 1997). Current research emphasizes characteristics of the natural analogue and the methods and opportunities to produce long-term solutions and lower-cost alternatives to traditional solutions by working with natural materials and processes to isolate waste rather than working without them. This approach is certainly appropriate and quite relevant in arid and semiarid environments (Markham 1997).

1.2 Deserts as Dumps?

One of the earliest comprehensive studies published on the natural hydrologic properties of the shallow vadose zone was conducted by Cole and Mathews (1939). These early researchers examined the quantity of soil water and its movement under semiarid conditions at U.S. Department of Agriculture (USDA) experimental stations in Montana, North Dakota, Nebraska,

and Kansas. The studies were conducted to investigate methods of crop production and tillage under semiarid conditions. Their review of 30 years of data demonstrated that no water moved below the root zone in these semiarid environments (Cole and Mathews 1939, Hauser et al. 2001).

Arid and semiarid regions of the western United States have received considerable attention over the past two decades in reference to hazardous waste disposal. The thick vadose zone of arid and semiarid environments has often been considered for storage and disposal of radioactive and mixed waste (Reith and Thomson 1992, Winograd 1981). Deserts were first explored as repositories for radioactive waste in a series of articles published by the Electric Power Research Institute (EPRI 1981, EPRI 1982). Disposal in deserts is based upon the premise that low, mean annual precipitation and high potential evapotranspiration yields low downward flux rates, favoring waste isolation from the environment for long periods of time. Little is known, however, about the hydraulic properties of the shallow vadose zone in arid and semiarid environments. The rate at which water flows through the vadose zone is highly sensitive to the hydraulic conductivity of the soil. This is especially true at low moisture contents (less than 10%) that are typical of desert environments such as those of the arid and semiarid regions of the western United States (Khaleel and Relyea 1995). The hydraulic conductivity versus volumetric moisture content relation is nearly vertical at low moisture contents, so that a slight change in moisture content can cause orders of magnitude increase or decrease in conductivity.

1.3 Objective of this Research

The main goal of this study is to demonstrate that containment of municipal and hazardous waste in arid and semiarid environments can be accomplished quite effectively without synthetic materials and costly, complex, multi-layer systems. The U.S. Environmental Protection Agency (EPA) encourages the development and deployment of alternative cover designs that are innovative and take advantage of site-specific conditions (USEPA 1989). This research will demonstrate that natural soils and native vegetation, namely, vegetative soil covers, will meet the technical equivalency criteria prescribed for Resource Conservation and Recovery Act (RCRA) Subtitle D and C caps as promulgated in 40 Code of Federal Regulations (CFR) Parts 264 and 258, respectively. This study will demonstrate that vegetative soil covers, utilizing readily-available, naturally-occurring materials and processes, will adequately address EPA-prescribed performance-based standards.

Alternative covers have many potential benefits over the current regulatory-prescribed landfill caps, while being equally protective of human health and the environment. These benefits include, but are not limited to, more readily available construction materials, ease of construction, less complex quality assurance/quality control programs, greater cost-effectiveness, and increased long-term sustainability and decreased maintenance (ITRC 2003).

In essence, a vegetative soil cover represents a cover designed and tested by nature. The natural analogue has minimized deep percolation for thousands of years (Cole and Mathews 1939; Hauser et al. 2001). Therefore, it seems logical that the science and engineering community charged with the management and disposal of our nation's waste should emulate that design.

Proper design of a vegetative soil cover depends on a thorough understanding of soil water storage, the physics of soil water movement, evapotranspiration, vegetative cover, and climate. The design of vegetative soil covers is an imprecise science, combining traditional engineering principles with shallow vadose zone geology, ecology, hydrology, climatology, sedimentology, botany, and agronomy. Principles from these applied sciences must be applied to develop an effective, site-specific design. Vegetative soil cover design combines layers of natural soil, native plant species, and climatic conditions to form a sustainable, functioning ecosystem that maintains the natural water balance (ITRC 2003).

Numerical codes incorporating relevant constitutive principles have become increasingly popular and necessary in the research and management of hydrologic and transport processes in landfill covers and in the shallow vadose zone. In this study, percolation through the natural analogue and an engineered cover is simulated using the numerical code Unsaturated Water and Heat Flow (UNSAT-H) (Fayer 2000). UNSAT-H is a Richards' equation-based model that simulates soil water infiltration, unsaturated flow, redistribution, evaporation, plant transpiration, and deep percolation. The two major objectives of the UNSAT-H code are to estimate percolation and to assist the design engineer and the regulator in evaluating and optimizing alternative landfill cover design (Fayer 2000).

The UNSAT-H code is a one-dimensional flow model. There is no provision for run-on or surface detention. Runoff is captured and represented by a uniform, hourly precipitation rate over the entire area of interest.

This study incorporates conservative, site-specific soil hydraulic and vegetation parameters obtained from the natural analogue and a constructed, engineered cover. Site-specific historical meteorological data from 1919 to 1996 are used to generate precipitation and infiltration data. Percolation is simulated through the natural analogue and the engineered cover both with and without native vegetation to evaluate the performance of covers 1, 2, 3, 4, and 5 feet (ft) in thickness. Deep percolation is used to optimize cover design that meets or exceeds the EPA-prescribed, technical equivalency criteria. The EPA performance-based, technical equivalency criteria used in this study are 31.5 millimeter (mm)/year (yr), or less, for net annual percolation and 1×10^{-7} centimeter (cm)/second (s) average flux, respectively, based on a hydraulic conductivity of 1×10^{-7} cm/s and the assumption of constant unit gradient conditions. Designs that incorporate conservative, site-specific information provide a satisfactory engineering safety factor and increase the understanding and confidence of the regulatory community and greatly facilitate the acceptance and permitting of alternative landfill covers.

1.4 Research Outline

This study outlines the research conducted for the design of vegetative soil covers for final closure of municipal waste landfills for the City of Albuquerque and for hazardous, radioactive, and mixed waste landfills at Sandia National Laboratories/New Mexico (SNL/NM) and Kirtland Air Force Base (KAFB). Chapters are presented on the federal and state regulatory basis (Chapter 2), location and characteristics of the field test area (Chapter 3), instantaneous profile (IP) test to determine the hydraulic properties of the natural analogue and an engineered cover (Chapter 4), laboratory soil tests to determine the hydraulic conductivity function for the natural analogue and an engineered cover (Chapter 5), performance modeling to simulate percolation through the natural analogue and an engineered cover (Chapter 6), performance modeling results

and design optimization for vegetative soil covers (Chapter 7), and conclusion and recommendations (Chapter 8).

1.5 Acknowledgments

The calculation set presented in this document is based upon fruitful collaborations with many scientists and engineers representing state and federal agencies, environmental science and geotechnical engineering firms, universities, and national laboratories. The authors benefited greatly from discussions with Paul Knight and Tom Ashton of Marron and Associates, Inc.; William Moats, Rich Kilbury, and Bill McDonald of the New Mexico Environment Department; Mike Fayer of Pacific Northwest National Laboratory (PNNL); Lewis Munk of Golder Associates, Inc.; and Jim Kelsey of Daniel B. Stephens and Associates, Inc.

The authors also acknowledge Danny Beets, Dirk Van Hart, Warren Strong, Mike McVey, Mike Mitchell, Doug Rizor, Mike Barthel, Don Helferich, Gary Bailey, Dave Grandi, Gilbert Quintana, Jeff Lee, and Ernie Ross for all the technical assistance they provided towards the completion of this project.

The authors greatly acknowledge Donna Reade, Lara Beasley, Elizabeth Edwards, Kim Murak, Zeke Carpio, Bonnie Little, and Christy Fischer of Shaw Environmental, Inc., for the quality review and production of this document. The authors are solely responsible for any errors or omissions in this document.

2. Regulatory Basis

2.1 Closure Requirements under RCRA

The primary federal program for regulation of shallow land burial of municipal and hazardous waste in the United States is RCRA of 1976, administered by the EPA. Under RCRA, Congress expanded significantly the federal role in controlling the management of solid waste in the United States. These federal regulations promulgated improved methods for disposal of municipal and hazardous waste. RCRA Subtitle C regulations governing the design of engineered liners and covers for hazardous waste landfills were issued in 1982. RCRA Subtitle D regulations governing the design of engineered liners and covers for municipal waste landfills were issued in 1991.

The EPA states that there are 226,000 municipal waste landfills that were operated and closed prior to promulgation of RCRA regulations (USEPA 1988). These pre-regulation landfills will require some form of capping technology as a final step in the regulatory closure process. The EPA examined data from 163 randomly selected landfills and found that 146 had ground water contamination (USEPA 1988). The severity of the contamination varied from simply elevated levels of various constituents in on-site groundwater to the contamination of major aquifers and/or production well fields.

2.2 Hazardous Waste Landfill Closure Requirements

Hazardous waste landfill closure requirements are codified under 40 CFR Part 264, "Standards for Owners and Operators of Hazardous Waste Treatment, Storage, and Disposal Facilities," Subpart G (Facility Closure Standards) and Subpart N (Landfills). These standards are performance-based: regulations that specify performance criteria without specifying design, construction materials, or operating parameters. The regulations require a low-permeability cover over landfills to minimize water infiltration into waste and provision for 30 years of post-closure monitoring and maintenance in order to prevent release of contaminants to the environment. The EPA has provided numerous guidance documents to aid in interpreting the level of performance required to design, construct, and operate a compliant closure cover. The closure performance standards for hazardous waste landfills are defined in 40 CFR 264.111:

> The owner or operator must close the facility in a manner that:
>
> (a) Minimizes the need for further maintenance; and
>
> (b) Controls, minimizes or eliminates, to the extent necessary to protect human health and the environment, post-closure escape of hazardous waste, hazardous constituents, leachate, contaminated runoff, or hazardous waste decomposition products to the ground or surface waters or to the atmosphere; and
>
> (c) Complies with the closure requirements of this subpart, including, but not limited to, the requirements of [Parts] 264.178; 264.197; 264.228; 264.258;

264.280; 264.310; 264.351; 264.601 though 603; and 264.1102 [Closure and Post-Closure Care; Environmental Performance Standards; Monitoring; Analysis; Inspection; Response; Reporting; and Corrective Action].

Performance-based requirements for hazardous waste landfill covers are established in 40 CFR 264.310:

> (a) At final closure of the landfill or upon closure of any cell, the owner or operator must cover the landfill or cell with a final cover designed and constructed to:
>
> (1) Provide long-term minimization of migration of water through the closed landfill;
>
> (2) Function with minimum maintenance;
>
> (3) Promote [surface] drainage and minimize erosion or abrasion of the cover;
>
> (4) Accommodate settling and subsidence so that the cover's integrity is maintained; and
>
> (5) Have permeability less than or equal to the permeability of any bottom liner system or natural subsoils present.

The New Mexico Environment Department (NMED), the lead regulatory agency for the state of New Mexico, is authorized by the EPA to implement the hazardous waste management provisions of RCRA for treatment, storage, and disposal facilities within the state. The NMED has adopted the federal regulations as written and incorporated them in New Mexico 20 New Mexico Annotated Code 4.1, Subpart V, 40 CFR 264.101, "Corrective Action for Solid Waste Management Units in April 1985."

2.3 RCRA Subtitle C Caps

A RCRA Subtitle C generic design consists of, at a minimum, a cap made up of three layers: 1) a vegetated or armored topsoil layer, 24 inches (in.) thick, graded at a slope of 3% to 5%, underlain by 2) a drainage layer, 12 in. thick, of a high-hydraulic conductivity sand layer, underlain by a flexible membrane liner in intimate contact with 3) a low-hydraulic conductivity compacted clay liner, 24 in. thick (USEPA 1991). The functional requirement of the topsoil layer is to promote surface run-off, prevent ponding and infiltration of water, and mitigate surface erosion. The topsoil layer functions as a water reservoir, storing water until removed by evapotranspiration. The functional requirement of the drainage layer is the rapid transport of water off and away from the compacted clay barrier via the underlying flexible membrane liner. Rapid and efficient removal of infiltrating water from the overlying topsoil layer prevents the build-up of infiltrating water and excess moisture that often leads to slope failure. The functional requirement of the compacted clay barrier is to prevent infiltrating water from entering waste

disposal cells. EPA considers the compacted clay barrier to be the most important component in controlling infiltration through the cap.

The overall goals of the EPA-prescribed design of final closure covers for RCRA Subtitle C facilities are 1) to minimize leachate by minimizing the contact of water with waste, 2) to minimize long-term maintenance, and 3) to protect human health and the environment considering the future use of the site. The fundamental concern of the EPA with alternative cover designs is that all cover components remain stable in the long-term, and that the cover performs as designed without posing a significant risk to human health and the environment.

2.4 RCRA Subtitle C Caps—Potential Problems

The fundamental shortcoming of any containment approach is that it falls short of the highest goal of waste management, which is to leave no hazardous residue whatsoever to future generations. Containment does not eliminate the problem, but simply isolates it for some period of time until it must be dealt with.

Disposal in engineering containment such as landfills and deep geologic repositories may be necessary and justified for the time being. The risks may be acceptably low and the costs of alternatives too high but it is a widely held axiom in the field that every landfill is a Superfund site waiting to happen (Reith and Thomson 1992). This may be true under RCRA Subtitle C using the most advanced engineering methods for hazardous waste. Serious questions exist about the longevity of synthetic materials used as liners (Allen 2001, Hewitt and Philip 1999).

The high level of confidence placed in RCRA Subtitle C caps and their ability to prevent release of contaminants to the environment may be premature (Allen 2001). Caps constructed according to EPA guidance have been in use for approximately 25 years. RCRA Subtitle C caps commonly employ the strategy of compacted clay and flexible membrane liners, sometimes in elaborate and redundant configurations, however, these caps may fail in dry climates due to desiccation and shrinkage of the compacted clay liner and tensile and shear stress failure of flexible membrane liners (Daniel and Wu 1993, USEPA 1991, Allen 2001, Yesiller et al. 2000, USEPA 2002).

Very little attention is paid to local hydrological conditions and the natural attenuation properties of closure covers and the shallow vadose zone. The long-term durability of compacted clay liners and flexible membrane liners such as high-density polyethylene (HDPE) is as yet unknown. The liner containment strategy employs purely engineering solutions to water infiltration mitigation and leachate management, representing high construction complexity, cost, and maintenance. There are a number of potential flaws in the liner containment approach, some of which may have serious long-term environmental implications. Apart from the high cost of purchase and installation, and the need for long-term maintenance, the long-term durability of synthetic flexible membrane liners and compacted clay liners is questionable (Allen 2001, Hewitt and Philip 1999, Yesiller et al. 2000, Daniel and Wu 1993, USEPA 1991, Landreth et al. 1991, Suter et al. 1993, USEPA 2002).

2.4.1 Flexible Membrane Liners

Numerous recent studies have drawn attention to the deficiencies of flexible membrane liners (Hakonson 1997, Melchior 1997, USEPA 2002). Flexible membrane liners require extreme care during manufacture and installation. Standard installation procedures, even with rigorous construction quality assurance, cannot guarantee the hydraulic integrity of a liner. Favorable weather conditions are essential during installation to prevent expansion of the liner creating waves and air pockets between the liner and the underlying compacted clay liner. HDPE liners can attain temperatures of 40 degrees Celsius (°C) (104 degrees Fahrenheit [°F]) in excess of ambient temperature (Hewitt and Philip 1999). Even manufacturer construction quality assurance is unlikely to produce a liner free of defects.

The EPA (2002) conducted a broad-based study to address issues related to the design, construction, and performance of waste containment systems at landfills. Waste containment system problems were identified at 74 modern landfill and surface impoundment facilities located throughout the United States. The purpose of the project was to better understand the identified problems and to develop recommendations to reduce the future occurrence of problems.

Flexible membrane liners have been used as essential design components of waste containment systems since the early 1980s. The EPA (2002) found that flexible membrane liners are susceptible to puncture and tears during manufacture and puncture, tears, faulty seams, and ultraviolet (UV) degradation during installation; high molecular diffusion rates caused by contact with concentrated organic chemicals; slippage, waves, and shear tears along interfaces between liners and adjacent soils during and after construction; low shear strength of hydrated bentonite and low internal shear strength in geosynthetic liners; and loss of liner elasticity over time.

Hakonson (1997) found that a potential problem leading to cap failure is slope failure at barrier interfaces caused by excessive soil moisture. Because many cap designs contain flexible membrane liners that generate lateral flow of soil water, saturated conditions at flexible membrane liner and soil interfaces can lead to reduced friction, especially on designs with steep lateral slopes.

In Germany, Melchior (1997) found that geosynthetic clay liners placed near the surface are readily penetrated by roots seeking soil moisture. He observed that desiccation cracks and root channels developed in the geosynthetic clay liners, increasing their permeability, thus compromising their performance.

Suter et al. (1993) notes that in recent decades, failure of caps on municipal and hazardous waste landfills results from subsidence, leakage through flawed or damaged flexible membrane liners, or intrusion by plants or animals.

The EPA (1991, 2002) found that the occurrence of cover soil instability in the form of sliding on flexible membrane liners is far too frequent. Additionally, there have been cases of wide width tension failures of the underlying flexible membrane liners when friction created by the overlying soil becomes excessive. Significant problems exist between the flexible membrane liner and the overlying soils or drainage geosynthetic liner and also between the underlying soils.

Percolation, drainage along liner interfaces, and seismic forces increase the cover soil instability when barriers are placed in direct contact with flexible membrane liners.

In summary, potential problems with flexible membrane liners include:

- Damage due to poor manufacturer and construction quality assurance;
- High temperature and UV degradation during installation;
- Waves and interfacial tension and shear failure along interfaces between liners and adjacent soils during and after construction due to slippage and excessive friction;
- Low shear strength of hydrated bentonite and low internal shear strength in geosynthetic liners;
- Layer instability in the form of sliding due to excessive interfacial moisture;
- Penetration by roots seeking soil moisture compromising liner performance;
- Tension and shear failure of liners due to subsidence;
- Corrosive affects on liners by organic chemicals; and
- Loss of liner elasticity over time.

2.4.2 Compacted Clay Liners

Despite the wealth of information recently developed on compacted clay liners, the performance of compacted clay liners in the field is largely undocumented (USEPA 2002). Compacted clay liners also require extreme care during installation. The compacted clay liner must be protected from desiccation both during and after construction. The saturated hydraulic conductivity of compacted clay liners is highly dependent on the molding water content and degree of compaction. As the molding water content increases, the shear strength and bulk density increases but the shrinkage and cracking potential increases as well. The clay barrier must be placed at wet of optimum moisture content to produce the desired barrier strength and a saturated hydraulic conductivity of 1×10^{-7} cm/s or less to comply with EPA guidance (USEPA 1991).

The EPA (2002) found that some of the significant issues for compacted clay liners are 1) the accuracy of field hydraulic conductivity assessment and the use of laboratory tests on small undisturbed samples of the constructed compacted clay liner; 2) the compaction criteria to achieve the required compacted clay liner hydraulic conductivity; and 3) the long-term hydraulic performance of compacted clay liners in final cover systems.

The EPA (2002) states that the serious concerns with respect to using compacted clay liners, particularly when used alone, are 1) desiccation is a distinct possibility in almost every final cover system where the compacted clay liners is not protected by a flexible membrane liner; 2) a

desiccated compacted clay liner does not return to its original low hydraulic conductivity; 3) the freeze-thaw sensitivity has been demonstrated in laboratory studies and the compacted clay liner hydraulic conductivity is increased significantly and self-healing in not likely; 4) root penetration of compacted clay liners may occur resulting in the development of channels for preferential flow; 5) burrowing animals could lead to large pathways for water migration; and 6) distortion of compacted clay liners due to differential settlement of the underlying waste may lead to tensile and shear failure. For these reasons, it is critical that compacted clay liners stay hydrated, are adequately protected from deep percolation, and are not subject to unacceptable chemical interaction.

Allen (2001) states that compacted clay liners made from bentonite or bentonite blends are highly susceptible to desiccation. Bentonite is composed of the mineral smectite which has sodium and calcium in its matrix, the former having greater swelling potential and higher activity. Replacement of sodium in the mineral matrix results in shrinkage of the clay, development of cracks, increased permeability, and lower activity.

Yesiller et al. (2000) investigated the compacted clay liners in three landfills in southeast Michigan. The clay soils had low plasticity with varying fines content. The soils were subject to repeated cycles of wetting and drying. Yesiller et al. (2001) found that the fines affected the cracking behavior significantly—the greatest amount of cracking was observed in the clay soils with the greatest amount of fines and after repeated wetting and drying. Shrinkage during the first drying cycle caused irreversible soil fabric damage.

Hakonson (1997) states that freezing temperatures or drought can damage and disrupt the integrity of clay soils. Desiccation of clay soils, particularly those used for hydraulic barriers, is a potentially important problem in arid sites. The EPA (1989) notes that alternatives to clay hydraulic barriers should be considered for sites with a high risk for barrier desiccation.

Warren et al. (1997) performed a study on four cover designs at Hill Air Force Base 1.25 mile (mi) south of Ogden, Utah. A flexible membrane liner was not installed in a RCRA Subtitle C cap under the assumption that the liner had failed as EPA guidance (1989) specifies will occur after some unspecified time. During the summer months, it was apparent that moisture in the clay barrier was being influenced by the vegetative cover. The possibility of plant roots penetrating the clay layer was a concern and brought into question the ability of the clay layer to perform in arid environments. It is well known that clays have a high propensity to crack when desiccated (Miller and Mishra 1989, Montgomery and Parsons 1989, Corser et al. 1992, Suter et al. 1993) and that root channels remain after decay or desiccation of roots. Both cracks and root channels create preferential flow paths. Furthermore, desiccation cracks may not heal upon rehydration (Boynton and Daniel 1985).

Melchior (1997) in Germany has shown that compacted clay, placed within a meter of the surface, desiccated after several years and did not rehydrate even in a humid climate (31.5 in./yr precipitation). The inability to rehydrate is attributed to root channel development and alteration of the structure of the clay.

In summary, the serious concerns regarding the use of compacted clay liners include:

- Field-testing of the saturated hydraulic conductivity of compacted clay liners is extremely difficult and costly to perform and document (large-scale infiltrometers would be preferred but are labor-intensive and time-consuming to perform);

- Lab-testing of the *in situ* saturated hydraulic conductivity of compacted clay liners is difficult to perform because the sample size is usually not representative of actual field conditions;

- Reaction between Na^{+} and Ca^{++} in Bentonite clay causes irreversible soil fabric changes. Sodic clays are more expansive than calcic clays. The resulting shrinkage causes irreparable damage, cracks, air pockets, and consequently, an increase in permeability;

- Freeze-thaw sensitivity affects compacted clay liner hydraulic conductivity and self-healing is not likely;

- Root penetration of compacted clay liners causes a significant loss in soil moisture and may create pathways for preferential flow;

- Burrowing animals could lead to large pathways for water migration; and

- Desiccation cracking and distortion of compacted clay liners due to differential settlement of the underlying waste may cause collapse of overlying layers and create pathways of preferential flow.

2.5 Alternative Landfill Covers

The EPA accepts alternative designs that consider site- or regional-specific conditions, such as climate and the nature of the waste, and meet the intent of the regulations. This study will focus on *alternative landfill covers* as substitute for RCRA-driven Subtitle C caps for closure of hazardous waste landfills, as codified under 40 CFR Part 264. There are over 3000 landfills containing low-level radioactive and mixed waste within the U.S. Department of Energy (DOE) complex alone that will have to be closed under 40 CFR Part 264 (Hakonson 1994). Containment technology will be relied upon to contain these low-level radioactive and mixed wastes for hundreds, if not thousands, of years. Although much of the research conducted in this study will focus on identifying better engineering solutions for the disposal of hazardous waste, the results of this study are applicable to municipal solid waste disposal as well.

The obvious provision for substitution of an alternative design is that it has to be demonstrated as "equivalent" in performance to RCRA Subtitle C designs. This presents a dilemma for the design engineer because equivalency is not defined by the EPA. The EPA does not provide any guidance regarding evaluation criteria or procedures as to how one goes about demonstrating equivalency. If the EPA means "equivalent" in terms of performance objectives, then demonstration of equivalency is easy due to the qualitative nature of the performance-based standards. If "equivalent" is interpreted as including all the functional elements of a RCRA Subtitle C cap as outlined in Section 2.3, then equivalency would severely limit the range of

options available to the design engineer that would qualify an alternative cover. The subject of equivalency is invoked often, especially by the regulators, but no one seems to know what it means (Hakonson 1997). And equivalency is difficult to demonstrate quantitatively without costly, field-scale experiments.

Alternative covers that are intended to last hundreds if not thousands of years must be designed as evolving components of larger dynamic ecosystems (Waugh 1997). Four precepts accompany this premise: 1) cover components will not function independent of one another and, thus, should not be designed independent of one another; 2) physical and ecological conditions will change over time, therefore, initial conditions should not be extrapolated as tests of long-term performance; 3) designs should not rely on man-made materials of unknown durability; and 4) designs should not rely on physical barriers to natural processes but on the beneficial exploitation of those natural processes. The goal is to take advantage of beneficial ecological processes, and to design covers that improve rather than degrade over the long term as inevitable natural processes act on the ecosystem (Waugh 1997).

Any proposed alternative cover must meet the RCRA requirements of 40 CFR 264.310. Performance of alternative covers cannot be isolated from the performance of the site itself. Natural site conditions, integrated with a landfill cover, produce an "ecosystem performance" that will ensure that the alternative design adequately meets the regulatory requirements. The natural site conditions that should be relied upon as part of the "system" include:

- Low precipitation and high potential evapotranspiration;
- Negligible recharge to groundwater;
- An extensive vadose zone; and
- Diverse, native vegetation consisting of multiple plant life forms that will adapt to climatic change, revegetate after severe damage (fire, disease, drought), and persist indefinitely with little or no maintenance.

2.5.1 Vegetative Soil Covers

Vegetative soil covers were introduced by Charles Reith, an ecologist with Jacobs Engineering Group, Advanced Systems Division, Albuquerque, New Mexico in 1987 (DOE 1988). Jacobs Engineering Group conducted a special study on vegetative covers for the DOE. The objectives of the study were to evaluate the feasibility of using vegetative covers for stabilizing Uranium Mill Tailings Remediation Action (UMTRA) waste piles; to define the advantages and disadvantages of using vegetative covers; and to develop guidelines for the design and construction of vegetative covers for the UMTRA project.

The definition Reith offered of a vegetative cover can be found in the DOE report (1988):

> Before proceeding, it is important to define what is meant by a vegetative cover. Two components are fundamental: (1) a layer of soil that serves as a

rooting medium and moisture reservoir, and (2) a plant community that is established based upon its maximal degree of adaptation to the local environment, its resistance to disturbance and its ability to meet performance objectives for controlling water balance and preventing erosion. Features may be applied such as rock mulches on top of the cover and cobble bio-barriers beneath the soil layer to enhance durability and performance.

Vegetative covers are based upon the overarching premise that the amount of total precipitation refracted back to the atmosphere annually via evapotranspiration is on the order of 80% to 100% in arid and semiarid environments (Anderson et al. 1993). The evapotranspiration potential in the southwestern United States far exceeds the amount of water received from precipitation. The climate in the southwest is sufficiently arid (Houghton 1972) that the possibility of prolonged periods of saturation in the shallow vadose zone of a properly selected site is highly unlikely (Hawley and Longmire 1992).

2.6 Proposed Demonstration of Equivalency

Quantitative demonstration of equivalency to the prescribed RCRA Subtitle C cap is very difficult to accomplish without side-by-side field-scale demonstrations. Field-scale demonstrations of this magnitude and scope are extremely time-consuming and costly to construct and monitor. Hydraulic equivalency generally means that percolation from the base of an alternative cover is less than or equal to the percolation from the base of a prescriptive cover. Commonly employed field-scale water-balance methods using meteorological data are inadequate for demonstrating equivalency because the precision within which precipitation and percolation can be measured is less than the actual equivalency requirement. Thus, performance assessment using the field-scale water balance method is insufficient in precision to demonstrate that an alternative cover is achieving the desired percolation rate (Benson et al. 2001). Due to the lack of definitive field data, design engineers have come to rely upon the predictive capability of hydrologic models to estimate the flux of water moving through the vadose zone. Despite the limitation of hydrologic models, they can still provide great benefit for cover design decision-making.

Numerical codes incorporating relevant constitutive principles have become increasingly popular and necessary in the research and management of transport processes in the shallow vadose zone. In this study, percolation through the natural analogue and an engineered soil cover is simulated using the numerical code UNSAT-H (Fayer 2000) developed at PNNL, Hanford, Washington. The UNSAT-H code was developed for assessing the water dynamics of arid sites and, in particular, estimating recharge for waste disposal facilities at Hanford. The code accomplishes this by simulating soil water infiltration, redistribution, evaporation, plant transpiration, and deep percolation. The two major objectives of the UNSAT-H code are to estimate percolation and to assist the design engineer and regulator in evaluating and optimizing alternative landfill cover design (Fayer 2000).

The UNSAT-H code uses a one-dimensional, finite-difference implementation of a modified form of Richards' equation to describe unsaturated liquid and vapor flow in soil layers and water removal through evaporation and transpiration. The code employs rigorous mechanistic methods to compute liquid water and vapor flow near the soil surface (Khire et al. 1997, Fayer 2000).

The unsaturated hydraulic functions are integral input parameters in this numerical model. Extensive data describing meteorological conditions, unsaturated soil and vegetation characteristics are required by the code. These data can be measured directly in the field or indirectly in the laboratory. Field data can be obtained using the IP technique (Watson 1966). This method is based upon monitoring the transient-state drainage of a soil profile as suggested by Richards and Weeks (1953) and by Ogata and Richards (1957), and later by Rose et al. (1965) and Watson (1966). Laboratory data can be obtained using soil samples collected from the soil profile with thin-walled sampling tubes or augers. The computer code Retention Curve (RETC), developed by the Soil Physics group of the U.S. Salinity Laboratory, Riverside, California, can be used to determine the unsaturated hydraulic conductivity functions of the soil samples. Collectively, these field- and laboratory-derived soils data can be used as input parameters for the UNSAT-H code to simulate deep percolation through vegetative soil covers and to optimize cover thickness. The RETC and UNSAT-H codes are described in detail in Chapters 5 and 6, respectively.

3. Characterization of the Field Test Area

The field tests in the study were conducted in Technical Area 3 (TA-3) at SNL/NM, Albuquerque, New Mexico. TA-3 was selected because of its proximity to several hazardous waste landfills operated for the disposal of low-level radioactive and mixed waste. TA-3 provides a secure area for the operation and maintenance of the instrumentation needed for long-term monitoring of various test sites and the undisturbed natural analogue for conducting the tests, the very "natural ecosystem" designed by nature that one should endeavor to emulate.

SNL/NM is located within the boundaries of KAFB, immediately south of the City of Albuquerque in Bernalillo County, New Mexico (Figure 3-1). SNL/NM research and administration facilities are divided into five technical areas designated 1 through 5. TA-3 forms a 4.5-square-mile rectangular area in the southwestern portion of KAFB.

3.1 Weather Characteristics of the Test Area

The weather for Albuquerque and vicinity, including TA-3, is typical of high-altitude, dry continental climates. The normal daily temperature ranges from -5°C to 11°C (23°F to 52°F) during winter months and from 14°C to 33°C (57°F to 91°F) during summer months. The average annual relative humidity is 46%, however, the relative humidity can range from a low of 5% to a high of 70% (Bonzon et al. 1974).

Under normal conditions, wind speeds rarely exceed 32 miles per hour (mph) and are generally less than 8 mph (Bonzon et al. 1974). Strong winds, often accompanied by blowing dust, occur mostly in late winter and early spring. During these months, the prevailing surface winds are from the southwest. Rapid nighttime ground cooling produces strong temperature inversions and strong winds through mountain canyons.

The average annual precipitation for the Albuquerque area is 8.65 in. Monthly precipitation can range from a minimum of less than 0.5 in. during winter months to 1.5 in. during summer months. Average annual snowfall in the Albuquerque area is 11 in. Summer precipitation, particularly from July through August, is usually in the form of heavy thundershowers that typically last less than 1 hour (hr) at any given location (Williams 1986). Average annual Class A pan evaporation at Albuquerque International Sunport is 89 in., approximately 10 times the average annual precipitation.

New Mexico, however, has experienced severe drought since 1999. Historical stream flow records and the forecast for 2004 make the current (1999–2004) drought in the southwestern United States the worst in the past 80 years and the seventh worst in an approximately 500-year proxy record (Piechota et al. 2004). New Mexico statewide and basin reservoir totals dropped from approximately 5 million acre-ft in 1999 to 2 million acre-ft in 2004, a reduction of 60%.

3.2 Geology and Geomorphology of the Test Area

TA-3 occurs within a sequence of coalescing alluvial fans emanating from the Manzanita Mountains to the east that forms an expansive, relatively featureless, arid mesa. TA-3 is

underlain by an extensive vadose zone (Figure 3-2). The upper part of the vadose zone is a thin cap, generally 20 to 40 ft in thickness, of Late Pleistocene to Holocene, post-Santa Fe Group alluvial-fan and eolian sediments. This cap consists chiefly of very-fine-grained sands, with a number of local west-trending lenses of coarse gravel. The lower part of the vadose zone consists of unconsolidated sands and gravels of the Late Pleistocene Santa Fe Group. In the eastern part of the area, including that below the IP test site, the Santa Fe Group consists of alluvial-fan sediments that generally exhibit a decrease in average grain size with depth. In the western part of the area, the Santa Fe Group consists of relatively well-sorted fluvial sands of the ancestral Rio Grande. The regional water table beneath TA-3 occurs within the Santa Fe Group approximately 500 ft below ground surface (bgs) (Van Hart 2003).

The study area lies in the north-central portion of TA-3. Fine-grained sediments dominate the shallow vadose zone. According to the USDA soil classification system, soils in the study area are predominantly very fine sandy loam. According to the Unified Soil Classification System (USCS), soils are predominantly silty sand (SM). Dry bulk density ranges from 106 to 120 pounds/cubic ft (lb/ft^3). All sediments at the surface or in the shallow vadose zone are of Late Pleistocene to Holocene age, on the order of 30,000 years or younger (Peace et al. 2002). Elevation of the study area is 5381 ft above sea level. There are no perennial streams in the immediate vicinity of the study area. Surface runoff is regionally controlled and generally to the west.

3.3 Flora in the Test Area

The flora within TA-3, as described by Sullivan and Knight (1992), represents the Mesa and Desert Grassland habitat dominated by grassland vegetation. Flora exhibit influences from the Great Basin Desert, the Rocky Mountains, and the Great Plains. Typical plant species occurring in TA-3 include 1) grasses: black grama, dropseed, galleta, burrograss, bush and ring muhly; 2) wildflowers: globemallow, spiny aster, spectacle pod, and desert aster; and 3) shrubs: sandsage, winterfat, mormon tea, yucca, prickly pear, and snakeweed. Most of TA-3 is occupied by grasslands with sandsage communities occurring on deep sandy soils. An estimated 150 to 175 plant species are likely to occur within the area on an average year (Sullivan and Knight 1992). During wetter years, more conducive to growth and development of annuals, this number could increase to over 200 species. Frequency and coverage of these plant species vary but most of TA-3 is composed of elements of the black grama grass series.

3.4 Characterization of the Natural Analogue

Extensive field investigations and analytical studies were undertaken during this study to assess and characterize the natural analogue to a depth of 30 ft bgs. Soil samples, both disturbed and thin-walled, were collected from pits, trenches, and boreholes for determination of soil moisture, grain-size distribution, bulk density, porosity, saturated hydraulic conductivity, and Atterberg limits.

3.4.1 Geotechnical Characterization of Soils

Five trenches were excavated within a 8.5-acre area northeast of the IP test site (Figure 3-3). Each trench was excavated to a minimum depth of 6 ft to obtain disturbed samples for

determination of soil moisture content, grain-size distribution, standard Proctor tests, and Atterberg limits. Results of these analyses are provided in Tables 3-1 and 3-2.

Persaud and Wierenga (1982) conducted a detailed analysis of soils in the study area by obtaining soil samples from various soil horizons for physical and geochemical characterization. Their detailed description of the soil profile to approximately 30 ft (9 meters [m]) below the ground surface is presented in Table 3-3 (Persaud and Wierenga 1982).

As part of Persaud and Wierenga's study (1982), saturation extracts from the soil core samples were prepared and analyzed for geochemical parameters. Core samples were analyzed for particle size distribution. Table 3-4 presents the results of these analyses, including the electrical conductivity and pH of the saturation extracts, the percentages $CaCO_3$ and organic matter, the cation exchange capacity of the samples, and particle size fraction data from these samples (Persaud and Wierenga 1982).

3.5 Vegetation Characterization

The dominant vegetation type within the study area and throughout the north-central portion of TA-3 is classified as Desert Grassland (Dick-Peddie 1992). The species composition within the study area best fits the Desert Grassland Shrub-Black Grama Series. The dominant grass and indicator of Desert Grassland is black grama. Much of the habitat in the north-central portion of TA-3 is dominated by black grama. Within the study area, black grama forms almost monospecific stands where it accounts for nearly 62% of the total foliar coverage of the native plant community.

In the area, the six most common perennial species by foliar coverage are black grama (*Bouteloua eriopoda*), threadleaf snakeweed (*Gutierrezia microcephala*), galleta grass (*Pleuraphis jamesii*), spike dropseed (*Sporobolus contractus*), sand sage (*Artemisia filifolia*), and ring muhly (*Muhlenbergia torreyi*) (Peace et al. 2004). In aggregate, these six species account for 85% of the total foliar coverage. Deertongue (*Cryptantha crassisepala*) and Russian thistle (*Salsola tragus*) are the most common annual species accounting for 12% of the total foliar coverage. Basically, eight species (black grama, threadleaf snakeweed, galleta grass, spike dropseed, sand sage, ring muhly, deertongue, and Russian thistle) account for 97% of the foliar cover (annual and perennial) within the study area. Although conspicuous by their size and unique appearance, species such as prickly pear cactus (*Opuntia phaeacantha*) and small soapweed yucca (*Yucca glauca*) are insignificant in the total foliar coverage and composition of the native plant community.

Detailed studies were conducted on the six most common perennial species in the native plant community to obtain vegetative input for the UNSAT-H code. These studies included root depth, root length density, growing season, leaf area index, and percent foliar coverage. These studies were conducted in undisturbed areas east of the IP test site.

3.5.1 Root Depth

Root depth and distribution data was obtained for the six most common perennial species in the native plant community. These data were obtained by direct excavation and profiling of each

species' root system. The data were obtained from pits excavated with a shovel to depths varying from 50 to 100 cm. Each of these pits was excavated adjacent to the species under study. Once the primary pit was excavated, the sidewalls of the pits were carefully worked backward toward the root system of the species under study utilizing a trowel, paintbrushes, and canned air. Eventually, a two-dimensional picture of the root system of the plant was exposed. Once the root system was profiled, a series of pins were placed in the sidewall of the pit at decimeter increments along the vertical axis of the root system. The illustrated root system was then photographed utilizing a digital camera. Root depth was measured for black grama, threadleaf snakeweed, galleta grass, spike dropseed, sand sage, and ring muhly.

3.5.1.1 Black Grama

Black grama has a well-developed and finely divided root system with the greatest concentration of roots found within the uppermost 30 cm of the soil profile (Figure 3-4). These roots are arranged in a dense reticulate pattern and permeate the entire soil profile. Below 25 cm, smaller roots continue to penetrate the soil profile up to 80 cm but steadily decrease in abundance. Below 80 cm, roots are very scarce and minute. Based on field observations, minute roots are expected to penetrate the soil profile to a depth of 1.3 m below the surface.

The water-regulating physiology and root morphology of this dominant species place it in the 'intensive exploiter' classification (Burgess 1995). Intensive exploiters are plants that derive the majority of their moisture through dense rooting networks situated within shallow soil horizons. They exploit the moisture from ephemeral storm events with rapid root growth and water absorption. Intensive exploiters are also good competitors for limited, shallow soil moisture and recover rapidly from stress or damage with readily available soil moisture.

3.5.1.2 Threadleaf Snakeweed

Threadleaf snakeweed has a well-developed taproot and lateral root system with the greatest concentration of roots found within the upper 60 cm of the soil profile (Figure 3-5). The shortest taproot penetrated to approximately 40 cm where smaller lateral roots extended another 20 cm. The longest taproot penetrated to approximately 60 cm where smaller lateral roots extended additional 20 to 30 cm. Based on field observations, the taproot and the smaller lateral roots are expected to penetrate the soil profile to a depth of 100 cm below the surface.

3.5.1.3 Galleta Grass

Galleta grass has a rhizomatous root system with the greatest concentration of roots found within the uppermost 30 cm of the soil profile (Figure 3-6). Below 30 cm, smaller roots continue to penetrate the soil profile to 60 cm but steadily decrease in abundance. Below 60 cm, roots are very scarce and minute. Based on field observations, minute roots are expected to penetrate the soil profile to a depth of 75 cm below the surface.

3.5.1.4 Spike Dropseed

Spike dropseed has a well-developed and finely divided root system with the greatest concentration of roots found within the uppermost 30 cm of the soil profile (Figure 3-7). These roots are arranged in a dense reticulate pattern and penetrate the entire soil profile. Below

30 cm, smaller roots continue to penetrate the soil profile to 70 cm but steadily decrease in abundance. Below 70 cm, roots are very scarce and minute. Based on field observations, minute roots are expected to be found up to a depth of 100 cm below the surface.

3.5.1.5 Sand Sage

Sand sage has a well-developed pronounced taproot and lateral root system with the greatest concentration of roots found within the uppermost 80 cm of the soil profile (Figure 3-8). Taproots penetrated to approximately 80 to 150 cm where numerous, lateral roots extended another 20 to 50 cm. Based on field observations, the taproot and the smaller lateral roots are expected to penetrate the soil profile to a depth of 200 cm below the surface.

3.5.1.6 Ring Muhly

Ring Muhly has a fibrous root system with the greatest concentration of roots found within the uppermost 40 cm of the soil profile (Figure 3-9). Below 40 cm, smaller roots continued to penetrate the soil profile to 70 cm but steadily decrease in abundance. No roots were observed below 70 cm. Ring muhly appears to have the same root configuration as black grama but does not appear to root as deeply. Based on field observations, minute roots are expected to penetrate the soil profile to a depth of 100 cm below the surface.

3.5.2 Root Length Density

Root length density (RLD) was measured in two hand-excavated pits, RLD-1 and RLD-2 during the 2003 growing season. Each pit was 100 x 100 cm in area at the surface and 100 cm in depth. Root biomass was extracted and collected at successive 10 cm intervals to 100 cm in depth. Root biomass from each interval was screened and floated, then placed on a rack for one week and allowed to dry at an ambient temperature of 24°C (75°F) and a humidity of 10% to 15%. Root biomass from each interval was measured with a triple beam balance to an accuracy of 0.1 gram (g).

The distribution of root biomass with depth from RLD-1 and RLD-2 is shown in Figure 3-10. The root biomass exhibits a high degree of correlation. One factor contributing to the high degree of correlation may be the homogeneity of the dominant native plant species within the study area. Black grama accounts for over 60% of the total foliar coverage. There was very little variation in the composition or structure of the native plant community between the two pits. If there were greater variability in species composition, the root biomass would most likely exhibit greater variation. An additional factor that may contribute to root biomass correlation is the protracted drought at the time of the tests. All of the native plants exhibited signs of stress. It is likely that root biomass was low in relation to what might be expected if the native plant community had not been subject to such a protracted drought.

The labor and time to excavate and process 100,000-cubic-cm (cm^3) samples from RLD-1 intervals 1, 2, and 3 proved to be prohibitive so subsequent intervals were excavated in lesser volumes. A 25,000-cm^3 sample was excavated from intervals 4 and 5. A 12,500-cm^3 sample was excavated from interval 6. A 6250-cm^3 sample was excavated from interval 7 and 1576-cm^3 samples were excavated from intervals 8, 9, and 10. RLD-2 was excavated in 5000-cm^3 samples

from each interval. RLD-2 samples were floated, sifted, and dried in the manner described for RLD-1.

Root biomass data from RLD-1 and RLD-2 are summarized in Table 3-5. Approximately 90% of the root biomass occurs within 50 cm of the surface and approximately 98% of the root biomass occurs within 80 cm of the surface.

Because the greatest concentration of roots for the six most common perennial species within the study area is found between 0 and 80 cm of the soil profile, root biomass from RLD-1 and RLD-2 is normalized for biomass measured between 0 and 80 cm. Normalized biomass data for RLD-1 and RLD-2 is summarized in Tables 3-6 and 3-7, respectively.

Assuming that the normalized root biomass is directly related to RLD, RLD can then be related to the depth, z, below the surface by the exponential equation

$$\mathrm{RLD} = ae^{-bz} + c \tag{3-1}$$

where a, b, and c are coefficients that optimize the fit to the normalized root biomass data. Equation 3-1 is used in the UNSAT-H code to generate root density variation with depth in the soil profile, which drives the transpiration model. Normalized root biomass of RLD-1 and RLD-2 are shown related to Equation 3-1 in Figures 3-11 and 3-12. The root biomass data for RLD-1 and RLD-2 were fitted using the Levenberg-Marquardt algorithm for non-linear least squares fit of coefficients. The coefficients a, b, and c for RLD-1 are 0.5079, -0.0764, and 0.044, respectively with $r^2 = 0.979$. The coefficients a, b, and c for RLD-2 are 0.5172, -0.0516, and 0.0032, respectively with $r^2 = 0.995$. Combining the root biomass data for RLD-1 and RLD-2 in Figure 3-13 and again using the Levenberg-Marquardt algorithm for non-linear least squares fit of coefficients provides final coefficients $a = 0.5090$, $b = -0.0630$, and $c = 0.0262$ with $r^2 = 0.999$. These final coefficients optimize the exponential fit to the combined, normalized root biomass data of RLD-1 and RLD-2.

To calculate the root density function, the values of RLD are multiplied by their respective root length to obtain the root density function value for each depth. Tables 3-6 and 3-7 contain the root density function values for depths of root penetration between 0 and 80 cm.

3.5.3 Leaf Area Index and Growing Season

Growth of the dominant species within the study area is seasonal and to a large degree depends upon the availability of water. There was almost no growth among the dominant perennial grasses in the study area during the 2003 growing season. New Mexico experienced severe drought conditions in 2003 and prior years. Virtually all of the vegetation within the study area was dormant. There was essentially no rainfall to stimulate growth until late in the summer, and even then only a few sprouts developed leaving most perennial grasses dormant. Most of the leaves from prior years had been shattered or shredded from wind action over the prior winter. In essence, there was no leaf area to measure during the 2003 growing season, leaving no suitable platform to measure leaf area.

Many types of vegetation react to stress in the environment by producing canopies with lower leaf area. Thus the leaf area of a particular biome compared with typical values for such a biome may provide an indicator of stress, such as drought, nutrient deficiency, excessive heat or cold, as well as disease (Scurlock et. al. 2001).

Leaf area index (LAI) is broadly defined as the amount of leaf area in a vegetation canopy per unit land area. LAI is a key structural characteristic of vegetation and land cover because of the role of green leaves in a wide range of biological and physical processes. In the simplest terms, LAI can be described as the functional leaf area of a canopy standing above a defined ground area. LAI may be described as

$$\mathrm{LAI} = \frac{s}{G} \tag{3-2}$$

where s is the functional (green) leaf area of the canopy standing on the ground area, G. Because s and G are normally measured in units of area (m^2), LAI is dimensionless. However, LAI is sometimes presented in units of m^2/m^2 (Scurlock et. al. 2001).

Very few comprehensive reviews of LAI data exist in the literature. Scurlock et al. (2001) provide the most recent LAI data for biomes from 1000 published estimates of LAI from nearly 400 unique field sites covering the period 1932 to 2000. The maximum and minimum LAI values for a desert biome are 2.84 and 0.59, respectively, with a mean of 1.31 and a standard deviation of 0.85.

Without directly measured LAI data, the literature was consulted on prior studies of LAI in desert biomes. Scurlock et al. (2001) presents LAI data from two unique desert biomes in New Mexico, both of which are geographically close to and biologically similar to the TA-3 study area. The closest of these biomes is Sevilletta Wildlife Refuge, located approximately 45 mi south of TA-3. Much of the habitat of Sevilletta Wildlife Refuge is a mixture of scrubland and desert grassland. The desert grassland biomes of Sevilletta are very similar to those of TA-3. Scurlock et al. (2001) reports an LAI range of 0.8 to 1.9 for Sevilletta. The second biome in New Mexico occurs at the Jornada Research Station located approximately 35 mi north of Las Cruces. The Jornada Research Station is a large area composed of a mixture of Plains Mesa Sand Scrub, Closed Basin Scrub, and Desert Grassland (Dick-Peddie 1992). Dick-Peddie (1992) and Scurlock et al. (2001) report a LAI range of 0.8 to 3.9. In both of these New Mexico biomes, a minimum LAI value of 0.8 was reported.

At any given time, LAI is a measure of the functional photosynthetic area of the leaves. However, over the growing season, the size and abundance of leaves on any particular plant vary. Consequently, LAI is not a constant but varies across the growing season and from year to year depending upon annual climatic conditions. In order to address this issue, an analysis of the growth characteristics of the dominant species within the project area was conducted. These species include black grama, threadleaf snakeweed, galleta grass, and spike dropseed. These data are derived from the USDA Forest Service Fire Effects Information Database (2003) and

information provided by Reggie Fletcher, US Forest Service Regional Ecologist (retired) (2003), and Paul J. Knight, Ecologist, Marron and Associates, Inc. (Knight and Ashton 2003).

3.5.3.1 Black Grama

Black grama, although a grass, almost behaves like a small shrub in that it maintains a large amount of standing living biomass throughout the year. The growth of black grama has been found to correspond with season and amount of precipitation. Paulson and Ares (1962) found that precipitation received between July and September is more important than total annual precipitation, as most of the foliar growth occurs in the summer. The stems of black grama remain green throughout the year (Brown 1982, Brown and Gersmehl 1985) maintained with carbohydrate reserves stored in the stem, root, and root crown (Herbel and Nelson 1969). The plants can also be dormant for long periods of time during drought, but rapid development and growth occur under periods of relatively abundant moisture and high nighttime temperature (Canfield 1934).

Black grama can maintain green stems even in the winter months. However, it is unlikely that these stems would function below biological zero, generally considered 5°C (41°F). Depending on available moisture, the standing biomass of black grama can rapidly green in the spring. Fletcher (2003) estimates that during a normal spring, the standing biomass of black grama available from past year growth can reach perhaps 70% of its total expected LAI for the year soon after the onset of the growing season in the spring, and that the full potential or growth and leaf area on this species generally occurs just after the onset of the summer monsoon season. Nelson (1934) found that in arid areas of southern New Mexico, the start of the growing season for black grama corresponds with the onset of the summer rainy period (usually in early July through August). Depending upon the availability of moisture, this growth can continue until the end of September or October. With the end of the growing season, the plants enter into a period of dormancy. Nelson (1934) reports that if fall, spring, and winter precipitation is high and if temperatures are not too low, the onset of new growth of leaves may start as early as March and April, and with continued moisture, growth may extend into the main summer growing period.

3.5.3.2 Threadleaf Snakeweed

Much like black grama, threadleaf snakeweed can retain green leaves throughout the winter in some areas of New Mexico. Comstock et al. (1988) reports that new terminal growth begins on basal stems from January through March. This growth continues through the spring, and depending upon available moisture, can continue into the summer. Flowering is initiated in the spring and early summer. Fletcher (2003) estimates that the plants are probably at about 70% of their full LAI potential in the spring and likely reach 100% of their LAI potential during the summer rainy season starting in July and August.

3.5.3.3 Galleta Grass

West et al. (1972) reports that the availability of moisture is the cue for vegetative growth in galleta grass and the growth of this species corresponds to periods of available moisture. Goodrich (1986) reports that the most common growing season for this species is May to September. Fletcher (2003) notes that this species is completely dormant throughout the winter,

and depending upon moisture, can rapidly begin leaf development at the onset of the growing season. Within the Albuquerque area, Fletcher (2003) reports an annual period of dormancy in late June through July. With the onset of the summer rainy season, the plants green up to full LAI. Fletcher (2003) believes that by the end of the growing season, the functional LAI for this species drops to zero.

3.5.3.4 Spike Dropseed

Fletcher (2003) reports that the seasonal growth and development of spike dropseed is much like that of galleta grass. This species is generally completely dormant in winter, and depending on available moisture, can have an immediate response in the spring with beginning growth. During prolonged dry periods, moisture during the early growing season is spotty and much like galleta grass, spike dropseed will remain dormant. Fletcher (2003) estimates that during most years from May through July this species may reach only 10% to 20% of its LAI, but with the onset of the summer rains in late July and August, rapid growth occurs. Fletcher (2003) estimates that during normal precipitation years, the full LAI potential of this species would be reached by August and would continue into October.

3.5.3.5 Leaf Area Index and Growing Season Summary

The seasonal variation of LAI among the dominant plant species in the study area consists of a complex interaction of variation in annual wet and dry cycles intermeshed with the ecological growth and development strategies that have developed within each of these species. Although LAI probably varies greatly on a short-term basis among these species, there are some overall predictable seasonal trends in growth and development among the common grasses found in the project area (USDA Forest Service 2003).

Although evaporation from the soil continues year round, plants and transpiration are active only during the growing season of the established plant community. Within a growing season, different species initiate and achieve peak growth at different times depending on seasonal variation in precipitation, wind, atmospheric pressure, and temperature. The growing season begins when air and soil temperatures are high enough to allow plant growth and ends when day length and temperature decrease below a metabolic threshold for vegetation.

The growing season and corresponding LAI data for the study area are summarized in Table 3-8 and shown in Figure 3-14. The growing season data were derived from the plant species databases of the USDA Forest Service Fire Effects Information Database, Reggie Fletcher, U.S. Forest Service Regional Ecologist (retired) (2003), and Paul J. Knight and Tom S. Ashton (Knight and Ashton 2003). The LAI data were obtained from Scurlock et al. (2001) and discussions with Lewis P. Munk (Munk 2004). Growing season and LAI are used in the UNSAT-H code to drive the transpiration model.

3.5.4 Percent Bare Area

Ground cover can be composed of live and dead plant material, mosses, lichen, rock, litter, and miscellaneous debris (ITRC 2003). Two methods were employed to measure ground cover within the study area. In this study, ground cover is defined as live and dead plant material or

"foliar" coverage. The first method used to measure foliar coverage involved linear transects. Linear transects are commonly employed by botanists to determine the coverage and frequency distribution of plants and plant communities. Ten linear transects, each 50 m in length, were surveyed within the 8.5-acre study area (Figure 3-15). Foliar coverage was measured along a total of 500 m of linear transects.

The second method used to measure foliar coverage involved aerial digital photography. Five surface plots for digital photography, each 4 x 4 m in area, were randomly selected within the 8.5-acre study area (Figure 3-16). Digital photographs were taken from 9 m above each plot to delineate foliar coverage. The photographs framed the perimeter of each plot and clearly identified vegetation in contrast to bare ground. The root crown of the perennial grasses and shrubs within each surface plot were outlined with white flour. The flour was applied 4 to 5 cm wide with an Irwin straight-line marking chalk bottle. The digital photographs were imported into Adobe Illustrator 8.0 where the approximate boundaries of the root crown were outlined in red and the foliar cover was outlined in yellow. The digital images where then transferred to a computer aided design system where foliar coverage was recorded. Digital photographs of surface plots DP-1 through DP-5 are shown in Figures 3-17 through 3-21.

3.5.4.1 Linear Transects Results

The results of linear transects are presented in Table 3-9. Seventeen perennial and annual species were identified along the transects. These data indicate a total foliar coverage of 22.5%. Perennial species accounted for 19.2% of total foliar coverage where black grama represents the most abundant species with an individual coverage of 13.8%. Annual species accounted for 3.3% of the total foliar coverage. The fraction of the ground surface not covered by plants, e.g., percent bare area (PBA), is 77.5%.

3.5.4.2 Digital Photography Results

The results of digital photography are presented in Table 3-10. These data indicate an average foliar coverage of 26.1%, somewhat higher than the 22.5% total foliar coverage measured from the linear transects. The higher foliar coverage measured by digital imagery is the result of recording pockets of plant litter which could not be distinguished from standing vegetation on the digital images. Based on the methodology employed to collect the two sets of data, the linear transect method is considered to be the most accurate in determining PBA. PBA is also used in the UNSAT-H code to drive the transpiration model.

4. Instantaneous Profile Test

The IP method (Watson 1966) for determination of the unsaturated hydraulic conductivity of soil requires the construction of a soil profile that allows free vertical drainage of water. The technique is not applicable where significant lateral movement of water occurs. The technique requires frequent and simultaneous measurement of soil wetness and tension under conditions of drainage alone. From these measurements, one can determine instantaneous values of the potential gradients and fluxes operating within the profile and also the hydraulic conductivity function of soils. This technique provides a practical, direct method for measuring the unsaturated hydraulic conductivity of soils on a realistic scale (Hillel 1998). The IP method of Watson (1966) is preferred over laboratory tests (Jaynes and Tyler 1980). Data obtained *in situ* are used as a standard by which comparisons are made from the results of indirect laboratory methods; however, laboratory methods are less costly and less laborious than *in situ* testing (Marion et al. 1994). In this study, directly measured field and indirectly measured laboratory soil parameters provide a good practical basis for the evaluation of alternative landfill cover design. The use of these parameters for model input produces less modeling uncertainty than using empirical reference values from the literature.

4.1 Instantaneous Profile Test Site

An IP test site was constructed in the north-central portion of TA-3 at SNL/NM (Figure 3-1) to obtain site-specific, soil hydraulic parameters representative of the natural analogue. The test site was constructed by excavating trenches around an undisturbed soil profile, 16 x 16 ft in area. Hillel (1998) recommends that IP sites be at least 5 x 5 m such that internal drainage is unaffected by the boundaries and that lateral movement of soil moisture is not appreciable. The trenches, 1 ft wide, were excavated to a depth of 6 ft and filled with a 10% bentonite-soil slurry that was dispensed from a cement truck. Directly above the trenches and the slurry wall at the ground surface, a concrete retaining wall, 1 ft high, was formed around the perimeter of the soil profile to allow for ponding of water.

The soil profile was instrumented with 2 neutron probe access tubes and 3 clusters of paired tensiometers and time domain reflectometry (TDR) probes (Figure 4-1). The neutron probe access tubes consisted of 2-in. inside-diameter Schedule 80 polyvinyl chloride (PVC) pipe installed to a depth of 9 ft. The neutron probe access holes were installed by hand-augering to the desired depth and gently forcing the PVC tubes into place. Each of the 3 instrument clusters, A, B, and C, contained tensiometers and TDR probes that were installed at depths of 1, 2, 3, 4, 5, and 6 ft. The tensiometers and TDR probes were installed by hand-augering to the desired depth, gently forcing the instruments into place, and backfilling to grade. Two additional neutron probe access tubes were installed outside the perimeter of the soil profile to determine if any leakage had occurred through the bentonite-soil barrier.

All instrumentation was calibrated in the field or in the lab before installation and operation. After installation, the instrumentation was tested for continuity and allowed to equilibrate with the soil profile. Tensiometers and TDR probes were multiplexed to a Campbell Scientific CR7 electronic data logger. Baseline neutron probe and tensiometer data within the soil profile were obtained before the test was initiated. Neutron probe data were recorded manually as counts of

thermalized neutrons using a CPN Model 503DR neutron probe. Counts were obtained over 64 s at successive 1-ft intervals to 9 ft in depth. Thermalized neutron counts were converted to volumetric moisture content using a soil calibration curve. Tensiometer data were obtained using Soil Moisture Systems, Inc. 1-bar porous cup tensiometers equipped with pressure transducers. Tensiometer data were recorded using a Campbell CR7 data logger.

4.1.1 Instantaneous Profile Test—Flooding Phase

The soil profile was flooded with 5500 gallons of water over a period of 48 hrs. Flow was monitored electronically with an EG&G flow meter. Elevation (pressure) head within the concrete retaining wall was maintained at 2 in. during flooding. Flooding was discontinued once instrumentation indicated that the 6-ft soil profile was field saturated.

The advance of the wetting front was monitored with the neutron probe, tensiometers, and TDR probes. The wetting front moved quite rapidly through the soil profile due to redistribution of water within the profile. Rapid redistribution is caused by strong suction gradients because the underlying soil in the profile is quite dry compared to the overlying wetted soil. Over time, the wetting front slowed as the suction gradients diminish and the hydraulic conductivity of the soil increases. As the suction gradient decreases and the hydraulic conductivity increases, the flux (i.e., water flow rate) diminishes even more rapidly and the advance of the wetting front gradually dissipates (Hillel 1998).

The advance of the wetting front as recorded by the neutron probe in the center and southeast access tubes is shown in Figures 4-2 and 4-3. Each curve represents the moisture content at the depth indicated. Time in days is shown as negative because Day 0 represents the time, T_0, when flooding was discontinued and drainage of the soil profile was initiated. The data at 7, 8, and 9 ft were collected below the depth of the bentonite-soil barrier. These data are represented as dashed lines. The advance of the wetting front at these depths is more diffuse due to lateral flow.

Figures 4-2 and 4-3 demonstrate the effective water storage capacity of the soil profile at the IP test site. The redistribution process described above determines the amount of water retained at various times and depths in the soil profile. The rate and duration of downward flow during redistribution determines the effective water storage capacity of the soil profile. The effective storage capacity may be determined from the figures by measuring the area between the residual water and the quantity of water the soil profile holds against the force of gravity when suction gradients hardly exist and drainage occurs under the influence of gravity only. In Figures 4-2 and 4-3, if the soil profile has an average storage capacity of 30% by volume, and gravity and plants extract water to an average of 10% by volume, the effective storage capacity is 20% by volume. If the soil profile were 100 cm (39 in.) in thickness, it would store 200 mm (8 in.) of water.

4.1.2 Instantaneous Profile Test—Drainage Phase

Once the IP test site instrumentation confirmed that the 6-ft soil profile was field saturated and had attained steady-state, flooding was discontinued and the soil profile was allowed to drain. In the field, soil rarely attains complete saturation, as air remains within the soil matrix. The soil surface was covered with an opaque blue tarp to minimize soil heating and prevent evaporation

from the soil profile. As the soil profile drained, data was obtained on the distribution of soil moisture and tension throughout the soil profile. Neutron probe data were acquired manually every hr for the first 32 hrs of the test with the neutron probe and then every 4 hrs for the next 48 hrs. Thereafter, the frequency of moisture readings was decreased to one reading every 8 hrs, every 12 hrs, daily, weekly, and then monthly, as the rate of drainage decreased. Collection of tensiometer data was computer controlled, allowing for more rapid data acquisition. Tensiometer data was acquired automatically every 10 minutes for the first 32 hrs of the test with the Campbell CR7 data logger and then every 30 minutes for the next 70 hrs. Thereafter, the frequency of tensiometer data acquisition was decreased to hourly and then twice daily. Neutron probe data were acquired on a continual basis for 890 days whereas tensiometer data was acquired on a continual basis for 200 days.

The neutron probe provides uniform precision and reliable results throughout the entire range of moisture content variation in the soil profile. Tensiometer measurements are limited to values below 1 atmosphere (atm) (1 bar), however, in the field, the useful limit of most tensiometers is about 0.85 atm. Although the tension range of 0 to 0.85 atm is a minor part of the total range of tension one encounters in the field, it actually encompasses a major part of the soil profile-wetness range (Hillel 1998).

Despite considerable planning and effort, the tensiometers proved problematic during the IP test. A few tensiometers failed or operated intermittently as the test progressed. Very few tensiometers were operational beyond 200 days into the test. As a result, tension measurements were discontinued at 200 days. The TDR probes proved completely unreliable during the test. Therefore, TDR data were eliminated from consideration in this study.

4.1.3 Data Conditioning

Neutron probe and tensiometer data were evaluated for errors in data acquisition and instrument failure. All data were converted to appropriate units of volumetric moisture content, θ, or tension, Ψ. Tension describes the water pressure difference from atmospheric pressure. When the water pressure is equal to or greater than the atmospheric pressure, the soil profile is field saturated. When the water pressure is less than the atmospheric pressure, the soil profile is unsaturated. Positive tension values will be used as the convention in this study.

Volumetric moisture content and tension with the respect to time, $\theta(t)$ and $\Psi(t)$, were conditioned (e.g., smoothed) using Butterworth digital filters (Stearns 1975). Conditioned data were then fitted mathematically with low-order polynomials to obtain numerical arrays for determining the hydraulic properties of the soil profile. The soil properties that determine the behavior of water flow in the soil profile are the hydraulic conductivity and water-retention characteristics. The hydraulic conductivity of the soil profile is a measure of its ability to transmit water; the water-retention characteristic of the soil profile is a measure of its ability to store water. These combined properties are often called the hydraulic conductivity function of soils (Klute and Dirkson 1986).

4.1.4 Hydraulic Conductivity Function—Theoretical Overview

Hillel (1998) provides a detailed description for determining the intrinsic hydraulic properties of a soil profile *in situ* based on the IP test method. The general equation describing the redistribution of water in a vertical soil profile is

$$\frac{\partial \theta}{\partial t} = \frac{\partial}{\partial z}\left[K(\theta)\frac{\partial H}{\partial z} \right] \tag{4-1}$$

where θ is the volumetric moisture content (measured by neutron probe), t is time, z is the vertical depth of the soil profile, $K(\theta)$ is the hydraulic conductivity as a function of volumetric moisture content, and H is the total hydraulic head, gravitational and tensional ($Z+\Psi$) (the latter measured by tensiometry).

Integrating, one obtains

$$\int_0^z \frac{\partial \theta}{\partial t}\partial z = \left[K(\theta)\frac{\partial H}{\partial z} \right]_Z \tag{4-2}$$

where z is the depth in the soil profile to which the measurement applies. Since the soil profile is covered to prevent evaporation and only internal drainage is allowed, the total volumetric water content per unit time is

$$\left[\frac{dW}{dt} \right]_Z = K\left[\frac{\partial H}{\partial z} \right]_Z \tag{4-3}$$

where W is the total volumetric water content stored at time t in the profile between the surface and depth z, that is

$$W_T = \int_0^z \theta(z,t)dz \tag{4-4}$$

This technique is used to determine the hydraulic properties of soil, and was named the IP method by Watson (1966).

During the internal drainage of a thoroughly-wetted soil profile, $(\partial H/\partial z)_Z$, is often found to be near unity; that is, the tension is near zero and only the gravitational gradient operates. If so, then

$$K = \left(\frac{dW}{dt} \right)_Z \tag{4-5}$$

Otherwise, the suction gradient must be considered and the hydraulic conductivity is obtained from the ratio of flux to the total hydraulic head gradient (gravitational plus matric). This can be done successively at gradually diminishing water content during drainage to obtain a series of K versus θ values and thus establish the functional dependence of hydraulic conductivity upon soil wetness or moisture content for each depth in the soil profile (Hillel 1998).

4.1.5 Hydraulic Conductivity Function—Application

Moisture content data from the center and southeast neutron probe access tubes are shown in Figures 4-4 and 4-5, respectively. The moisture content within the soil profile decreases rapidly during the first 60 days of drainage. Rapid initial drainage reflects much higher hydraulic conductivity at field-saturated and near-field-saturated conditions. Beyond 60 days, drainage decreases significantly with time, becoming near-asymptotic as one approaches 330 days.

Tension figures from tensiometer clusters A, B, and C are shown in Figures 4-6 through 4-11. The tension within the soil profile increases rapidly during the first 10 days of drainage. The marked decrease in drainage with time represents a simultaneous increase in tension and decrease in hydraulic conductivity.

Tension and volumetric moisture content data from the IP test were analyzed using the IP test method discussed by Hillel et al. (1972) to determine the unsaturated hydraulic conductivity, K, as a function of volumetric moisture content, θ. This relationship was calculated at 1-ft intervals to 6 ft in depth for the center and southeast neutron access tubes by pairing volumetric moisture content data with tension data from tensiometer clusters A, B, and C. Data from days 1, 2, 4, 8, 16, 32, and 64 were analyzed to obtain specific points on the K versus θ curves.

4.1.6 Calculation of Hydraulic Conductivity Function

From Figures 4-4 and 4-5, the water flow rate (flux) through each depth increment 1, 2, 3, 4, 5, and 6 ft is calculated by integrating the moisture-time (θ,t) curves with respect to depth, z. The slope ($\partial\theta/\partial t$) of the moisture curves is measured at day 1, 2, 4, 8, 16, 32, and 64 using linear and polynomial regression. These slopes are then multiplied by their respective depth increment to obtain the per layer rate of water content change, $dZ(\partial\theta/\partial t)$. The flux, Q, through the bottom of each depth increment is obtained by accumulating the water content of each successive layer overlying that depth, i.e., $Q = dZ(\partial\theta/\partial t)$. These data are presented in Tables 4-1 and 4-2. From Figures 4-6 through 4-11, the hydraulic head, H, corresponding to the times for which the above flux values were calculated, is obtained by adding the depth of each tensiometer in clusters A, B, and C to their corresponding elevation head value.

The resulting hydraulic head change with depth during drainage is shown in Figure 4-12. The hydraulic head profiles exhibit a distinct change in slope between the lower and upper half of the profiles. The slope, $\partial H/\partial z$, of each hydraulic head profile was determined for the lower and upper segments using linear regression (Figure 4-13). The regression for each segment is presented in Table 4-3. The flux, Q, presented in Tables 4-1 and 4-2, was divided by the corresponding hydraulic head gradient ($\partial H/\partial z$), which represents the minimum and maximum slope of the hydraulic head profiles in Figure 4-13 (Table 4-3). The hydraulic conductivity, K, is then plotted against corresponding volumetric moisture content from Figures 4-4 and 4-5, and

shown in Figures 4-14 and 4-15 for the center and southeast neutron probe access tubes, respectively.

4.1.7 Soil Profile Moisture, Tension, and Conductivity Characteristics

The dynamic range of measurements obtained from the IP test on the natural analogue was limited to 30% to 35% volumetric moisture content (effective field saturation) and 15% to 20% volumetric moisture content. This limited range was due to the slow rate of drainage and the time and labor involved to continue monitoring incremental changes in soil moisture and tension within the profile. Even so, the IP test encompasses a significant portion of the soil profile-wetness range and provided valuable data describing the soil profile moisture, tension, and conductivity characteristics for the wet end of the soil profile.

The saturated hydraulic conductivity and conductivity near saturation is determined primarily by soil structural properties that are known to be subject to considerable spatial variability. This is in contrast to soil textural properties that generally are less variable and have a dominant effect on unsaturated conductivity. Saturated hydraulic conductivity is determined by an assemblage of macropores or channels of preferential flow that may have little effect on the overall pore-size distribution (texture) that determines the general shape of the predictive conductivity curve at intermediate water contents.

The saturated hydraulic conductivity of the soil profile was determined under steady-state conditions during the flooding phase of the IP test. Field tests are preferred over indirect laboratory tests for determining the saturated hydraulic conductivity because the soil structure and volume as it existed *in situ* is usually altered during sample collection and preparation. The saturated hydraulic conductivity at steady state was determined to be 4.05×10^{-4} cm/s.

Three soil samples from the IP test site were sent to an outside geotechnical laboratory for independent analysis of saturated hydraulic conductivity. The soil samples were remolded and tested for saturated hydraulic conductivity using the flexible wall permeability test. Although these samples do not reflect the *in situ* soil structure and fabric, the results of these tests show that the saturated hydraulic conductivity ranged between 1.2×10^{-4} cm/s to 3.1×10^{-4} cm/s, averaging 2.5×10^{-4} cm/s.

In Figures 4-14 and 4-15, the unsaturated hydraulic conductivity determined *in situ* is approximately log-normally proportional to the volumetric moisture contents observed during the IP test. This relationship can be described empirically by the exponential equation $K = ae^{b\theta}$ where K is the hydraulic conductivity, θ is the volumetric moisture content, and a and b are soil texture characteristics. The soil profile is not characterized by a unique hydraulic conductivity function but by an envelope of functions that represent the range of soil textures that govern the flow of water within the profile. Within the operating envelope, hydraulic conductivity as a function of θ varies by three orders of magnitude.

The hydraulic conductivity as a function of volumetric moisture content $K(\theta)$ determined from the IP test is compared to the $K(\theta)$ function obtained from the van Genuchten RETC code in Section 5.5.

Volumetric moisture content and soil tension for the center and southeast neutron probe access tubes at 1-ft intervals are shown in Figures 4-16 through 4-27. The observations are limited to the wet range of the $\theta(\Psi)$ curve with a tension range of 0 to 300 cm.

The $\theta(\Psi)$ data exhibit a sigmoidal-shaped curve as described and presented in the literature by numerous researchers (van Genuchten 1978, van Genuchten 1980, van Genuchten and Nielson 1985, van Genuchten et al. 1991, Marion et al. 1994, Khaleel and Relyea 1995, Paige and Hillel 1993, Shouse et al. 1992). The sigmoidal curve relates tension (or suction head) to volumetric moisture content in the soil profile as θ moves from effective field saturation to residual values along the drainage path. In a classic $\theta(\Psi)$ curve, the slope, $\partial\theta/\partial\Psi$, becomes zero when θ approaches both its effective field-saturated and residual values.

These $\theta(\Psi)$ data represent desorption rather than sorption of water within the soil profile because data were obtained during the drainage phase of the IP test (soil tension is measured over a greater desorption range in the laboratory—these laboratory tests and data will be discussed in Chapter 5). These directly measured field data encompass a significant portion of the soil profile-wetness range and will be used to develop the constitutive principles that will govern performance modeling using the UNSAT-H code in Chapter 6.

4.2 Construction of an Engineered Cover

Once the IP test of Section 4.1 was completed, the IP test site was excavated to a depth of 6.5 ft and replaced with an engineered cover. The engineered cover was built using traditional engineering practices and construction specifications. Conceptually, the simplest engineered cover consists of a monolithic soil layer overlain by a vegetative soil layer. Often referred to as an "evapotranspiration" cover, the monolithic soil layer has the advantage of being simple and economical to construct and maintain (ITRC 2003). The engineered cover was designed and constructed to emulate the natural analogue and to represent the vegetative soil covers proposed in this study.

The engineered cover consisted of 6 ft of compacted native soil overlain by 9 in. of uncompacted native topsoil. The soils were obtained from local stockpiles and screened to remove all rock and debris greater than 2 in. in diameter. The native soil and topsoil were mostly classified as SM according to the USCS in accordance with American Society for Testing and Materials (ASTM) D4318 and ASTM D2487.

The native soil layer was placed in maximum 8-in. loose lifts to attain maximum 6-in. compacted lift thickness. The native soil was compacted to not less than 90% of maximum dry density at -3 to +2 percentage points of optimum moisture content, as determined by ASTM D698 (Standard Proctor testing). The native topsoil was placed in a maximum 9-in. uncompacted lift to not more than 90% of maximum dry density at -3 to +2 percentage points of optimum moisture content, as determined by ASTM D698.

A total of 13 lifts, excluding subgrade, were placed to complete the construction of the engineered cover. Bulk density and moisture content were measured after construction of each lift utilizing a CPN MC-3 Portaprobe. A summary of the number of lifts along with bulk

densities and moisture contents for each lift is summarized in Table 4-4. The average volumetric moisture content and dry bulk density compare very well with the average volumetric moisture content and dry bulk density of the natural analogue presented in Tables 3-1 and 3-2.

The engineered test cover was instrumented with 2 neutron probe access tubes (Figure 4-28). The neutron probe access tubes consisted of 2-in. inside-diameter 6061-T6 aircraft aluminum pipe installed to a depth of 8 ft. The test cover was not instrumented with tensiometers because of their limited range, intermittent operation, and early failure during the IP test on the natural analogue. The engineered cover was instead instrumented with optical time-domain reflectometry (OTDR) fiber optics to detect localized measurand-induced (temperature) variations in the scattering coefficient of continuous sensing fibers. This phenomenon forms the basis of the distributed (rather than point source) temperature sensing systems that are being considered for deployment in landfill covers for long-term performance monitoring.

An important advantage of fiber optic sensors is that they are electrically passive, and thus the whole system exhibits low intrinsic susceptibility to the effects of electromagnetic interference and electromagnetic pulse. Experience to date in environmental monitoring indicates that electrically-based sensors are extremely susceptible to electrical storms, particularly in the semiarid and arid southwest. Therefore, issues of electrical passivity are of paramount importance when a sensor is required for long-term monitoring and performance in an electrically noisy environment.

4.2.1 Engineered Cover—Flooding Phase

The engineered cover was flooded with 5100 gallons of water over a period of 10 days. Elevation (pressure) head within the concrete retaining wall was maintained at 2.5 in. during flooding. Flooding was discontinued once instrumentation indicated that the engineered cover was field saturated. The advance of the wetting front was monitored with the neutron probe and fiber optics.

4.2.2 Engineered Cover—Drainage Phase

Once the engineered cover instrumentation confirmed that the 6-ft soil profile was field saturated and had attained steady-state, flooding was discontinued and the test cover was allowed to drain. As the test cover drained, data was obtained on the distribution of soil moisture throughout the soil profile for validation of the OTDR fiber optics and calibration of the variations in the scattering coefficient of continuous sensing fibers. The results of the OTDR distributed fiber optics tests are beyond the scope of this study, therefore are not included. Soil core samples were collected from the soil profile to determine the unsaturated conductivity function for the engineered cover by means of laboratory tests in Chapter 5. These laboratory data will be used to develop the constitutive principles that will govern performance modeling using the UNSAT-H code in Chapter 6.

5. Laboratory Soil Tests

Laboratory tests to obtain the hydraulic conductivity function of soils are less costly and laborious to conduct than IP tests and can be applied to a larger range of water contents and tension over which *in situ* measurements are not practical. Because of their simplicity, laboratory tests are convenient alternatives to the IP method. Laboratory tests incorporate the inverse approach for determining the hydraulic conductivity function of soils. Instead of taking direct field measurements of soil moisture content and soil tension in a draining soil profile to determine the hydraulic conductivity function, other flow variables are measured in the laboratory, such as the saturated hydraulic conductivity and the soil moisture characteristic curve. The best representative equation describing the hydraulic conductivity function is determined by fitting the theoretical solution of the actual transient flow to the corresponding laboratory-measured data.

In this chapter, soil samples from the natural analogue and the engineered cover are evaluated using the parametric model of van Genuchten (1980) and the predictive model of Mualem (1976) for moisture retention data to obtain the unsaturated conductivity function for the natural analogue and engineered cover soil profiles. The parametric and predictive models are available in the computer code RETC developed by the Soil Physics group of the U.S. Salinity Laboratory, Riverside, California (van Genuchten et al. 1991). The RETC code is described in Section 5.3.

The application of inverse methodology in the RETC code has become quite popular for obtaining the hydraulic properties and moisture characteristics of soils. The inverse method is based upon obtaining solutions to transient flow processes through the inversion of the governing flow equations. This approach combines laboratory-determined $\theta(\Psi)$ data, unsaturated flow equations with appropriate boundary conditions, and computer codes to parameterize the soil hydraulic function during transient flow. The numerical scheme determines the desired parameters in the hydraulic function by minimizing deviations between observed and model output. The inverse methodology is versatile and can be applied to multi-layered soil profiles. In this study, the inverse methodology is used on soil samples obtained from the natural analogue and the engineered cover.

5.1 Laboratory Testing—Natural Analogue

A total of 20 soil core samples were collected from the southwest corner of the natural analogue (Figure 4-1). The samples were collected to a depth of 6 ft using a hydraulically-driven, double-cylinder soil sampler. The sampler was driven to the desired depth into the soil profile, and the soil sample carefully removed to preserve the structure and volume of soil as it existed *in situ*. Undisturbed samples were preferred but due to the dry, friable nature of the soils within the soil profile, undisturbed soil samples were not always obtained nor was sample recovery complete. Soil samples were retained in removable, 2.0-in. diameter cylindrical sleeves, labeled, and stored in sealed containers to prevent drying during preparation for laboratory testing. The dry mass and volume of each soil sample was determined for calculation of dry bulk density by measuring the length and diameter of the sample. Saturated hydraulic conductivity, K_s, for each soil sample was determined according to the Constant Head Method of Klute and Dirkson (1986). The soil core characteristics of the natural analogue are presented in Table 5-1.

The relationship between the soil water content and tension (suction head) of a porous medium (referred to as the soil moisture characteristic or soil water retention curve) is a fundamental part of the hydraulic properties of a soil. A common laboratory method by which the soil moisture characteristic curve is determined is the pressure cell method (Klute and Dirkson 1986). Soil samples from the natural analogue were tested using a 0.1- to 15-bar pressure extractor assembly to determine the soil moisture characteristic curve and the hydraulic conductivity function.

Soil samples were tested at tensions ranging from 1 to 15 bar. After preparation, saturated soil samples were transferred to the pressure extractor assembly for testing. Undisturbed soil samples were trimmed to insure proper hydraulic contact with the ceramic plate. Disturbed samples were remolded to a representative bulk density and then trimmed to insure proper hydraulic contact with the ceramic plate.

In the pressure extractor method of determining the water retention characteristics of a soil, a soil sample is placed on a saturated, porous ceramic plate. The sample and the surface of the plate is subjected to an inlet air pressure, P_{in}, greater than the atmospheric air pressure, P_{atm}. The lower side of the ceramic plate is sealed from the inlet pressure and vented to the atmosphere. The ceramic plate, having an air entry pressure greater than the inlet pressure, creates a pressure gradient across the sample that results in the flow of water through the sample. When the flow of water from the sample ceases, the soil water tension in the sample, Ψ is considered to be in equilibrium with the pressure difference across the sample, $\Psi = P_{in} - P_{atm}$. At equilibrium, the volumetric moisture content, θ, of the sample is determined and paired with the soil tension, Ψ, of the sample. The data pair, (θ,Ψ), determines one point on the water retention curve. A complete water retention curve is mapped by establishing a series of equilibria and paired (θ,Ψ) values by applying sequential pressure gradients across the sample starting from an initial saturated condition to a final, residual water content.

The water content of a sample at equilibrium is determined by calculating the change in weight of the sample from the fully dried weight. Pressure plate testing begins using a pressure of 1 bar and an inlet pressure slightly greater than ambient air pressure. When equilibrium is attained, the pressure is released from the pressure vessel, and the sample is removed and weighed to determine the soil moisture content corresponding to the applied soil water tension. The time required to reach equilibrium is dependent on the soil sample properties, sample size, and the pressure gradient, but averages 2 to 3 days. This procedure is repeated with increasing inlet pressures, until the $\theta(\Psi)$ curve is fully mapped. This procedure defines the drying curve or "desorption" of the soil samples.

5.2 Laboratory Testing—Engineered Cover

A total of 13 soil core samples were collected from the southeast corner of the engineered cover (Figure 4-28). Bulk samples were obtained by hand-augering to a depth of 6 ft. Samples were stored in sealed plastic bags for laboratory testing at Daniel B. Stephens and Associates, Inc., Albuquerque, New Mexico. In the laboratory, the samples were remolded to not less than 90% of maximum dry density at -2 to +2 percentage points of optimum moisture content, as determined by ASTM D698. The dry mass and volume of each soil sample was determined for

calculation of dry bulk density. Saturated hydraulic conductivities for each soil sample were determined according to the Constant Head Method of Klute and Dirkson (1986). The soil core characteristics of the engineered cover are presented in Table 5-2.

Remolded soil samples from the engineered cover were tested using a combination of hanging column, pressure plate, water activity meter, and relative humidity chamber at tensions ranging from 0 to 850 bar to determine the soil moisture characteristic curve and the hydraulic conductivity function.

5.3 The RETC Code—Overview

The RETC code (van Genuchten et al. 1991) can be used to fit several parametric models to observed water retention and hydraulic conductivity data. Water retention data is dependent primarily on the texture or particle size of the soil and the structure or arrangement of the individual soil particles (Klute and Dirkson 1986). The soil water retention function may be described with the analytical equations of Brookes and Corey (1964) or van Genuchten (1980). The pore-size distribution models of Burdine (1953) or Mualem (1976) may be used to predict the unsaturated hydraulic conductivity function. The van Genuchten model (1980) has the greatest flexibility in describing retention data from various soils, has a simple inverse function, and permits the derivation of closed-form analytical solutions for hydraulic conductivity when combined with the predictive theories of Burdine (1953) or Mualem (1976). The van Genuchten (1980) model graphically displays a continuously differentiable (smooth), S-shaped retention curve between the saturated and residual water contents. Of the two hydraulic conductivity models, Mualem's model has been found to be applicable to a wider range of soils. In this study, the parametric model of van Genuchten (1980) and the pore-size distribution model of Mualem (1976) are used exclusively to determine the hydraulic conductivity function of the IP soil profile from soil cores and their related water retention data. The combined van Genuchten-Mualem approach is routinely used by soil physicists to estimate the unsaturated hydraulic conductivity function of soils.

5.3.1 Soil Water Retention Model

Van Genuchten (1980) derived an empirical relationship to describe the soil water retention function:

$$\theta = \theta_r + \frac{\left(\theta_s - \theta_r\right)}{\left[1 + \left|\alpha\Psi\right|^{n}\right]^{m}} \tag{5-1}$$

where θ is the volumetric moisture content, θ_r is the residual moisture content, θ_S is the saturated moisture content, α, m, and n are empirical curve-fitting parameters that affect the shape of the curve, and Ψ is the tension (or suction head). To obtain relatively simple predictive closed-form analytical solutions for the unsaturated hydraulic conductivity, van Genuchten (1980) assumed unique relations between m and n. Van Genuchten and Nielsen (1985) found that when fitting observed retention data, the restriction m=1-1/n yields stable, well-defined unsaturated hydraulic conductivity functions.

The Mualem (1976) model used to predict the hydraulic conductivity function of soils from moisture retention data using the restriction m=1-1/n is

$$K(S_e) = K_s S_e^{\ell}\left[1-(1-S_e^{1/m})^m\right]^2 \tag{5-2}$$

where

$$S_e = \left(\frac{\theta-\theta_r}{\theta_s-\theta_r}\right) \tag{5-3}$$

S_e is referred to as the effective saturation; K_s is the saturated hydraulic conductivity; ℓ is a dimensionless pore-connectivity parameter estimated by Mualem (1976) to be approximately 0.5 for many soils; and $\theta_r \le \theta \le \theta_s$; $0 \le S_e \le 1$; and $0 < m < 1$.

Equation 5-3 is a form of the popular Brooks and Corey (1964) empirical expression

$$\theta = (\theta_r + (\theta_s-\theta_r)(ah)^{-\lambda} \text{ (for } ah > 1) \text{ and} \tag{5-4}$$

$$\theta = \theta_s \text{ (for } ah \le 1) \tag{5-5}$$

which is used to describe the water retention curve for unsaturated soils, where *a* is an empirical parameter whose inverse is referred to as the air entry value; and λ is a pore-size distribution parameter affecting the slope of the retention curve. Equations 5-4 and 5-5 generate two straight lines on a logarithmic plot that intersect at the air entry value *a*. Because of its simple form, the Brooks and Corey (1964) equation has been used in numerous unsaturated flow studies but the expression ignores the smooth transition around the air entry pressure that is characteristic of observed water retention functions.

The van Genuchten (1980) model and Equation 5-1 provides a smooth continuous transition between the saturated and residual water contents improving the description of the observed water retention function. Because of their attractive properties, Equations 5-1 and 5-2 are used in this study to determine the soil water retention function and the hydraulic conductivity function for the natural analogue and engineered test cover soil profiles.

5.4 The RETC Code—Application

The RETC code provides several options for describing or predicting the hydraulic properties of unsaturated soils. These properties involve the soil water retention curve, (θ,Ψ), and the hydraulic conductivity function, K(Ψ) or K(θ). The retention function is given by Equation 5-1 which contains five independent parameters, the residual water content, θ_r, the saturated water content, θ_s, and the curve shape parameters, α, *m*, and *n*. The predictive equation for the hydraulic conductivity function (Equation 5-2) adds two additional parameters, the pore connectivity parameter, ℓ, and the saturated hydraulic conductivity, K_s. The RETC code may be

used to fit any given parameter, several parameters, or all seven parameters simultaneously to observed data. The RETC code maps the water retention curve by fitting θ_r, θ_s, α, *m*, and *n* to laboratory-observed soil water retention data. The fitted retention curve parameters are subsequently used along with ℓ and K_s to predict the hydraulic conductivity function, (K,θ), using Equation 5-2. The RETC code allows one to keep parameters *m* and *n* independent in Equation 5-1, or dependent through the restriction of m=1-1/n for the Mualem-based formulation. Mualem (1976) recommends that the pore-connectivity parameter, ℓ, remain fixed at an average value of 0.5 for most soils.

The RETC code uses a nonlinear least-squares optimization approach to estimate the unknown model parameters from laboratory-observed laboratory data. The aim of the curve fitting process is to find an equation that maximizes the sum of squares associated with the model, while minimizing the residual sum of squares. In this study, the RETC code is used to predict K(θ) from laboratory-observed θ(Ψ) data using the parametric model of van Genuchten (1980) with m=1–1/n and the pore-size distribution model of Mualem (1976) using ℓ = 0.5. No other options offered by RETC were used in the analysis of laboratory data.

Unknown retention curve parameters θ_r, θ_s, α, *m*, and *n* were determined using an iterative approach. The inverse problem (i.e., optimization of parameters in the hydraulic model) was initiated by using initial estimates for sandy loam obtained from code-imbedded average parameter values of θ_r, θ_s, α, *m*, and *n* for soil textural groups according to USDA classification (Carsel and Parrish 1988, Rawls et al. 1982). These average values serve as a guide for making initial parameter estimates. The initial fitting effort allows RETC to fit all parameters to the laboratory-observed data. The sum of squares and r^2 of observed versus fitted values were checked to determine accuracy of the fitted curves. Code-imbedded correlation matrices were also evaluated to identify non-unique relationships between parameters. Once the van Genuchten parameters θ_r, θ_s, α, *m,* and *n* were accurately determined based on the sum of squares and r^2, the entire process was repeated with different original input parameters to insure that the values obtained were global and did not represent local minimum solutions. The final van Genuchten parameters were subsequently used to predict K(θ) using ℓ and K_s to predict the hydraulic conductivity function, (K,θ) for the full range of *K* versus θ (initial saturated conditions to residual moisture content).

5.5 The RETC Code—Natural Analogue Results

Figures 5-1 through 5-18 show calculated soil moisture characteristic and unsaturated hydraulic conductivity curves for natural analogue soil samples IP-00 through IP-20. IP-07, IP-09, and IP-13 were omitted *a priori* because RETC could not fit a reasonable α. Fitted van Genuchten parameters are presented in Table 5-3. The average van Genuchten values are used to calculate the average soil moisture characteristic curve shown in red on Figure 5-19.

The soil moisture characteristic curves exhibit the classic, sigmoidal, or S-shape curve relating tension to volumetric moisture content in soil core samples as θ moves from laboratory saturation to residual values along the pressure induced drainage path. At each end of each soil moisture characteristic curve $\partial\theta/\partial\Psi$ is zero.

Figure 5-19 shows the combined soil moisture characteristic and unsaturated hydraulic conductivity curves for natural analogue soil samples IP-00 through IP-20. The curves fall within a well-defined range of Ψ versus θ and *K* versus θ values that represent the hydraulic conductivity function of the natural analogue.

A comparison of the (*K,*θ) obtained from the IP test (Section 4.1.7) and the (*K,*θ) obtained from RETC is shown in Figure 5-20. The range of (*K,*θ) from the IP test is limited to values below 1 bar but encompasses a major part of the soil profile-wetness range. Only five of the (*K,*θ*)* curves from RETC (IP-00, IP-02, IP-04, IP-15, and IP-20) are shown for easy comparison. The (*K,*θ) match remarkably well with approximately 50% overlap in the 1 bar range. This satisfactory comparison indicates that the van Genuchten (1980) and Mualem (1976) models performed very well in characterizing the hydraulic conductivity function for these soils. These laboratory data provide the complete (θ,Ψ) and (*K,*θ) relationship required by the UNSAT-H code as input parameters for the natural analogue simulation. These input parameters are discussed in Chapter 6.

5.6 The RETC Code—Engineered Cover Results

Figures 5-21 through 5-33 show the calculated soil moisture characteristic and unsaturated hydraulic conductivity curves for engineered cover soil samples EC-00 through EC-12. Fitted van Genuchten parameters are presented in Table 5-4. The average van Genuchten values are used to calculate the average soil moisture characteristic curve shown in red on Figure 5-34.

Again, the soil moisture characteristic curves exhibit the classic, sigmoidal, or S-shape curve relating tension to volumetric moisture content in soil core samples as θ moves from laboratory saturation to residual values along the pressure induced drainage path. At each end of each soil moisture characteristic curve, $\partial\theta/\partial\Psi$ is zero.

Figure 5-34 shows the combined soil moisture characteristic and unsaturated hydraulic conductivity curves for soil samples EC-00 through EC-12. The curves fall within a much narrower range of Ψ versus θ and *K* versus θ values than those of the natural analogue in Figure 5-19. The narrower range of values reflects less anisotropy and heterogeneity within the constructed soil profile than in the natural analogue. These laboratory data provide the full range of (θ,Ψ) and (*K,*θ) required by the UNSAT-H code as input parameters for the engineered cover simulation. These input parameters are described in Chapter 6.

6. Performance Modeling

Numerical codes incorporating relevant constitutive principles have become increasingly popular and necessary in the research and management of hydrologic and transport processes in landfill covers and in the shallow vadose zone. Percolation through the natural analogue and the engineered cover is simulated using the Richards' equation-based code UNSAT-H (Fayer 2000). The UNSAT-H code was developed from the UNSAT model of Gupta et al. (1978). The UNSAT model was used to predict the water dynamics of agricultural land. The UNSAT model was modified in 1979 for waste management purposes at PNNL, Hanford, Washington (Fayer et al. 1986). The result was the UNSAT-H code, with the added "H" signifying Hanford (Fayer and Jones 1990). The UNSAT-H code was developed specifically for assessing the water dynamics of arid sites and, in particular, estimating recharge rates for waste disposal facilities at Hanford. The UNSAT-H code accomplishes this by simulating soil water infiltration, redistribution, evaporation, plant transpiration, and deep percolation. The two major objectives of the UNSAT-H code are to estimate deep percolation and to assist the design engineer and the regulator in evaluating and optimizing cover design (Fayer 2000).

6.1 Code Validation

In 1998, the EPA initiated the Alternative Cover Assessment Program (ACAP) to address the growing interest in the use of alternative landfill covers in lieu of prescribed landfill cap designs. The Desert Research Institute (DRI), with support from the PNNL, was contracted by the EPA to assess sites where alternative covers had been or are currently being tested. In addition, DRI and PNNL provided an evaluation of computer codes to assess the current capabilities of hydrologic models to quantify both water balance and performance of landfill cover systems (Albright et al. 2002).

ACAP evaluated ten computer codes commonly used for cover design assessment and performance according to their capabilities and limitations. Four codes were selected for detailed evaluation: the water balance codes HELP (Hydrologic Evaluation of Landfill Performance) (Schroeder et al. 1994) and EPIC (The Erosion Productivity Impact Calculator) (Williams et al. 1984) and the Richards' equation-based codes HYDRUS-2D (Simunek et al. 1996) and UNSAT-H (Fayer 2000). These codes were subjected to extensive tests for verification, validation, and sensitivity to input parameters.

HELP and EPIC demonstrated several process oversimplifications in testing performance of alternative cover designs. HYDRUS-2D and UNSAT-H provided the most consistent and physically realistic results; however, ACAP suggested that future use of HYDUS-2D and UNSAT-H by the engineering and regulatory communities would require more user-friendly modifications.

The ACAP study indicates that Richards' equation-based codes are better suited to capture the behavior of alternative covers under both arid and humid conditions than water balance codes and recommended that Richards' equation-based codes be adapted for alternative landfill cover designs (Albright et al. 2002). ACAP determined that UNSAT-H provided the most accurate predictions of deep percolation (Albright et al. 2002).

6.2 UNSAT-H Code—Overview

The UNSAT-H code is designed to simulate water and heat flow processes in one dimension, typically vertical. UNSAT-H can simulate the isothermal flow of liquid water and water vapor, the thermal flow of water vapor, the flow of heat, the surface energy balance, soil-water extraction by plants, and deep drainage. Liquid water flow is simulated using the Richards equation, water vapor diffusion using Fick's law, and sensible heat flow using the Fourier equation. The description of the UNSAT-H code that follows is paraphrased from the UNSAT-H Version 3.0 User Manual (Fayer 2000).

6.2.1 Code Processes and Input Requirements

The UNSAT-H code simulates evaporation in two ways. In the isothermal mode, UNSAT-H uses the potential evapotranspiration (PET) concept for evaporation. The user supplies either daily values of PET or daily weather data with which the code calculates daily PET values using the Penman equation. In the thermal mode, UNSAT-H calculates evaporation as a function of the vapor density difference between the soil and a reference height and the resistance to vapor transport. The resistance to vapor transport is a function of several factors including air temperature, wind speed, solar radiation, and precipitation.

The UNSAT-H code simulates the effects of plant transpiration using the PET concept. Plant information is supplied to the code to partition the PET into potential evaporation (E_p) and potential transpiration (T_p). The T_p is applied to the root zone using a root distribution function to apportion it among the computational nodes that have roots. The withdrawal of water from a particular node is dependent on the suction head at the node. The user provides suction head values that define how the T_p rate applied to a particular node is reduced. Below a minimum assigned value, often referred to as the wilting point, transpiration is unable to remove any water. When all nodes with roots reach this level of suction head, transpiration is reduced to zero.

Code input requirements include the number of computational nodes to completely discretize the conceptual soil profile (up to 250 nodes are available) and the number of materials, e.g., soil types, that make up the profile. Initial suction heads must be assigned to each node in the soil profile. Plant parameters include the seasonal variation in LAI, root depth, root density variation with depth in the soil profile, and the suction head limits or wilting point that governs the withdrawal efficiency of plants. Surface boundary conditions include options for daily PET values or daily weather conditions (temperature, wind speed, solar radiation, and precipitation). Lower boundary conditions include the options of unit gradient, constant suction head, daily water flux, or impermeable boundary.

6.2.2 Code Implementation

In this study, the UNSAT-H code is used to simulate the isothermal flow of liquid water and water vapor, soil-water extraction by plants, and deep drainage, e.g., percolation. Use of the code in the isothermal mode means that water vapor moves and redistributes within the soil in response to matric potential gradients only. Temperature-induced thermal water vapor flow is not considered. Use of the code in the thermal mode would not allow the user to evaluate the performance of a vegetative soil cover because there is no provision in the code to simulate both

water and heat flow in a plant canopy. Analyses by Campbell (1985) imply that isothermal vapor flow can affect the near-surface water-content profile, and Fayer and Gee (1997) determined that the inclusion of heat flow has only a minor effect on surface evaporation and vapor flow within the soil. Fayer and Gee (1997) obtained these results during a 6-yr record of water storage, suction, and drainage data on a 5 ft non-vegetated soil profile consisting of silt loam over sand and gravel at Hanford, Washington.

6.3 UNSAT-H Code—Mathematical Model

The UNSAT-H code uses a finite difference implementation of a modified form of Richards' equation to describe unsaturated water flow in soil layers and water removal through evaporation and transpiration. The development of the modified Richards' equation begins with Darcy's law. In its original form, Darcy's law represented an empirical relationship between the rate of flow in saturated sand and the hydraulic head gradient. The one-dimensional differential form of Darcy's law is

$$q_L = -K_s \frac{\partial H}{\partial z} \tag{6-1}$$

where q_L is flux density of water, cm/hr; K_s is the saturated hydraulic conductivity, cm/hr; and z is depth below the surface, cm. Darcy's law can be extended to unsaturated flow by replacing the saturated conductivity term with liquid conductivity, K_L, as a function of suction head yielding

$$q_L = -K_L(\Psi)\frac{\partial H}{\partial z} \tag{6-2}$$

Equation 6-2 must be combined with the continuity equation to describe transient flow. For one-dimensional flow, the continuity equation is

$$\frac{\partial \theta}{\partial t} = -\frac{\partial q_L}{\partial z} \tag{6-3}$$

where θ is the volumetric water content, cm^3/cm^3, and t is time, hr. Combining Equations 6-2 and 6-3 yields

$$\frac{\partial \theta}{\partial t} = \frac{\partial}{\partial z}\left[K_L(\Psi)\frac{\partial H}{\partial z} \right] \tag{6-4}$$

In Equation 6-4, the hydraulic head, H, is equal to the matric head, Ψ, plus the gravitational head, Z, e.g., $H = (\Psi + Z)$. In UNSAT-H, there are two sign conventions that relate to heads: z is replaced by $-z$ and Ψ is replaced by suction head, h, which is the negative of matric head. Therefore, $H = (\Psi + Z)$ is replaced by $H = -(h + z)$.

Combining Equation 6-4 with $H = -(h + z)$ and adding a sink term, S, for water uptake by plants gives

$$\frac{\partial \theta}{\partial t} = -\frac{\partial}{\partial z}\left[K_L(h)\left(\frac{\partial h}{\partial z}\right) + 1 \right] - S(z,t) \tag{6-5}$$

where $S(z,t)$ indicates that the sink term is a function of depth and time.

Equation 6-5 does not take vapor flow into consideration. Diffusion of water vapor from the soil to the atmosphere can be an important mode of water loss. The fundamental equation used to calculate the diffusion of water vapor in soils is Fick's law. When applying Fick's law to soils, adjustments must be made for 1) tortuosity and the reduced cross-sectional area available for flow; 2) gradients for suction head and temperature; and 3) the effect of soil temperature on vapor diffusion (Fayer 2000).

Equation 6-5 can now be rewritten to include the contribution from vapor flow

$$\frac{\partial \theta}{\partial t} = -\frac{\partial}{\partial z}\left[K_T(h)\frac{\partial h}{\partial z} + K_L(h) + q_{vT} \right] - S(z,t) \tag{6-6}$$

where θ is volumetric moisture content; t is time; h is suction head (or tension); z is depth in the soil profile; K_T is equal to $K_L + K_{vh}$; K_L is the liquid water conductivity; K_{vh} is the isothermal vapor conductivity; q_{vT} is the thermal vapor flux density; and $S(z,t)$ is the sink term representing volumetric water uptake by plants as a function of depth and time (Feddes et al. 1978).

Equation 6-6 is the modified Richards' equation that serves as the primary differential equation solved by the UNSAT-H code. Equation 6-6 describes changes in water storage, isothermal redistribution of liquid water, thermal redistribution of water vapor, and water uptake by plants (Fayer 2000).

Hysteresis of the soil moisture characteristic curve and preferential flow is not considered in this study. Although preferential flow has important implications with regard to the movement of water through macropores, the process is multidimensional and occurs via distinct pathways that constitute only a fraction of the soil's total volume (Hillel 1998). The UNSAT-H code lacks a comprehensive, multidimensional model to describe preferential flow.

The UNSAT-H code must have mathematical descriptions of the hydraulic and vapor properties of soil and air. To solve the flow equation for liquid water, the UNSAT-H code must be provided with the relationship for both water content and hydraulic conductivity as a function of suction head, h. The water content relationship is the soil moisture characteristic curve (or water retention curve) and the hydraulic conductivity relationship is the unsaturated hydraulic conductivity function.

The UNSAT-H code contains eight options for describing the soil hydraulic properties of soil. In this study, the soil moisture characteristic curve is described by the van Genuchten (1980) function (Equation 5-1)

$$\theta = \theta_r + \frac{(\theta_s - \theta_r)}{\left[1 + (\alpha h)^n\right]^m}$$

When the van Genuchten (1980) function is combined with the Mualem (1976) conductivity function, the equation solved by the UNSAT-H code is

$$K_L = K_s \frac{\left\{1 - (\alpha h)^{nm}\left[1 + (\alpha h)^n\right]^{-m}\right\}^2}{\left[1 - (\alpha h)^n\right]^{\ell m}} \qquad (6\text{-}7)$$

where m=1-1/n.

6.4 Code Input Parameters

The UNSAT-H code must be provided with relationships for water content and hydraulic conductivity as a function of suction head, vegetative data, climate data, and initial and boundary conditions. The water content relationship is determined from the soil moisture characteristic curves of van Genuchten (1980), and the hydraulic conductivity relationship is determined from the hydraulic conductivity function of Mualem (1976).

Vegetative parameters include the root depth of the common perennial plant species, growing season and the seasonal variation in LAI, root depth, root density variation with depth in the soil profile, and the suction head limits or wilting point that governs the withdrawal efficiency of plants. Vegetative parameters are described in Section 6.5.8.

Climate data includes daily precipitation. Precipitation rates are entered directly into the code as hourly liquid water flow. The historical rainfall record is described in Section 6.5.7.

Initial conditions are obtained from the *in situ* volumetric water content measured in the natural analogue soil profile as a function of depth and the RETC-derived average soil moisture characteristic curves. Initial conditions are described in Sections 6.5.1 and 6.5.2.

The boundary conditions consist of options for the upper and lower boundaries of the soil profile. The upper surface conditions are based on the availability of daily weather data or daily PET data. The lower surface conditions are based on four options for flow across the boundary: unit gradient; constant suction head; daily flux; and impermeable boundary, e.g., zero flux. Boundary conditions are described in Sections 6.5.1 and 6.5.2.

6.5 Problem Formulation and UNSAT-H Code Input

Application of the UNSAT-H code to the problem in this study requires the problem to be formulated in terms understood by the numerical model. Problem formulation entails specifying program control options, discretizing the spatial and temporal domain of interest, assigning soil properties, and defining the boundary conditions (Fayer 2000).

Numerous trial runs were conducted to optimize the number of nodes needed to adequately discretize the problem while balancing solution accuracy with computer time. A satisfactory balance occurs when one uses a minimum of 30 nodes—the solution remains essentially the same; therefore 30 nodes are used to discretize a conceptual soil profile.

The problem in this study is formulated in one dimension, vertically, and as such, is discretized by placing computational nodes at predetermined vertical spacing in a conceptual soil profile to emulate the performance of covers 1, 2, 3, 4, and 5 ft in thickness. Figure 6-1 shows a cross-section of the conceptual soil profile and its code representation. A total of 30 nodes are used to discretize a conceptual soil profile 6 ft in thickness. A thickness of 6 ft is used so that the overlying nodes of interest are not adversely impacted by the lowermost boundary conditions. Node spacing is very small near the surface and becomes progressively larger as one moves downward through the soil profile. The smaller node spacing near the surface is necessary for an accurate numerical solution because very large and rapid changes in suction head occur as the surface dries and wets in response to evaporation and precipitation (Fayer 2000). Further down in the soil profile, suction head changes are less dramatic and node spacing can be increased. Soil and vegetative properties, and initial suction head values are assigned to each node. By code convention, nodal depths in the soil profile are assigned metric values. Node numbers 10, 14, 18, 22, and 26 are assigned depths of 30, 61, 91, 122, and 152 cm, respectively, to represent the lower boundary of covers 1, 2, 3, 4, and 5 ft in thickness. The lowermost boundary of the soil profile, node 30, is assigned a depth of 6 ft (183 cm).

The code contains some features that translate into conservative estimates of downward liquid water flow. These features are introduced into the simulation through inherent code limitations or by means of the various code input parameters. In this study, the term "conservative" is used to designate a code feature that tends to overestimate percolation. An inherent code limitation that translates into a significant conservative estimate of liquid water flow is the code's one-dimensionality. Use of the UNSAT-H code is considered valid where water flow is strictly vertical (Fayer 2000). There is no provision for run-off, surface detention of water, or internal lateral drainage. All precipitation and liquid water flow is directed downward through the soil profile.

The conceptual soil profile is simulated as a lithologic monolayer. A soil profile with uniform soil and hydrologic properties translates into a significant conservative estimate of liquid water flow. If multiple layers are simulated, the water potential in the underlying layer must equal the water potential in the overlying layer before flow into the lower layer occurs. Multiple layering in performance modeling as well as multiple layers in nature attenuate the downward flow of liquid water (e.g., multiple capillary barriers).

In this study, the conceptual soil profile that represents the natural analogue and the engineered cover is simulated with and without vegetation. Modeling a soil profile without vegetation yields a conservative estimate of liquid water flow. A significant amount of liquid water is removed from the soil profile by transpiration. Even in the absence of vegetation, evaporation is limited by the ability of near-surface soils to conduct liquid water to the surface from soils deeper in the profile. Once near-surface soils dry below a certain threshold, the rate of transfer of water from deep within the soil profile to the soil surface limits the rate of evaporation. Additional features that translate into conservative estimates of liquid water flow will be highlighted in the following sections as code input is discussed. UNSAT-H input parameters for the natural analogue and the engineered cover are summarized in Table 6-1. All parameters are site-specific and have been carefully measured to obtain the most conservative estimate of percolation possible.

6.5.1 Initial and Boundary Conditions—Natural Analogue

Initial suction head assigned to nodes 1 through 30 is obtained from the *in situ* volumetric water content measured in the natural analogue soil profile as a function of depth (prior to flooding) and the RETC-derived average soil moisture characteristic curve shown in Figure 5-19. The average i*n situ* volumetric water content is obtained from Figures 4-2 and 4-3. The average moisture content prior to flooding (Day -2.0) is 11.9%. From the average soil moisture characteristic curve shown in red on Figure 5-19 and its corresponding RETC code output file, the suction head corresponding to 11.9% moisture content is approximately 17.2 bar (17,200 cm).

The water flow for the upper boundary (i.e., through the surface of the soil profile), is specified as an evaporation flux boundary and an infiltration boundary equivalent to hourly precipitation over a 24-hr period. The water flow for the lower boundary or the base of the soil profile at 6 ft is specified as a unit downward gradient —flow is always directed downward. A lower boundary specified as a unit gradient is conservative because in nature, movement of water is either upward or downward as the soil profile responds to precipitation, evaporation, and transpiration. Since hourly precipitation is designated and the model regards daily precipitation as occurring over a 24-hr period, all flow is directed downward through the soil profile. There is little or no predicted runoff.

6.5.2 Initial and Boundary Conditions—Engineered Cover

Initial suction head assigned to nodes 1 through 30 is obtained from the *in situ* volumetric water content measured in the engineered cover soil profile as a function of depth (prior to flooding) and the RETC-derived average soil moisture characteristic curve shown in Figure 5-34. The *in situ* volumetric water content is obtained from Table 4-4. The average moisture content prior to flooding is 9.9%. From the average soil moisture characteristic curve shown in red in Figure 5-34 and the corresponding RETC code output file, the suction head corresponding to 9.9% moisture content is approximately 5.62 bar (5620 cm).

As in Section 6.5.1, the water flow for the upper boundary is specified as an evaporation flux boundary and an infiltration boundary equivalent to hourly precipitation over a 24-hr period.

The water flow for the lower boundary or the base of the soil profile at 6 ft is specified as a unit downward gradient —flow is always directed downward.

6.5.3 Soil Hydraulic Properties—Natural Analogue

Input values for θ_s, θ_r, α, and *n* are obtained from the RETC-derived average soil moisture characteristic curve shown in red in Figure 5-19. The average values for θ_s, θ_r, α, and *n*, summarized in Tables 5-3 and 6-1, are used to initialize the simulation.

Input for the saturated hydraulic conductivity, K_s, is obtained from the IP test site while under steady state conditions during flooding. The *in situ* K_s obtained from the IP test site is 4.05×10^{-4} cm/s. The laboratory K_s obtained from soil samples is 4.01×10^{-5} cm/s and the K_s obtained from the RETC code is 7.27×10^{-4} cm/s (see Tables 5-1 and 5-3). The log average (geometric mean) is used because hydraulic conductivity is a log-normally distributed property. These saturated conductivity values are remarkably similar when one considers the inherent anisotropy and heterogeneity that exist in any given soil profile and the different methods of measurement. Hydraulic conductivity is a highly variable soil property, often varying by two or three orders of magnitude. The *in situ*, laboratory, and RETC values are all within one order of magnitude of one another (Table 5-3). Since field methods of determining hydraulic conductivity are generally regarded as more reliable than laboratory methods, 4.05×10^{-4} cm/s is used as the code input parameter for K_s. The *in situ* conductivity is a conservative estimate of liquid water flow because it is greater than the RETC-derived conductivity and laboratory-measured conductivity.

6.5.4 Soil Hydraulic Properties—Engineered Cover

Input values for θ_s, θ_r, α, and *n* are obtained from the RETC-derived average soil moisture characteristic curve shown in red in Figure 5-34. The average values for θ_s, θ_r, α, and *n*, summarized in Tables 5-4 and 6-1, are used to initialize the simulation.

Input for the saturated hydraulic conductivity, K_s, is obtained from the engineered cover prior to flooding. The *in situ* K_s obtained from the IP test site is 3.46×10^{-4} cm/s. The laboratory K_s obtained from soil samples is 1.1×10^{-4} cm/s and the K_s obtained from the RETC code is 2.89×10^{-4} cm/s (see Tables 5-2 and 5-4). Again, the log average (geometric mean) is used because hydraulic conductivity is a log normally distributed property. The *in situ*, laboratory, and RETC values are all very similar. Since field methods of determining hydraulic conductivity are generally regarded as more reliable than laboratory methods, 3.46×10^{-4} cm/s is used as the code input parameter for K_s.

6.5.5 Evaporation

In the isothermal mode, the UNSAT-H code simulates evaporation and transpiration using the PET concept of Penman (1963). Either daily values of PET or daily meteorological data are supplied from which the code calculates daily PET using the modified Penman equation reported by Doorenbos and Pruitt (1992). The daily weather data consist of the following factors:

- Daily maximum and minimum air temperatures;
- Daily average dewpoint temperature;
- Total daily solar radiation;
- Average daily wind speed; and
- Daily average cloud cover.

These daily weather data are not available for the historical meteorological record selected for this study so daily values of PET are supplied. Daily PET values can be calculated external to the UNSAT-H code using programs such as FAOPET (Doorenbos and Pruitt 1977) and HELP (Schroeder et al. 1994).

Daily PET values were calculated using the HELP code Version 3 (Schroeder et al. 1994) with its embedded functions and database for Albuquerque, New Mexico. The HELP code is widely used by the regulatory community to assess water movement across, into, through, and out of landfills. The HELP code calculates daily PET using the approach recommended by Ritchie (1972) and incorporating USDA Agricultural Research Service temperature and solar radiation equations of Richardson and Wright (1984). Daily PET is distributed by the UNSAT-H code as a sine function that approximates the daily variation of solar radiation, with the maximum value occurring at 1200 hr. This option allows 88% of the daily PET to be applied sinusoidally between 0600 and 1800 hr. During the remaining time, hourly PET is 1% of the daily value (Fayer 2000).

To validate the PET data calculated by the HELP code, the daily PET values are shown along with pan evaporation data from two New Mexico National Weather Service stations in Figure 6-2. The average annual PET calculated by the HELP code for the historical precipitation data is 75.4 in., approximately nine times the average annual precipitation for the Albuquerque area. A comparison of average annual PET calculated by the HELP code for the historical precipitation data (1932 through 1996) with average monthly pan evaporation for Bosque Farms and Los Lunas, New Mexico demonstrates that they are essentially identical. Figure 6-3 shows monthly pan evaporation and Penman PET for Los Lunas, New Mexico (Sammis et al. 1977). Annual pan evaporation is 72.4 in. and Penman PET is 72.8 in. demonstrating that the two are, again, essentially identical.

6.5.6 Transpiration

Transpiration is also based on the concept of PET. Vegetative input parameters are supplied to the code to partition PET into E_p and T_p. T_p is applied to the root zone using the root depth and RLD data to apportion T_p among the computational nodes that have been assigned roots. The withdrawal of water from a particular node is dependent on the suction head at that node. The user assigns suction head values that define how T_p applied to a particular node is reduced. Below a minimum value, referred to as the wilting point, transpiration is unable to remove any water. When all the nodes in the soil profile reach this level of suction head, transpiration is reduced to zero (Fayer 2000).

The removal of soil water by transpiring plants is modeled as a sink term, $S(z,t)$, in Equation 6-6. The calculation is accomplished in three steps. First, PET is partitioned into T_p and E_p, subject to

the constraint that PET = $E_p + T_p$. Second, T_p is distributed over the root zone in proportion to the relative root density at each depth, establishing a potential sink term for each depth. Third, the sink term for each node in modified based on water content to obtain the actual sink term for that node (Fayer 2000). Calculation of the sink term is according to the macroscopic scale or root system model of water uptake by roots proposed by Feddes et al. (1974), Feddes et al. (1978) and Hillel (1998).

T_p is calculated from the LAI using the equation

$$T_p = \text{PET}[a + b(\text{LAI})^c] \tag{6-8}$$

where $a = 0.0$, $b = 0.52$, and $c = 0.5$ (Fayer 2000). Equation 6-8 was developed by Ritchie and Burnett (1971) for cotton and grain sorghum.

Once T_p is determined, the transpiration demand is applied to the root zone using the sink term $S(z,t)$ in Equation 6-6. The sink term at each node in the model domain is assigned a fraction of the transpiration demand, with the fraction calculated as the RLD of the node divided by the total root length within the soil profile.

After T_p is distributed throughout the root zone, the final step is to calculate the actual transpiration or sink term, S, at each depth. This is done by multiplying the potential sink term reduction factor, α_f, a factor that is less than or equal to 1.0 and is a function of the soil water content of the respective node. The factor α_f relates the transpiration rate to the water status and suction head in the root zone. The relationship between α_f and suction head is shown in Figure 6-4. Water uptake by roots is considered to be a function of the suction head, Ψ. When the suction head at a node is greater than Ψ_n, α_f equals zero due to anaerobic conditions. When the suction head is between Ψ_n and Ψ_d, α_f is 1.0 and the rate of withdrawal is equal to S_{pot}. If the suction head is between Ψ_d and Ψ_w, the rate of withdrawal is reduced linearly from 1.0 to 0.0 as the suction head increases. When the suction head is greater than Ψ_w, α_f equals zero to indicate that the plant has stopped withdrawing water from that node (Feddes et al. 1974, Feddes et al. 1978, Hillel 1998). The head values selected for Ψ_n, Ψ_d, and Ψ_w, are 30, 3000, and 30,000 cm, respectively. These suction head values are quite conservative for native plants in arid and semiarid environments.

Although the suction head at which agricultural plants stop withdrawing water from the soil (commonly referred to as the wilting point) is often considered to be 15 bar (15,000 cm) (Penman 1963, van Genuchten 1980), suction heads corresponding to the wilting point of native plants in arid and semiarid environments are reported to be 25 to 30 bar (25,000 to 30,000 cm) (HDR Engineering 2000), 60 bar (60,000 cm) (ITRC 2003), and as high as hundreds of bar (Hillel 1998).

The difficulty encountered in attempting to describe soil water uptake by plants in physical terms is the inherently complicated nature of the space-time relationship involved in this process. The rate of water uptake from a given volume of soil depends on root depth and density, hydraulic conductivity, and the net difference between average soil suction head and root suction. Overall

root growth consists of several sequential and concurrent root growth processes, including proliferation, extension, senescence, and death. Roots proliferate and extend in different directions and density, so it is extremely difficult to measure the gradients and fluxes of water in their immediate vicinity. Furthermore, root distribution is not uniform or constant within the soil profile. Neither does water uptake correspond to the root density and distribution, since at any given time some roots may be more absorptive than others and some regions in the soil profile may yield moisture more readily than other regions. One of the main limitations of water uptake models is that they consider vegetative growth only and make no provision for the development of reproductive structures such as flowers, fruits, and seeds at the appropriate stage of the plant's physiological cycle (Hillel 1998).

6.5.7 Climatic Data

Climatic data should represent the site-specific conditions to the maximum extent possible, and the longer the historical record, the better (ITRC 2003). The historical rainfall record from Albuquerque International Sunport, dating from 1919 to 1996, is used to input precipitation and simulate percolation through the natural analogue and the engineered cover. Two discrete sets of precipitation data were compiled from the historical record. The first data set, the "historical precipitation data," included 65 years of daily rainfall recorded from 1932 to 1996. The second data set, the "maximum precipitation data," included the 8 heaviest years' rainfall recorded between 1919 and 1996, repeated 8 times for a total of 64 years. The heaviest rainfall years were 1919, 1929, 1940, 1941, 1982, 1986, 1988, and 1992. These maximum precipitation data represent a significant climate change, and would have the greatest influence on the long-term performance of any cover system. Precipitation during these years ranged 12 in. to over 15 in. The current average annual precipitation for the Albuquerque area is 8.65 in./yr.

6.5.8 Vegetative Parameters

Plants play a vital role in the success of a vegetative soil cover design. Vegetative soil cover design combines layers of natural soil, native plant species, and climatic conditions to form a sustainable, functioning ecosystem that maintains the natural water balance (ITRC 2003). Plants function as an elaborate pumping and conveyance system extending into various soil depths to extract water in a manner that maximizes the plant's chances for survival and self-perpetuation (Hillel 1998).

Plant transpiration is the primary mechanism in removing water from a vegetative soil cover. Without plants, soil covers would only depend on evaporation to remove water from the cover soil profile (ITRC 2003). Vegetative input for the UNSAT-H code includes root depth, RLD, LAI, growing season, and PBA (Fayer 2000). Root depth, RLD, LAI and growing season, and PBA were determined from the natural analogue in Sections 3.5.1, 3.5.2, 3.5.3, and 3.5.4, respectively.

The value selected for root depth is 80 cm because approximately 98% of the dominant native plant species root biomass within the study area occurs within 80 cm of the surface. The coefficients for RLD determined from the exponential fit to the combined, normalized root biomass of RLD-1 and RLD-2 are $a = 0.5090$, $b = -0.0630$, and $c = 0.0262$ (Equation 3-1). Two discrete sets of LAI data have been generated for the historical precipitation data and the

maximum precipitation data (Table 3-8). The maximum LAI values for the historical precipitation data and the maximum precipitation data are 0.8 and 1.2, respectively. The NMED recommends a maximum LAI of 0.8 for Albuquerque corresponding with "poor" vegetation (NMED 1998). The value selected for PBA is 81%. This PBA represents the foliar coverage of the perennial plant species only in the study area. Annual plant species are excluded. All of the vegetative input parameters are summarized in Table 6-1.

7. Modeling Results and Design Optimization

7.1 Modeling Results

The UNSAT-H code simulated percolation through soil covers of 1, 2, 3, 4, and 5 ft in thickness. Percolation varied as a function of thickness, precipitation, and vegetation. The modeling results for the natural analogue and the engineered cover are discussed in the following sections and compared to the EPA-prescribed, technical equivalency criteria of 31.5 mm/yr and 1 x 10^{-7} cm/s for net annual percolation and average flux, respectively.

Soil moisture profiles are provided to show the vertical distribution of moisture within the soil profile. Each line represents volumetric moisture content as a function of depth and time. Differences in line position reflect changes in moisture content within the soil profile depending on climate conditions and the rainfall record.

Percolation profiles are provided to show net percolation through the soil profiles of the natural analogue and the engineered cover. Each line represents cumulative percolation as a function of depth and time. A rising line indicates net downward percolation and a falling line indicates net upward percolation.

7.1.1 Modeling Results Using Historical Precipitation Data—Natural Analogue

The 65-yr historical precipitation data delivered 562.3 in. of precipitation to the surface of the soil profile. The average annual precipitation during these years was 8.65 in./yr. Volumetric moisture content and cumulative percolation as a function of depth and time are shown in Figures 7-1 and 7-2 and Figures 7-3 and 7-4, respectively. Cumulative percolation, net annual percolation, and average flux as a function of depth are presented in Tables 7-1 and 7-2.

7.1.1.1 Moisture Content

Figure 7-1 shows the volumetric moisture content at depths of 1 through 5 ft in the soil profile without vegetation. It takes approximately 12 years for the soil profile to reach steady state from an initial moisture content of 12%. The soil profile then experiences approximately 16 years of drying followed by numerous wetting and drying cycles. During drying cycles, the moisture content in the soil profile is "inverted"—the upper few feet tracks below the lower few feet in the graph due to more rapid drying. During wetting cycles, the upper few feet tracks above the lower few feet in the graph due to more rapid wetting.

Due to rapid wetting and drying, the moisture contents within the upper few feet of the soil profile fluctuate dramatically. These fluctuations decrease in amplitude with increasing depth, indicating that moisture is being stored primarily in the upper few feet of the soil profile from where it is rapidly removed by evaporation. Lower moisture content at depth is indicated by less fluctuation and a significant decrease in amplitude. Lower moisture contents at depth result in a unit gradient and low unsaturated hydraulic conductivity, yielding very low rates of percolation.

Figure 7-2 shows the volumetric moisture content at depths of 1 through 5 ft in the soil profile with vegetation. The moisture content in the upper few feet fluctuates dramatically with repeated wetting and drying cycles, again indicating that moisture is being stored and removed primarily within the upper few feet of the soil profile. The moisture content at 3 ft is unaffected by the wetting and drying cycles and exhibits a gradual drying over time, reaching steady state at approximately 11% volumetric moisture content. The moisture content and gradual drying at 4 and 5 ft lag behind the moisture content at 3 ft indicating no downward percolation and a much slower rate of drying compared to shallower depths.

7.1.1.2 Cumulative Percolation

Figure 7-3 shows the cumulative percolation at depths of 1 through 5 ft in the soil profile without vegetation. Percolation increases dramatically in the first 10 years then plateaus during the 16-yr drying period, as shown in Figure 7-1. Percolation then increases gradually over time, spiking during repeated wetting cycles. The cumulative percolation through the soil profile ranges from 4.6% of the total precipitation at 1 ft to 2.2% of the total precipitation at 5 ft during this 65-yr historical precipitation record. Cumulative percolation without vegetation is presented in Table 7-1.

Figure 7-4 shows the cumulative percolation at depths of 1 through 5 ft in the soil profile with vegetation. Percolation decreases significantly with depth, falling to 5 mm at 2 ft. At 3 ft, percolation is directed upward at a rate of 3.3 mm/yr due to transpiration and the soil profile gradually dries (Figure 7-2). Below 3 ft, transpiration continues to exert an upward influence on percolation and the soil profile gradually dries (Figure 7-2). Cumulative percolation with vegetation is presented in Table 7-2.

7.1.1.3 Net Annual Percolation

Net annual percolation decreases gradually with depth in the soil profile without vegetation (Table 7-1), ranging from 3.99 mm/yr at 1 ft to 1.9 mm/yr at 5 ft. These percolation rates are approximately one order of magnitude less than the EPA-prescribed percolation rate of 31.5 mm/yr.

Net annual percolation decreases significantly with depth in the soil profile with vegetation (Table 7-2), ranging from 3.68 mm/yr at 1 ft to 0.08 mm/yr at 2 ft. At 3 ft, net annual percolation is directed upward at a rate of 0.05 mm/yr due to transpiration. Overall, net annual percolation with depth in the soil profile with vegetation decreases dramatically as thickness increases from 1 to 3 ft. Although the code indicates net annual percolation is directed upwards for covers 3, 4, and 5 ft in thickness, net annual percolation is effectively zero.

7.1.1.4 Average Flux

Average flux decreases gradually with depth in the soil profile without vegetation (Table 7-1), ranging from 1.27×10^{-8} cm/s at 1 ft to 6.02×10^{-9} cm/s at 5 ft. This flux is approximately one to two orders of magnitude less than the EPA-prescribed flux of 1×10^{-7} cm/s.

Average flux decreases significantly with depth in the soil profile with vegetation (Table 7-2), ranging from 1.17 x 10^{-8} cm/s at 1 ft to 2.44 x 10^{-10} cm/s at 2 ft. This flux is approximately one to three orders of magnitude less than the EPA-prescribed flux of 1 x 10^{-7} cm/s. At 3 ft, average flux is directed upward at 1.61 x 10^{-10} cm/s due to transpiration. Overall, average flux with depth in the soil profile with vegetation decreases dramatically as thickness increases from 1 to 3 ft. For covers 3, 4, and 5 ft in thickness, average flux is effectively zero.

The best performance in average flux, whether with or without vegetation, is achieved by a soil profile 3 ft in thickness, with diminishing performance as thickness increases to 4 and 5 ft.

7.1.2 Modeling Results Using Maximum Precipitation Data—Natural Analogue

The 64-yr maximum precipitation data delivered 865.5 in. of precipitation to the surface of the soil profile. The average annual precipitation during these years was 13.5 in./yr. Volumetric moisture content and cumulative percolation as a function of depth and time are shown in Figures 7-5 and 7-6 and Figures 7-7 and 7-8, respectively. Cumulative percolation, net annual percolation, and average flux as a function of depth are presented in Tables 7-1 and 7-2.

7.1.2.1 Moisture Content

Figure 7-5 shows the volumetric moisture content at depths of 1 through 5 ft in the soil profile without vegetation. Similar to Figure 7-1, the soil profile takes approximately 10 years to reach steady state from an initial moisture content of 12%. The soil profile then tracks along at a moisture content of approximately 25% while reflecting wetting and drying cycles. As indicated by the fluctuation and amplitude of moisture contents within the upper few feet of the soil profile, moisture is stored primarily within the upper few feet of the soil profile from where it is rapidly removed by evaporation. Lower moisture content at depth is indicated by less fluctuation and a decrease in amplitude.

Figure 7-6 shows the volumetric moisture content at depths of 1 through 5 ft in the soil profile with vegetation. The soil profile in Figure 7-6 behaves similarly to the soil profile in Figure 7-2, with the exception that the moisture content in the upper few feet in Figure 7-6 fluctuates more dramatically with repeated wetting and drying cycles. This is due to a 50% increase in precipitation. Even so, this additional moisture is being stored and removed primarily within the upper few feet of the soil profile. The moisture content at 3 ft is unaffected by the increase in precipitation and exhibits a similar gradual drying over time, reaching steady state at approximately 11% volumetric moisture content. The moisture content and gradual drying at 4 and 5 ft lag behind the moisture content at 3 ft, indicating no downward percolation and a much slower rate of drying.

7.1.2.2 Cumulative Percolation

Figure 7-7 shows the cumulative percolation at depths of 1 through 5 ft in the soil profile without vegetation. Percolation increases uniformly in the first 10 years as the soil profile reaches steady state as shown in Figure 7-5. Percolation then increases gradually over time, spiking during repeated wetting cycles. The cumulative percolation through the soil profile ranges from 6.9%

of the total precipitation at 1 ft to 5.2% of the total precipitation at 5 ft during this 64-yr maximum precipitation record. Cumulative percolation without vegetation is presented in Table 7-1.

Figure 7-8 shows the cumulative percolation at depths of 1 through 5 ft in the soil profile with vegetation. Percolation decreases significantly with depth, falling to 20.9 mm at 2 ft. At 3 ft, percolation is directed upward at a rate of 3.2 mm/yr due to transpiration. Below 3 ft, transpiration continues to exert an upward influence on percolation. Cumulative percolation with vegetation is presented in Table 7-2.

7.1.2.3 Net Annual Percolation

Net annual percolation decreases gradually with depth in the soil profile without vegetation (Table 7-1), ranging from 9.35 mm/yr at 1 ft to 7.06 mm/yr at 5 ft. These percolation rates are approximately four times less than the EPA-prescribed percolation rate of 31.5 mm/yr.

Net annual percolation decreases significantly with depth in the soil profile with vegetation (Table 7-2), ranging from 11.16 mm/yr at 1 ft to 0.33 mm/yr at 2 ft. At 3 ft, net annual percolation is directed upward at a rate of 0.05 mm/yr due to transpiration. Overall, net annual percolation with depth in the soil profile with vegetation decreases dramatically as thickness increases from 1 to 3 ft even though precipitation increases by 50%. For covers 3, 4, and 5 ft in thickness, net annual percolation is effectively zero.

7.1.2.4 Average Flux

Average flux decreases gradually with depth in the soil profile without vegetation (Table 7-1), ranging from 2.97×10^{-8} cm/s at 1 ft to 2.24×10^{-8} cm/s at 5 ft. This flux is approximately one order of magnitude less than the EPA-prescribed flux of 1×10^{-7} cm/s.

Average flux decreases significantly with depth in the soil profile with vegetation (Table 7-2), ranging from 3.53×10^{-8} cm/s at 1 ft to 1.04×10^{-9} cm/s at 2 ft. This flux is approximately one to two orders of magnitude less than the EPA-prescribed flux of 1×10^{-7} cm/s. At 3 ft, average flux is directed upward at 1.59×10^{-10} cm/s due to transpiration. Even under significantly wetter climatic conditions, average flux with depth in the soil profile with vegetation decreases dramatically as thickness increases from 1 to 3 ft. For covers 3, 4, and 5 ft in thickness, average flux is effectively zero. Again, the best performance in average flux, whether with or without vegetation, is achieved by a soil profile 3 ft in thickness, with diminishing performance as thickness increases to 4 and 5 ft.

7.1.3 Modeling Results Using Historical Precipitation Data—Engineered Cover

The 65-yr historical precipitation data delivered 562.3 in. of precipitation to the surface of the soil profile. The average annual precipitation during these years was 8.65 in. Volumetric moisture content and cumulative percolation as a function of depth and time are shown in Figures 7-9 and 7-10 and Figures 7-11 and 7-12, respectively. Cumulative percolation, net annual percolation, and average flux as a function of depth are presented in Tables 7-3 and 7-4.

7.1.3.1 Moisture Content

Figure 7-9 shows the volumetric moisture content at depths of 30 through 1 through 5 ft in the soil profile without vegetation. It takes approximately 6 years for the soil profile to reach steady state from an initial moisture content of 10%. The soil profile then experiences similar fluctuations in moisture content due to numerous wetting and drying cycles as described in Section 7.1.1.1. The engineered soil cover profile reaches steady state in less time than the natural analogue soil profile, and the engineered cover soil profile moisture content tracks at approximately 5 percentage points lower than that of the natural analogue moisture content. This is due to the difference in van Genuchten parameters between the two soil profiles (Table 6-1).

Figure 7-10 shows the volumetric moisture content at depths of 1 through 5 ft in the soil profile with vegetation. The moisture content in the upper few feet fluctuates dramatically with repeated wetting and drying cycles, again indicating that moisture is being stored and removed primarily within the upper few feet of the soil profile. The moisture content at 3 ft is slightly affected by the wetting and drying cycles yet exhibits a gradual drying over time, reaching steady state at approximately 7% volumetric moisture content. The moisture content and gradual drying at 4 and 5 ft lag behind the moisture content at 3 ft indicating no downward percolation and a much slower rate of drying.

7.1.3.2 Cumulative Percolation

Figure 7-11 shows the cumulative percolation at depths of 1 through 5 ft in the soil profile without vegetation. Percolation increases dramatically in the first 6 years then decreases (i.e., is directed upward) during the 16-yr drying period shown in Figure 7-9. Percolation then increases gradually over time, spiking during repeated wetting cycles. The cumulative percolation through the soil profile ranges from 4% of the total precipitation at 1 ft to 2.5% of the total precipitation at 5 ft during this 65-yr historical precipitation record. Cumulative percolation without vegetation is presented in Table 7-3.

Figure 7-12 shows the cumulative percolation at depths of 1 through 5 ft in the soil profile with vegetation. Percolation decreases significantly with depth, falling to 24.2 mm at 2 ft. At 3 ft, percolation is directed upward at a rate of 18.5 mm/yr due to transpiration and the soil profile gradually dries (Figure 7-10). Below 3 ft, transpiration continues to exert an upward influence on percolation and the soil profile gradually dries (Figure 7-10). Cumulative percolation with vegetation is presented in Table 7-4.

7.1.3.3 Net Annual Percolation

Net annual percolation decreases gradually with depth in the soil profile without vegetation, ranging from 3.48 mm/yr at 1 ft to 2.15 mm/yr at 5 ft. These percolation rates are approximately one order of magnitude less than the EPA-prescribed percolation rate of 31.5 mm/yr.

Net annual percolation decreases significantly with depth in the soil profile with vegetation, ranging from 5.79 mm/yr at 1 ft to 0.37 mm/yr at 2 ft. At 3 ft, net annual percolation is directed upward at a rate of 0.28 mm/yr due to transpiration. Overall, net annual percolation with depth

in the soil profile with vegetation decreases dramatically as thickness increases from 1 to 3 ft. For covers 3, 4, and 5 ft in thickness, net annual percolation is effectively zero.

7.1.3.4 Average Flux

Average flux decreases gradually with depth in the soil profile without vegetation, ranging from 1.10×10^{-8} cm/s at 1 ft to 6.82×10^{-9} cm/s at 5 ft. This flux is approximately one to two orders of magnitude less than the EPA-prescribed flux of 1×10^{-7} cm/s.

Average flux decreases significantly with depth in the soil profile with vegetation, ranging from 1.84×10^{-8} cm/s at 1 ft to 1.18×10^{-9} cm/s at 2 ft. This flux is approximately one to two orders of magnitude less than the EPA-prescribed flux of 1×10^{-7} cm/s. At 3 ft, average flux is directed upward at 9.03×10^{-10} cm/s due to transpiration. Overall, average flux with depth in the soil profile with vegetation decreases dramatically as thickness increases from 1 to 3 ft. For covers 3, 4, and 5 ft in thickness, average flux is effectively zero.

The best performance in average flux, whether with or without vegetation, is achieved by a soil profile 3 ft in thickness, with diminishing performance as thickness increases to 4 and 5 ft.

7.1.4 Modeling Results Using Maximum Precipitation Data—Engineered Cover

The 64-yr maximum precipitation data delivered 865.5 in. of precipitation to the surface of the soil profile. The average annual precipitation during these years was 13.5 in./yr. Volumetric moisture content and cumulative percolation as a function of depth and time are shown in Figures 7-13 and 7-14 and Figures 7-15 and 7-16, respectively. Cumulative percolation, net annual percolation, and average flux as a function of depth are presented in Tables 7-3 and 7-4.

7.1.4.1 Moisture Content

Figure 7-13 shows the volumetric moisture content at depths of 1 through 5 ft in the soil profile without vegetation. Similar to Figure 7-9, the soil profile takes approximately 6 years to reach steady state from an initial moisture content of 10%. The soil profile then tracks along at a moisture content of approximately 19% while reflecting wetting and drying cycles. The engineered cover soil profile moisture content tracks at approximately 5 percentage points lower than that of the natural analogue moisture content. This is again due to the difference in van Genuchten parameters between the two soil profiles (Table 6-1).

Figure 7-14 shows the volumetric moisture content at depths of 1 through 5 ft in the soil profile with vegetation. The soil profile in Figure 7-14 behaves similarly to the soil profile in Figure 7-10 with the exception that the moisture content in the upper few feet in Figure 7-14 fluctuates more dramatically with repeated wetting and drying cycles. This is due to a 50% increase in precipitation. Even so, this additional moisture is being stored and removed primarily within the upper few feet of the soil profile. The moisture content at 3 ft is only slightly affected by the increase in precipitation yet exhibits a similar gradual drying over time, reaching steady state at approximately 7.5% volumetric moisture content. The moisture content and gradual

drying at 4 and 5 ft lag behind the moisture content at 3 ft indicating no downward percolation and a much slower rate of drying.

7.1.4.2 Cumulative Percolation

Figure 7-15 shows the cumulative percolation at depths of 1 through 5 ft in the soil profile without vegetation. Percolation increases rapidly in the first 6 years as the soil profile reaches steady state as shown in Figure 7-13. Percolation then increases gradually over time, spiking during repeated wetting cycles. The cumulative percolation through the soil profile ranges from 6.2% of the total precipitation at 1 ft to 5.0% of the total precipitation at 5 ft during this 64-yr maximum precipitation record. Cumulative percolation without vegetation is presented in Table 7-3.

Figure 7-16 shows the cumulative percolation at depths of 1 through 5 ft in the soil profile with vegetation. Percolation decreases significantly with depth, falling to 107.7 mm at 2 ft. At 3 ft, percolation is directed upward at a rate of 18.0 mm/yr due to transpiration. Below 3 ft, transpiration continues to exert an upward influence on percolation. Cumulative percolation with vegetation is presented in Table 7-4.

7.1.4.3 Net Annual Percolation

Net annual percolation decreases gradually with depth in the soil profile without vegetation (Table 7-3), ranging from 8.32 mm/yr at 1 ft to 6.81 mm/yr at 5 ft. These percolation rates are approximately one fourth of the EPA-prescribed percolation rate of 31.5 mm/yr.

Net annual percolation decreases significantly with depth in the soil profile with vegetation (Table 7-4), ranging from 15.67 mm/yr at 1 ft to 1.68 mm/yr at 2 ft. At 3 ft, net annual percolation is directed upward at a rate of 0.28 mm/yr due to transpiration. Overall, net annual percolation with depth in the soil profile with vegetation decreases dramatically as thickness increases from 1 to 3 ft even though precipitation increases by 50%. For covers 3, 4, and 5 ft in thickness, net annual percolation is effectively zero.

7.1.4.4 Average Flux

Average flux decreases gradually with depth in the soil profile without vegetation, ranging from 2.64×10^{-8} cm/s at 1 ft to 2.16×10^{-8} cm/s at 5 ft. This flux is approximately one order of magnitude less than the EPA-prescribed flux of 1×10^{-7} cm/s.

Average flux decreases significantly with depth in the soil profile with vegetation, ranging from 4.97×10^{-8} cm/s at 1 ft to 5.34×10^{-9} cm/s at 2 ft. This flux is approximately one to two orders of magnitude less than the EPA-prescribed flux of 1×10^{-7} cm/s. At 3 ft, average flux is directed upward at 8.92×10^{-10} cm/s due to transpiration. Even under significantly wetter climatic conditions, average flux with depth in the soil profile with vegetation decreases dramatically as thickness increases from 1 to 3 ft. For covers 3, 4, and 5 ft in thickness, average flux is effectively zero. Again, the best performance in average flux, whether with or without vegetation, is achieved by a soil profile 3 ft in thickness, with diminishing improvement in performance as thickness increases to 4 and 5 ft.

7.2 Design Optimization

The modeling results for the natural analogue and the engineered cover are quite similar using both historical and maximum precipitation data and vegetation. With each precipitation record, the net annual percolation and average flux through the soil profile represent only a small percentage of the total precipitation. The soil profiles for the natural analogue and the engineered cover show a significant decrease in net annual percolation and average flux as the soil profile increases in thickness from 1 to 3 ft (Figures 7-4, 7-8, 7-12, and 7-16) (Tables 7-2 and 7-4). The most significant improvement in performance is achieved by increasing the soil profile thickness from 1 to 3 ft with diminishing improvement in performance occurring as the soil profile thickness increases to 4 and 5 ft. The simulated performance values for net annual percolation and average flux presented in Tables 7-2 and 7-4 exceed the EPA-prescribed technical equivalency criteria of 31.5 mm/yr and 1 x 10^{-7} cm/s for net annual percolation and average flux, respectively.

Although the simulated performance values indicate that a 1- or 2-ft-thick cover will significantly limit net annual percolation and average flux, "spikes" or peaks in moisture content and flux occur during years with higher precipitation. These spikes are fewer and lower in amplitude as cover thickness is increased to 3 ft and as the storage capacity of the cover increases. The storage capacity of a 3-ft cover is 50% greater than the storage capacity of a 2-ft cover and would provide an additional degree of conservatism should there be extreme precipitation events or significant, long-term climatic changes. This study indicates that a 3-ft-thick cover is the minimum design thickness necessary to exceed EPA-prescribed technical equivalency criteria by two to three orders of magnitude. Additional cover thickness does not lead to significantly better performance.

Increasing cover thickness to 4 or 5 ft results in limited additional improvement in cover performance yet increases construction costs. Cover construction costs are directly proportional to the thickness of any given cover, and the optimal cover design is one that meets the performance criteria with the minimum cover thickness (Ankeny et al. 1997). A reduced finished elevation above grade would provide additional environmental benefits, reducing the cover's exposure to wind and water erosion and the need for long-term maintenance.

8. Conclusions and Recommendations

The goals of the EPA-recommended design of landfill closure covers for hazardous waste facilities are to 1) minimize leachate by minimizing the contact of water with waste, 2) to minimize further maintenance, and 3) to protect human health and the environment considering future use of the site. The EPA accepts alternative cover designs that consider site-specific conditions, such as climate and soil and hydrological properties that meet the intent of the regulations. A fundamental concern of the EPA with cover design is that the cover must be stable; and perform as intended without posing a significant risk to human health and the environment.

In this study, an alternative cover design consisting of a thick layer of natural soil and native vegetation, namely a vegetative soil cover, is proposed as the closure path for hazardous, radioactive, and mixed waste landfills at SNL/NM and KAFB. The proposed design relies upon soil thickness and evapotranspiration to provide long-term performance and stability. The proposed design is also inexpensive to build and maintain because of the availability of suitable on-site soils. The results of this study are applicable to municipal waste landfills within the City of Albuquerque and Bernalillo County.

EPA regulations are qualitative, which leave adequate flexibility for exploring and developing any number of alternatives for designing landfill closure covers. The alternative cover proposed in this study is conceptualized and simulated as a lithologic monolayer. A lithologic monolayer with uniform soil and hydrologic properties translates into a significant conservative estimate of performance. A multiple-layered cover, whether simulated as a multiple-layered cover or as multiple layers in nature, attenuates the downward flow of liquid water (e.g., multiple capillary barriers).

Capillary barriers, consisting of fine-over-coarse soil layers, have been proposed as another alternative for landfill covers in dry climates (Hakonson 1997, Stormont 1997). Conceptually, the fine-over-coarse arrangement functions as a moisture barrier impeding downward flow. Water is held in the fine layer by capillary forces and does not move into the coarse layer until the fine layer near the interface approaches saturation. Soil water is removed from the fine layer by evaporation and transpiration, or breakthrough into the underlying coarse layer. If the fine layer is sloped, water in the fine layer may drain laterally under unsaturated conditions. Capillary barriers are effective if the combined effect of evaporation, transpiration, and lateral drainage exceeds infiltration and percolation, keeping the cover system sufficiently dry so that appreciable breakthrough does not occur (Stormont 1997).

In this study, a conceptual cover that represents the natural analogue and an engineered cover was simulated with and without vegetation. Modeling a cover without vegetation yields a conservative estimate of liquid water flow. A significant amount of liquid water is removed from a cover by evaporation and transpiration. In the absence of vegetation, evaporation is limited by the ability of near-surface soils to conduct liquid water to the surface from soils deeper in the profile. Once near-surface soils dry below a certain threshold, the rate of transfer of water from deep within the soil profile to the soil surface limits the rate of evaporation. Additional features that translated into conservative estimates of liquid water flow were

highlighted in this study. All code input parameters were site-specific with the exception of LAI. Each parameter was carefully measured to obtain the most conservative estimate of net annual percolation and average flux possible. The practical approach used in this study yields code-generated performance values for net annual percolation and average flux that are two to three orders of magnitude less than the EPA-prescribed technical equivalency criteria of 31.5 mm/yr and 1 x 10^{-7} cm/s for net annual percolation and average flux, respectively. This approach, along with the application of conservative site-specific input parameters, provides a satisfactory engineering safety factor that forms the basis for decision-making by the regulatory community. Ultimately, model simulations should help the regulator establish appropriate performance criteria to optimize landfill final closure cover design.

Under current climatic conditions, e.g., historical precipitation, net annual percolation and average flux through a 3-ft cover is effectively zero (Table 7-4). Even under a maximum precipitation scenario, one that represents a 50% increase in future precipitation, net annual percolation and average flux through a 3-ft cover is, again, effectively zero. In reality, a 3-ft cover's performance will actually approximate that of a 4- or 5-ft cover due to the placement of subgrade fill. Several feet of compacted subgrade fill is usually placed over an existing landfill surface prior to construction of a cover.

This study cannot be concluded without citing the concerns expressed by the scientific and engineering community regarding the use of predictive models to simulate the performance of proposed alternative covers. Computer simulations are used to support the engineering design of landfill closure covers, interpret field data collected to verify post-closure performance, and evaluate the effectiveness of a cover at isolating waste well into the future. At this time, however, no model can account for all of the potentially relevant issues regarding cover performance such as preferential flow and the complex dynamics of soil water availability to plants.

Because of the complexity of the soil-plant-atmosphere continuum, it is practically impossible to define its exact physical state at any given time. The research community is generally obliged to simplify their approach by concentrating on the factors that appear to have the greatest and most direct bearing on the problem at hand (Hillel 1998). In many cases, the theories and attendant equations employed in soil physics describe not the soil itself, but some ideal and well-defined model that is invoked to predict the soils' behavior. Examples of ideal and well-defined models used in this study include Darcy's and Richards' equations, van Genuchten's (1980) and Mualem's (1976) models, the transpiration equation of Ritchie and Burnette (1971), the macroscopic scale plant-uptake model of Feddes et al. (1978), and the UHSAT-H code (Fayer 2000). The value of these models depends on the degree of approximation and/or realism with which the models portray the relevant constitutive principles. However, even the best models cannot provide anything but a simplified version of the highly dynamic soil-plant-atmosphere continuum (Hillel 1998).

The primary advantage of numerical modeling is the ability to enhance engineering and regulatory judgment, not the ability to enhance predictive capabilities. Numerical modeling should focus on improving our ability to understand key processes and characteristics that affect the long-term performance of cover systems. Cover materials evolve over time in response to

site-specific physical, chemical, and biological processes such that as-built performance, and performance after two to five years, does not represent long-term performance. The timeframe over which the cover system will come into equilibrium with its environmental setting has yet to be determined.

Field data from test sites is commonly collected to verify post-closure performance and validate performance modeling. However, field tests are much shorter than the design life of a landfill closure cover and the period of time being simulated. Field tests are far shorter than they should be to allow the test sites to reach steady state before percolation data is used for performance assessment. Field tests typically consist of lysimeters, which are, in essence, buried containers or test covers underlain by an impermeable synthetic liner and open to the atmosphere to capture precipitation. Lysimeters are instrumented to measure moisture content in the soil profile and to measure percolation at the base of the test cover.

A significant disadvantage of lysimeters is the artificial no-flow boundary induced by the synthetic liner at the base of the test cover (Benson et al. 2001). This artificial boundary does not exist beneath an actual cover and prevents the downward and upward flow of liquid water and water vapor across the liner. Other disadvantages with lysimeters are the potential capillary break effect caused by the artificial liner that does not exist under natural conditions (Albright et al. 2002) and the artificial pressure at the test cover-liner interface that is equal to zero or, in essence, a water table (O'Kane and Barbour 2003). Questions regarding the validity of lysimeter studies that need to be addressed include 1) whether the percolation seen in any given year is the result of that years' precipitation; 2) the length of time water is retained in the test cover at various depths before it is seen as percolation; 3) how deep lysimeters must be constructed to avoid pan evaporation effects; and, very importantly, 4) the length of time it takes for a lysimeter to reach steady state.

The results of this study indicate that an engineered cover does not reach steady state for at least 6 years and the natural analogue does not reach steady state for at least 12 years. Even then, more time may be needed to capture significant hydrological events. As much as 10 to 20 years should be the minimal length of time used to evaluate cover performance when employing lysimeters and test covers. At this time, the lysimeter data needed to evaluate cover performance and validate model simulations do not exist. These data, as well as improvements in lysimetry and performance modeling, are expected in coming years.

Even so, models are very useful tools and alternative covers have many potential benefits over the EPA-prescribed Subtitle C caps. Many scientists and engineers as well as the regulatory community support the use of models to simulate cover performance. As long as the basic practical limitations and the strengths and weaknesses of models are well understood, models will remain a valuable tool to evaluate alternative covers.

The performance of the alternative cover proposed in this study, when integrated with the natural site conditions in Albuquerque, New Mexico, produces a "system performance" that will ensure that the proposed cover is protective of human health and the environment. The natural site conditions that produce the desired system performance include:

- Extremely low precipitation and high evapotranspiration, and

- Versatile, native flora that persists indefinitely as a climax ecological community with little or no maintenance. For a vegetative cover to function effectively and consistently as designed, a healthy and diverse stand of perennial plants is essential (Anderson and Forman 2002).

Vegetative soil covers are 1) highly adapted to local soil and climate conditions, 2) less costly and easier to construct, 3) self-sustaining, and 4) capable of maintaining transpiration for much of the year. They can be easily constructed from readily available, naturally occurring materials using less rigorous construction quality assurance and construction quality control procedures, while providing long-term stability with less long-term maintenance. Long-term stability with less long-term maintenance is essential to the performance of vegetative soil covers.

Stability and maintenance are critical to the long-term performance of vegetative soil covers. Erosion of the cover by wind and water is a significant design consideration. The design should minimize the effects of wind and water erosion of the surface, side slopes, and toe of the cover. Vegetation plays a key role in stabilizing newly constructed surfaces.

The amount of water on the cover surface is a function of the amount of precipitation that falls on the cover surface less the amount of infiltrating water and water that runs off and away from the cover surface. Cover surfaces should be centrally crowned and sloped between 2% and 5% to minimize ponding and promote runoff of surface water while minimizing erosion of the topsoil layer.

The topsoil layer serves as the vegetation and erosion protection layer. Topsoil layers can include gravel admixtures up to 25% designed to control erosion much like a desert pavement, without adversely affecting the vegetation and soil water balance. The topsoil layer should be minimally compacted to facilitate the development of roots and root density.

Native vegetation is extremely versatile, adapting to climatic change through natural selection and severe disturbance, i.e., drought, fire, and herbivores. Species diversity of the selected plant mix is important for the long-term performance of a vegetative soil cover. Species diversity helps reduce susceptibility of the plant community to disease or blights, and better emulates the natural, climax ecosystem by encouraging wider environmental diversity within the restored habitat. By including a variety of warm-weather and cold-weather plants in the species mix, one can ensure that the plants will continue to grow and promote transpiration throughout the year.

The natural, climax ecosystem may take three to five years to develop, especially in arid and semiarid environments. Procedures can be developed to facilitate growth and provide erosion control until the climax ecosystem is established. These procedures include irrigation, fertilization, and mulching. Once the natural, climax ecosystem is established, it will persist indefinitely with little or no maintenance.

At this time, no hydrologic predictive model can account for all the potentially relevant issues regarding landfill cover performance. Progress can be made, however, at refining these models.

Significant progress is needed to capture relevant issues such as preferential flow and more accurately represent the transpiration model of Ritchie and Burnette (1971) and the macroscopic plant-uptake model of Feddes et al. (1978) for non-agricultural plants.

The most significant shortcoming in current models is the lack of a comprehensive theoretical framework that encompasses and integrates the relevant factors likely to influence the water regime of the highly dynamic soil-plant-atmosphere continuum. Biology *is* a form of engineering and must be incorporated into the design equation. Significant effort is needed to describe native plant soil-water uptake and response to dynamic soil-water conditions over both space and time.

9. References

Albright, W.H., G.W. Gee, G.V. Wilson, and M.J. Fayer, 2002. Alternative cover assessment project, Phase I report. DRI Rep. 41183, Division of Hydrologic Sci., Desert Res. Inst., Univ. of Nevada, Las Vegas, NV.

Allen, A., 2001. Containment landfills: The myth of sustainability. Eng. Geol. 60: 3–19.

Anderson, J.E., 1997. Soil-plant cover systems for final closure of solid waste landfills in arid regions. p. 27–38. In T.D. Reynolds and R.C. Morris (eds.) Landfill capping in the semi-arid West: Problems, perspectives, and solutions. Environ. Sci. and Res. Foundation, Idaho Falls, ID.

Anderson, J.E., and A.D. Forman, 2002. The protective cap/biobarrier experiment: A study of alternative evapotranspiration caps for the Idaho National Engineering and Environmental Laboratory. Environ. Sci. and Res. Foundation, Idaho Falls, ID.

Anderson, J.E., R.S. Nowak, T.D. Ratzlaff, and O.D. Markham, 1993. Managing soil moisture on waste burial sites in arid regions. J. Environ. Qual. 22:62–69.

Ankeny, M.D., L.M. Coors, N. Majumdar, J. Kelsey, and M. Miller, 1997. Performance and cost considerations for landfill caps in semi-arid climates. p. 243–261. In T.D. Reynolds and R.C. Morris (eds.) Landfill capping in the semi-arid West: Problems, perspectives, and solutions. Environ. Sci. and Res. Foundation, Idaho Falls, ID.

Benson, C., T. Abichou, W. Albright, G. Gee, and A. Roesler, 2001. Field evaluation of alternative earthen final covers. Int. J. Phytoremediation. 3(1):105–127.

Bonzon, L.L., J.S. Philbin, B.F. Estes, and J.A. Reuscher, 1974. Sandia Pulsed Reactor III (SPR III) safety analysis report. Rep. SLA-74-0349, Sandia National Laboratories, Albuquerque, NM.

Boynton, S.S., and D.E. Daniel, 1985. Hydraulic conductivity tests on compacted clay. J. Geotech. Eng. 111:465–477.

Brooks, R.H., and A.T. Corey, 1964. Hydraulic properties of porous media. Hydrology Paper No. 3, Colorado State Univ., Fort Collins, CO.

Brown, D.E., 1982. Biotic communities of the American Southwest-United States and Mexico, p. 322. In D.E. Brown (ed.) Desert plants, 4:1–14, University of Arizona, Boyce Thomson Southwestern Arboretum, Superior, AZ.

Brown, D.A., P.J. Gersmehl, 1985. Migration models for grasses in the American midcontinent. Ann. Assoc. Am. Geographers 75(3):383–394.

Burdine, N.T., 1953. Relative permeability calculations from pore-size distribution data. Petroleum Trans., Am. Inst. Mining Metall. Eng. 198:71–77.

Burgess, T.L., 1995. Desert grassland, mixed shrub savanna, shrub steppe, or semidesert scrub: The dilemma of coexisting growth forms. p. 31–67. In M.P. McClaran and T.R. Van Devender (eds.) The desert grassland. Univ. of Arizona Press, Tucson, AZ.

Campbell, G.S., 1985. Soil physics with BASIC. Elsevier, New York.

Canfield, R.H., 1934. Stem structure of grasses on the Jornada Experimental Range. Bot. Gazette 95:636–648.

Carsel, R.F., and R.S. Parrish, 1988. Developing joint probability distributions of soil water retention characteristics. Water Resources Res. 24:755–769.

Cole, J.S., and O.R. Mathews, 1939. Subsoil moisture under semiarid conditions. Tech. Bull. No. 637, USDA, Washington, DC.

Comstock, J.P., T.A. Cooper, and J.R. Ehleringer, 1988. Seasonal patterns of canopy development and carbon gain in nineteen warm desert shrub species. Oecologia 75(3):327–335.

Corser, P., J. Pellicer, and M. Cranston, 1992. Observations on long-term performance of composite clay liners and covers. Geotech. Fabrics Rep. Nov. 6–16.

Daniel, D.E., and Y.K. Wu, 1993. Compacted clay liners and covers for arid sites. J. Geotech. Eng., ASCE Publ. 119(2):223–237.

Dick-Peddie, W.A., 1992. New Mexico vegetation: Past, present and future. Univ. of New Mexico Press, Albuquerque, NM.

Doorenbos, J., and W.O. Pruitt, 1977. Guidelines for predicting crop water requirements. p. 1–107. In FAO Irrigation Paper No. 24, 2nd ed., FAO, Rome.

Doorenbos, J., and W.O. Pruitt, 1992. Crop water requirements. p. 1–144. In FAO Irrigation and Drainage Paper No. 24, FAO, Rome.

EPRI (Electric Power Research Institute), 1981. Siting of an international facility for storage of vitrified radiowastes. Rep. EC8-81-1-LD, Environ. Sci. and Eng. Program, Univ. of California, Los Angeles, CA.

EPRI (Electric Power Research Institute), 1982. Evaluation of great deserts of the world for perpetual international radiowaste storage. Rep. ESC-277-LD, Environ. Sci. and Eng. Program, Univ. of California, Los Angeles, CA.

Fayer, M.J., 2000. UNSAT-H Version 3.0: Unsaturated soil water and heat flow model. Pacific Northwest Natl. Lab., Richland, WA.

Fayer, M.J., and G.W. Gee, 1997. Hydrologic model tests for landfill covers using field data. p.53–68. In T.D. Reynolds and R.C. Morris (eds.) Landfill capping in the semi-arid West: Problems, perspectives, and solutions, Environ. Sci. and Res. Foundation, Idaho Falls, ID.

Fayer, M.J., G.W. Gee, and T.L. Jones, 1986. UNSAT-H Version 1.0: Unsaturated flow code documentation and application for the Hanford Site. Rep. PNL-5899, Pacific Northwest Natl. Lab., Richland, WA.

Fayer, M.J., and T.L. Jones, 1990. UNSAT-H Version 2.0: Unsaturated soil water and heat flow model. Rep. PNL-6779/UC-702, Pacific Northwest Natl. Lab., Richland, WA.

Feddes, R.A., E. Bresler, and S.P. Neuman, 1974. Field test of a modified numerical model for water uptake by root systems. Water Resources Res. 10:1199–1206.

Feddes, R.A., P.J. Kowalik, and H. Zaradny, 1978. Simulation of field water use and crop yield. John Wiley and Sons, New York.

Fletcher, R., 2003. "Ecological Concepts," Personal Communication, Albuquerque, New Mexico. November 15, 2003.

Goodrich, S., 1986. Vascular plants of the Desert Experimental Range, Millard County, Utah. General Tech. Rep. INT-209, USDA, Forest Serv., Intermountain Res. Stn., Ogden, UT.

Gupta, S.K., K.K. Tanji, D.R. Nielson, J.W. Biggar, C.S. Simmons, and J.L. MacIntyre, 1978. Field simulation of soil-water movement with crop water extraction. Water Sci. and Eng. Paper No. 4013, Dep. of Land, Air, and Water Resources, Univ. of California, Davis, CA.

Hakonson, T.E., 1994. Capping as an alternative for remediating radioactive and mixed waste landfills. Los Alamos Natl. Lab., Los Alamos, NM.

Hakonson, T.E., 1997. Capping as an alternative for landfill closures: Perspectives and approaches. p. 1–18. In T.D. Reynolds and R.C. Morris (eds.) Landfill capping in the semi-arid West: Problems, perspectives, and solutions, Environ. Sci. and Res. Foundation, Idaho Falls, ID.

Hauser, V.L., B.L. Weand, and M.D. Gill, September 2001. Natural covers for landfills and buried waste. J. Environ. Eng. 127(9):768–775.

Hawley, J.W., and P.A. Longmire, 1992. Site characterization and selection. p. 57–99. In C.C. Reith et al. (eds) Deserts as dump, Univ. of New Mexico Press, Albuquerque, NM.

HDR Engineering, Inc. and Daniel B. Stephens & Associates, Inc., 2000. Alternate cover design report for Waste Management of Nebraska, Inc., Douglas County Recycling and Disposal Facility, Bennington, Nebraska. HDR Engineering, Inc. and Daniel B. Stephens & Associates, Inc., Omaha, NE.

Herbel, C.H., and A.B. Nelson, 1969. Grazing management of semidesert ranges in southern New Mexico. Jornada Experimental Range Rep. No. 1. Agric. Res. Serv., Crops Res. Division, USDA, Las Cruces, NM.

Hewitt, P.J., and K.K. Philip, 1999. Problems of clay desiccation in composite lining systems. Eng. Geol. 53:107–113.

Hillel, D., 1998. Environmental soil physics. Academic Press, Harcourt Brace & Company, San Diego, CA.

Hillel, D., V. D. Krentos, and Y. Stylianou, 1972. Procedure and test of an internal drainage method for measuring soil hydraulic characteristics in situ. Soil Sci. 114:395–400.

Houghton, F.E., 1972. Climate of New Mexico. In U.S. Dep. of Commerce, Climates of the States Series, U.S. Gov. Print. Office, Washington, DC.

ITRC (Interstate Technology and Regulatory Council), 2003. Technical and regulatory guidance for design, installation, and monitoring of alternative final landfill covers. Alternative Landfill Tech. Team, Interstate Tech. and Regulatory Council, Washington, DC.

Jaynes, D.B., and E.J. Tyler, 1980. Comparison of one-step outflow laboratory method to an in-situ method for measuring hydraulic conductivity. Soil Sci. Soc. Am. J. 44:903–907.

Khaleel, R., and J.F. Relyea, 1995. Evaluation of van Genuchten-Mualem relationships to estimate unsaturated hydraulic conductivity at low water contents. Water Resources Res. 31(11):2659–2688.

Khire, M.V., C.H. Benson, and P.J. Bosscher, 1997. Water balance modeling of earthen final covers. J. Geotech. and Geoenviron. Eng. 123:744–754.

Klute, A., and C. Dirkson, 1986. Methods of soil analysis: Part 1, physical and mineralogical methods. 2nd ed. Soil Sci. Soc. Am., Inc., Madison, WI.

Knight, P.J., and T.S. Ashton, 2003. Vegetation studies in support of the design and optimization of vegetative soil covers at Sandia Natl. Laboratories, Albuquerque, New Mexico. Marron and Associates, Inc., Albuquerque, NM.

Landreth, R.E., D.E. Daniel, R.M. Koerner, P.R. Schroeder, and G.N. Richardson, 1991. Design and construction of RCRA/CERCLA final covers. USEPA Seminar Publ., Rep. EPA/625/4-91/025, U.S. Gov. Print. Office, Washington, DC.

Marion, J.M., D. Or, D.E. Rolston, M.L. Kavvas, and J.W. Biggar, 1994. Evaluation of methods for determining soil-water retentivity and unsaturated hydraulic conductivity. Soil Sci. 158(1):1–13.

Markham , O.D., 1997. Executive summary. p. i–ii. In T.D. Reynolds and R.C. Morris (eds.) Landfill capping in the semi-arid West: Problems, perspectives, and solutions. Environ. Sci. and Res. Foundation, Idaho Falls, ID.

Melchoir, S., 1997. In situ studies on the performance of landfill caps (compacted soil liners, geomembranes, geosynthetic clay liners, capillary barriers). In U.S. Dept. of Energy, USEPA, and DuPont Company, 1997 Int. Containment Tech. Conf. and Exhibition, February 1997, St. Petersburg, FL.

Miller, C.J., and M. Mishra, 1989. Modeling of leakage through cracked clay liners: A new perspective. Water Resource Bull. 25:557–563.

Montgomery, R.J., and L.J. Parsons, 1989. The Omega Hills final cover test pilot study: Three year data summary. 1989 Annu. Meeting of the Natl. Solid Waste Management Assoc., Washington, DC.

Mualem, Y., 1976. A new model for predicting the hydraulic conductivity of unsaturated porous media. Water Resources Res. 12:593–622.

Munk, L.P., 2004. "Growing Season and Leaf Area Index," Personal communication, Albuquerque, New Mexico, January 6, 2004.

Nelson, E.W., 1934. The influence of precipitation and grazing upon black grama grass range. Tech. Bull. No. 409. USDA, Washington, DC.

New Mexico Environment Department, 1998. Guidance document for performance demonstration for an alternate cover design under Section 502.A.2 of the New Mexico Solid Waste Management Regulations (20 NMAC 9.1) using HELP modeling and performance demonstration for an alternate liner design under Section 306.A.2 of the New Mexico Solid Waste Management Regulations (20 NMAC 9.1) using HELP modeling. Solid Waste Bureau Permit Section, New Mexico Environ. Dep., Santa Fe, NM.

Ogata, G., and L.A. Richards, 1957. Water content changes following irrigation of bare field soil that is protected from evaporation. Soil Sci. Soc. Am. Proc. 21:355–356.

O'Kane, M., and S.L. Barbour, 2003. Field performance of lysimeters used to evaluate cover systems for mine waste. Proc. 6th Int. Conf. for Acid Rock Drainage, Cairns, Qld., Australia.

Paige, G.B., and D. Hillel, 1993. Comparison of three methods for assessing soil hydraulic properties. Soil Sci. 155(3):175–189.

Paulsen, H.A., Jr., and F.N. Ares, 1962. Grazing values and management of black grama and tobosa grasslands and associated shrub ranges of the Southwest. Tech. Bull. No. 1270. U.S. Forest Serv., USDA, Washington, DC.

Peace, J.L., T.J. Goering, and M.D. McVey, 2002. Report of the Mixed Waste Landfill Phase 2 RCRA Facility Investigation, Sandia National Laboratories, Albuquerque, New Mexico. Rep. SAND2002-2997, Environ. Restoration Project, Sandia Natl. Laboratories, Albuquerque, NM.

Peace, J.L., P.J. Knight, T.S. Ashton, and T.J. Goering, 2004. Vegetation study in support of the design and optimization of vegetative soil covers. Rep. SAND2004-6144, Sandia Natl. Laboratories, Albuquerque, New Mexico.

Penman, H.L., 1963. Vegetation and hydrology. Tech. Comment No. 53, Commonwealth Bureau of Soils, Harpenden, England.

Persaud, N., and P.J. Wierenga, 1982. Report prepared for Sandia National Laboratories. Dep. of Agron., New Mexico State Univ., Las Cruces, NM.

Philip, J.R., and D.A. deVries, 1957. Moisture movement in porous materials under temperature gradients. Trans. Am. Geophys. Union 38:222–232.

Piechota, T., J. Timilsena, G. Tootle, and H. Hidalgo, 2004. The Western U.S. drought: How bad is it? Trans. Am. Geophysical Union 85(32):301–304.

Rawls, W.J., D.L. Brackensiek, and K.E. Saxton, 1982. Soil water characteristics. Trans. ASAE Publ. 25:1316–1328.

Reith, C.C., and B.M. Thomson, 1992. Deserts as dumps? The disposal of hazardous materials in arid ecosystems. Univ. of New Mexico Press, Albuquerque, NM.

Richards, S.J., and L.V. Weeks, 1953. Capillary conductivity values from moisture yield and tension measurements on soil columns. Soil Sci. Soc. Am. Proc. 17:206–209.

Richardson, C.W., and D.A. Wright, 1984. WGEN: A model for generating daily weather variables. Rep. ARS-8, Agric. Res. Serv., USDA, Washington, DC.

Ritchie, J.T., and E. Burnette, 1971. Dryland evaporative flux in a subhumid climate, II, plant influences. Agron. J. 63:56–62.

Ritchie, J.T., 1972. Model for predicting evaporation from a row crop with incomplete cover. Water Resources Res. 8(5):1204–1212.

Rose, C.W., W.R. Stern, and J.E. Drummand, 1965. Determination of hydraulic conductivity as a function of depth and water content for soil in situ. Aust. J. Soil Res. 3:1–9.

Sammis, W.T., E.G. Hanson, C.E. Barnes, H.D. Fuehring, E.J. Gregory, R.F. Hooks, T.A. Howell, and M.S. Finkner, 1977. Consumptive use and yields of crops in New Mexico. Completion Rep. Project No. B-054-NMEX, New Mexico Water Resources Res. Inst., New Mexico State Univ., Las Cruces, NM.

Schroeder, P.R., T.S. Dosier, P.A. Zappi, B.M. McEnroe, J.W. Sjostrom, and R.L. Peyton, 1994. The hydrologic evaluation of landfill performance (HELP) model: Engineering documentation for Version 3. Rep. EPA/600/R-94/168b, Office of Res. and Dev., USEPA, Washington, DC.

Scurlock, J.M.O., G.P. Asner, and S.T. Gower, 2001. Worldwide historical estimates of leaf area index, 1932–2000. Rep. ORNL/TM-2001/268, Oak Ridge Natl. Lab., Oak Ridge, TN.

Shouse, P.J., J.B. Sisson, T.R. Ellsworth, and J.A. Jobes, 1992. Estimating in situ unsaturated hydraulic properties of vertically heterogeneous soils. Soil Sci. Soc. Am. J. 56:1673–1679.

Simunek, J., M. Sejna, and M.T. van Genuchten, 1996. HYDRUS-2D: Simulating water flow and solute transport in two-dimensional variably saturated media. Int. Groundwater Modeling Cent., Colorado School of Mines, Golden, CO.

Stearns, S.D., 1975. Digital signal analysis. Hayden Book Company, Rochelle Park, NJ.

Stormont, J.C., 1997. Incorporating capillary barriers in surface cover systems. p. 39–51. In T.D. Reynolds and R.C. Morris (eds.) Landfill capping in the semi-arid West: Problems, perspectives, and solutions. Environ. Sci. and Res. Foundation, Idaho Falls, ID.

Sullivan, R.M., and P.J. Knight, 1992. Biological assessment for the Sandia National Laboratories Coyote Canyon Test Complex, Kirtland Air Force Base, Albuquerque, New Mexico. Spec. Tech. Rep. 1 (Contract AB4892), Phys. Sci. Lab., Las Cruces, NM.

Suter, G.W., R.J. Luxmoore, and E.D. Smith, 1993. Compacted soil barriers at abandoned landfills will fail in the long term. J. of Environ. Qual. 22:217–226.

USDA-Forest Service, 2003. Fire effects information database, Plant Species Sub-database. Available at http://www.fs.fed.us/database/feis/plants/. USDA Forest Serv., Rocky Mountain Res. Stn., Fire Sci. Lab., Missoula, MT.

U.S. Department of Energy, 1988. Vegetative covers. Rep. UMTRA-DOE/AL 400642.0000, Uranium Mill Tailings Remedial Action Project, U.S. Dep. of Energy, Washington, DC.

USEPA, 1988. Case studies on groundwater and surface water contamination from municipal waste landfills: Criteria for municipal solid waste landfills. Rep. EPA/530-SW-88-040, NTIS PD-88-242466, Office of Solid Waste, USEPA, Washington, DC.

USEPA, 1989. Technical guidance document: Final covers on hazardous waste landfills and surface impoundments. Rep. EPA/530-SW-89-047, USEPA, Washington, DC.

USEPA, 1991. Design and construction of RCRA/CERCLA final covers. Rep. EPA/625/4-91/025, USEPA, Washington, DC.

USEPA, 2002. Assessment and recommendations for improving the performance of waste containment systems Rpt. No. EPA/600/R-02/099. USEPA, Washington, D.C.

van Genuchten, M.T., 1978. Calculating the unsaturated hydraulic conductivity with a new closed-form analytical model. Res. Rep. 78-WR-08, Dept. of Civil Eng., Princeton Univ., Princeton, NJ.

van Genuchten, M.T., 1980. A closed-form equation for predicting the hydraulic conductivity of unsaturated soils. Soil Sci. Soc. Am. J. 44:892–898.

van Genuchten, M.T., and D.R. Nielson, 1985. On describing and predicting the hydraulic properties of unsaturated soils. Ann. Geophys. 3:615–628.

van Genuchten, M.T., F.J. Leij, and S.R. Yates, 1991. The RETC code for quantifying the hydraulic functions of unsaturated soils. p. 91–65. In USEPA, Environmental Protection Technology Series, Office of Res. and Dev., U.S. Salinity Lab., Agric. Res. Serv., Riverside, CA.

Van Hart, D., 2003. Geologic investigation: An update of subsurface geology on Kirtland Air Force Base, New Mexico. Rep. SAND2003-1869. Sandia Natl. Laboratories, Albuquerque, NM.

Warren, R.W., T.E. Hakonson, and K.V. Bostick, 1997. The hydrologic evaluation of four cover designs for hazardous waste landfills. p. 181–197. In T.D. Reynolds and R.C. Morris (eds.) Landfill capping in the semi-arid West: Problems, perspectives, and solutions. Environ. Sci. and Res. Foundation, Idaho Falls, ID.

Watson, K.K., 1966. An instantaneous profile method for determining the hydraulic conductivity of unsaturated porous materials. Water Resources Res. 2:709–715.

Waugh, W.J., 1997. Ecology of uranium mill tailings covers. p. 199–212. In T.D. Reynolds and R.C. Morris (eds.) Landfill capping in the semi-arid West: Problems, perspectives, and solutions, Environ. Sci. and Res. Foundation, Idaho Falls, ID.

Waugh, W.J., and G.N. Richardson, 1997. Ecology, design, and long-term performance of surface barriers: Applications at a uranium mill tailings site; barrier technologies for environmental management: Summary of a workshop, Washington, DC.

West, N.E., et al., 1972. Galleta: Taxonomy, ecology, and management of Hilaria jamesii on western rangelands. Bull. 487, Utah Agric. Experiment Stn., Utah State Univ., Logan, UT.

Williams, J.L., 1986. New Mexico in maps. 2nd ed. Univ. of New Mexico Press, Albuquerque, NM.

Williams, J.R., C.A. Jones, and P.T. Dyke, 1984. The EPIC Model and its application. p. 111–121. In Proc., ICRISAT-IBSNAT-SYSS Symposium on minimum data sets for agrotechnology transfer, March 1983, Hyderabad, India.

Winograd, I.J., 1981. Radioactive waste storage in thick unsaturated zones. Sci. 212:1457–1464.

Yesiller, N., C.J. Miller, G. Inci, and K. Yaldo, 2000. Desiccation and cracking behavior of three compacted landfill liner soils. Eng. Geol. 57:105–121.

FIGURES

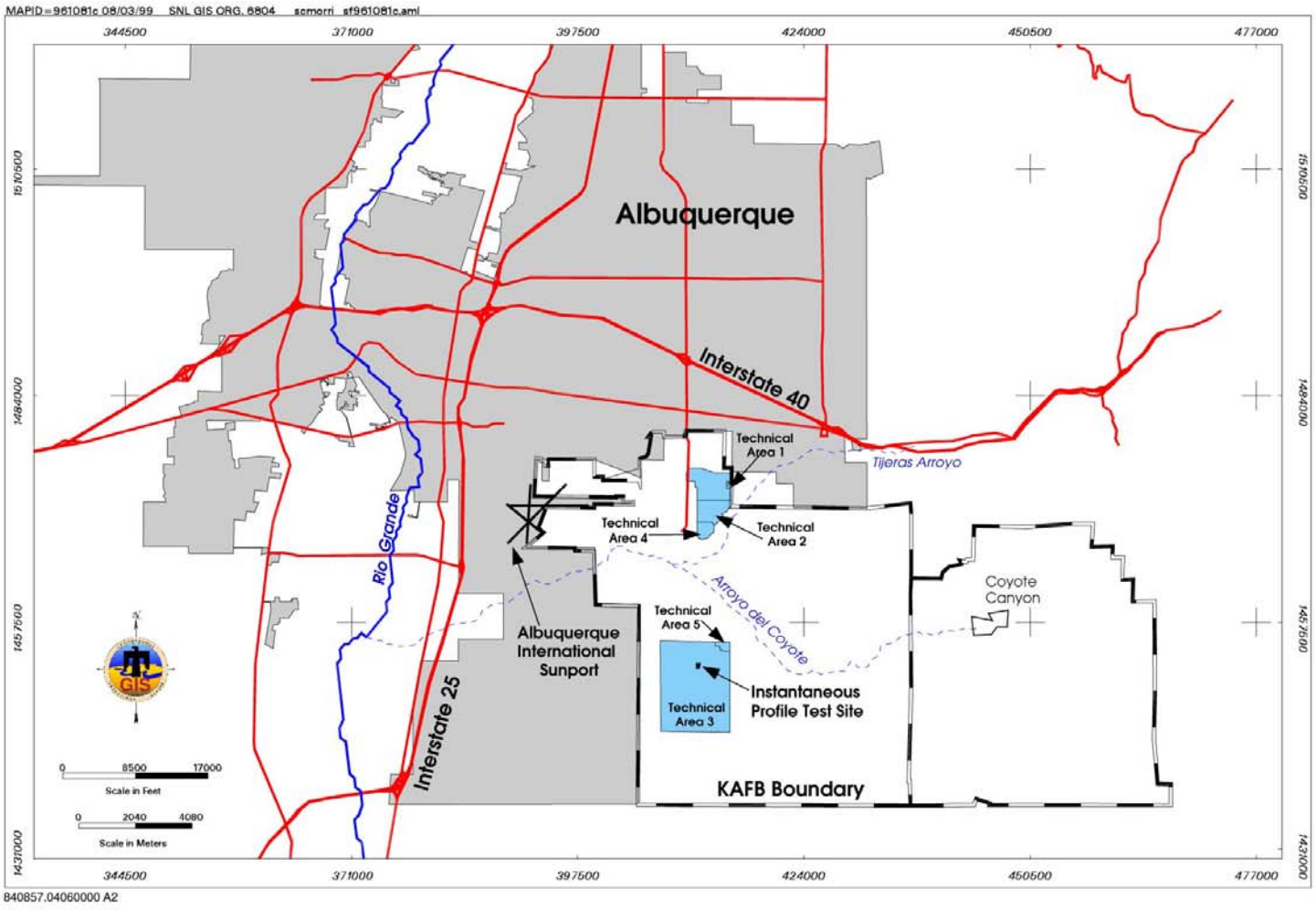

Figure 3-1 Location of Sandia National Laboratories, Kirtland Air Force Base and the Instantaneous Profile Test Site, Albuquerque, New Mexico

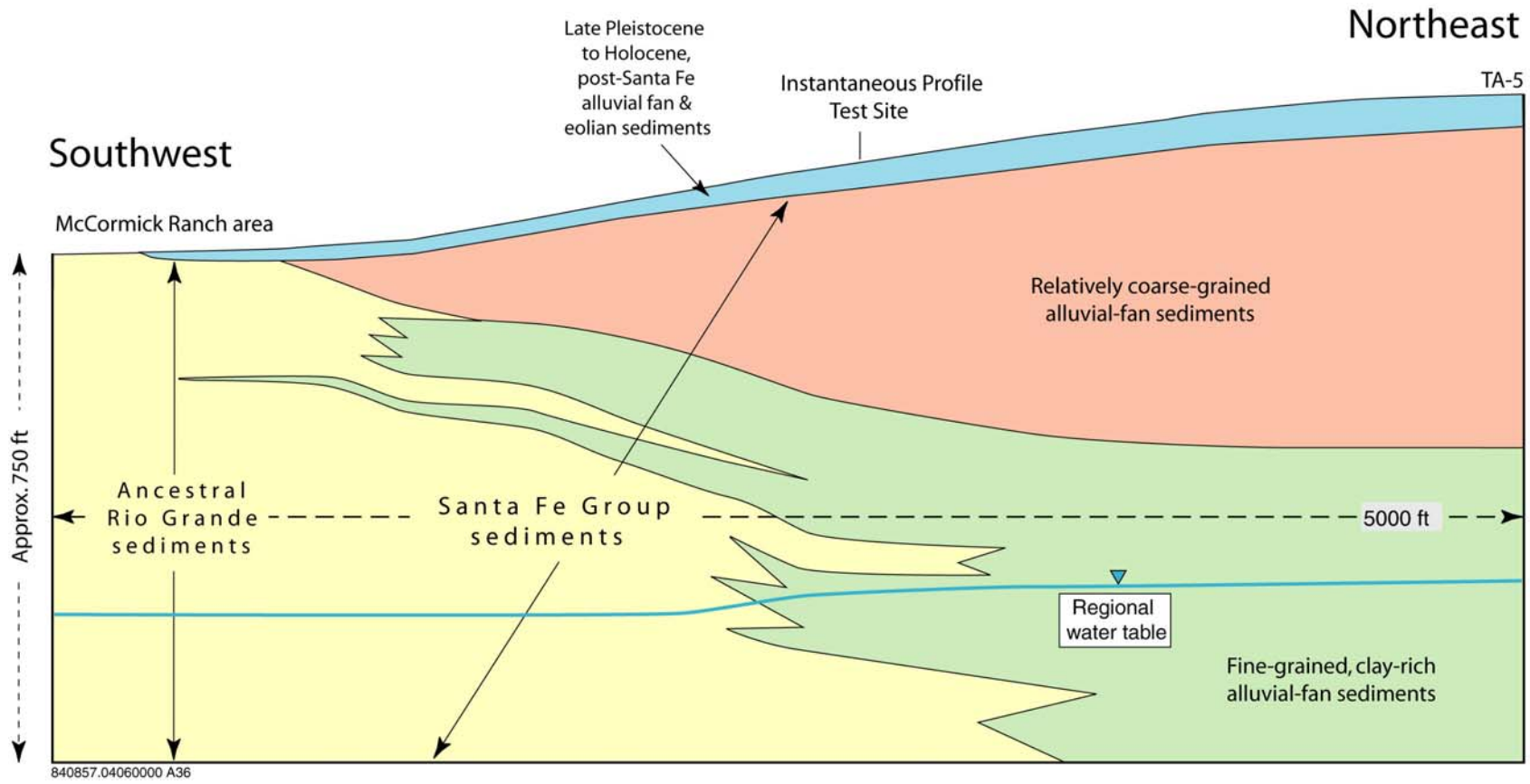

Figure 3-2 Generalized Geologic Cross-Section of TA-3 (Van Hart 2003)

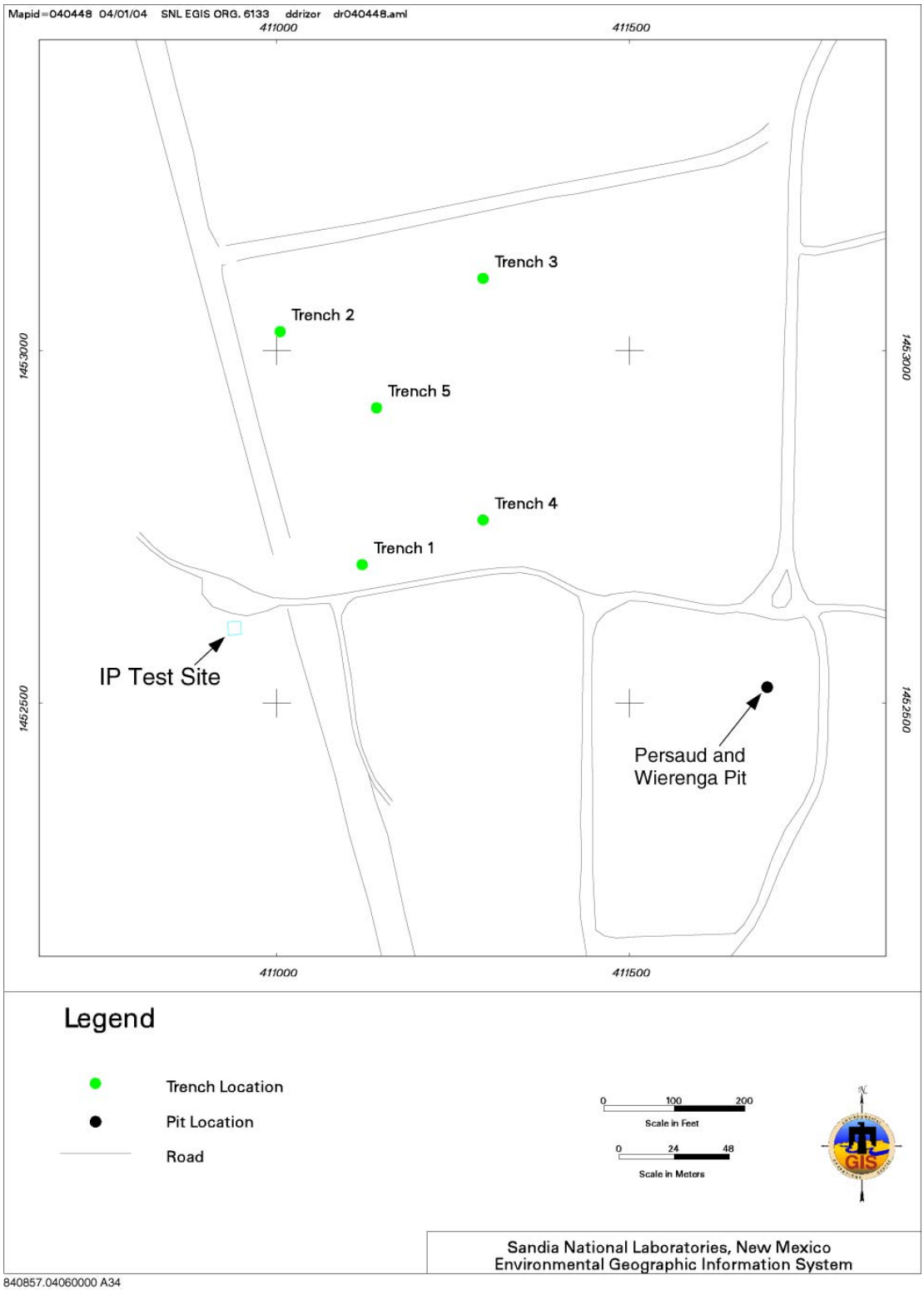

Figure 3-3 Location of Instantaneous Profile Test Site, Trenches, and Pit Within the Study Area

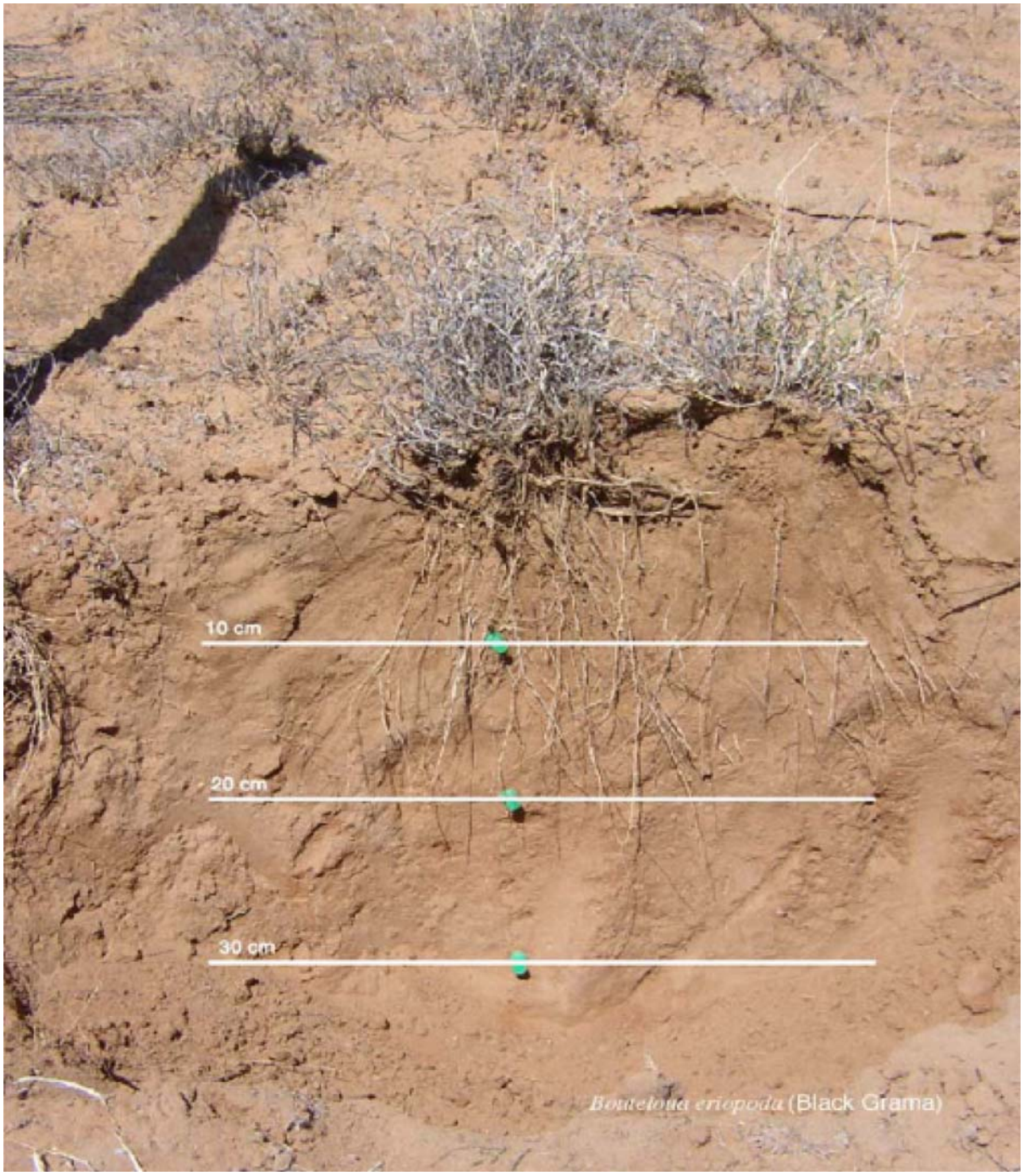

Figure 3-4 Root Depth and Density of Black Grama

Figure 3-5 Root Depth and Density of Threadleaf Snakeweed

Figure 3-6 Root Depth and Density of Galleta Grass

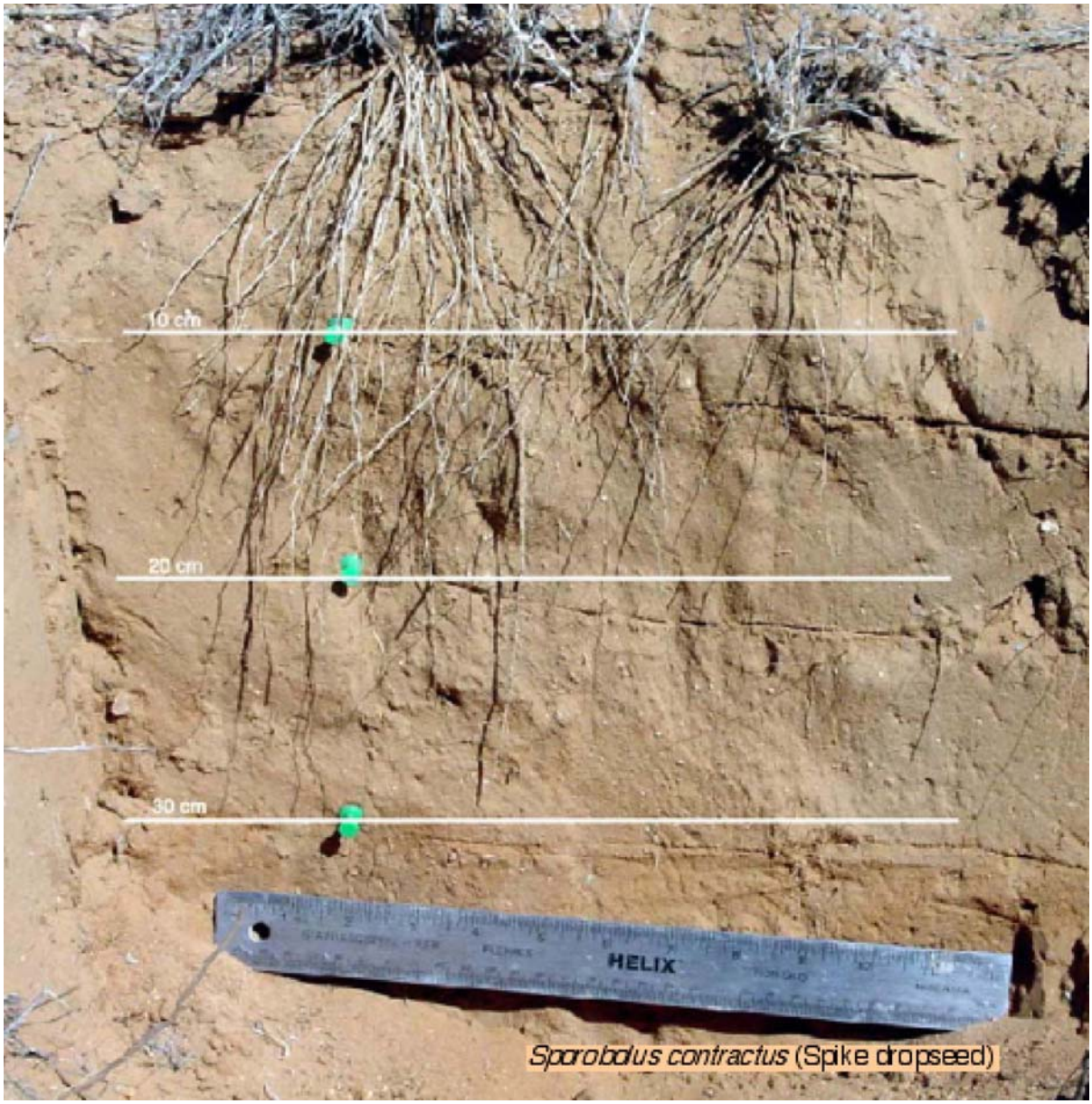

Figure 3-7 Root Depth and Density of Spike Dropseed

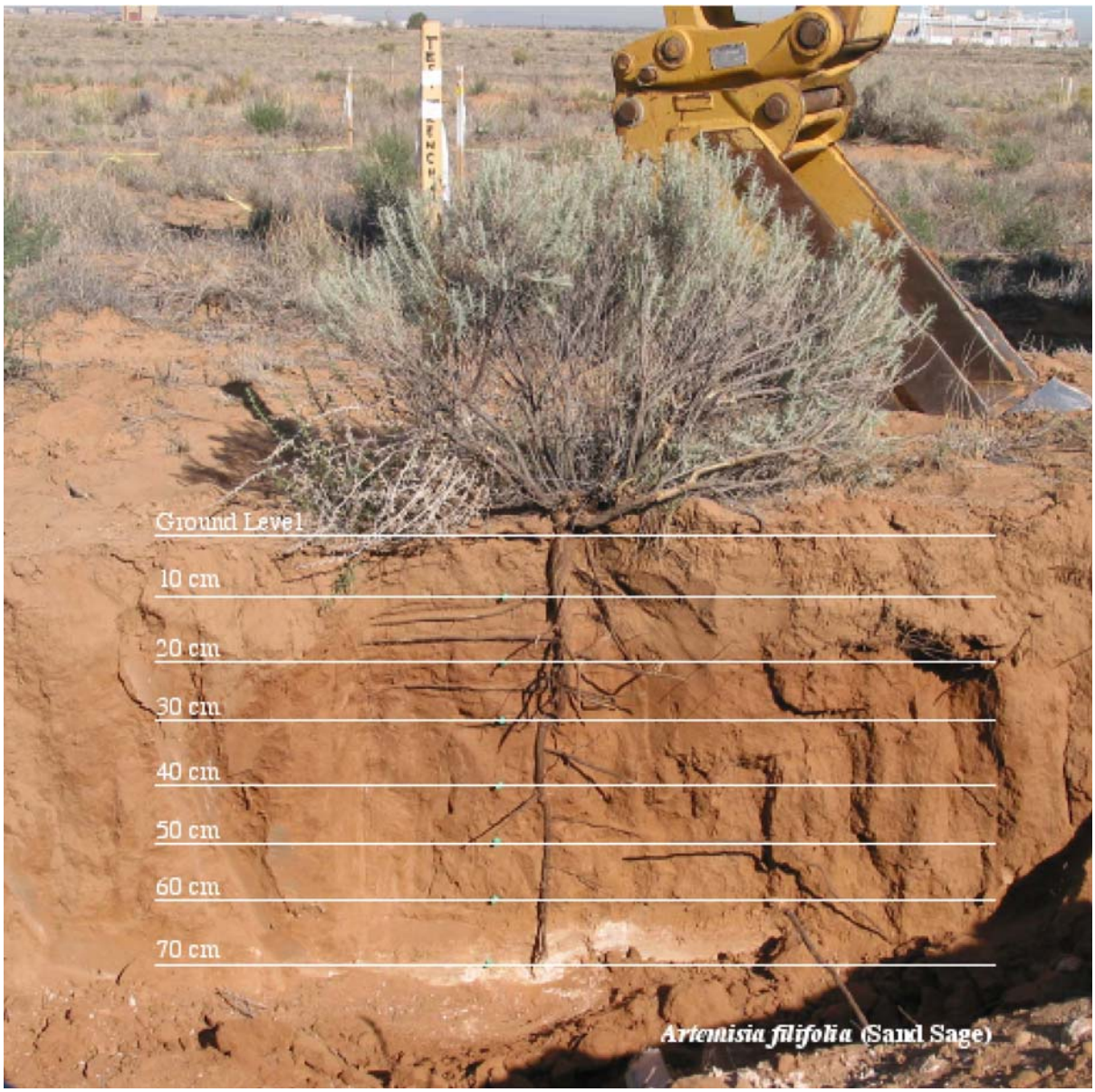

Figure 3-8 Root Depth and Density of Sand Sage

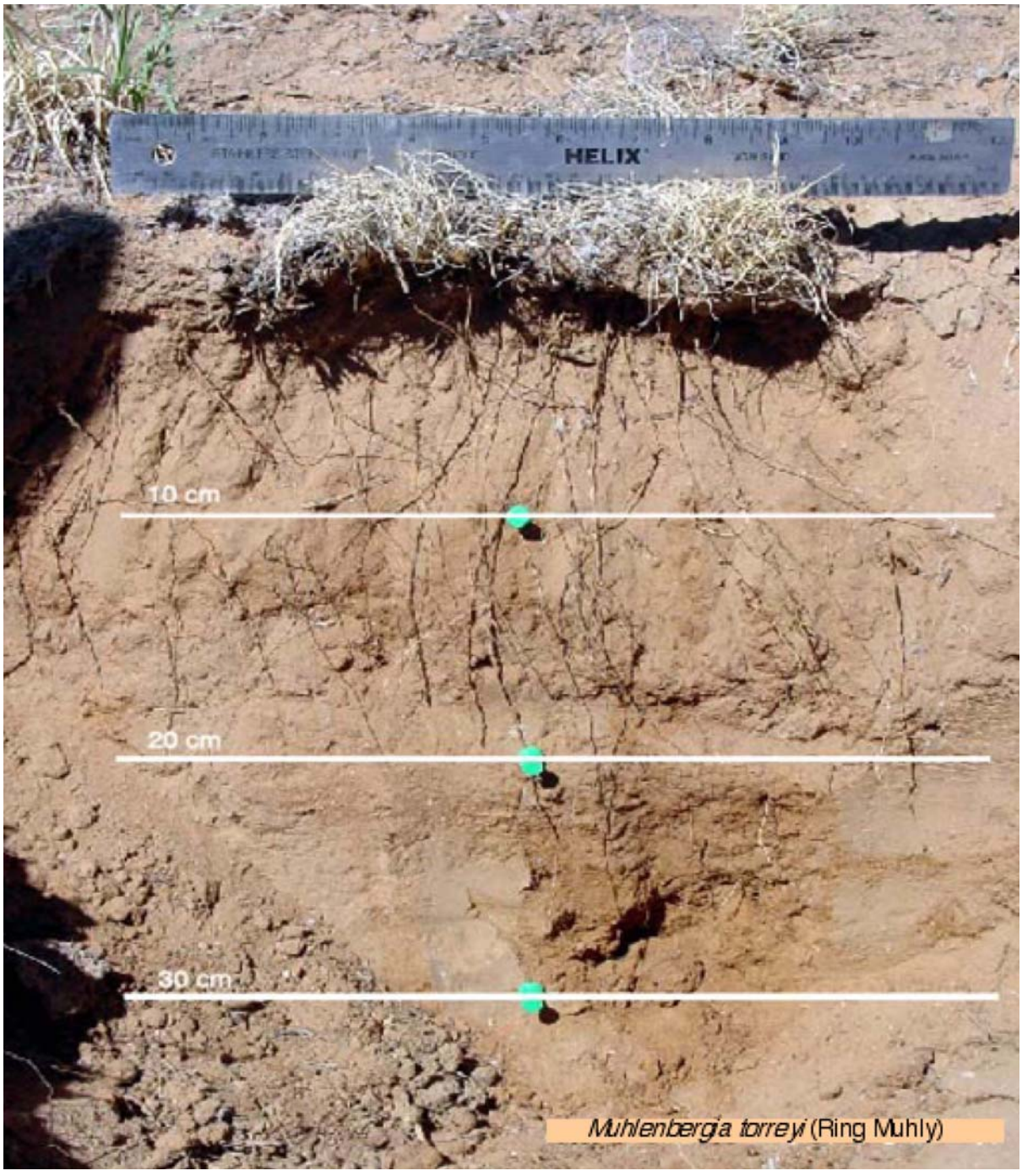

Figure 3-9 Root Depth and Density of Ring Muhly

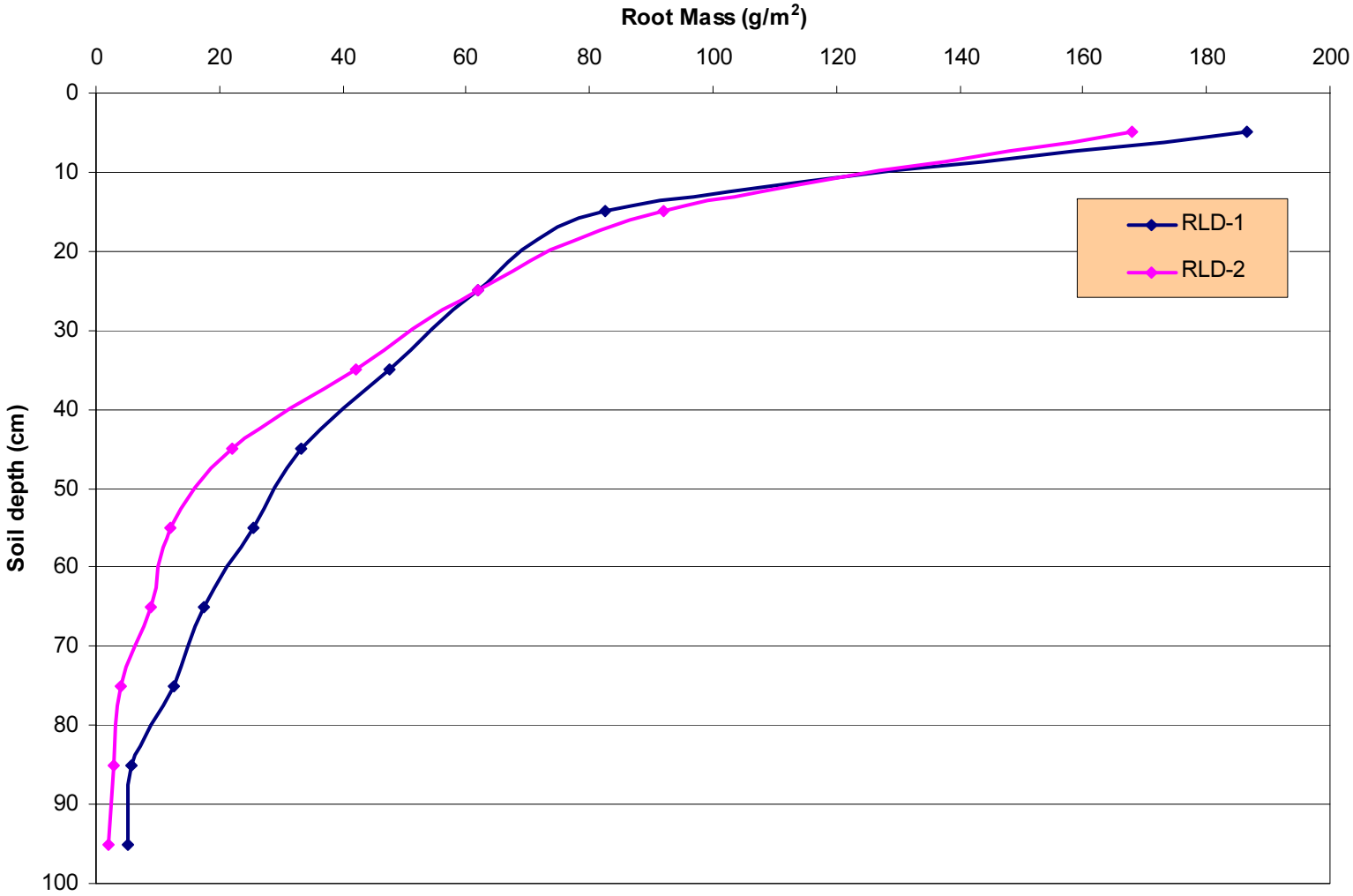

Figure 3-10 Distribution of Root Biomass for RLD-1 and RLD-2

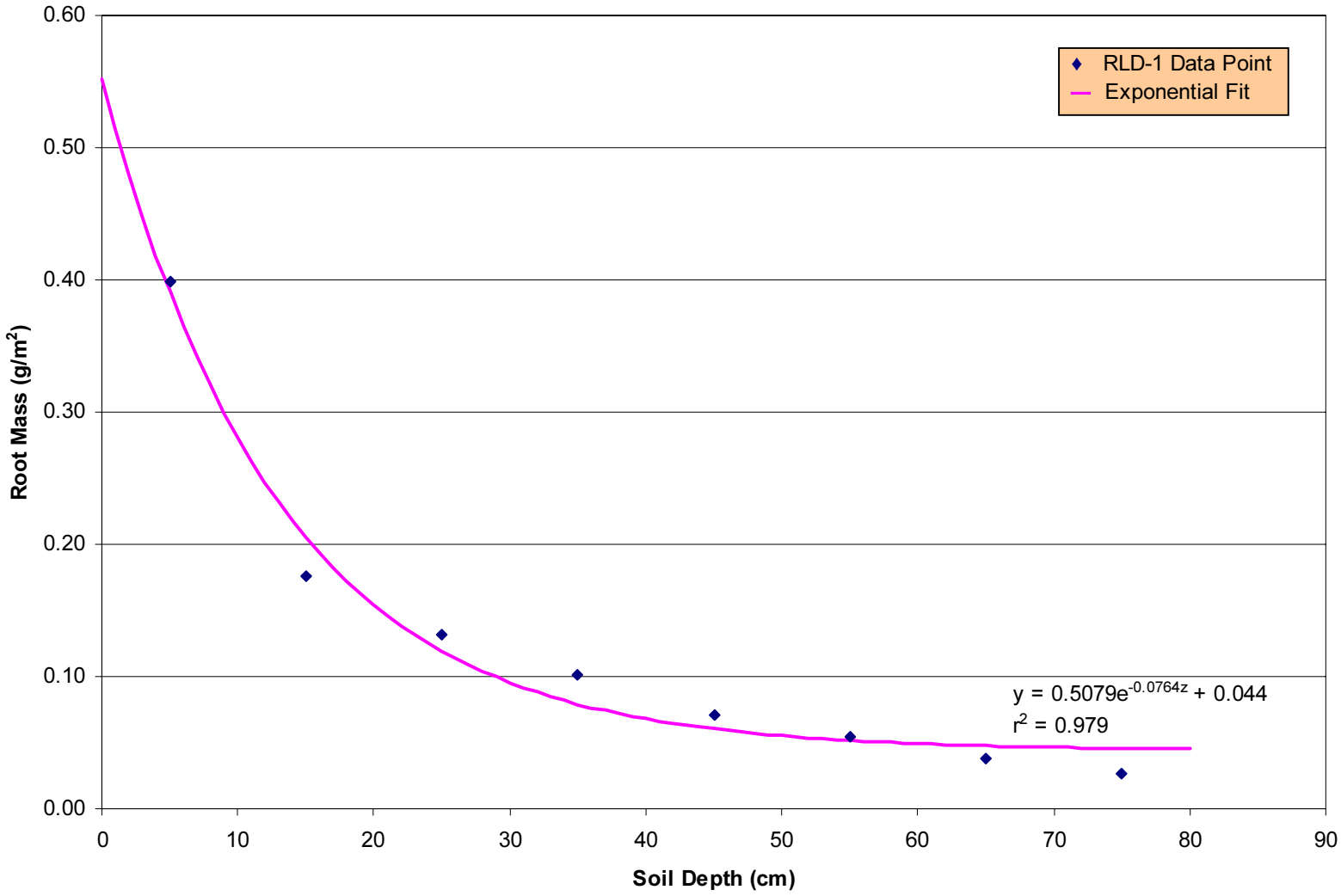

Figure 3-11 Exponential Fit of Normalized Root Biomass for RLD-1

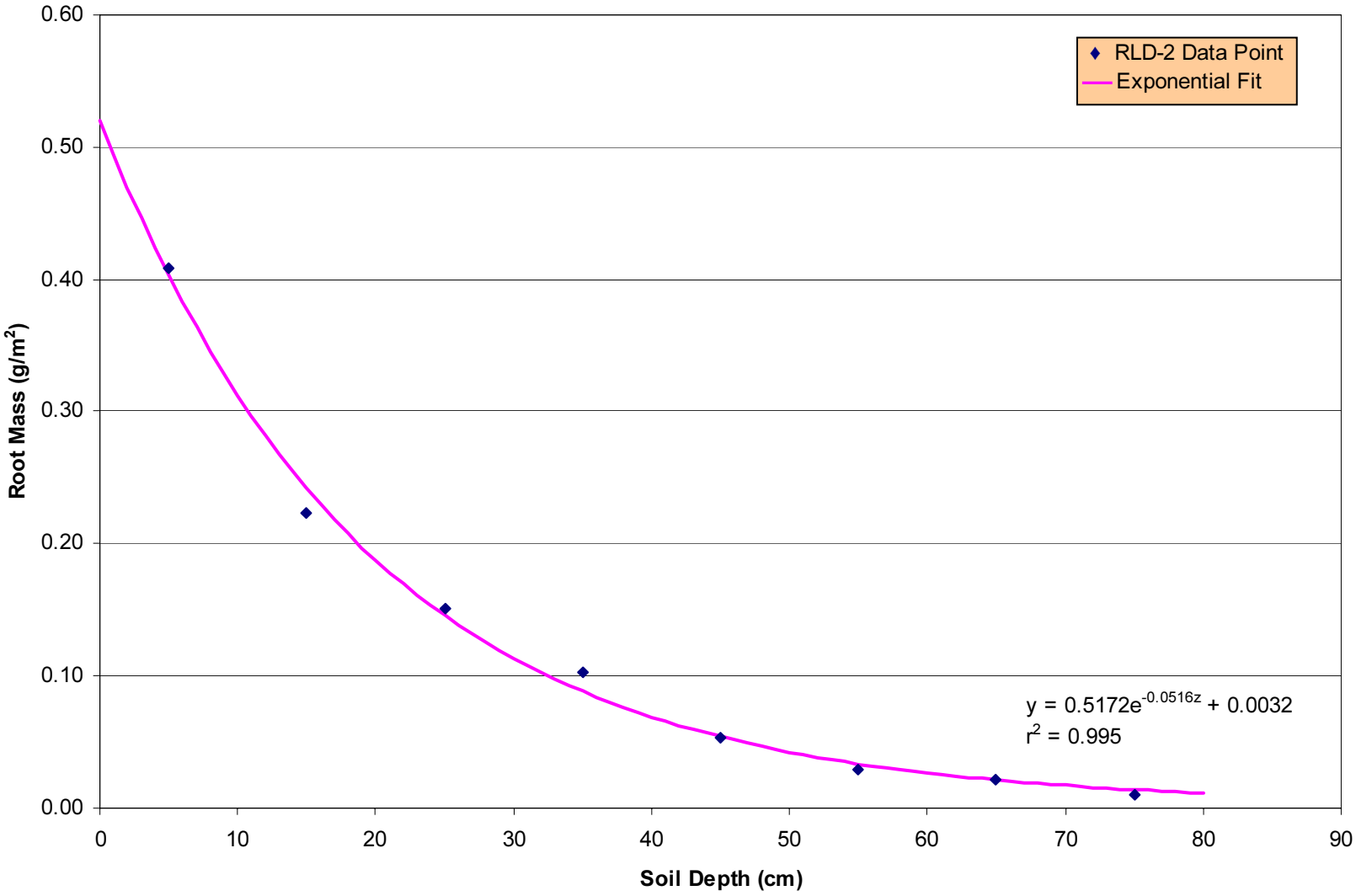

Figure 3-12 Exponential Fit of Normalized Root Biomass for RLD-2

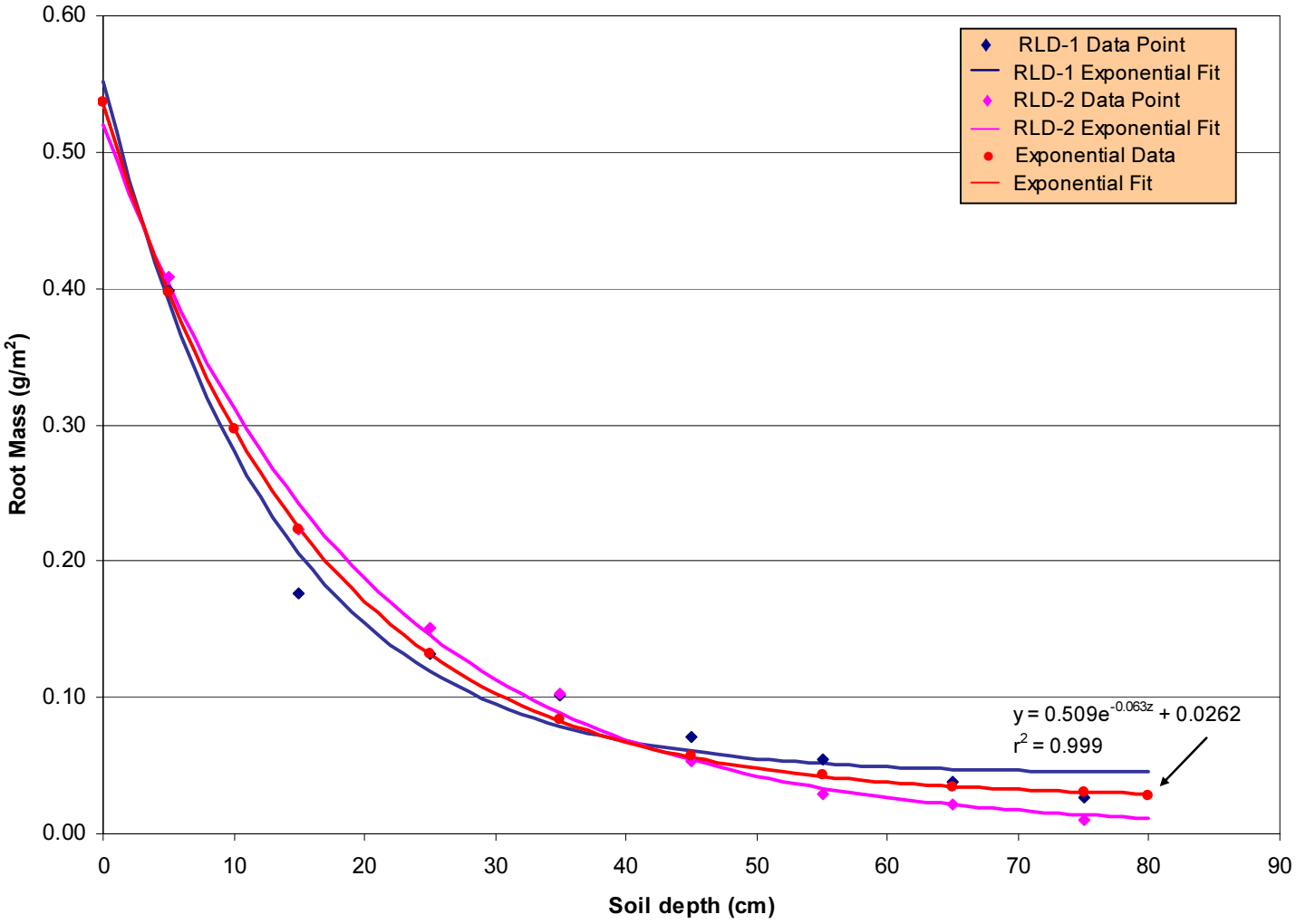

Figure 3-13 Exponential Fit of Combined Normalized Root Biomass for RLD-1 and RLD-2

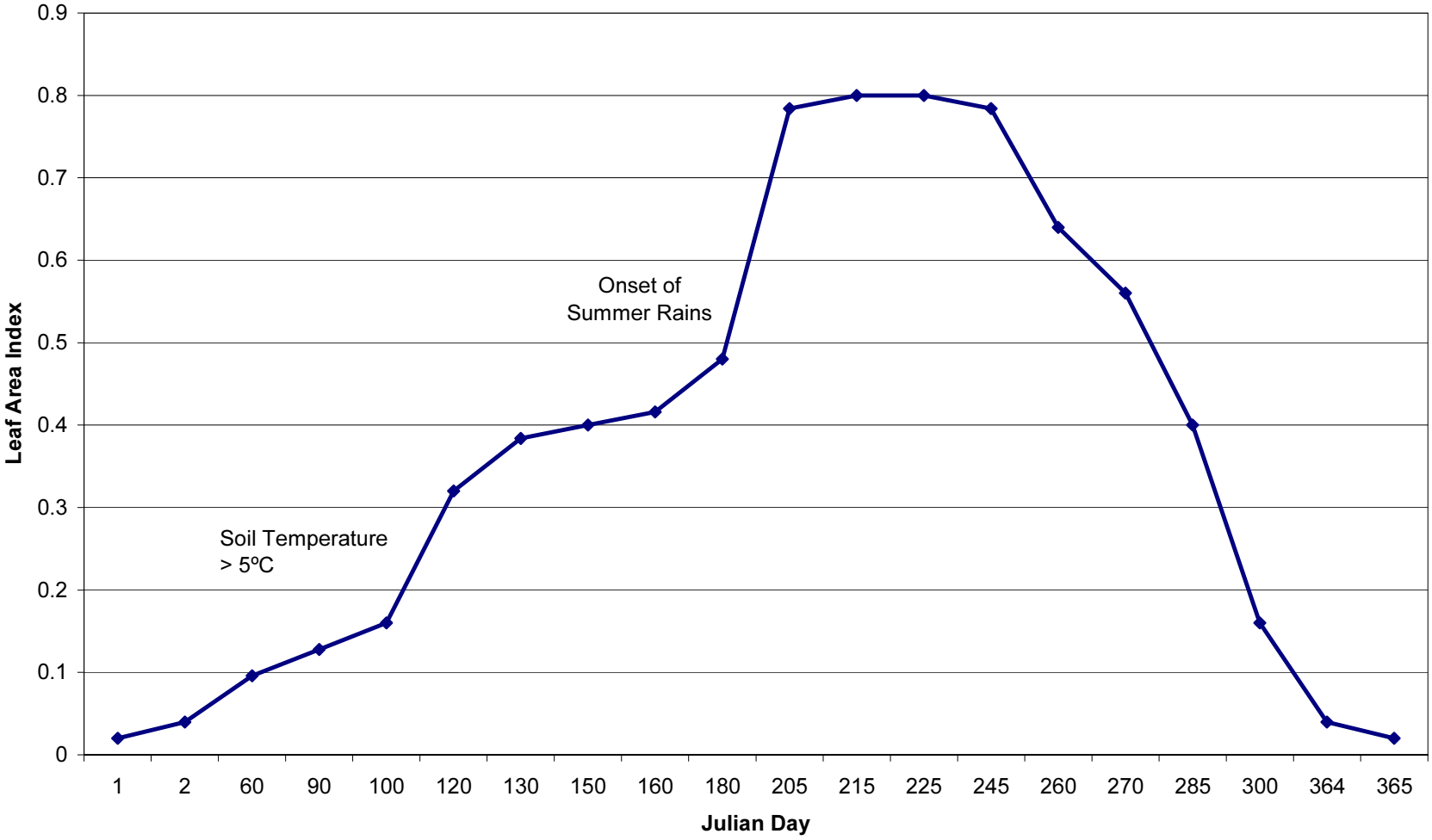

Figure 3-14 Growing Season and Leaf Area Index

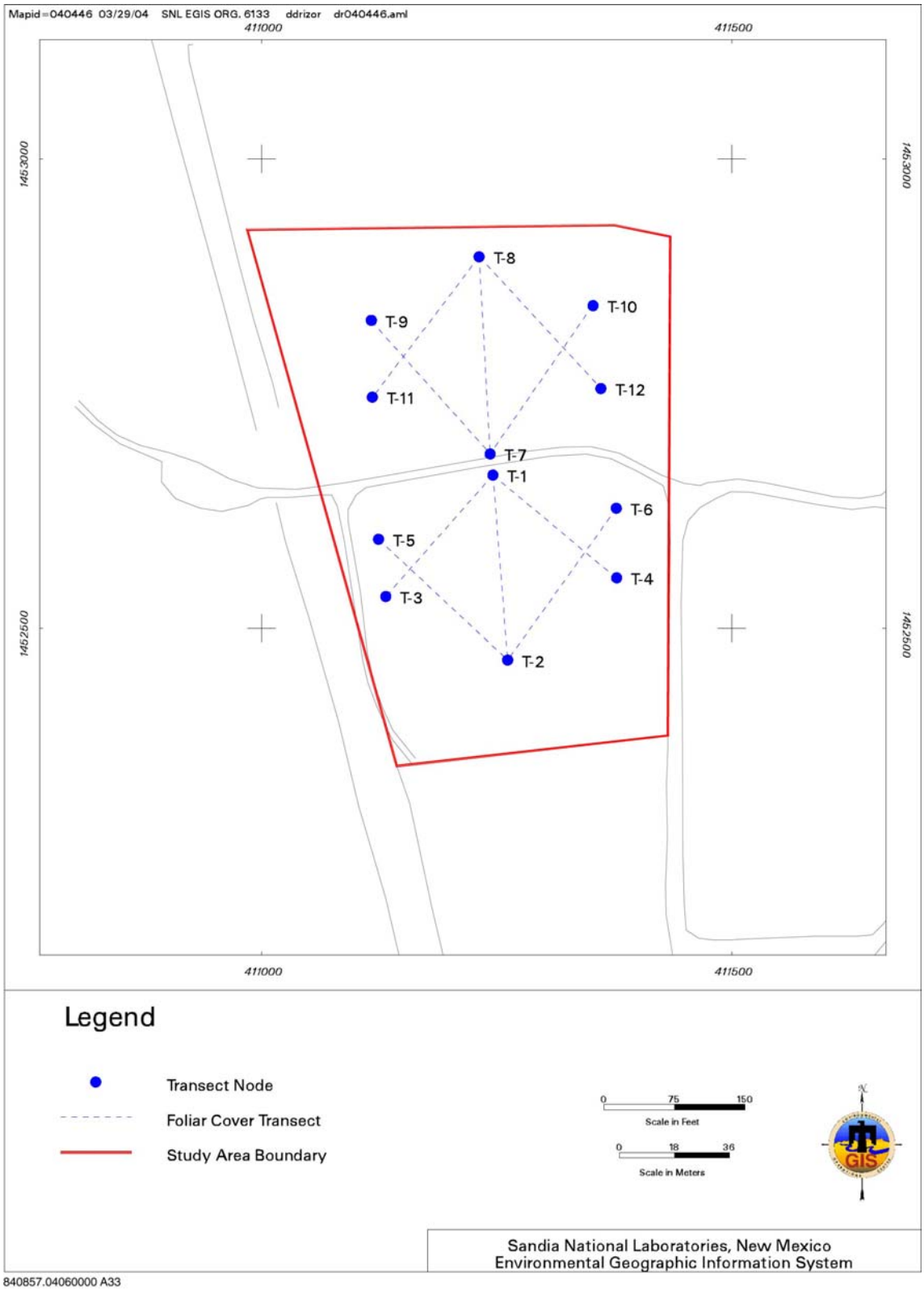

Figure 3-15 Location of Foliar Cover Linear Transects within the Study Area

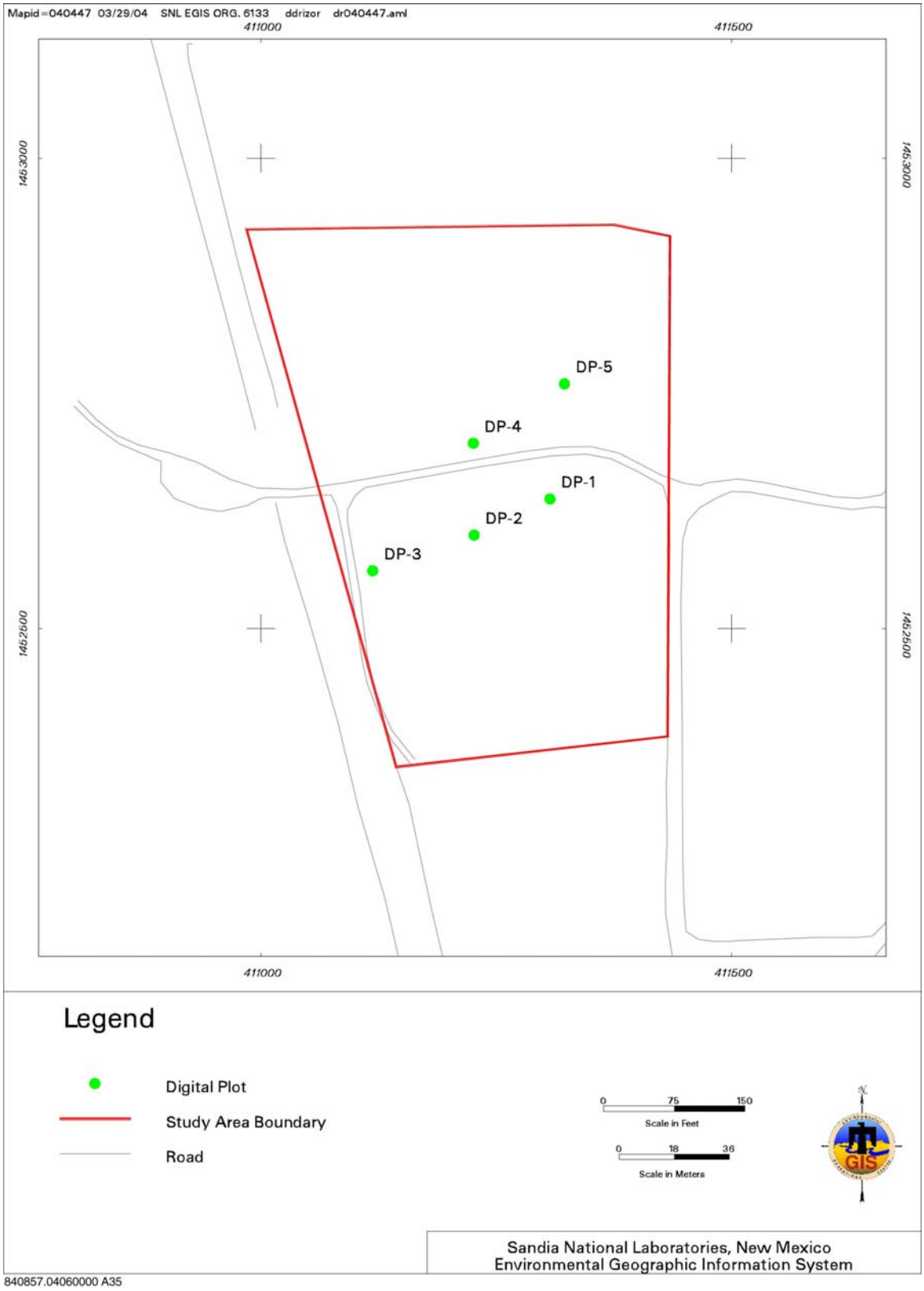

Figure 3-16 Location of Digital Photograph Surface Plots

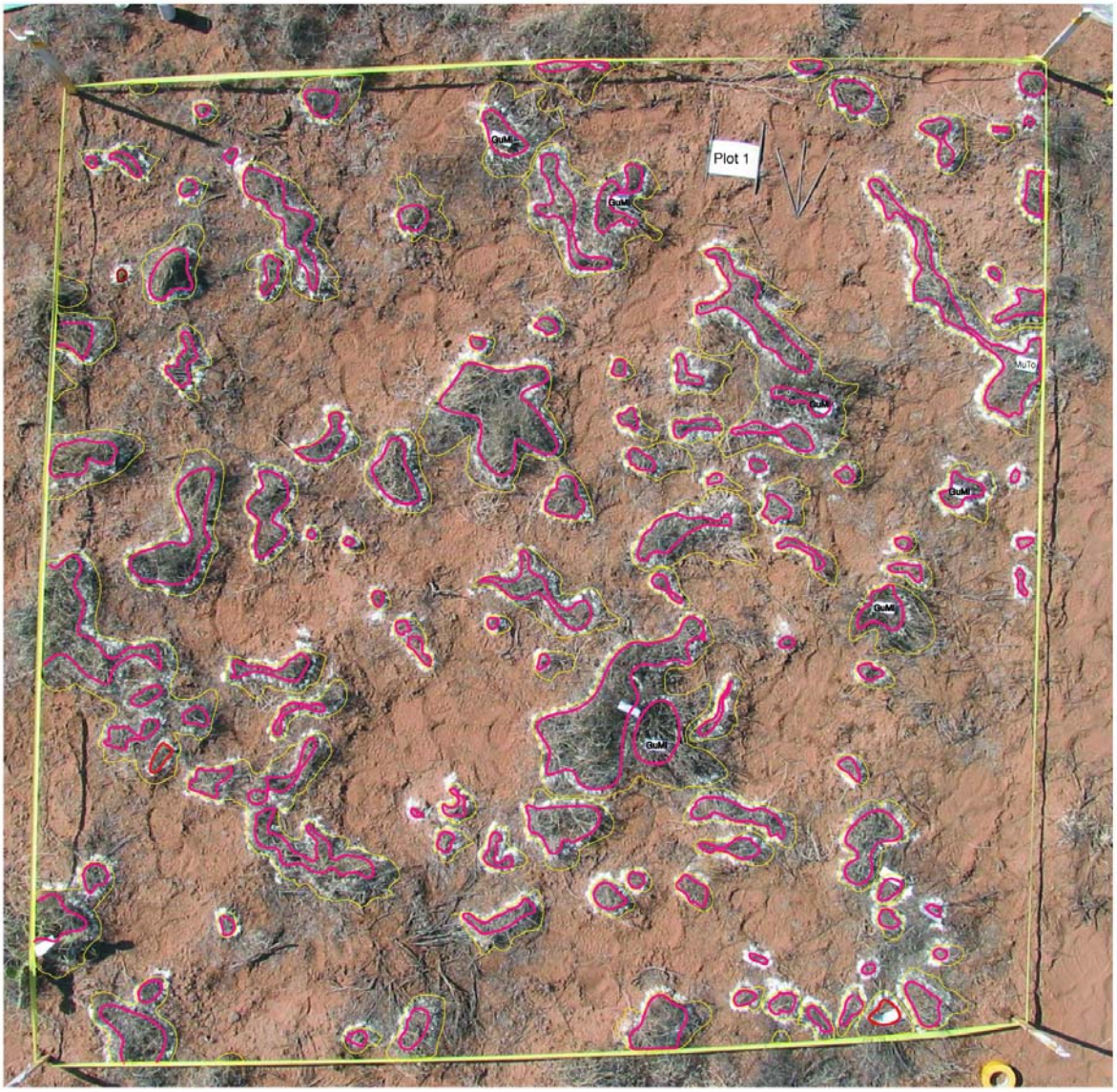

Figure 3-17 Digital Photograph DP-1

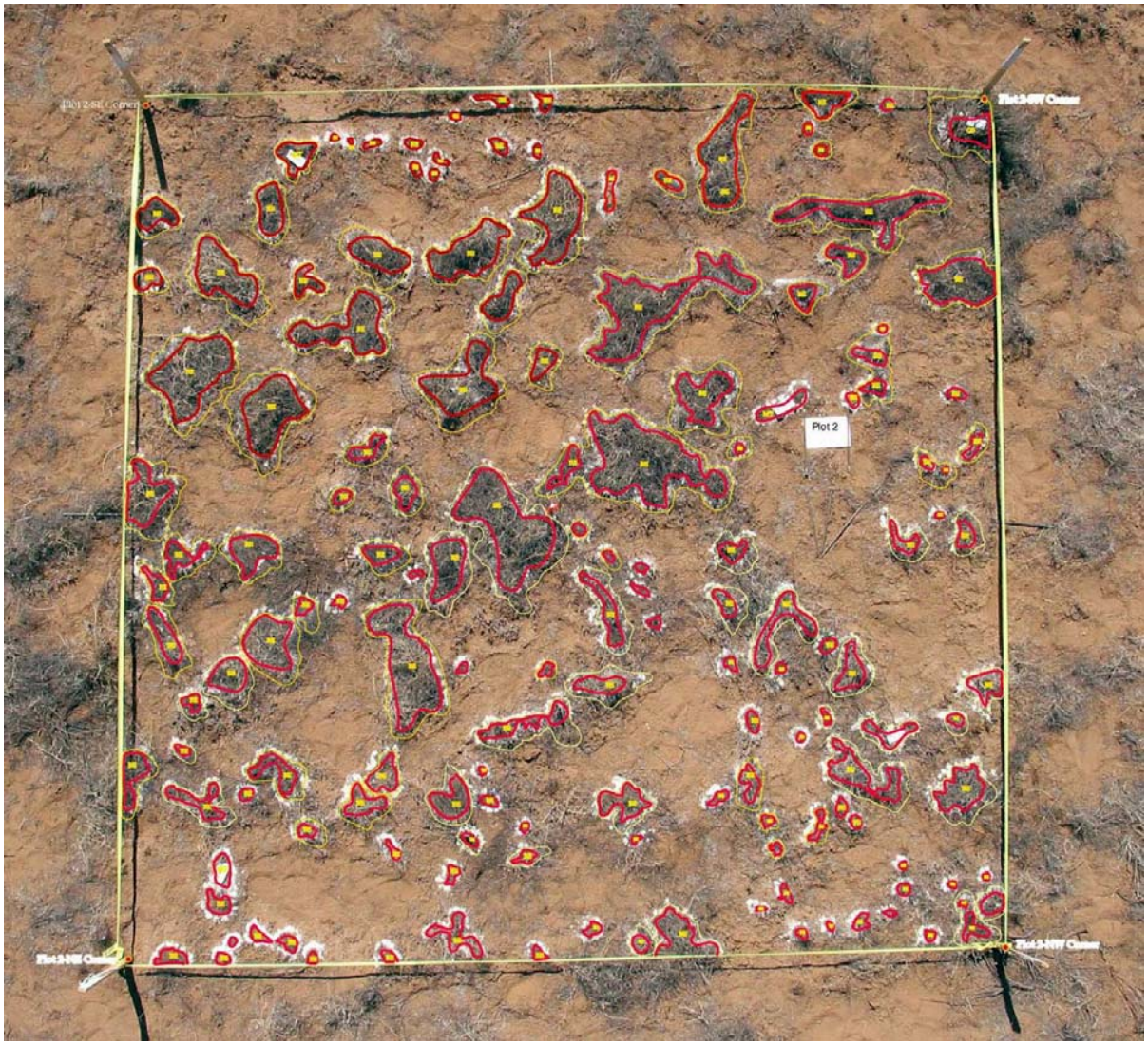

Figure 3-18 Digital Photograph DP-2

Figure 3-19 Digital Photograph DP-3

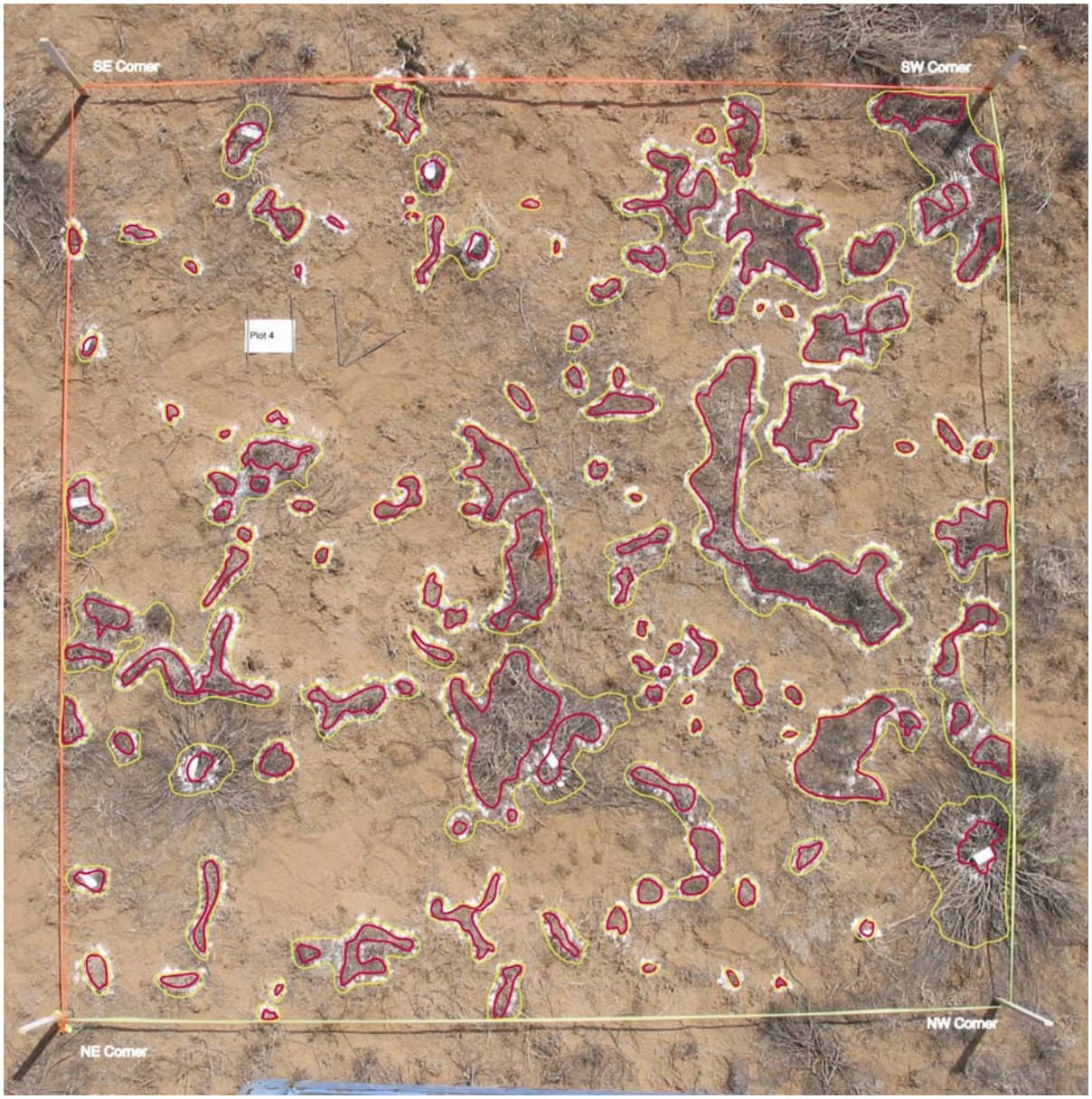

Figure 3-20 Digital Photograph DP-4

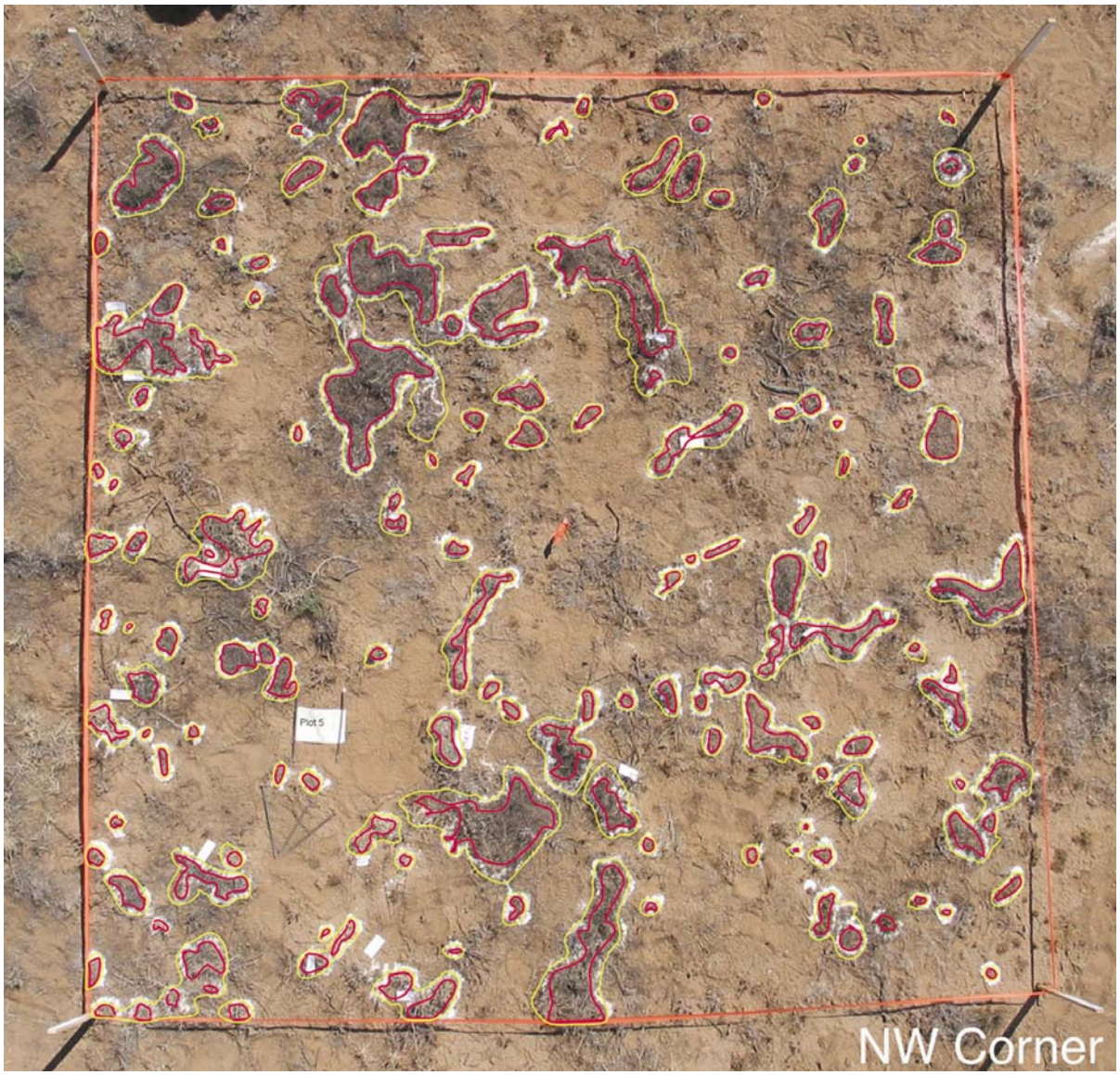

Figure 3-21 Digital Photograph DP-5

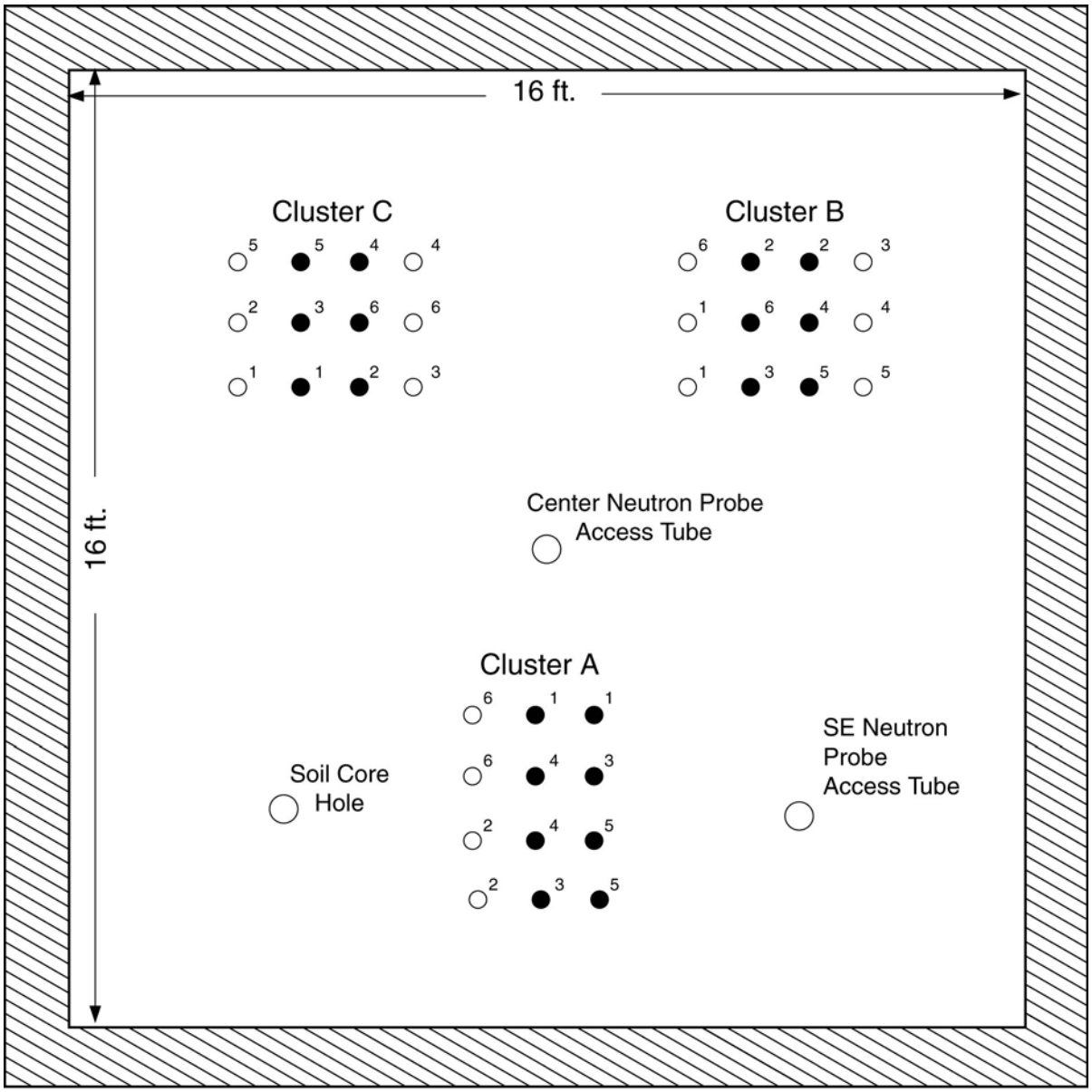

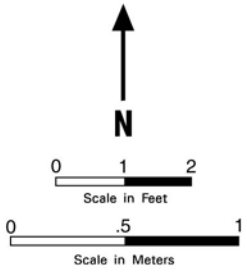

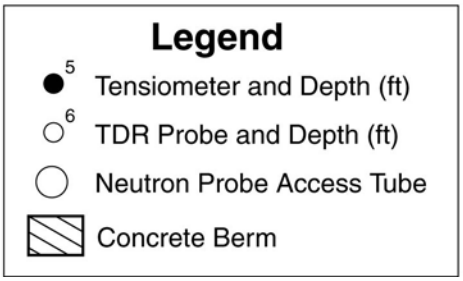

Figure 4-1 Schematic of Instantaneous Profile Test Site—Natural Analogue

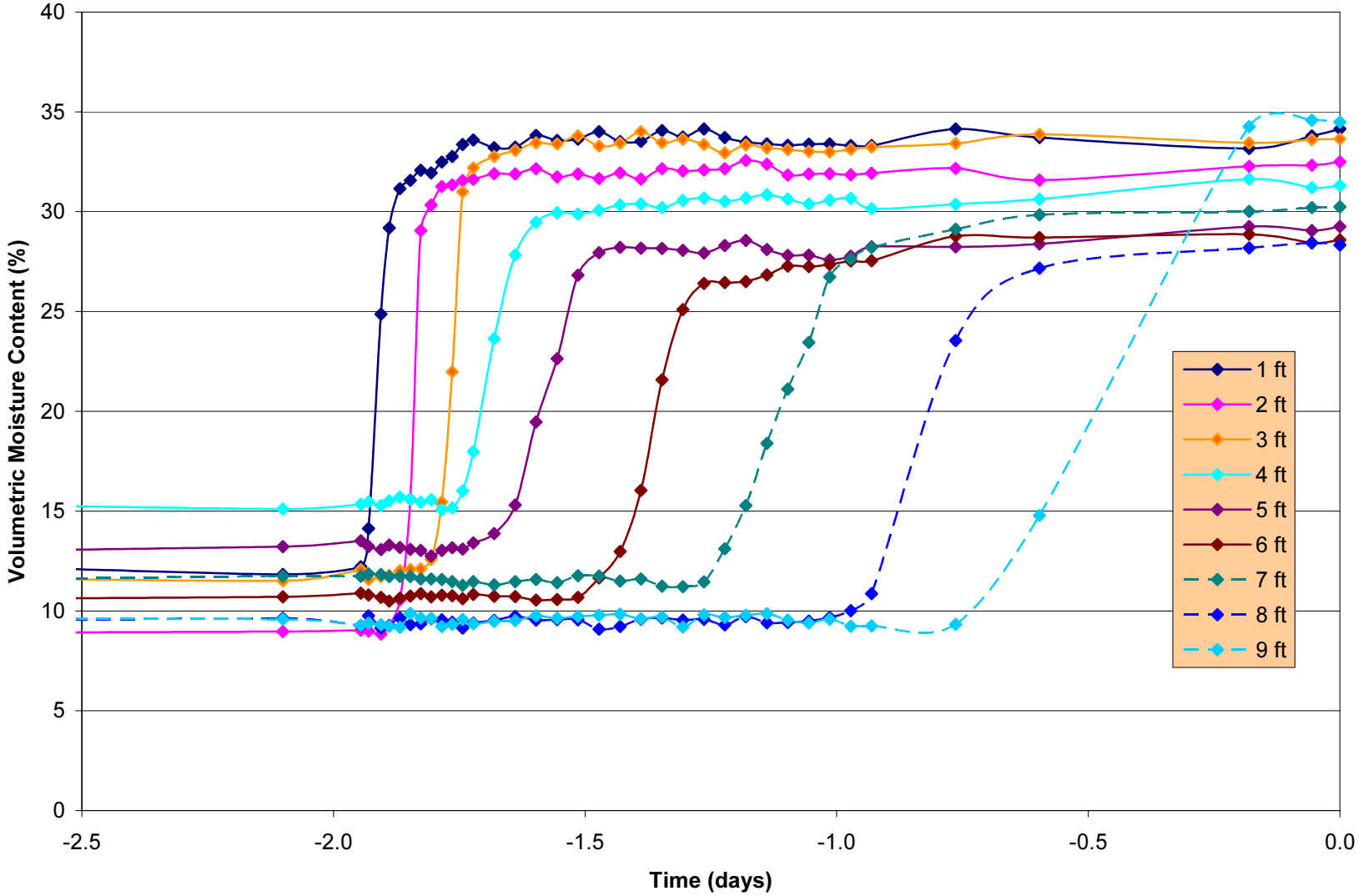

Figure 4-2 Advance of the Wetting Front, Center Neutron Probe Access Tube

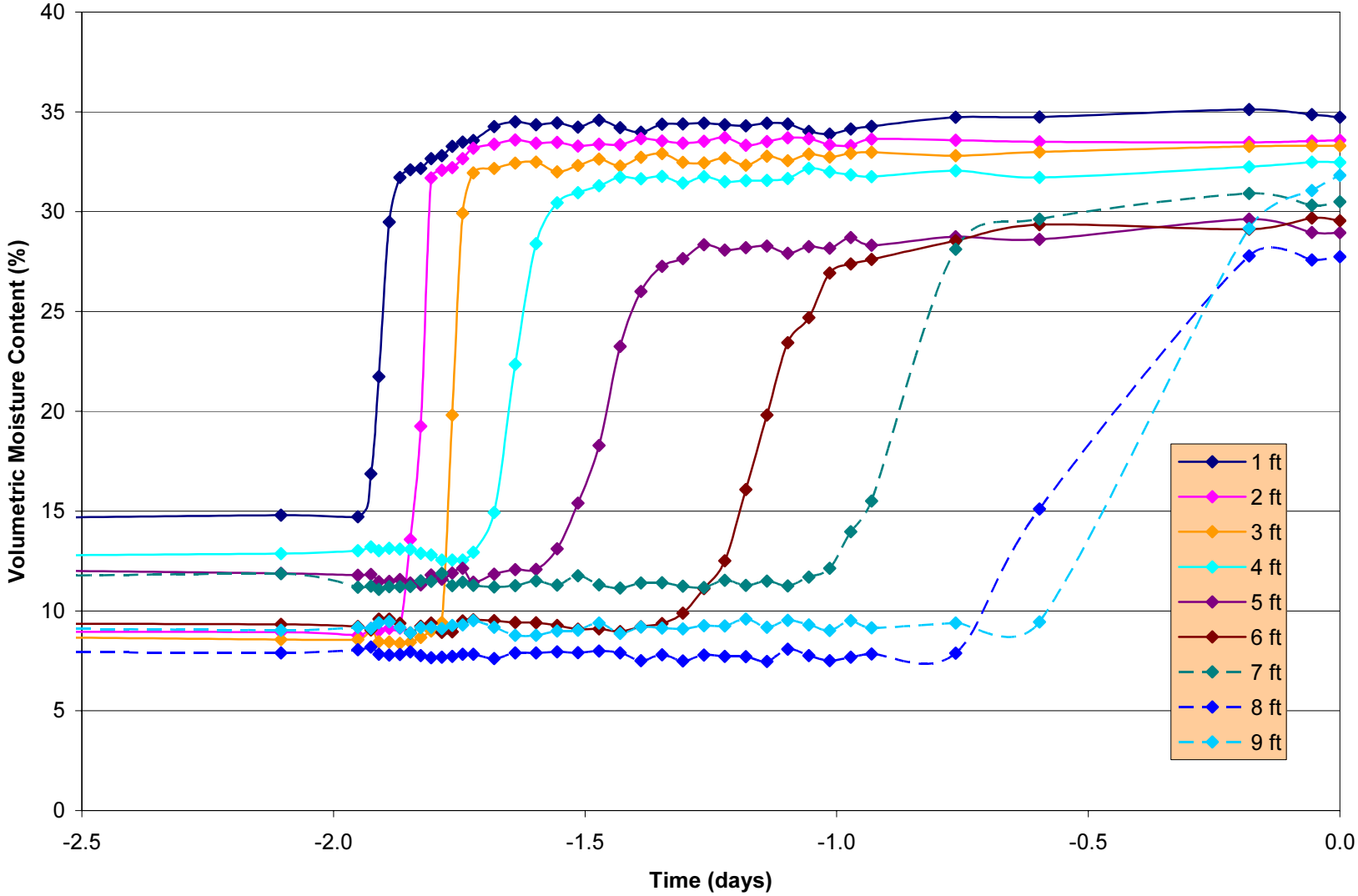

Figure 4-3 Advance of the Wetting Front, Southeast Neutron Probe Access Tube

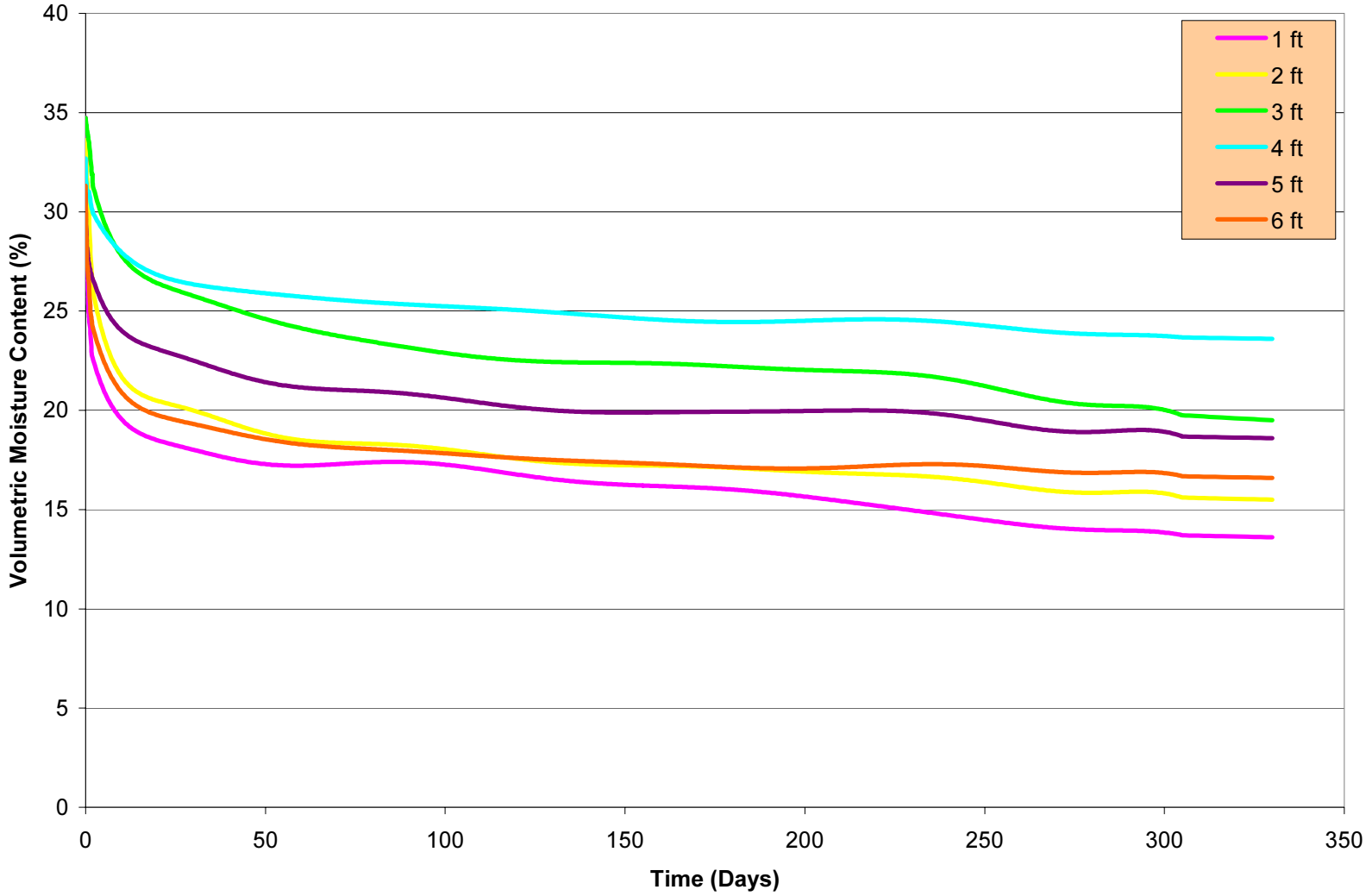

Figure 4-4 Moisture Content, Center Neutron Probe Access Tube, 0 to 330 Days

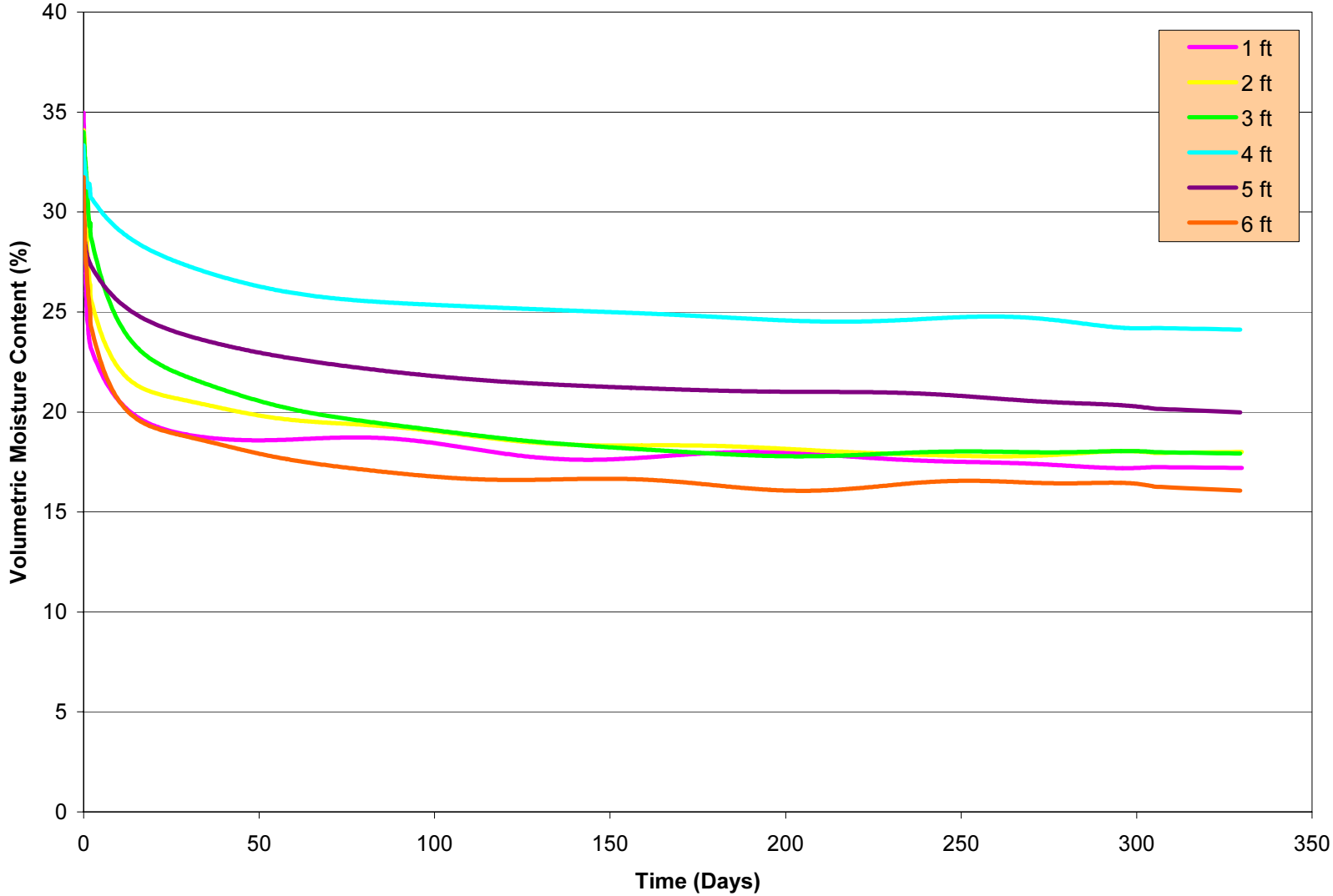

Figure 4-5 Moisture Content, Southeast Neutron Probe Access Tube, 0 to 330 Days

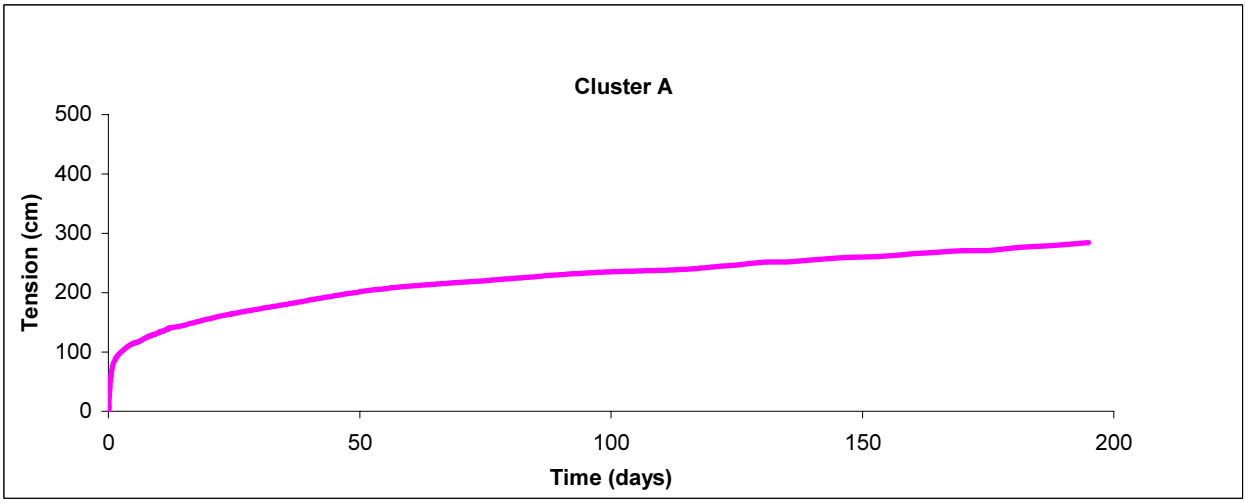

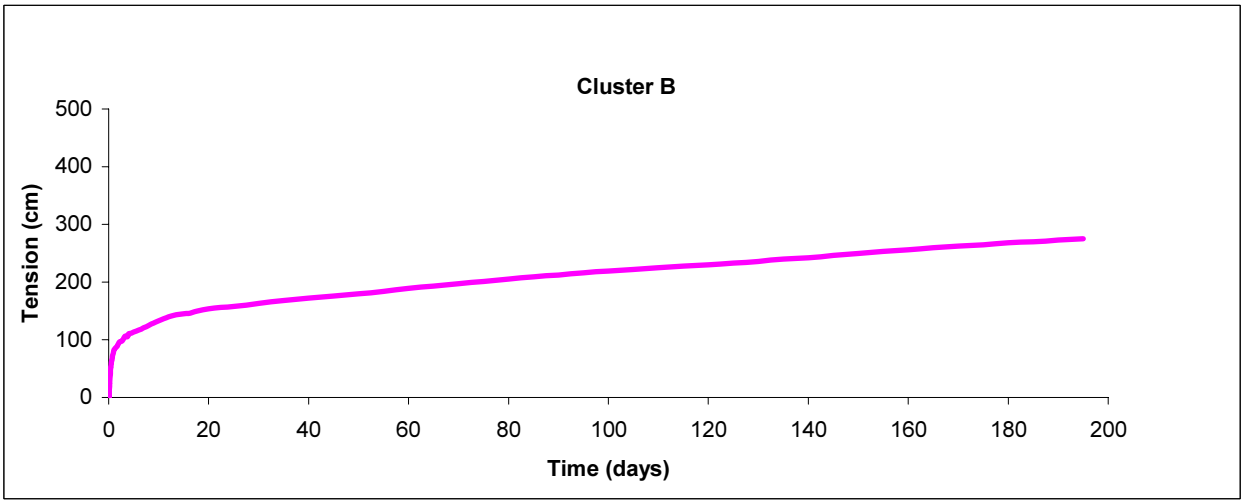

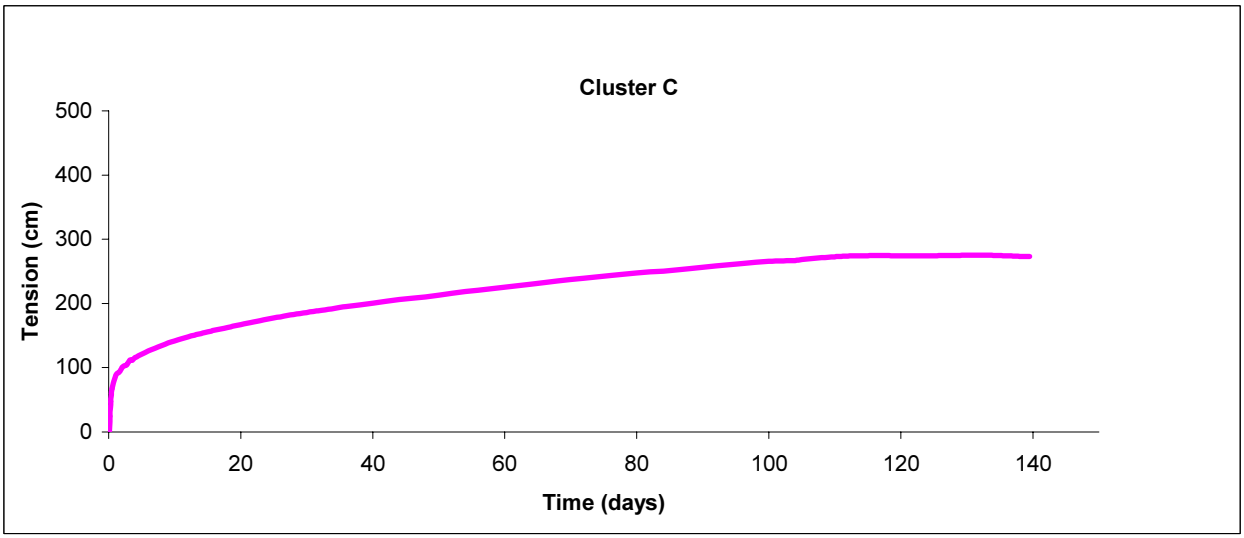

Figure 4-6 Tension Data at 1 ft

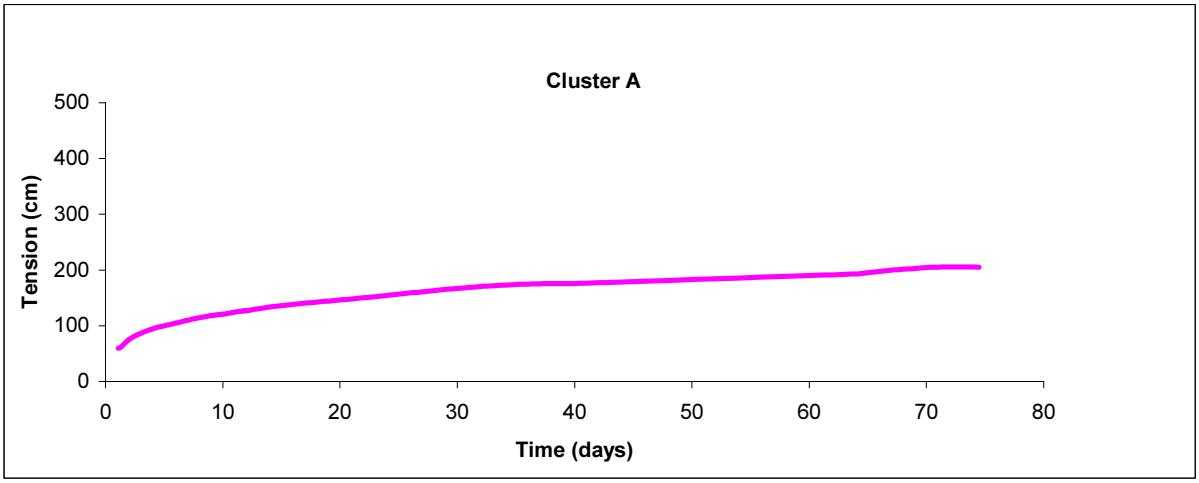

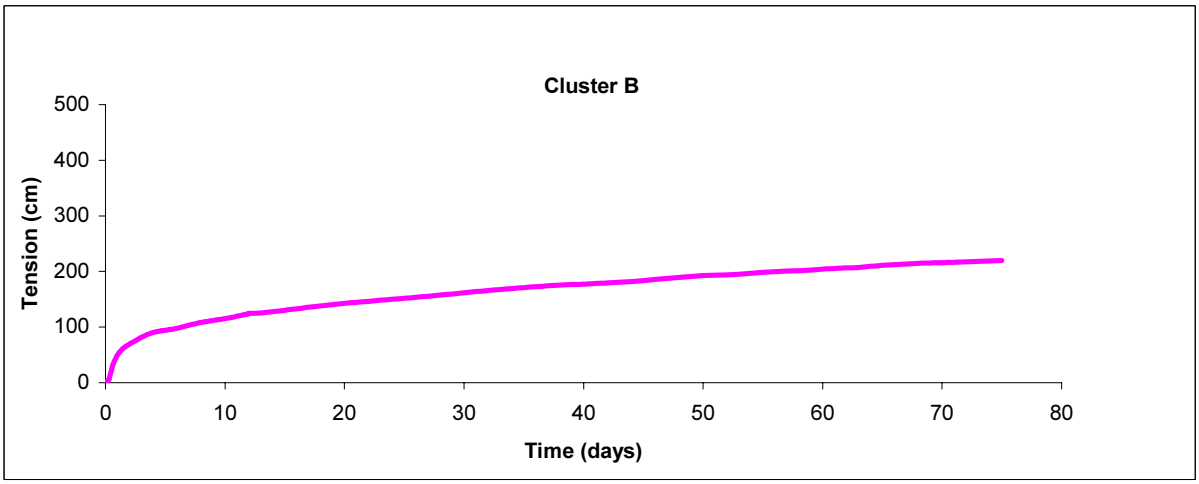

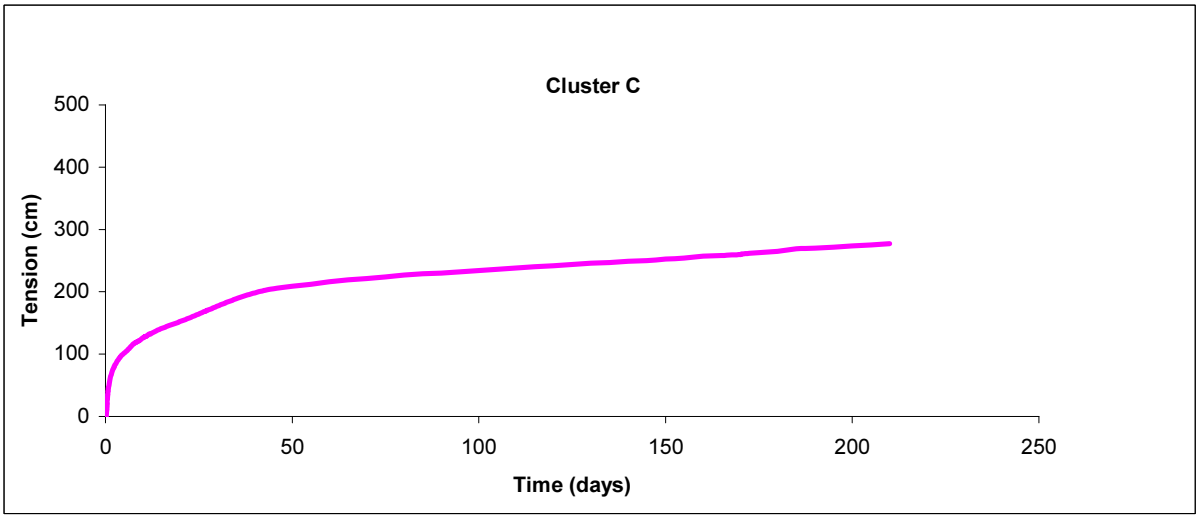

Figure 4-8 Tension Data at 3 ft

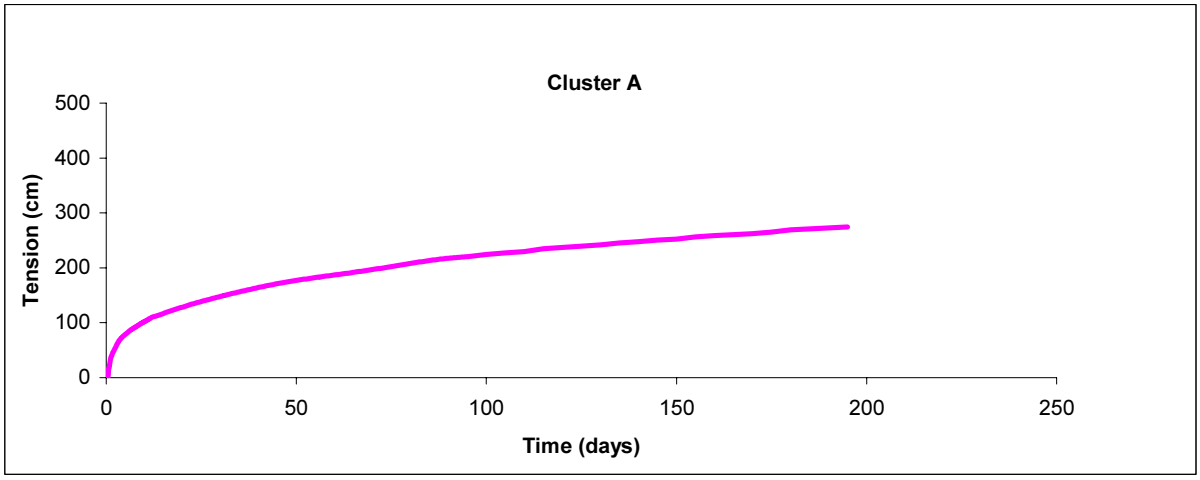

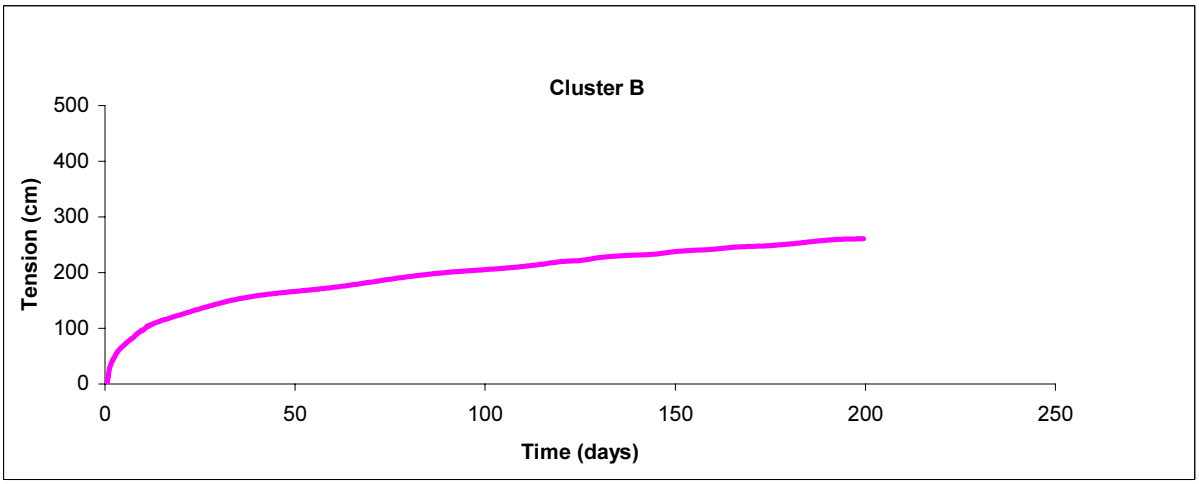

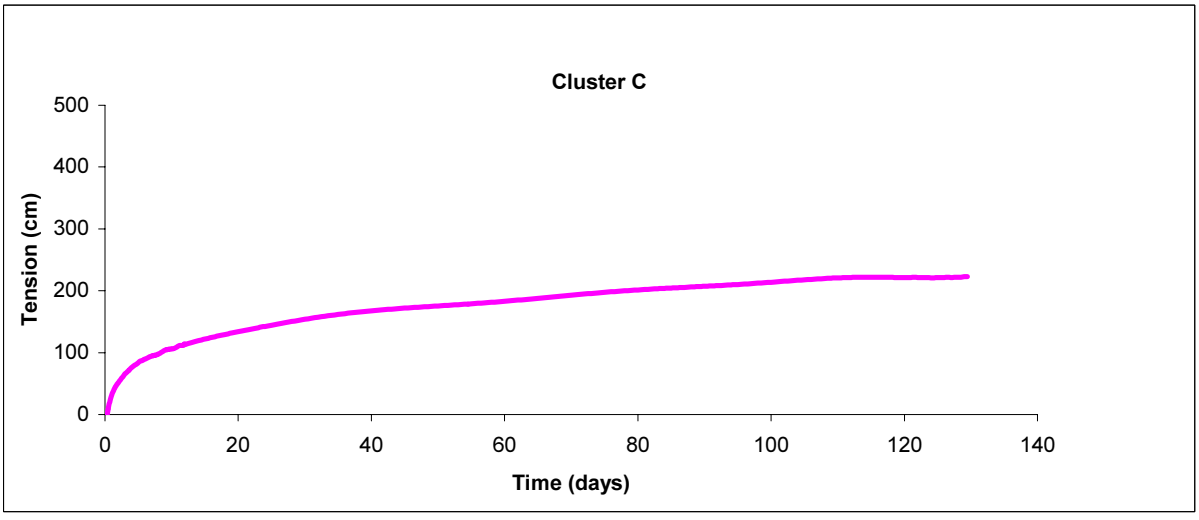

Figure 4-9 Tension Data at 4 ft

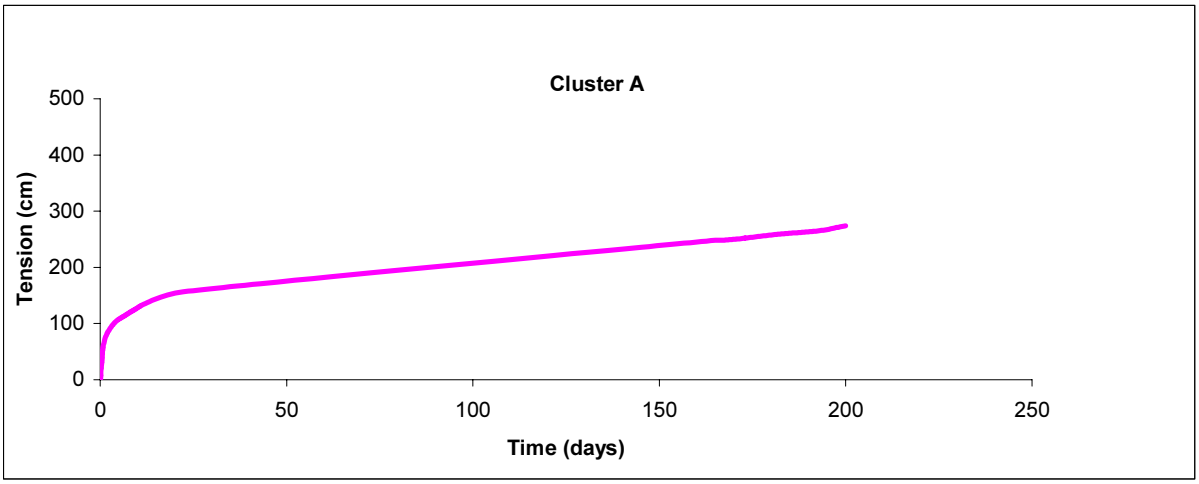

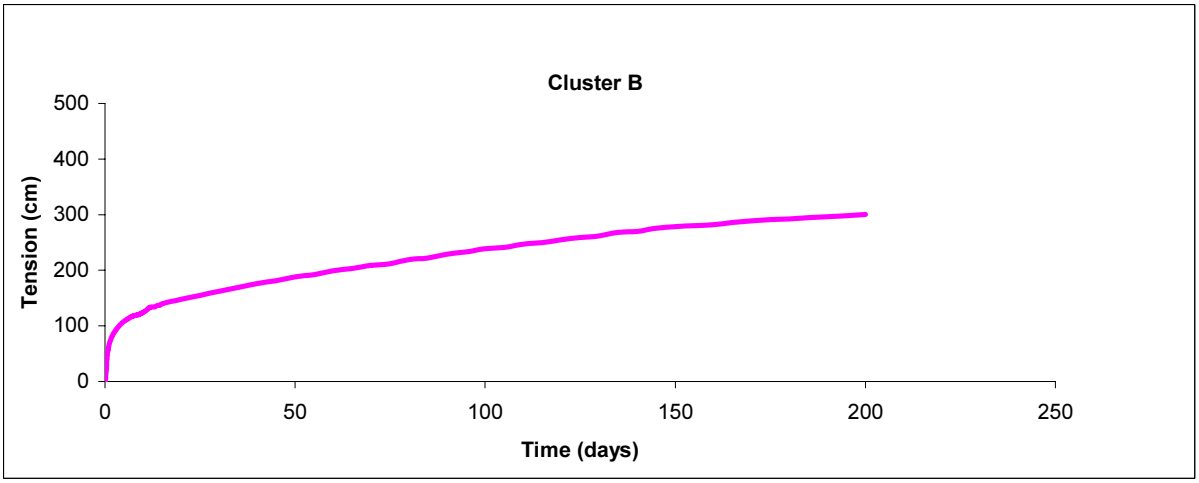

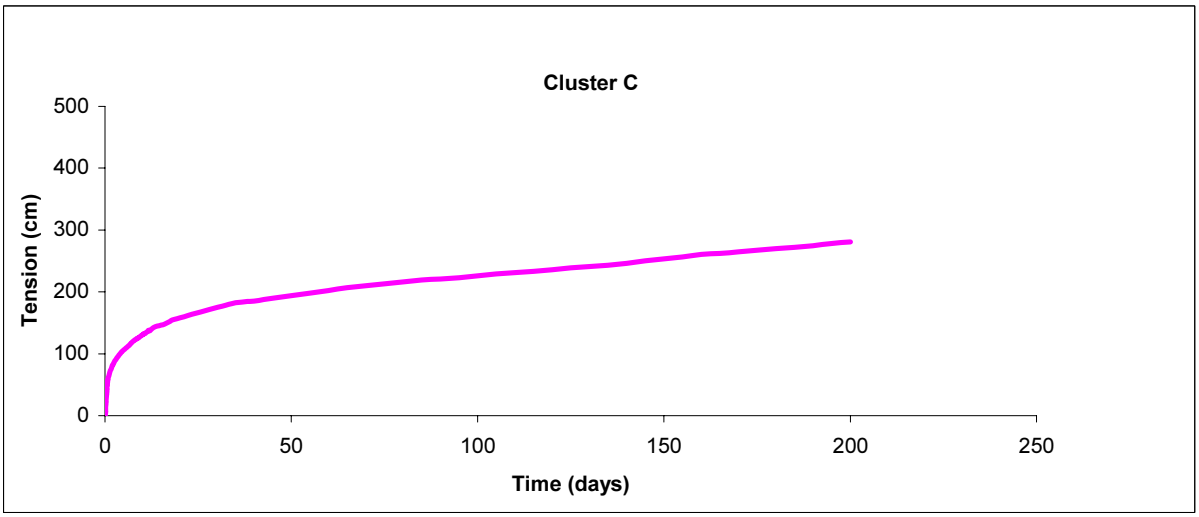

Figure 4-7 Tension Data at 2 ft

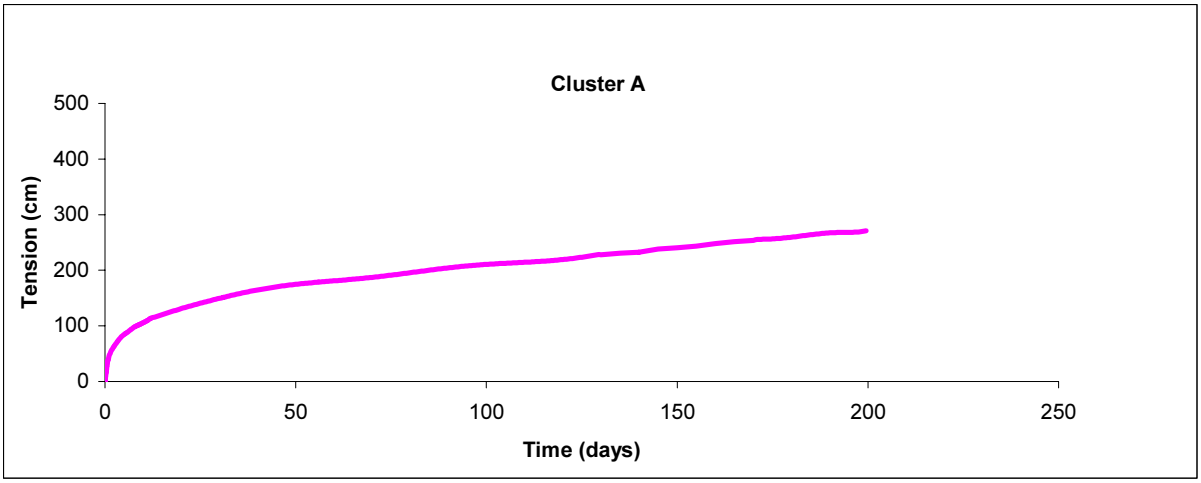

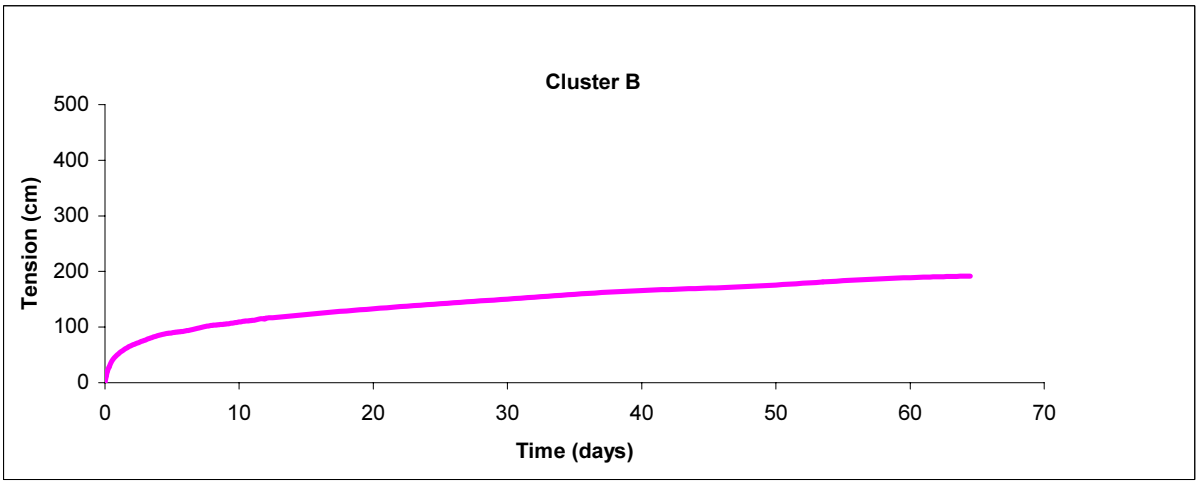

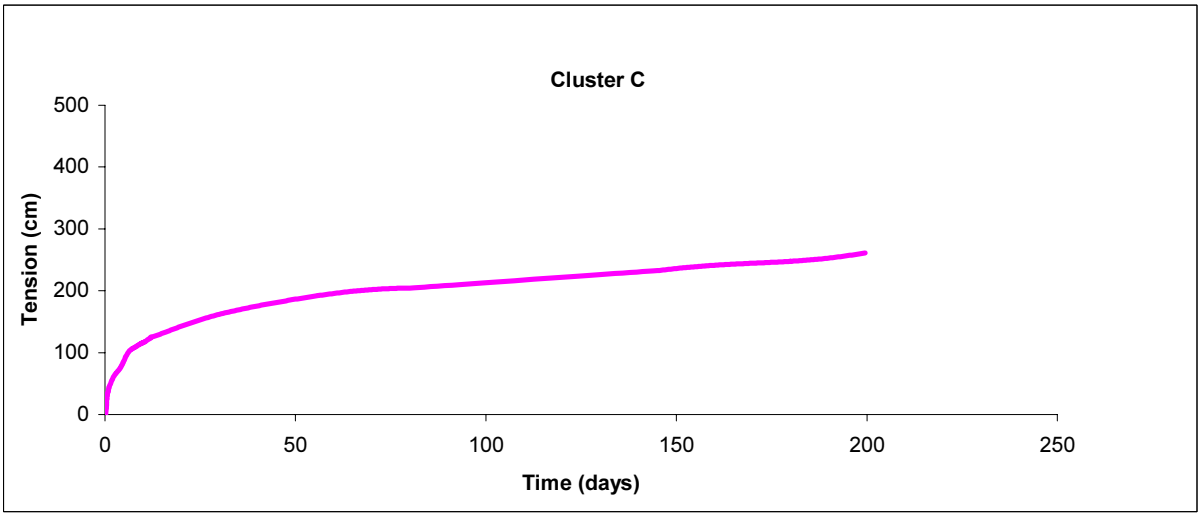

Figure 4-10 Tension Data at 5 ft

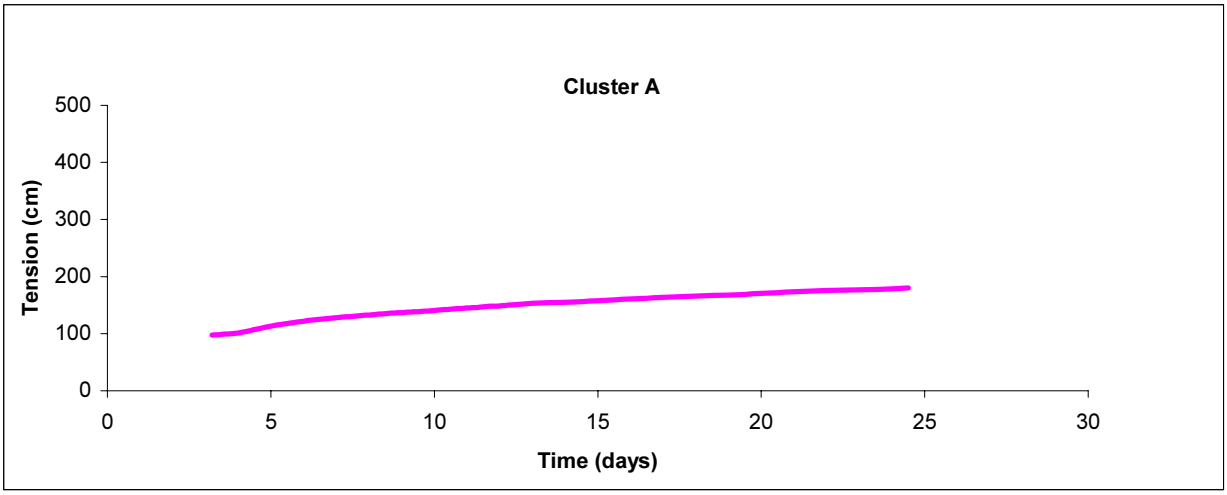

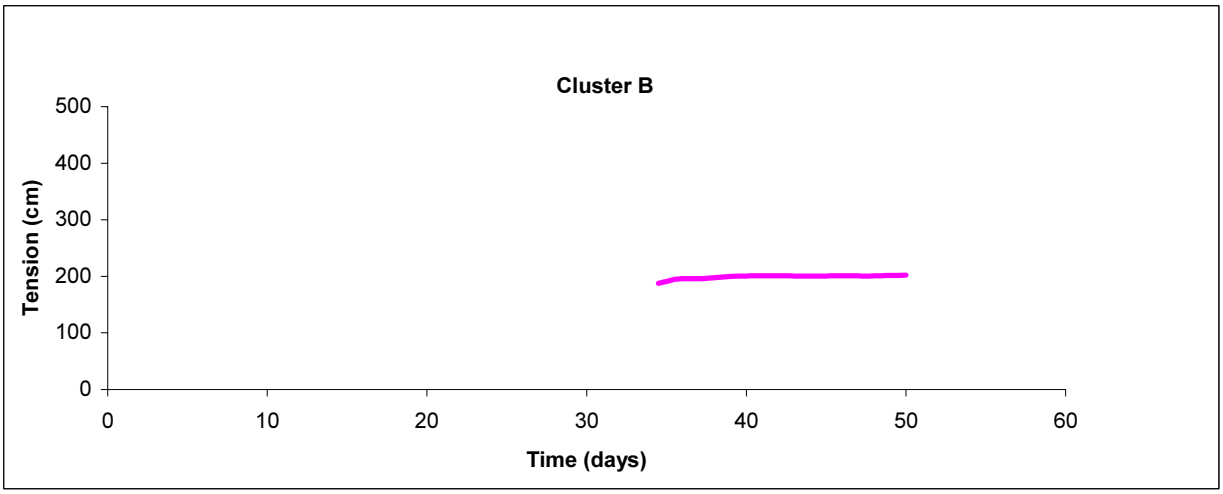

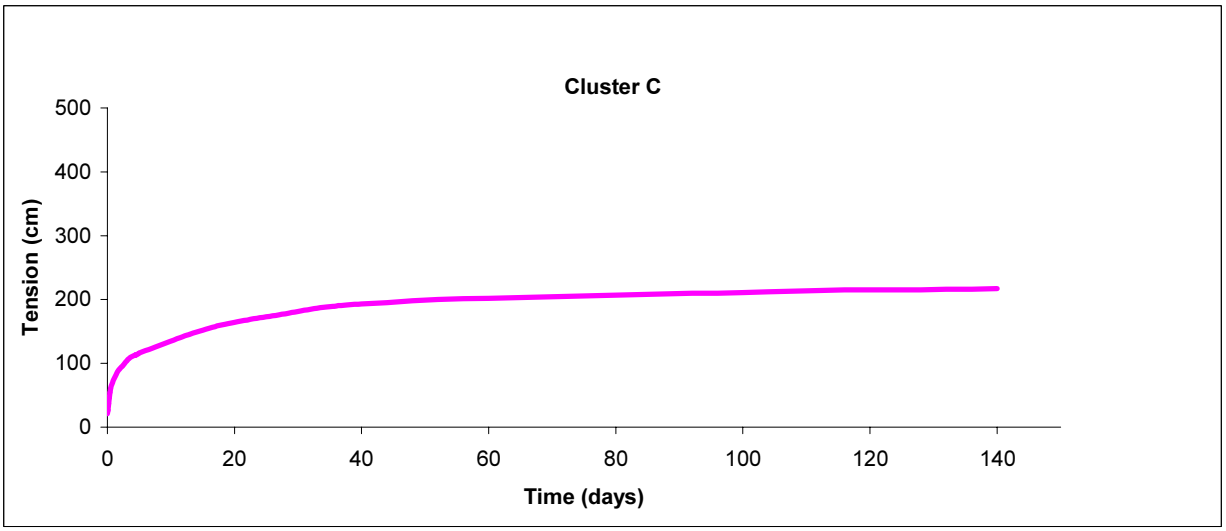

Figure 4-11 Tension Data at 6 ft

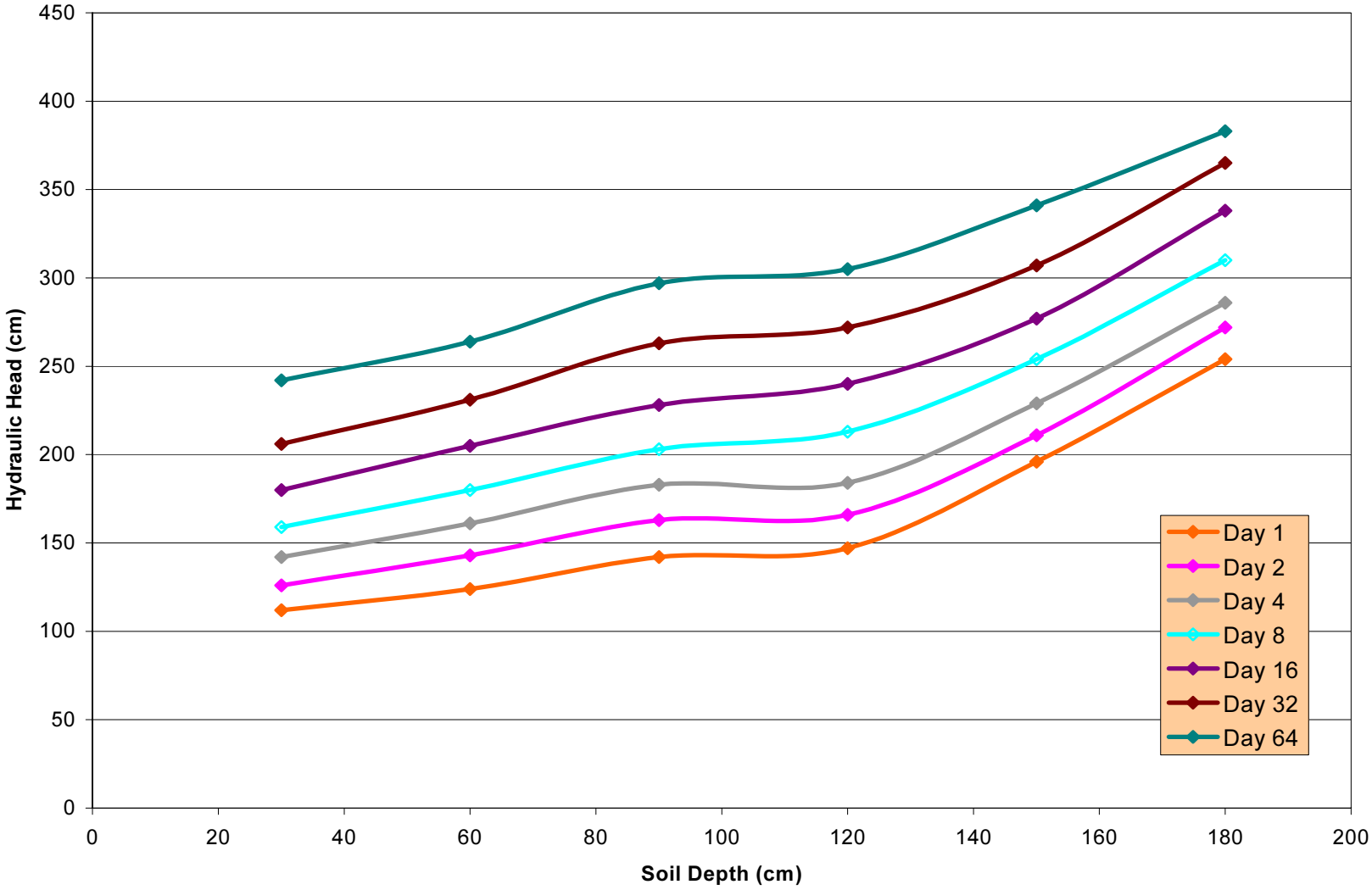

Figure 4-12 Hydraulic Head Change with Depth

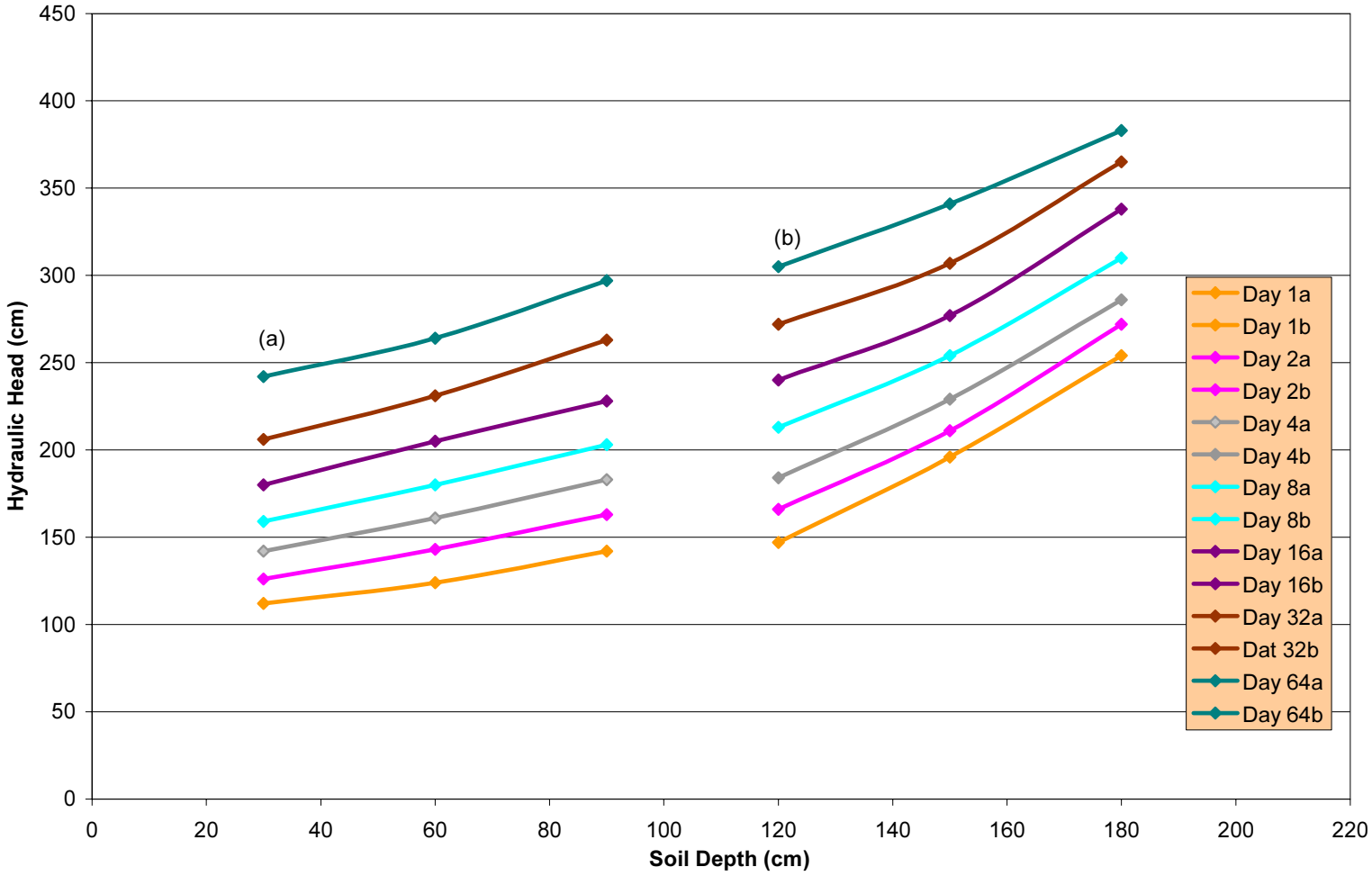

Figure 4-13 Hydraulic Head Profiles Used for Slope Calculations: (a) Lower Segment, (b) Upper Segment

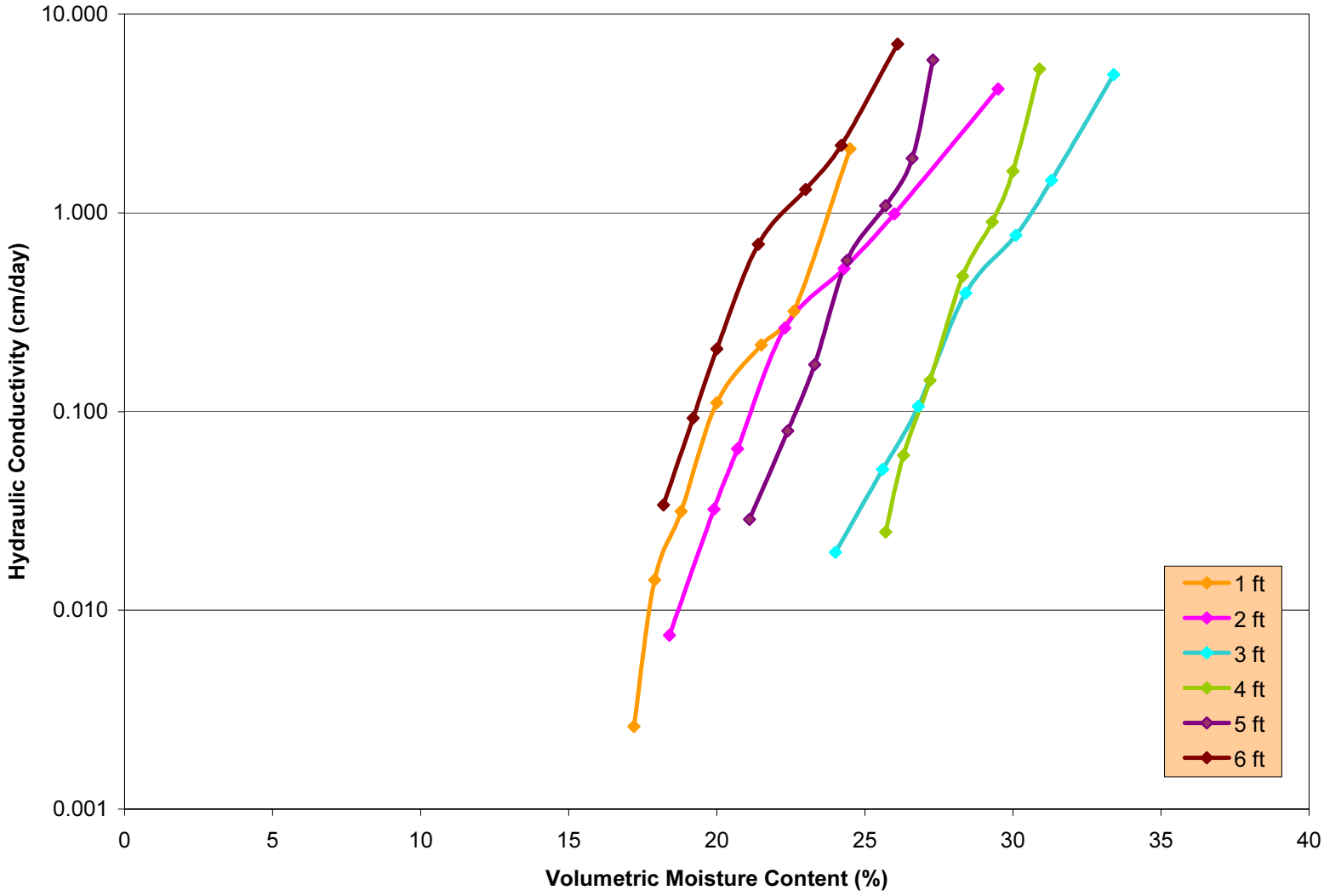

Figure 4-14 Hydraulic Conductivity as a Function of Moisture Content, K(θ), Center Neutron Probe Access Tube

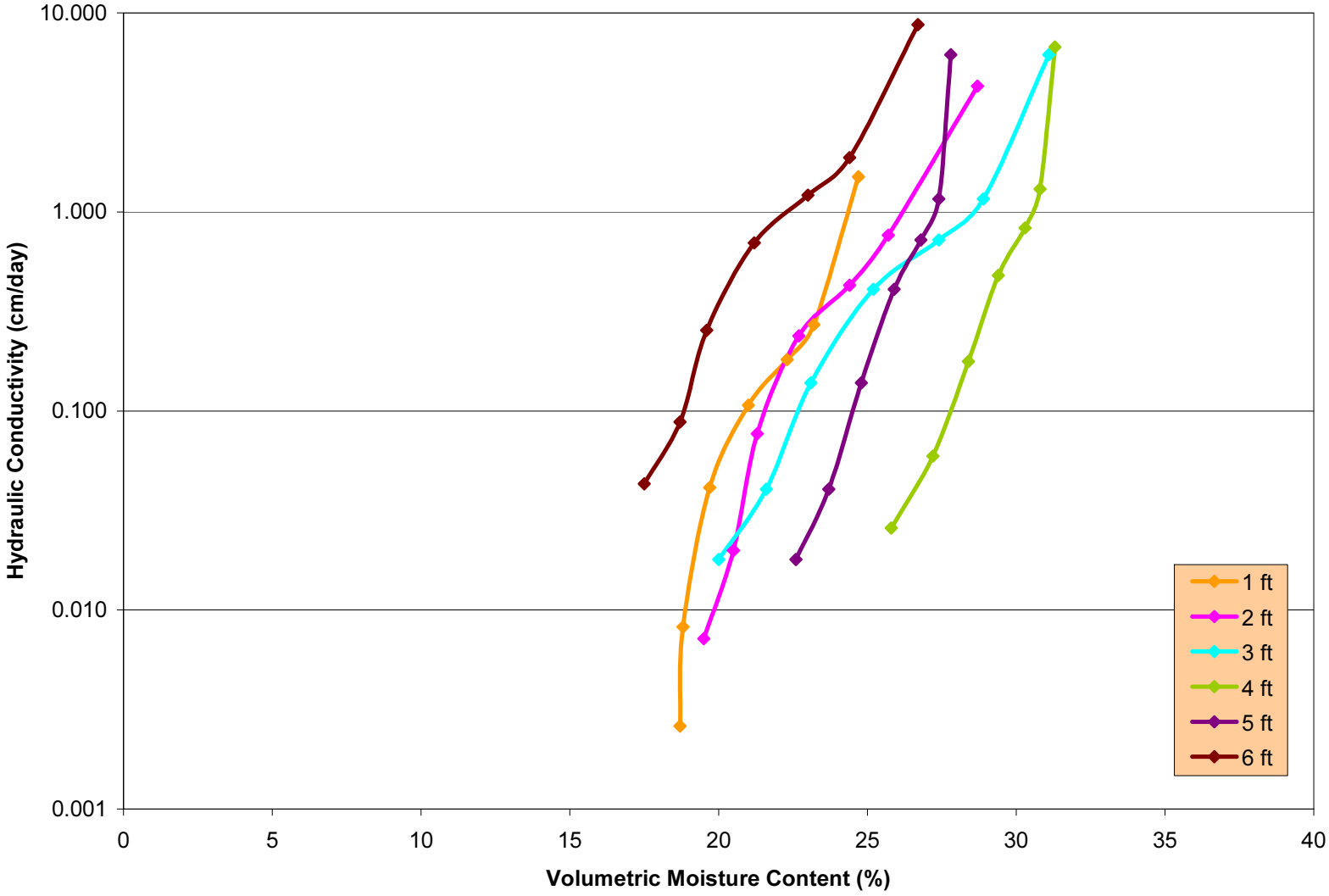

Figure 4-15 Hydraulic Conductivity as a Function of Moisture Content, K(θ), Southeast Neutron Probe Access Tube

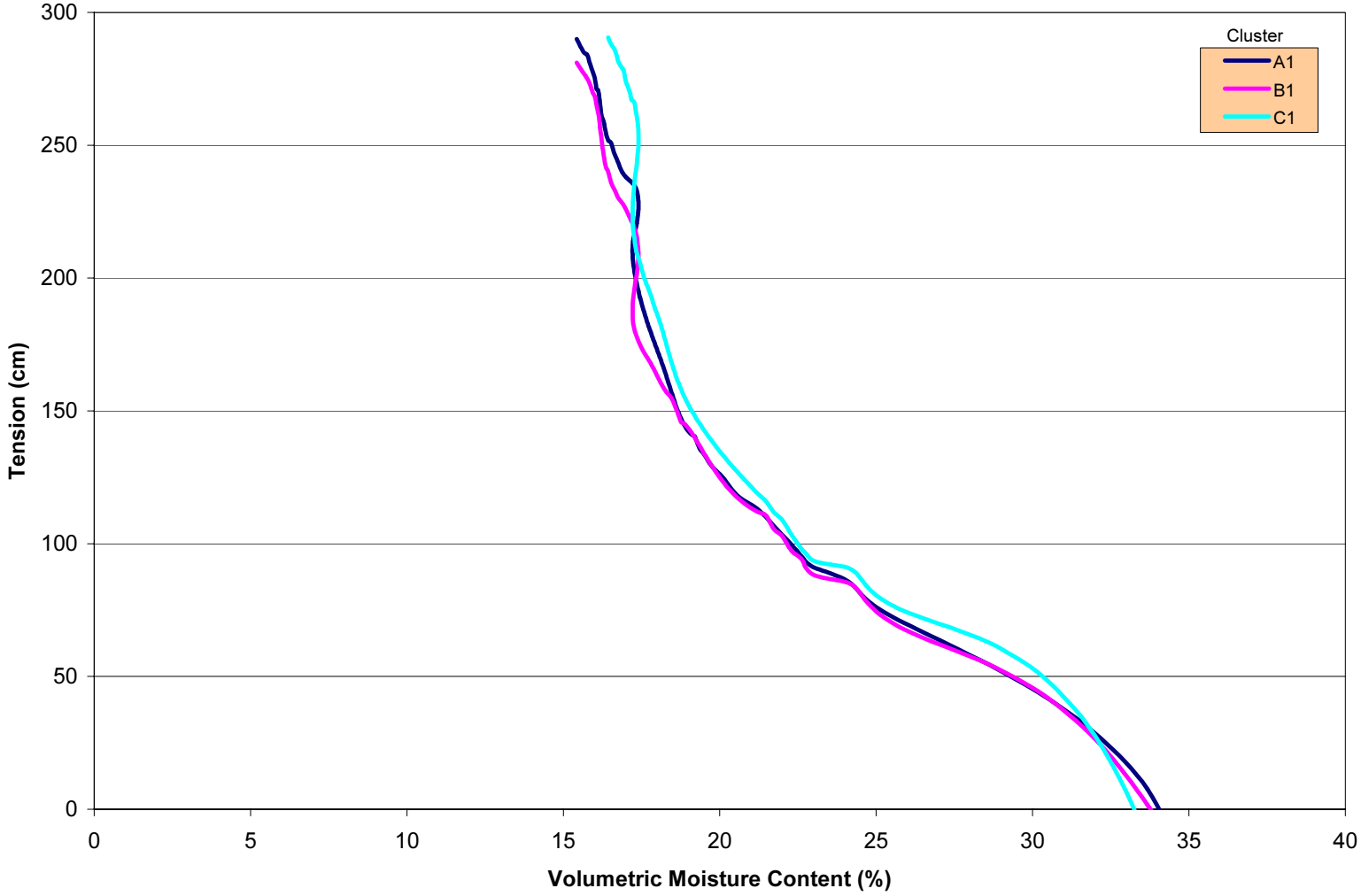

Figure 4-16 Volumetric Moisture Content and Tension at 1 ft, Center Neutron Probe Access Tube

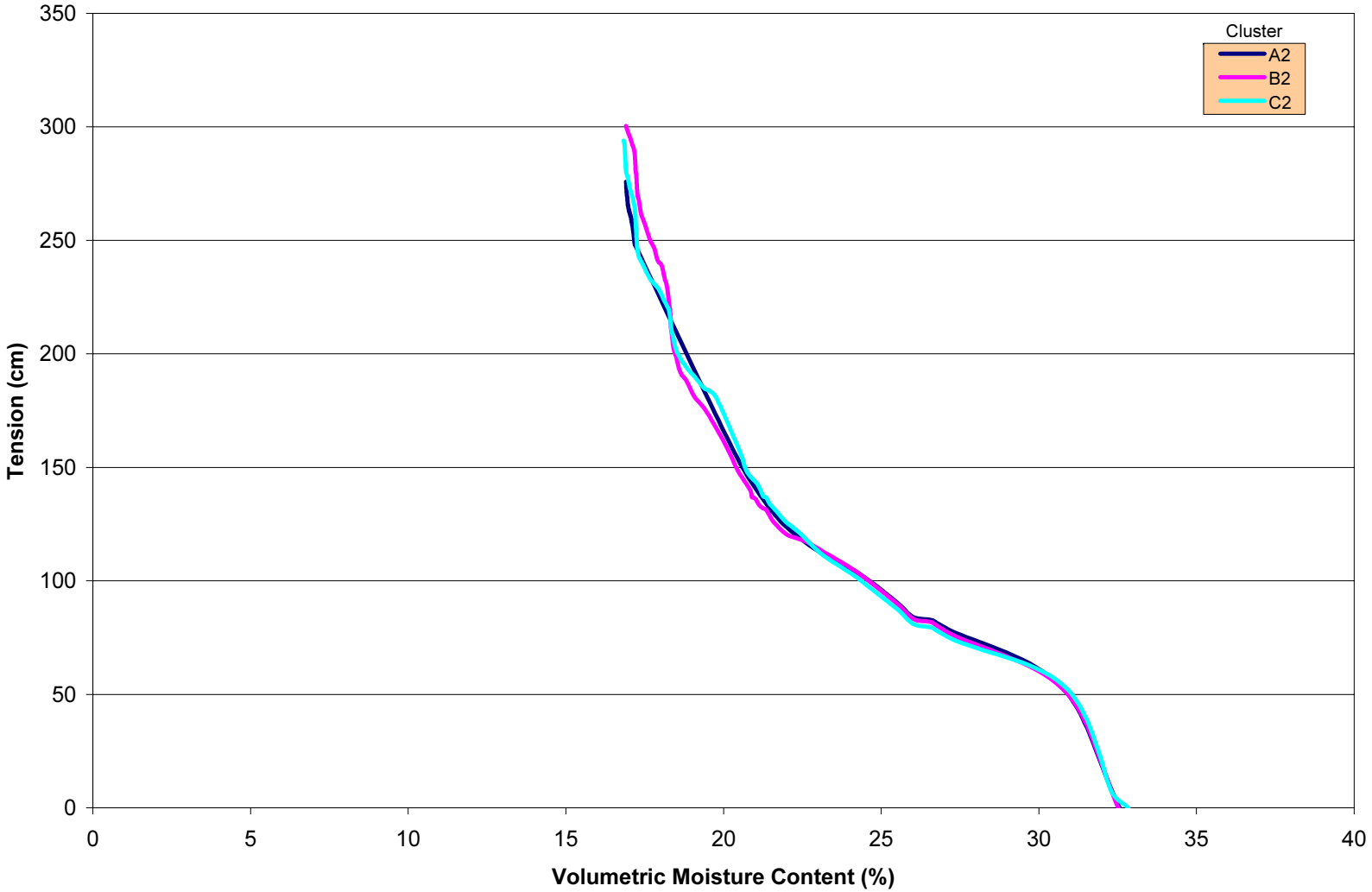

Figure 4-17 Volumetric Moisture Content and Tension at 2 ft, Center Neutron Probe Access Tube

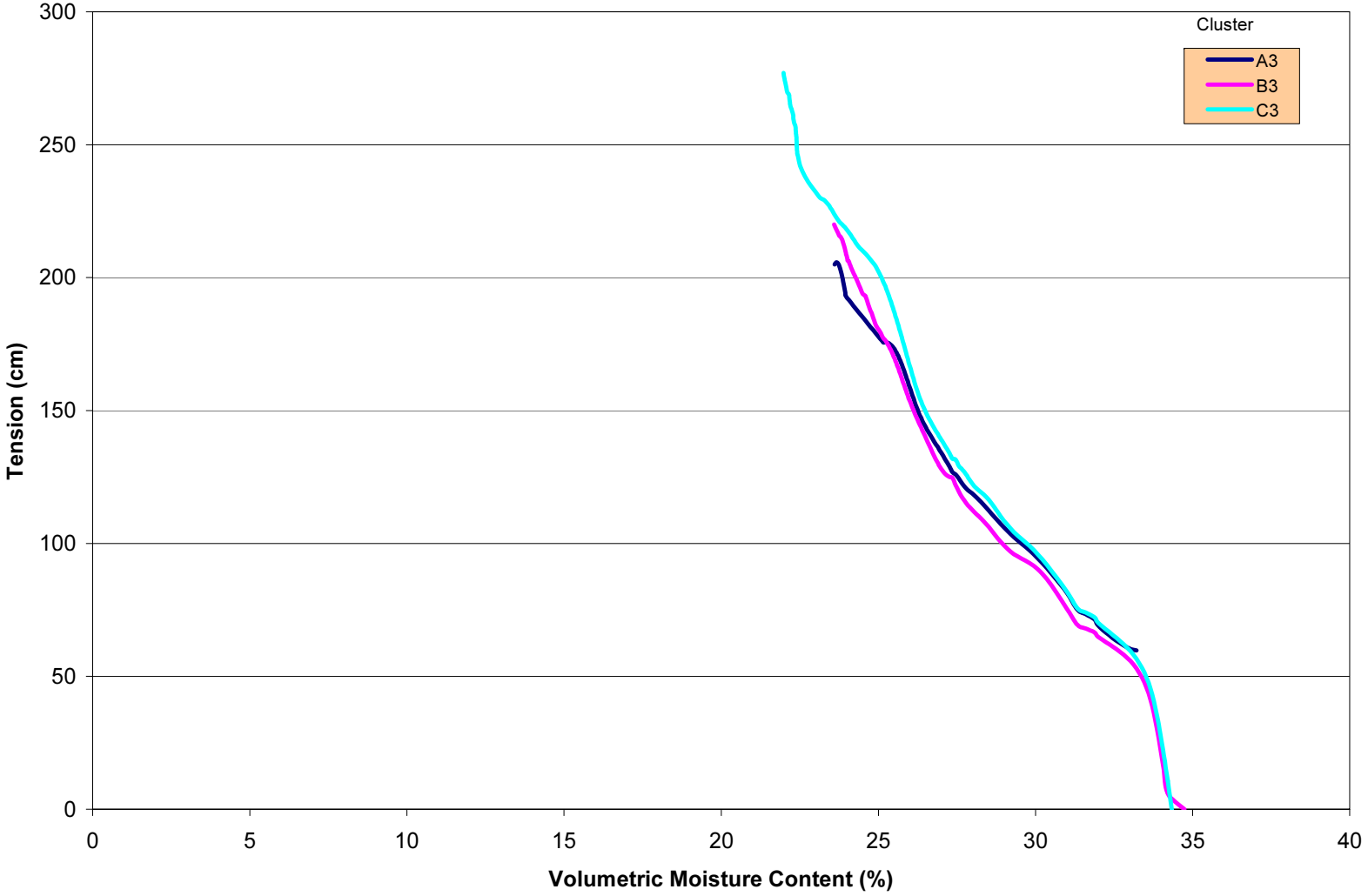

Figure 4-18 Volumetric Moisture Content and Tension at 3 ft, Center Neutron Probe Access Tube

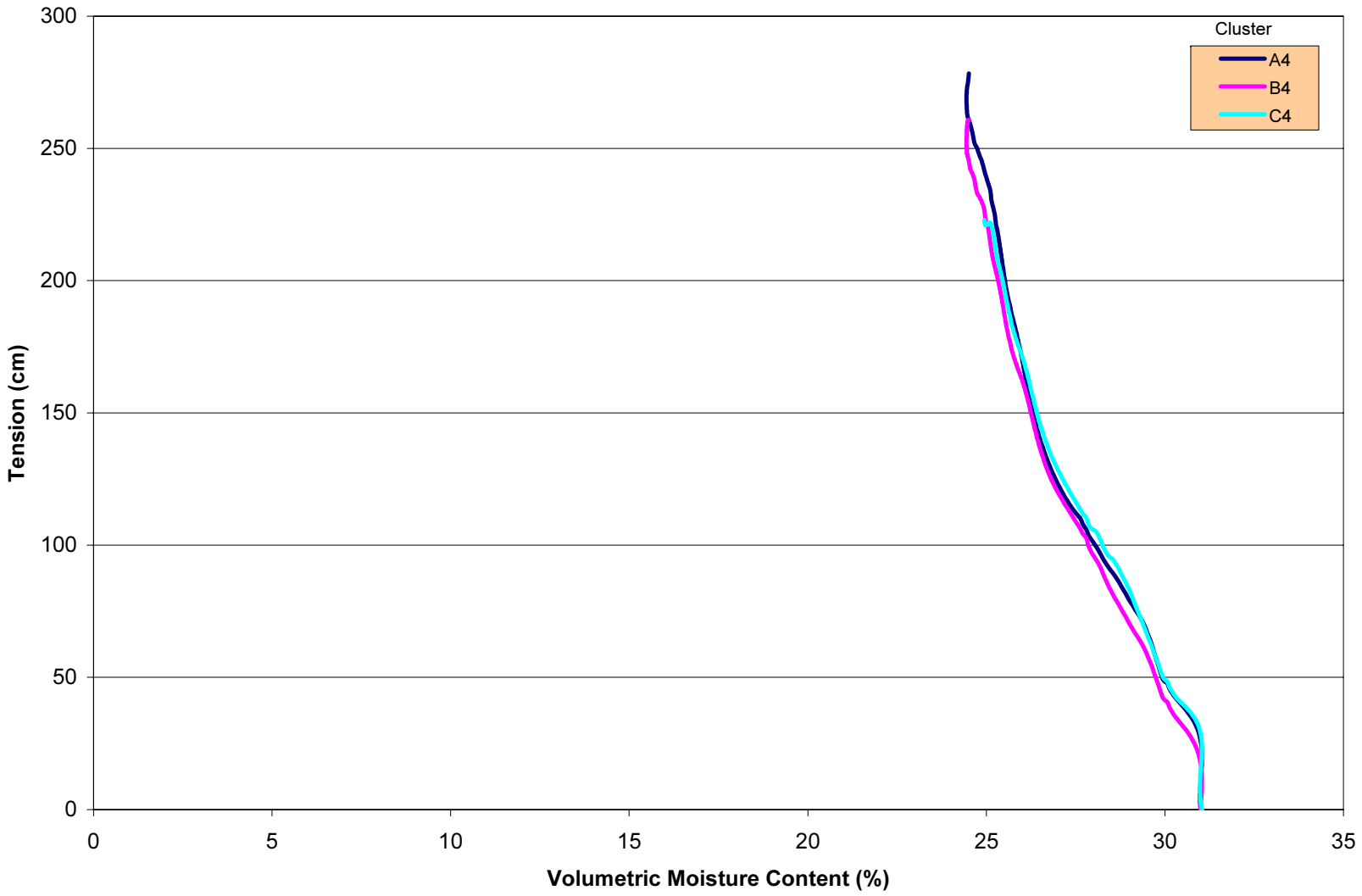

Figure 4-19 Volumetric Moisture Content and Tension at 4 ft, Center Neutron Probe Access Tube

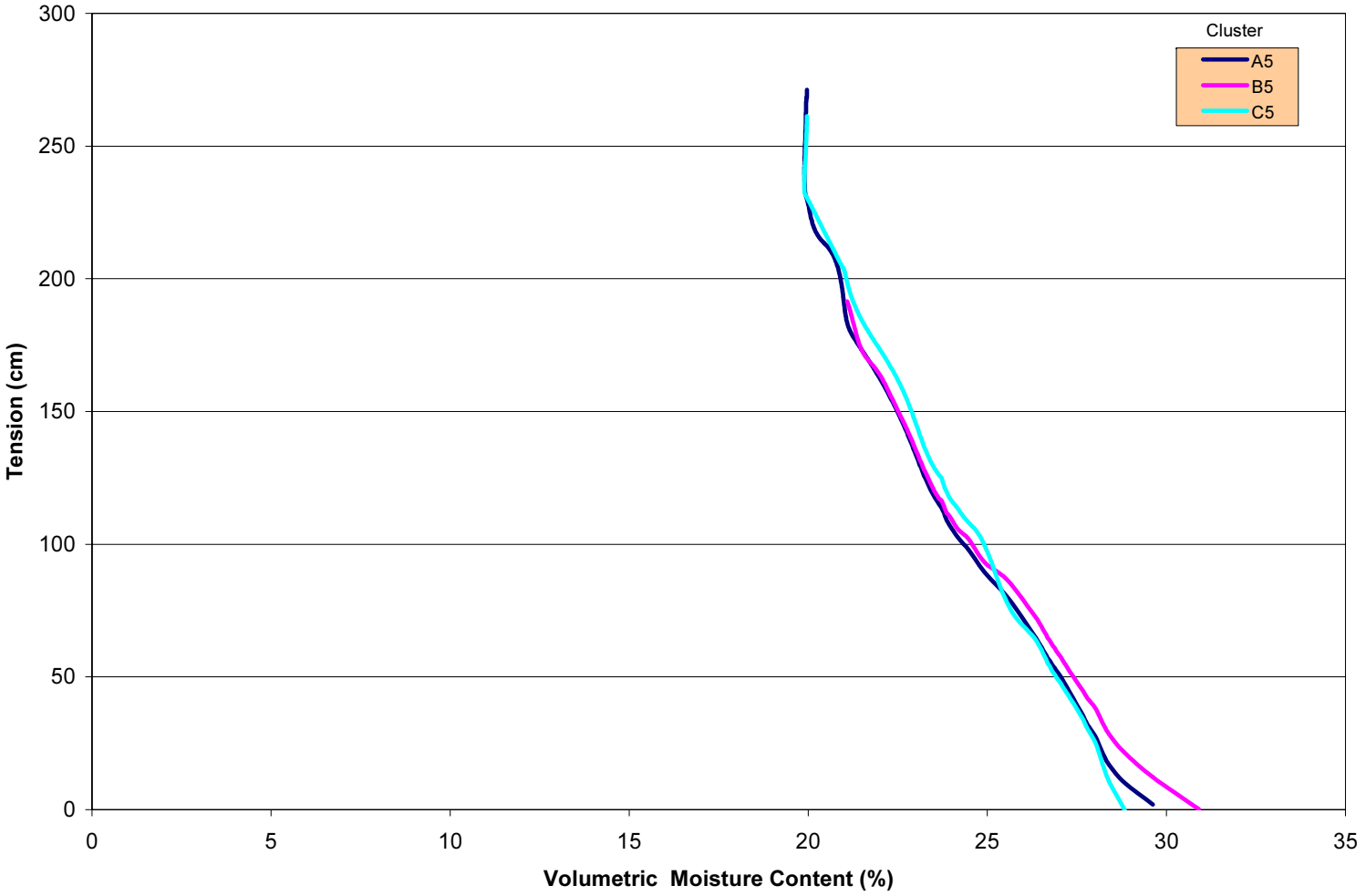

Figure 4-20 Volumetric Moisture Content and Tension at 5 ft, Center Neutron Probe Access Tube

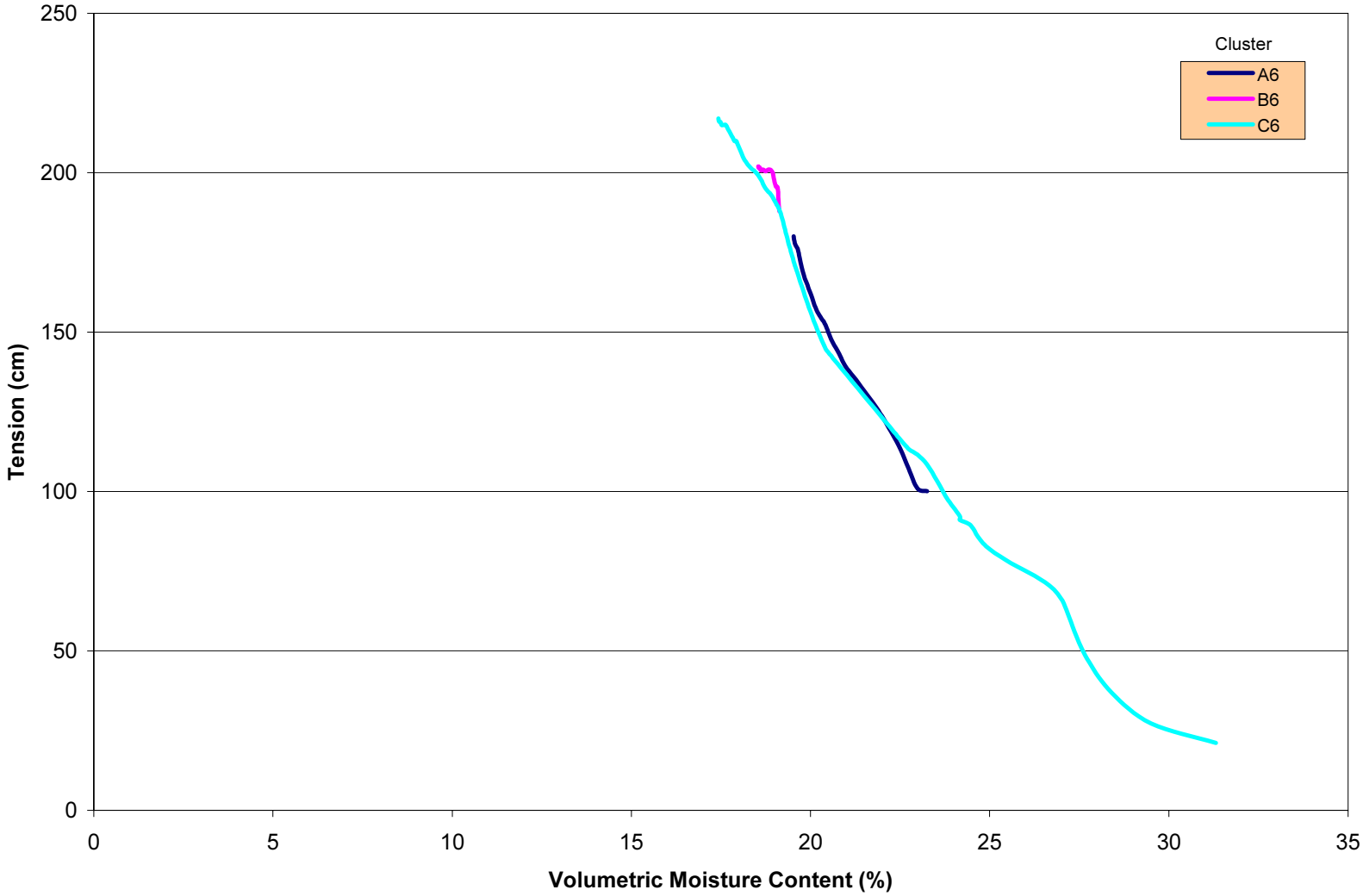

Figure 4-21 Volumetric Moisture Content and Tension at 6 ft, Center Neutron Probe Access Tube

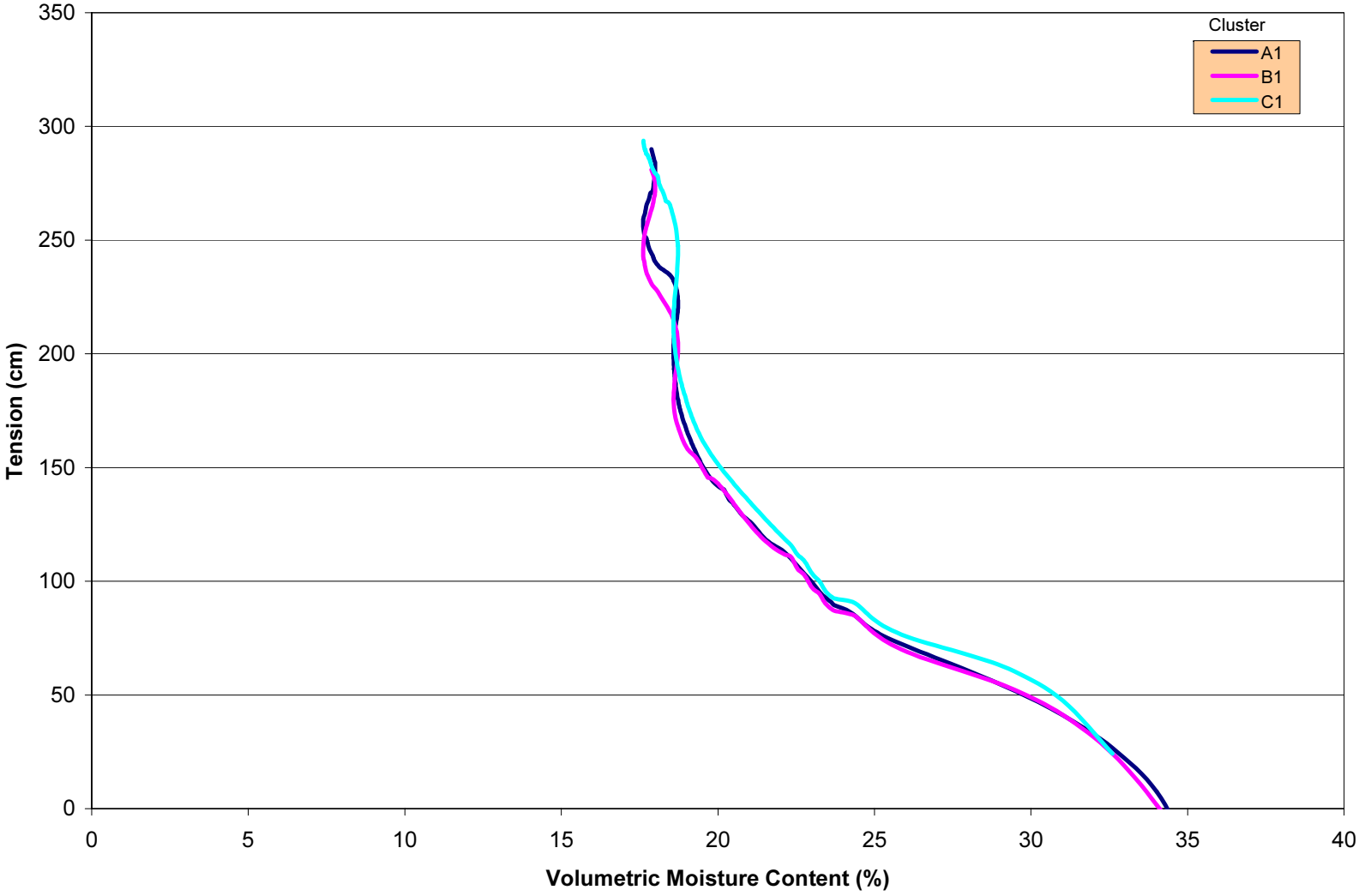

Figure 4-22 Volumetric Moisture Content and Tension at 1 ft, Southeast Neutron Probe Access Tube

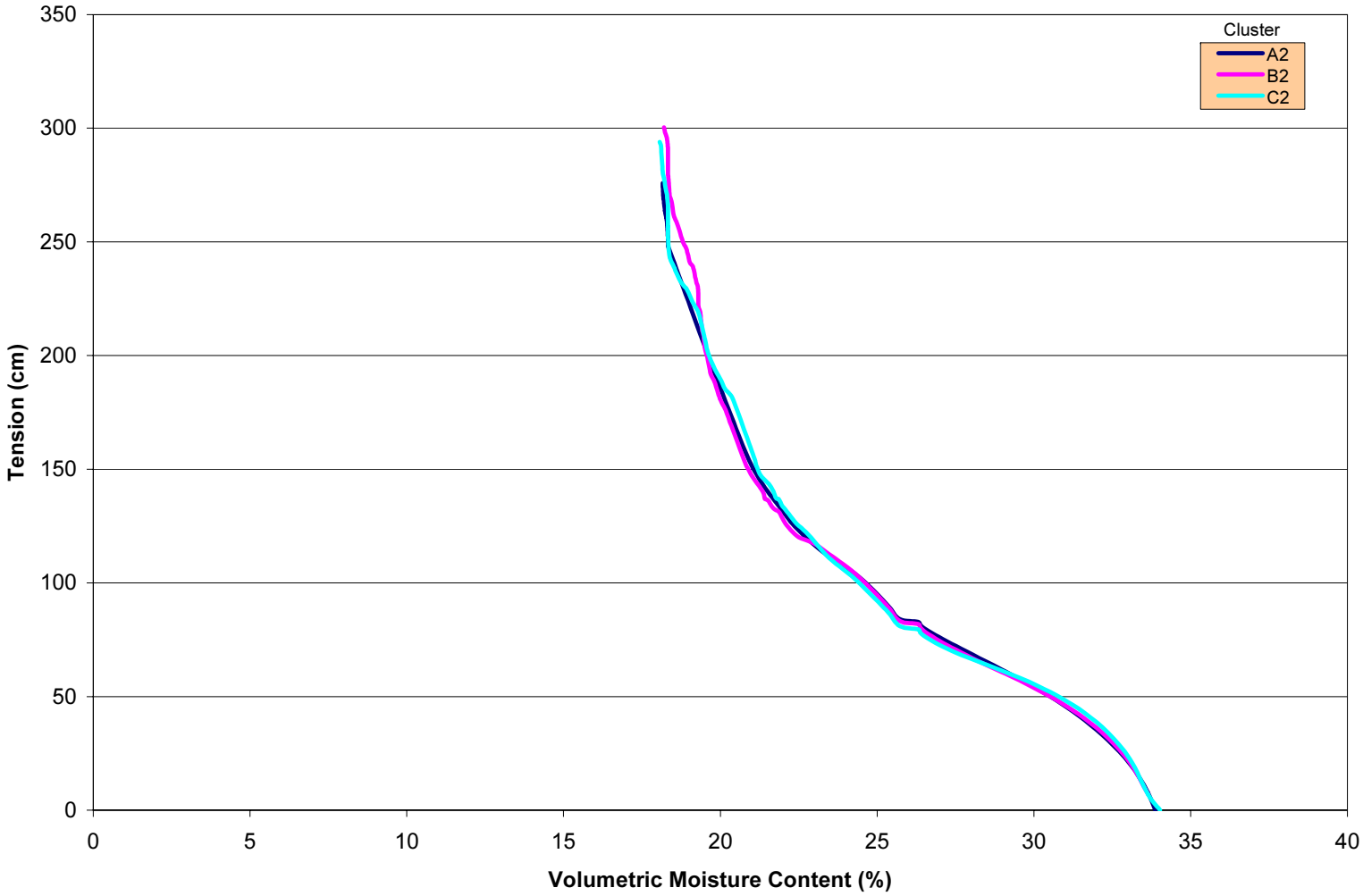

Figure 4-23 Volumetric Moisture Content and Tension at 2 ft, Southeast Neutron Probe Access Tube

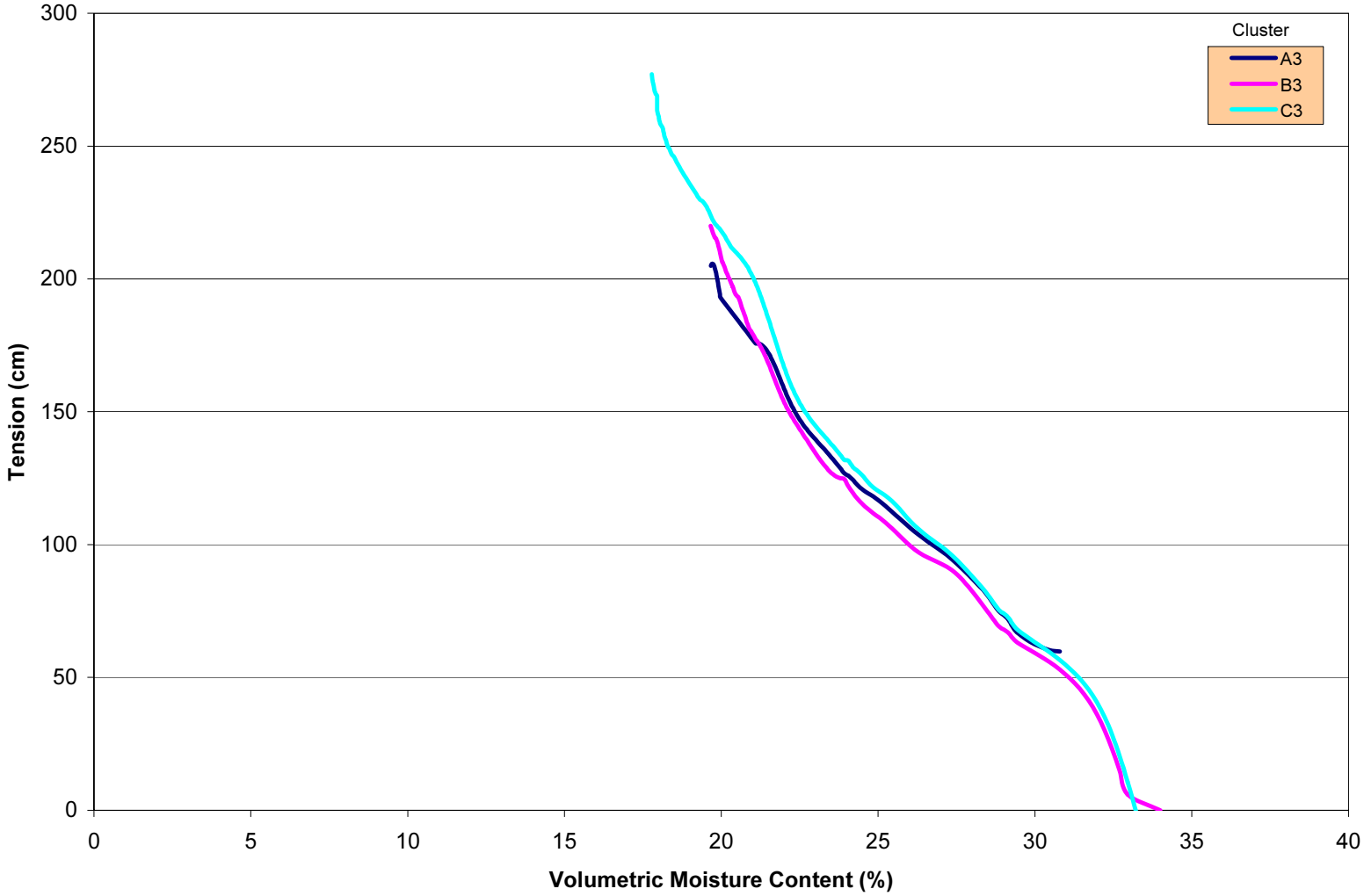

Figure 4-24 Volumetric Moisture Content and Tension at 3 ft, Southeast Neutron Probe Access Tube

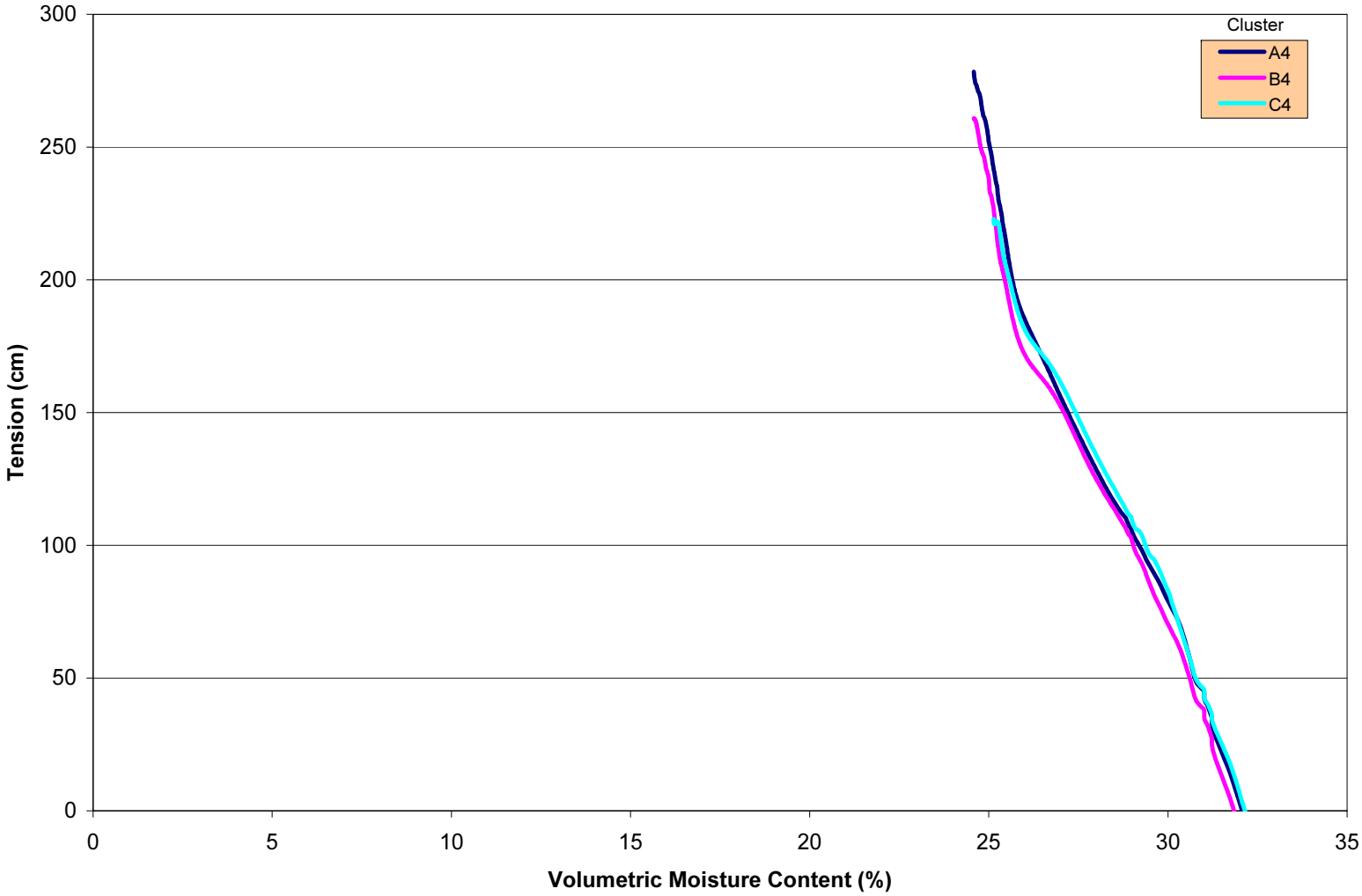

Figure 4-25 Volumetric Moisture Content and Tension at 4 ft, Southeast Neutron Probe Access Tube

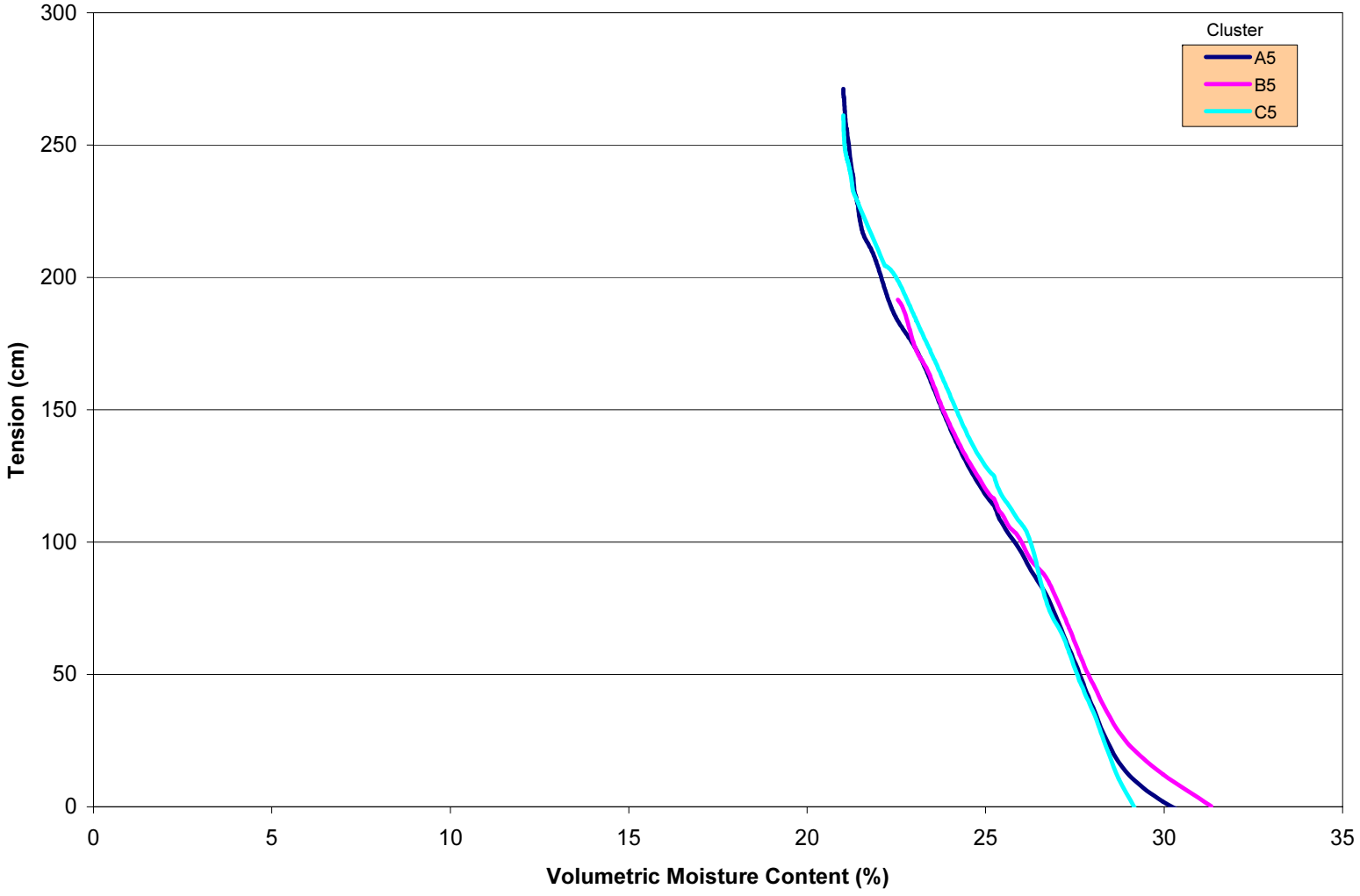

Figure 4-26 Volumetric Moisture Content and Tension at 5 ft, Southeast Neutron Probe Access Tube

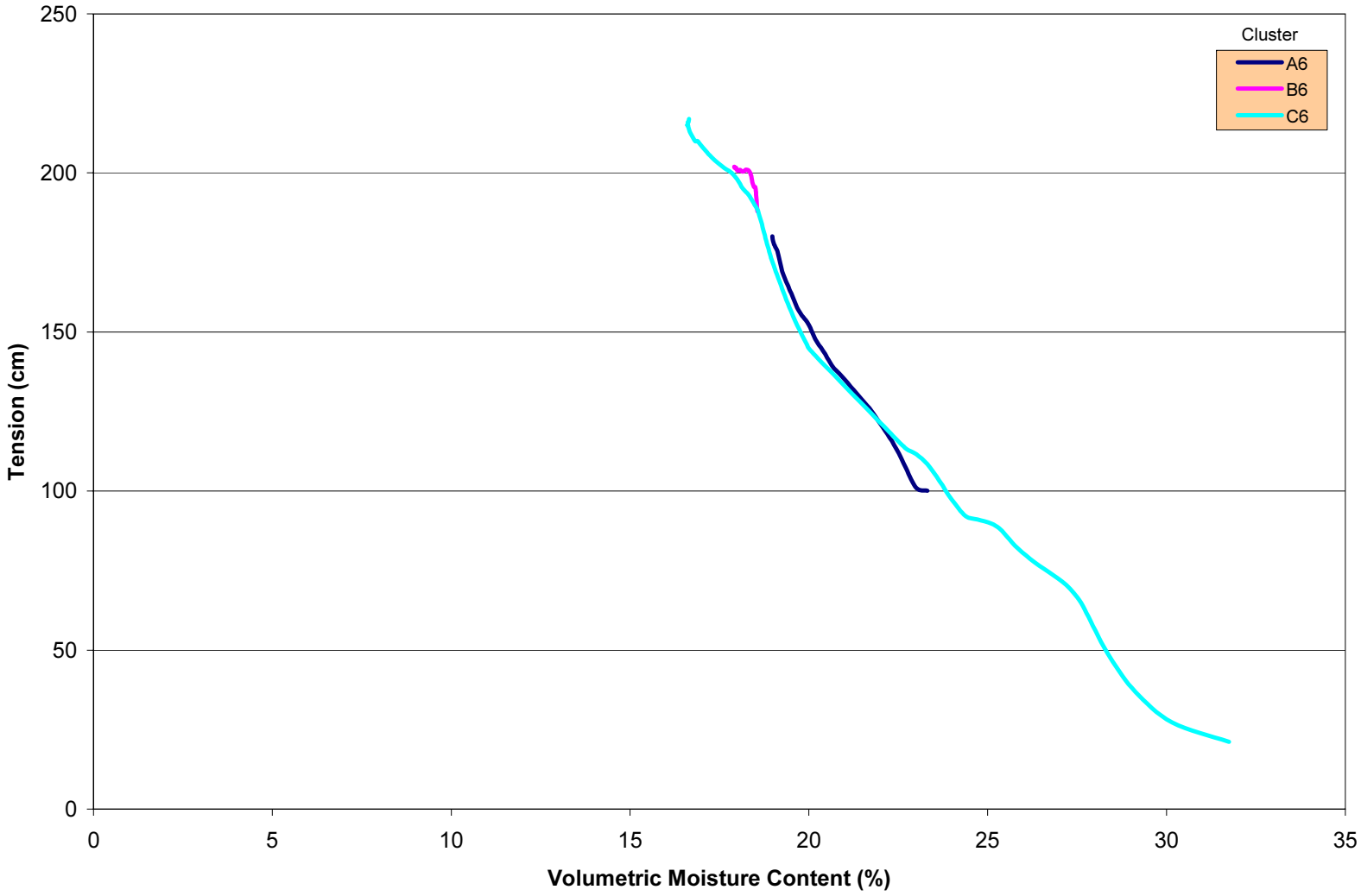

Figure 4-27 Volumetric Moisture Content and Tension at 6 ft, Southeast Neutron Probe Access Tube

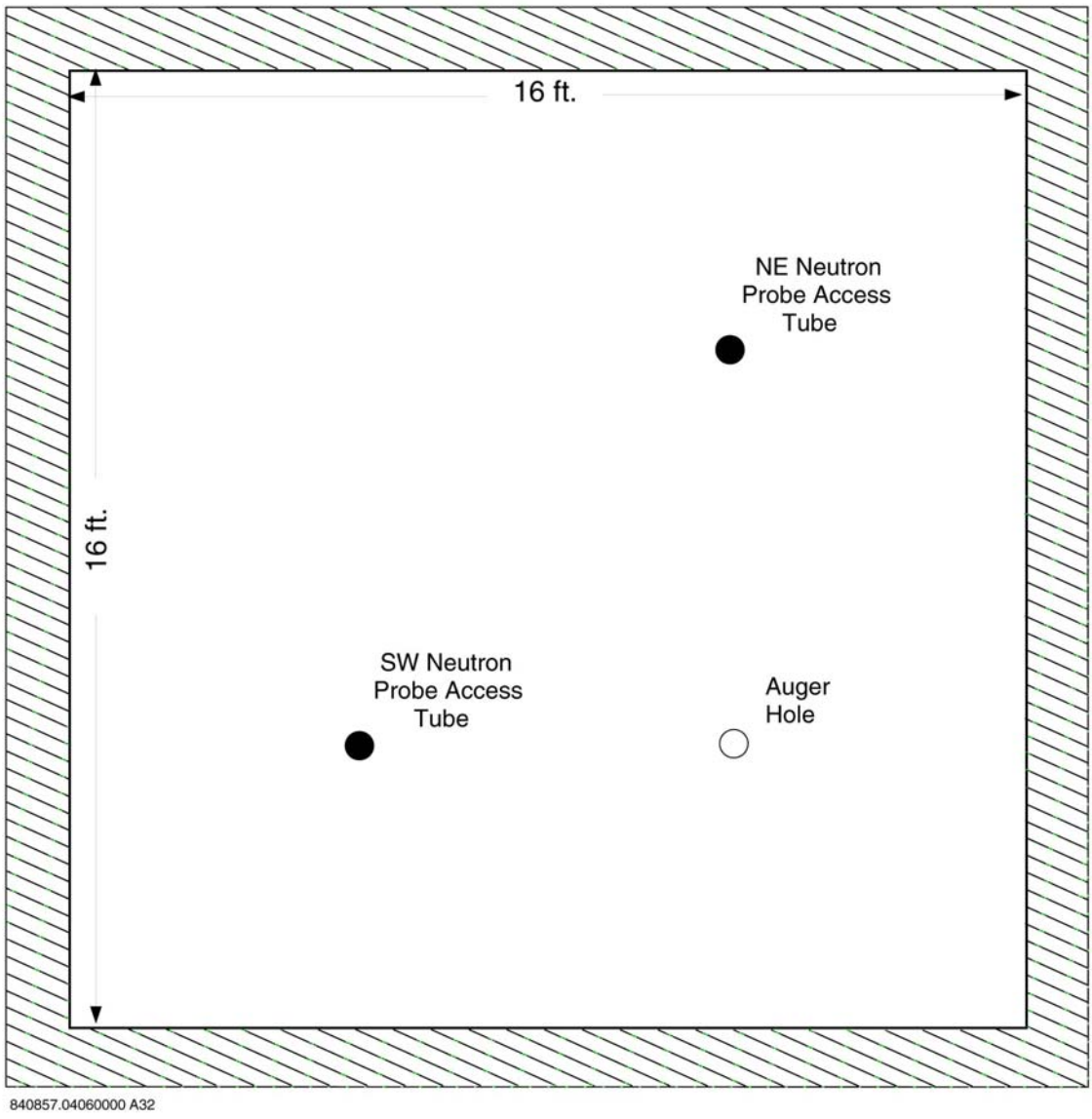

Figure 4-28 Schematic of Instantaneous Profile Test Site—Engineered Cover

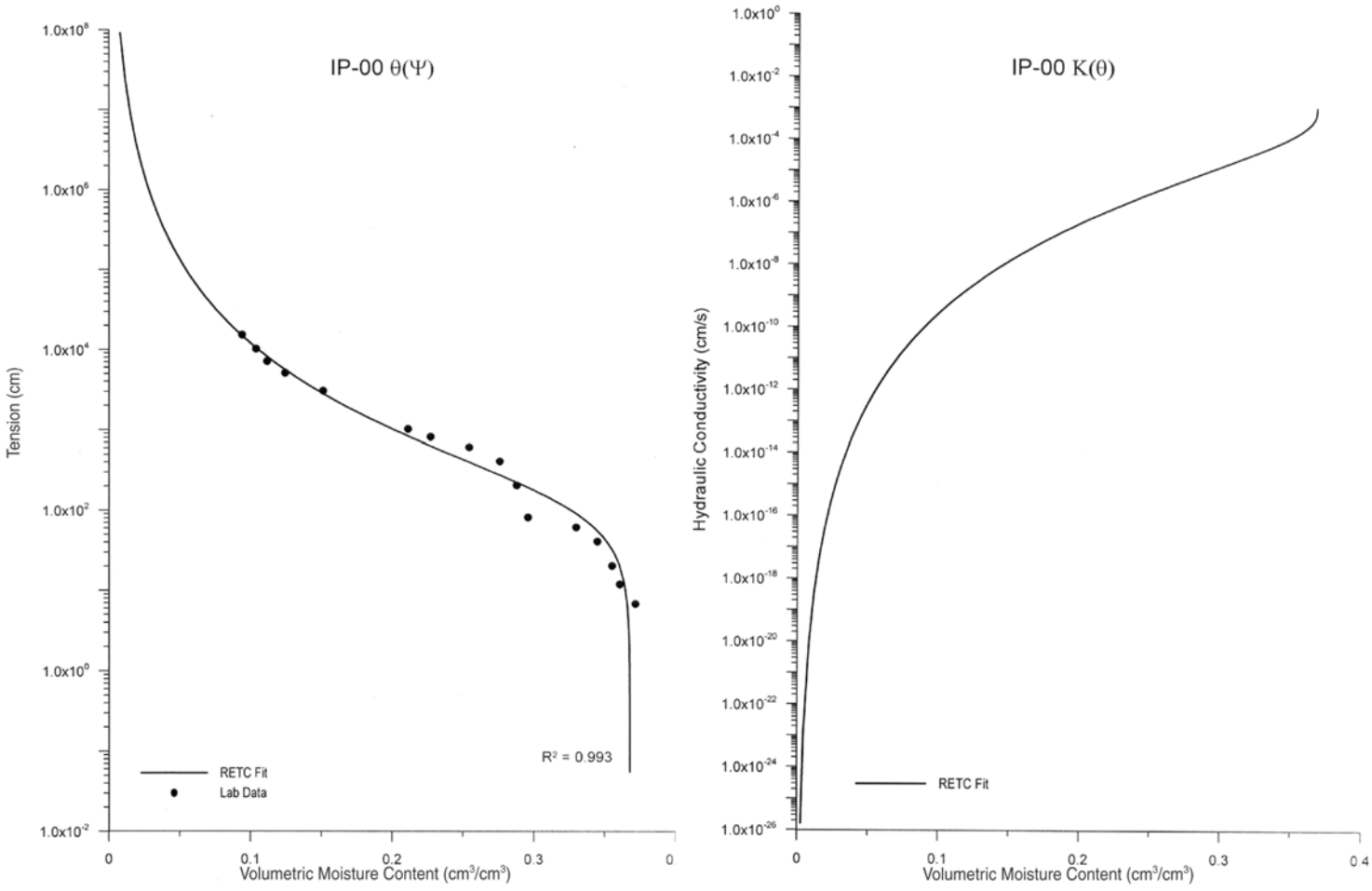

Figure 5-1 RETC Code Simulation of θ(Ψ) and K(θ) Hydraulic Properties for IP-00

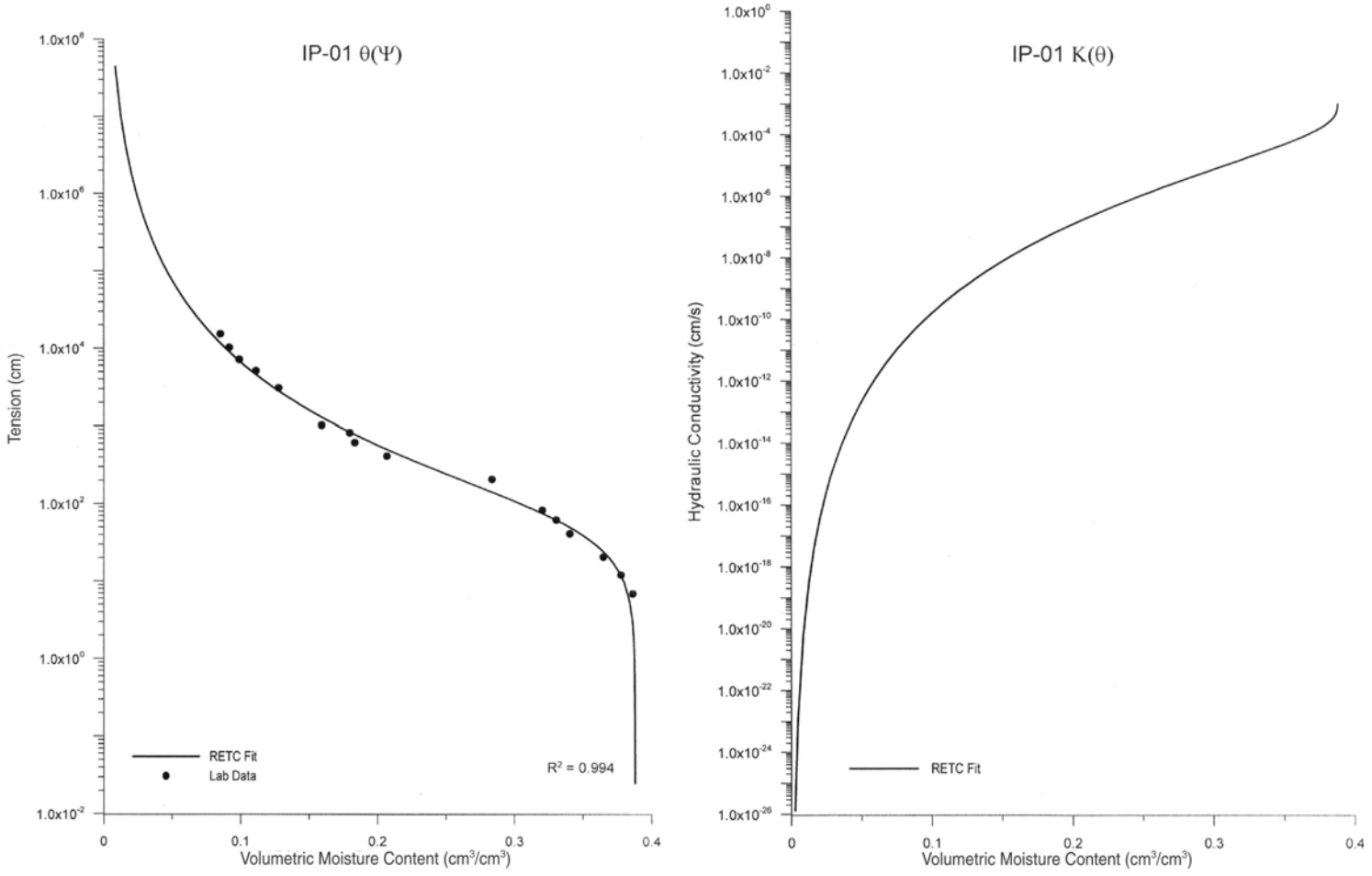

Figure 5-2 RETC Code Simulation of θ(Ψ) and K(θ) Hydraulic Properties for IP-01

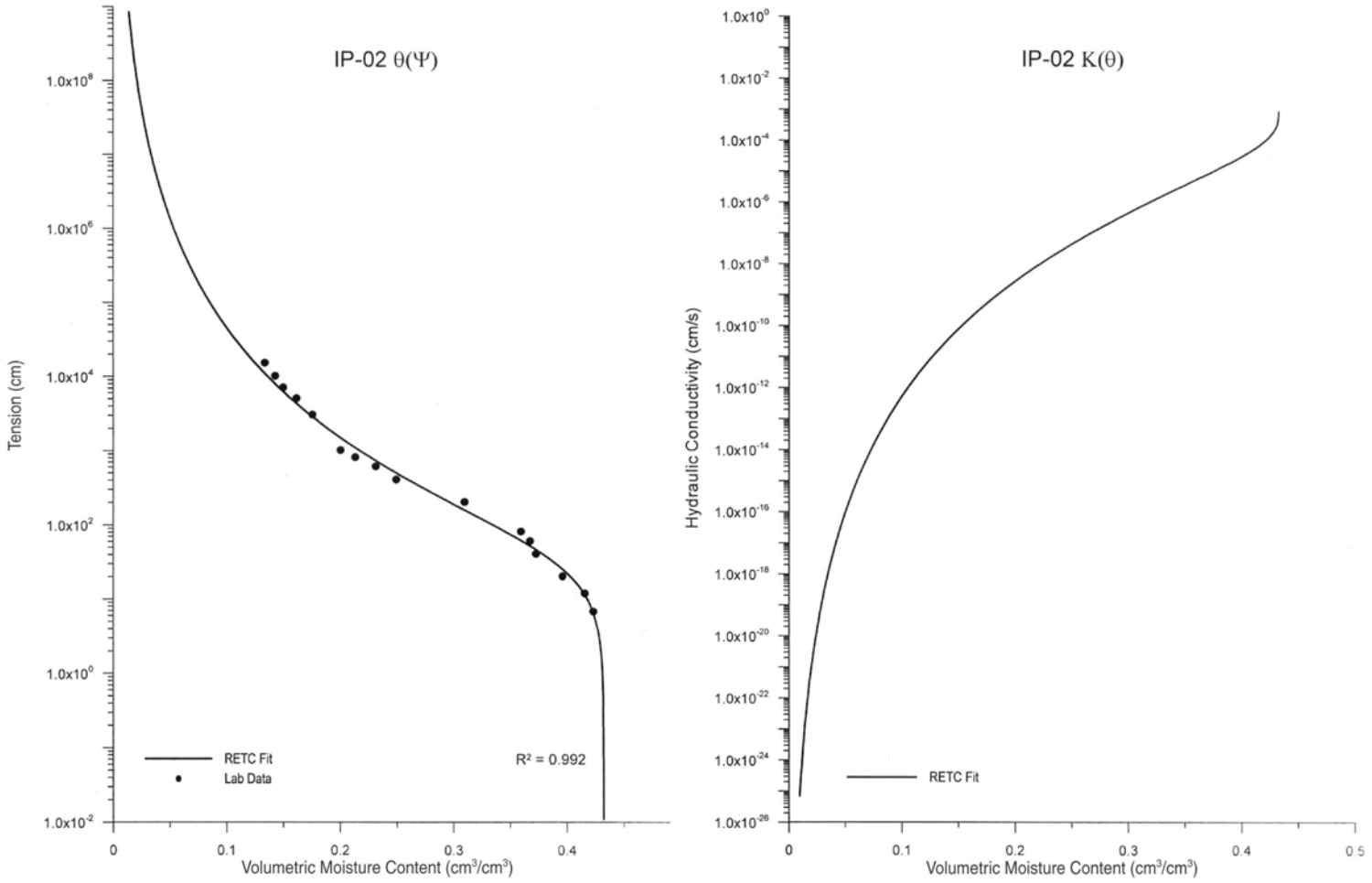

Figure 5-3 RETC Code Simulation of θ(Ψ) and K(θ) Hydraulic Properties for IP-02

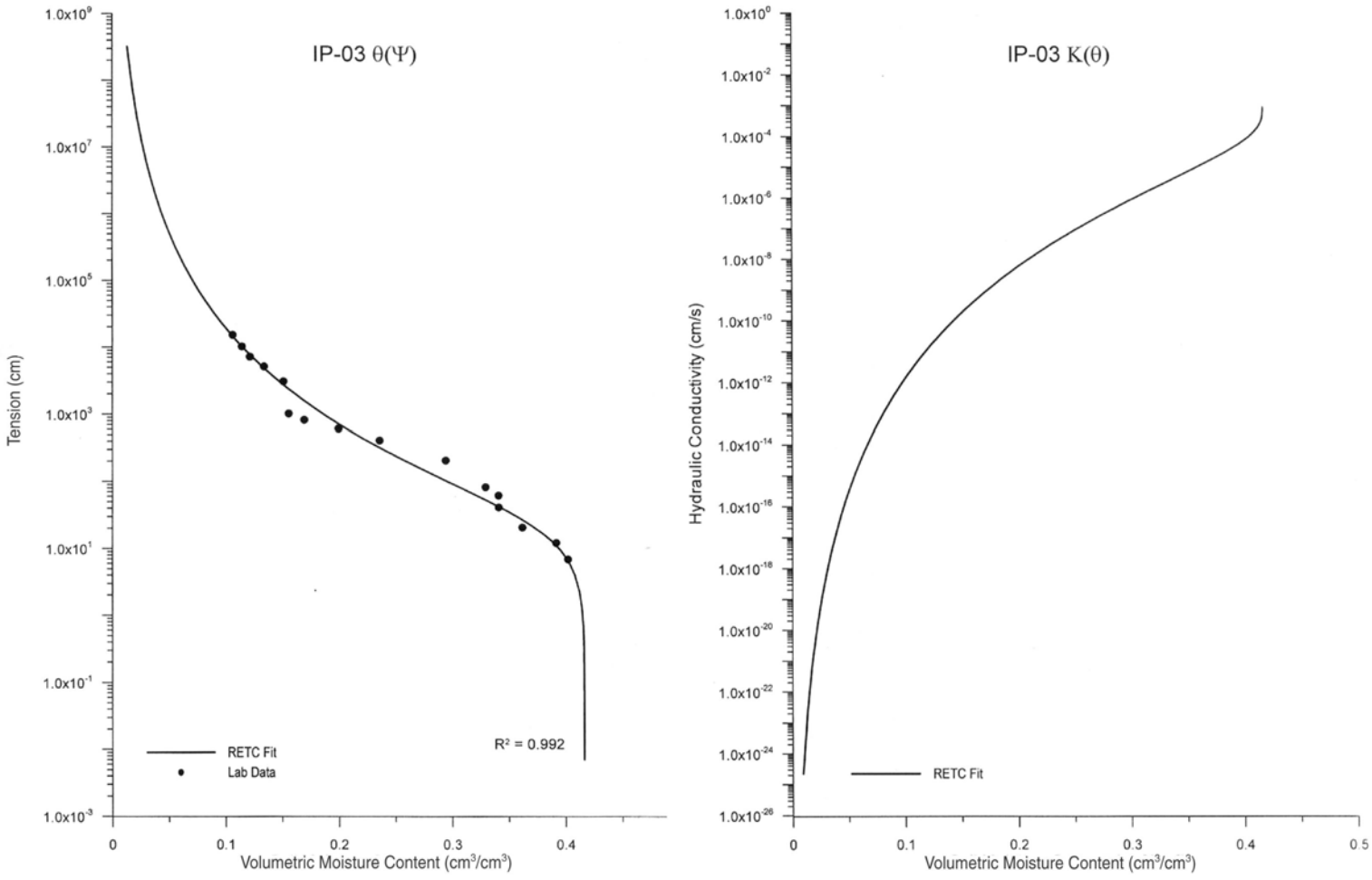

Figure 5-4 RETC Code Simulation of θ(Ψ) and K(θ) Hydraulic Properties for IP-03

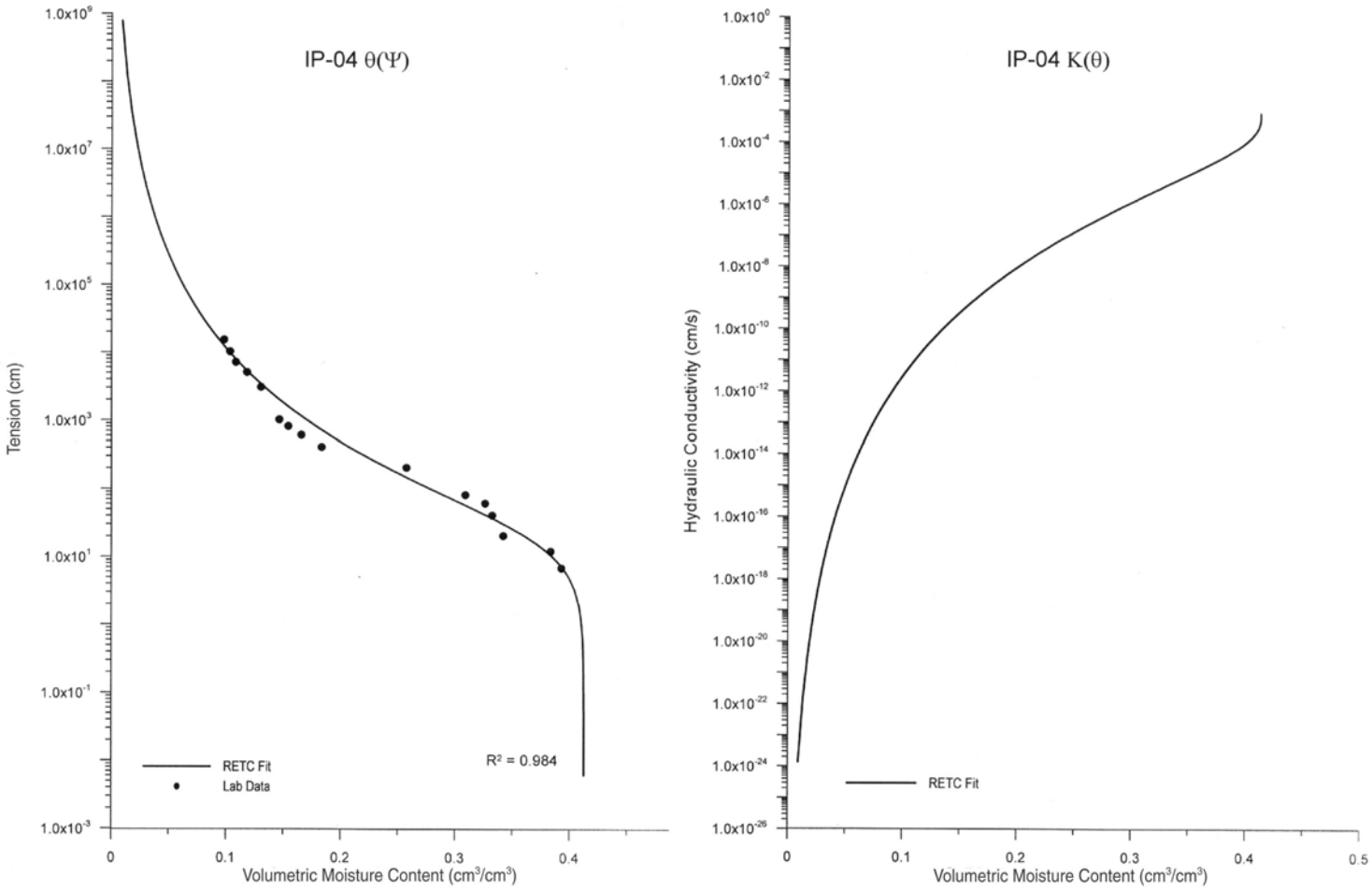

Figure 5-5 RETC Code Simulation of θ(Ψ) and K(θ) Hydraulic Properties for IP-04

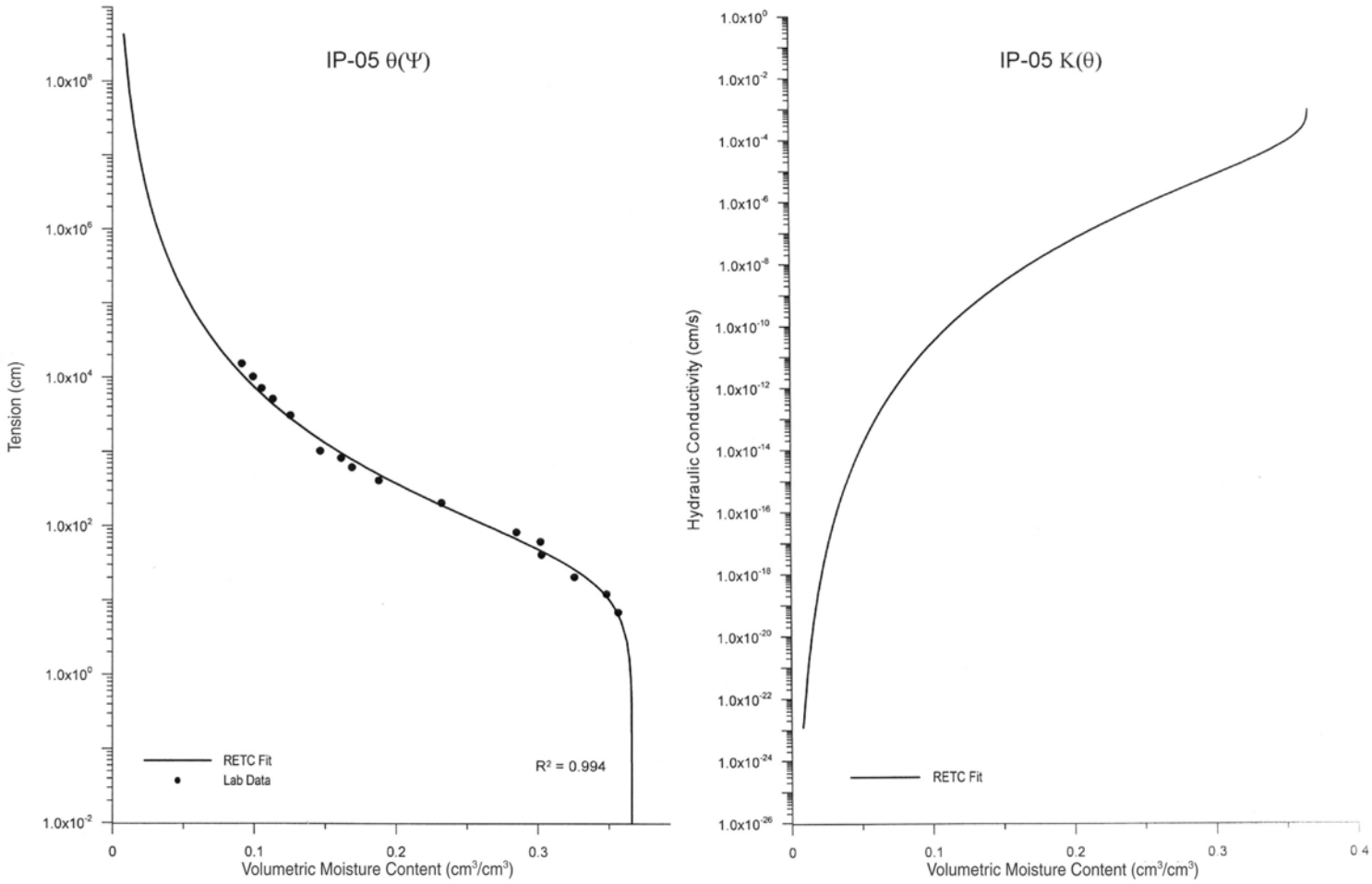

Figure 5-6 RETC Code Simulation of θ(Ψ) and K(θ) Hydraulic Properties for IP-05

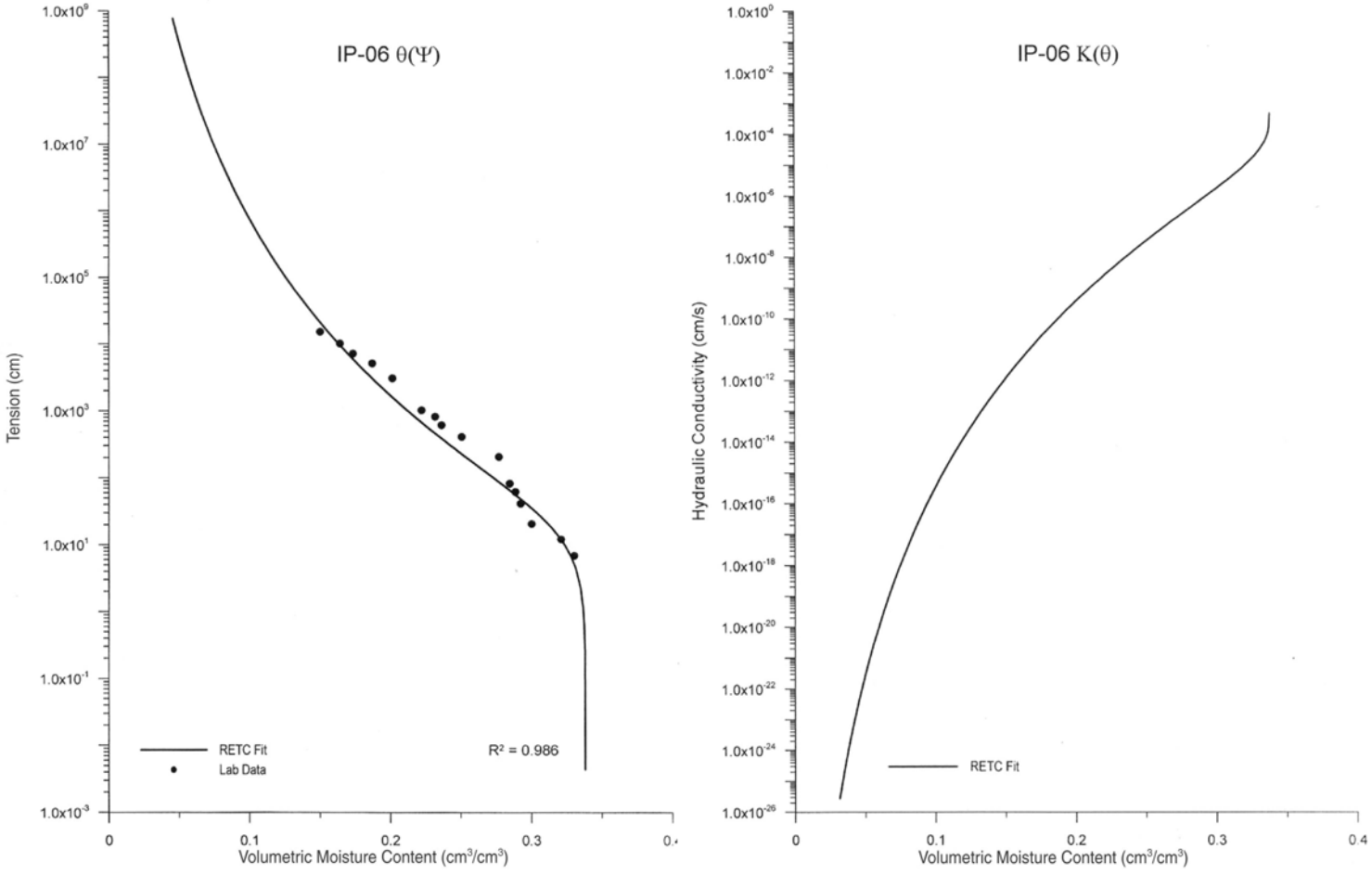

Figure 5-7 RETC Code Simulation of θ(Ψ) and K(θ) Hydraulic Properties for IP-06

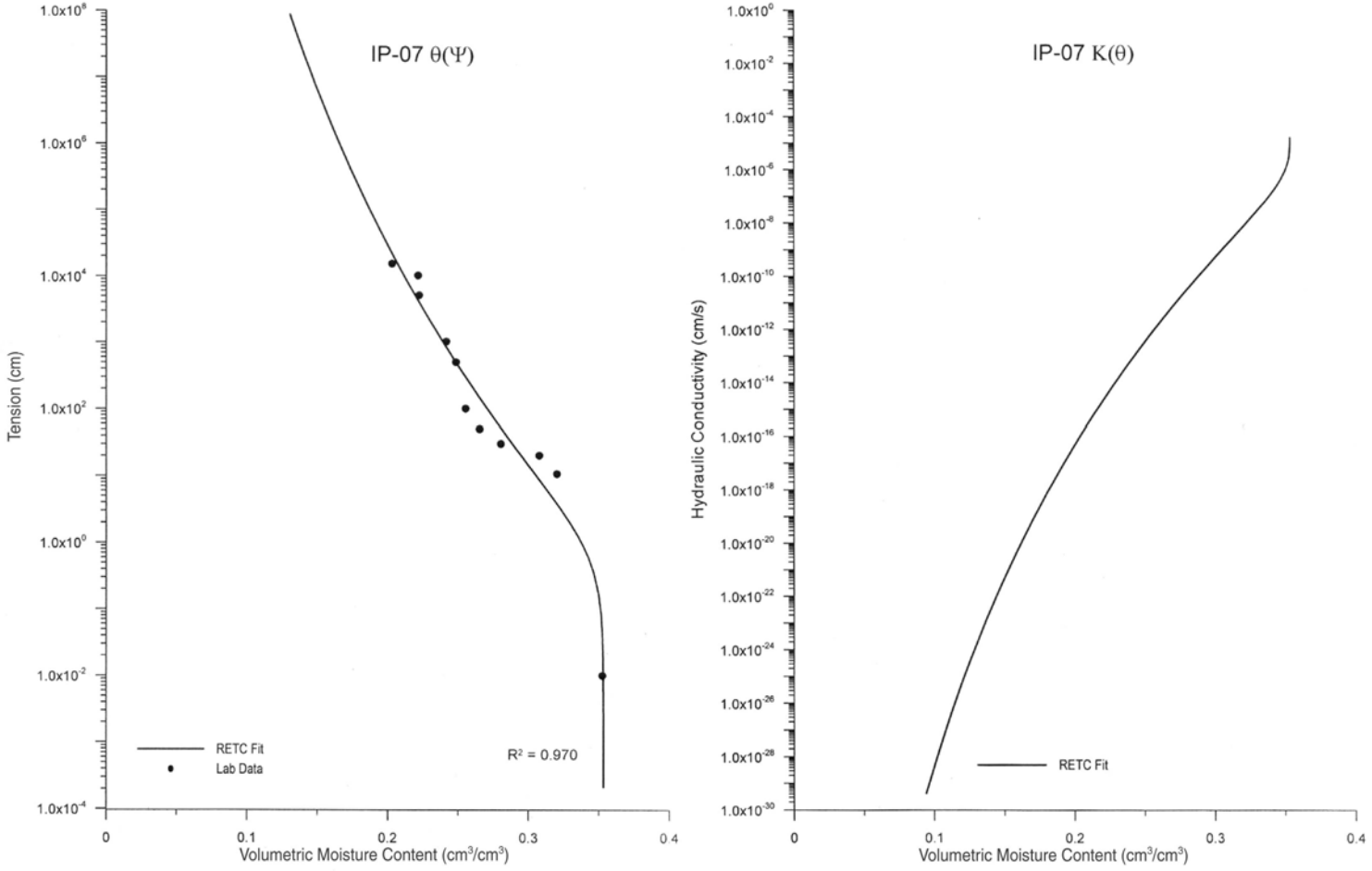

Figure 5-8 RETC Code Simulation of θ(Ψ) and K(θ) Hydraulic Properties for IP-07

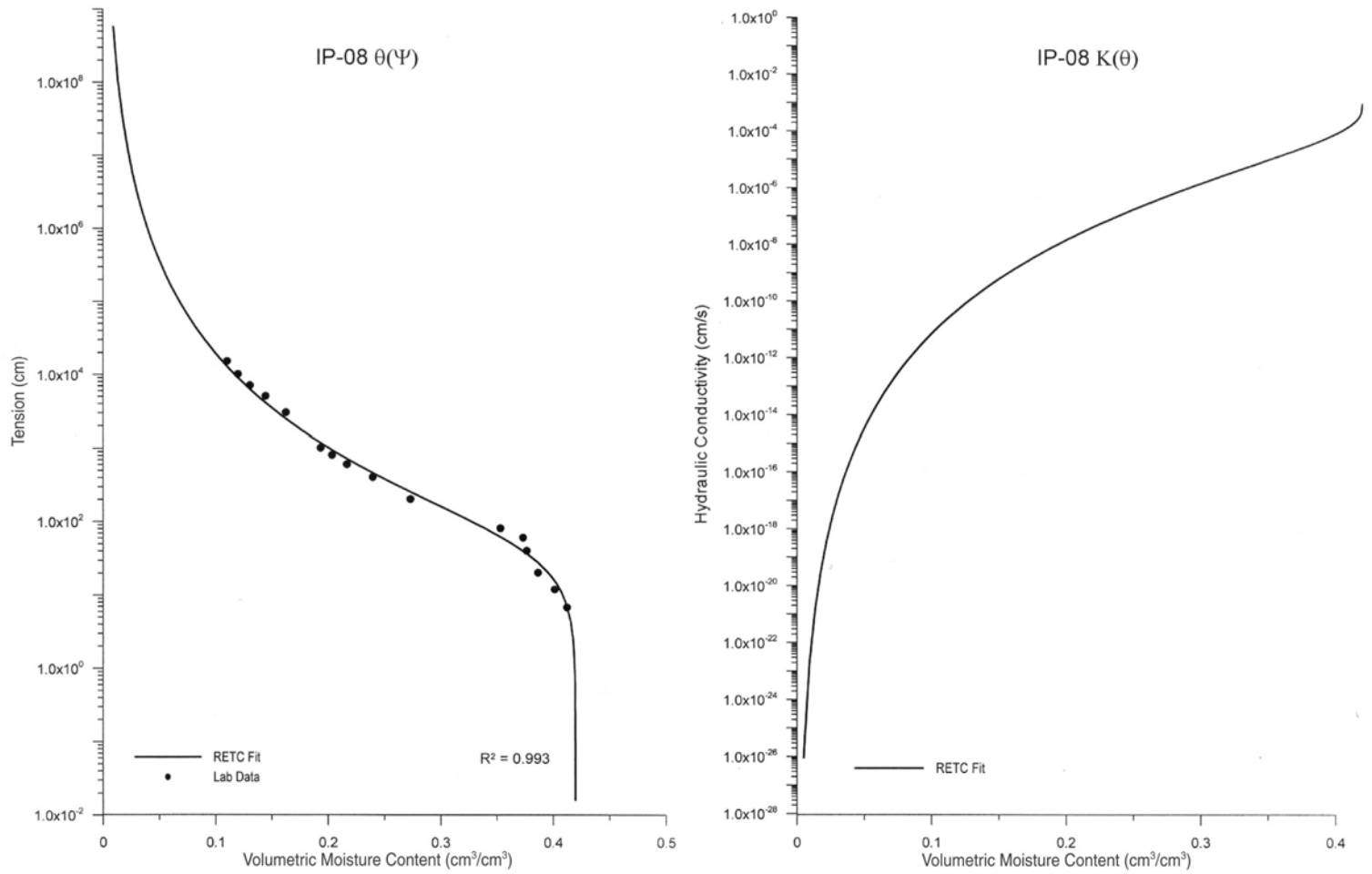

Figure 5-9 RETC Code Simulation of θ(Ψ) and K(θ) Hydraulic Properties for IP-08

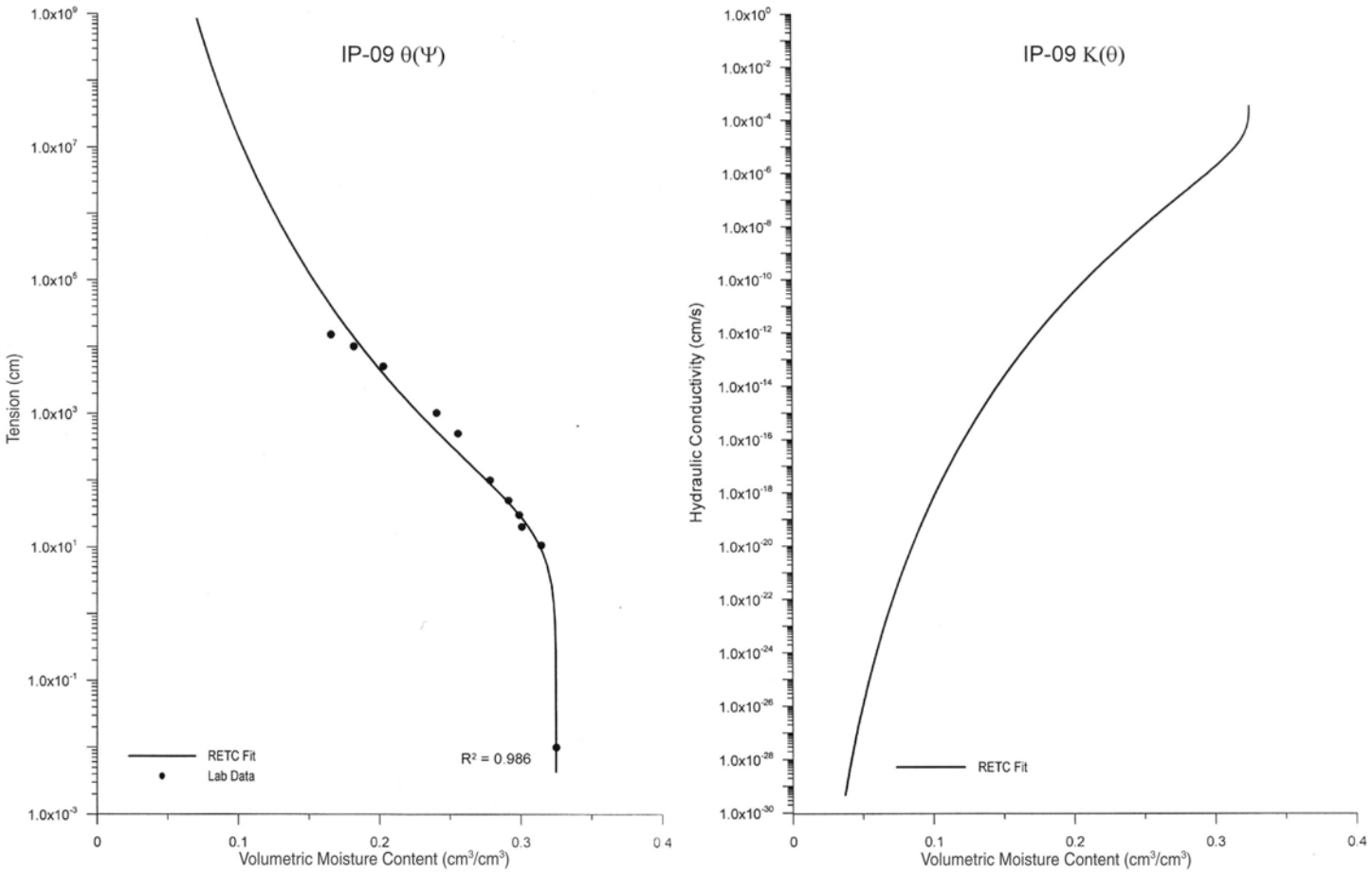

Figure 5-10 RETC Code Simulation of θ(Ψ) and K(θ) Hydraulic Properties for IP-09

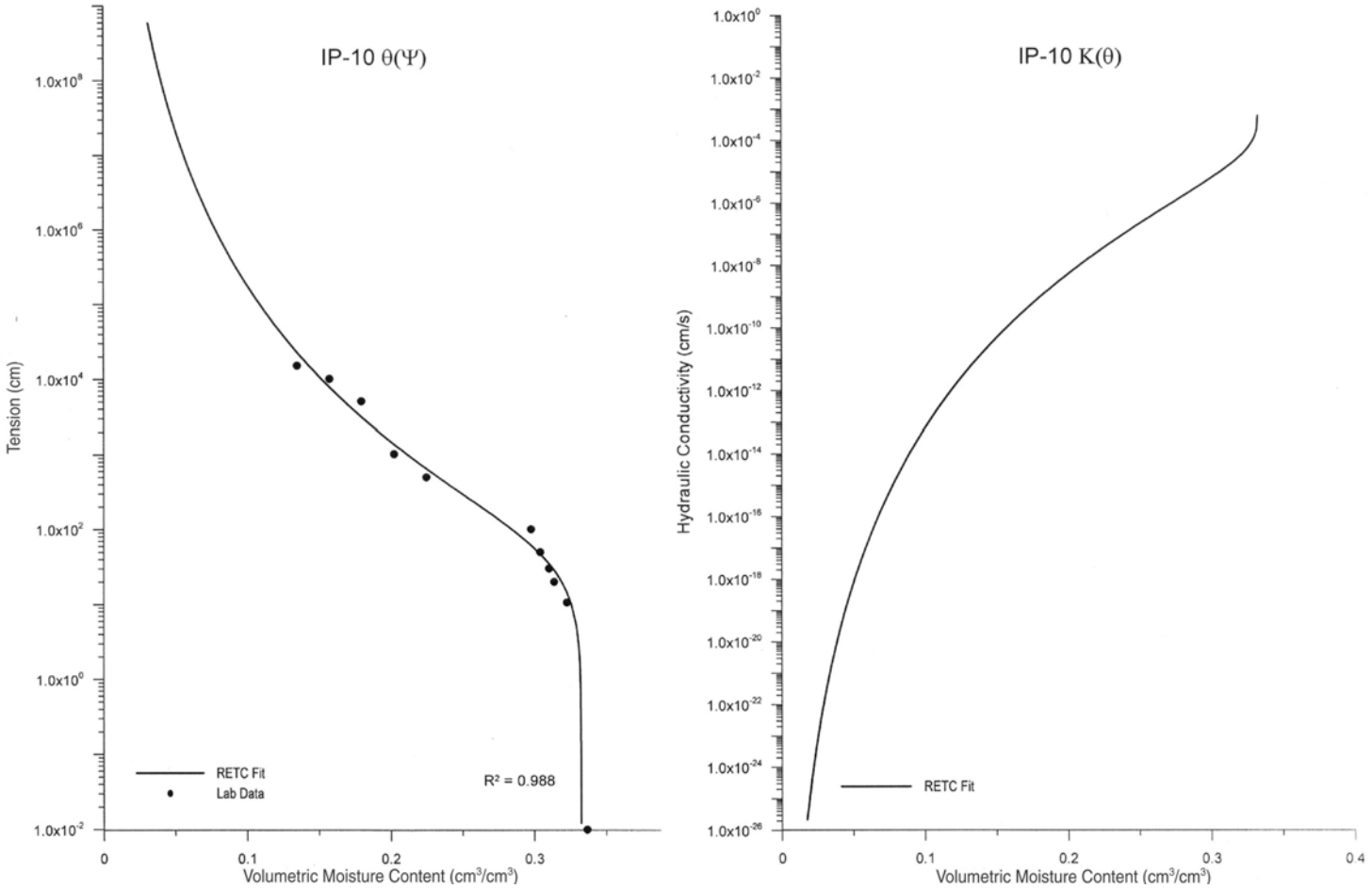

Figure 5-11 RETC Code Simulation of θ(Ψ) and K(θ) Hydraulic Properties for IP-10

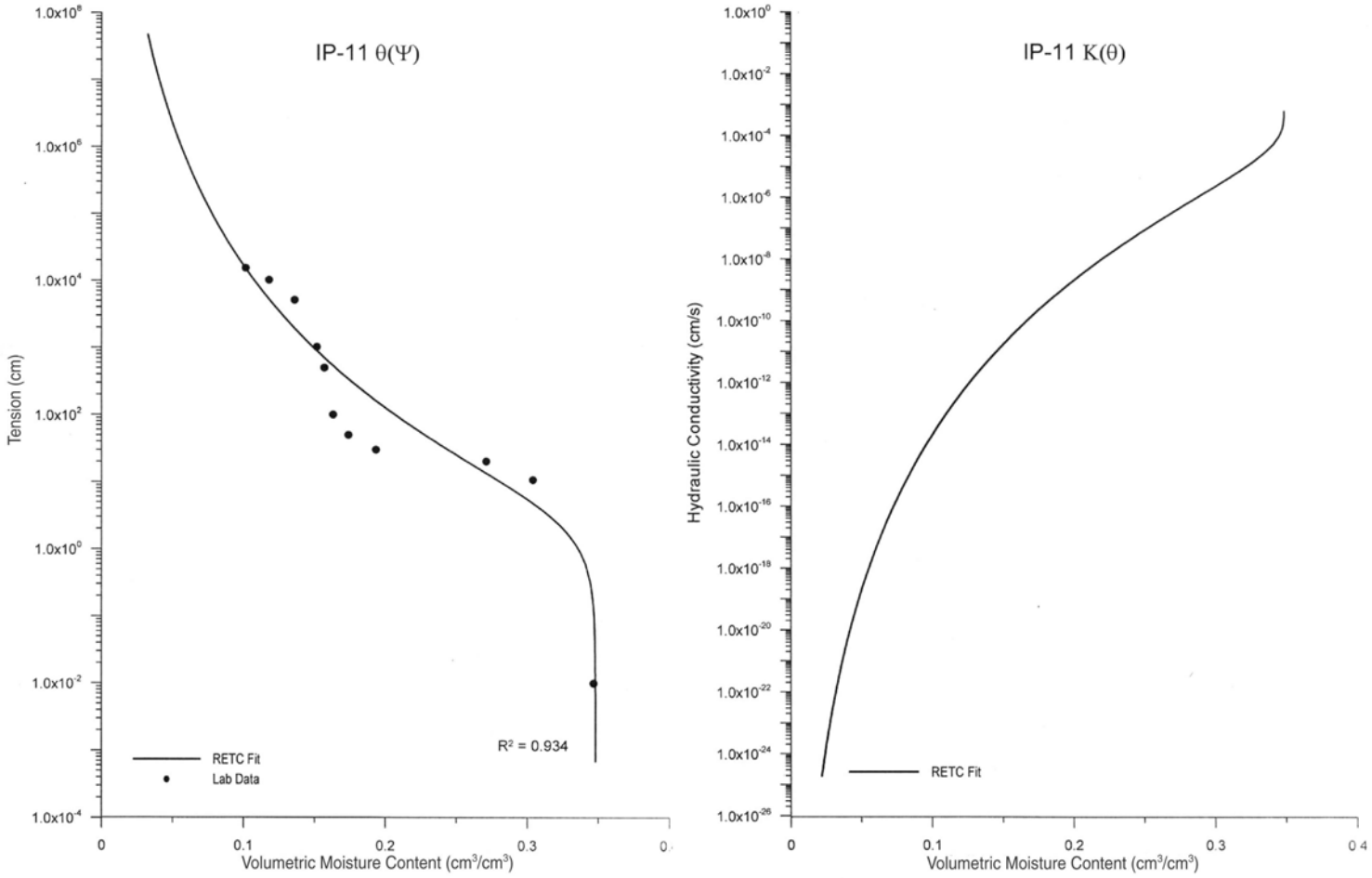

Figure 5-12 RETC Code Simulation of θ(Ψ) and K(θ) Hydraulic Properties for IP-11

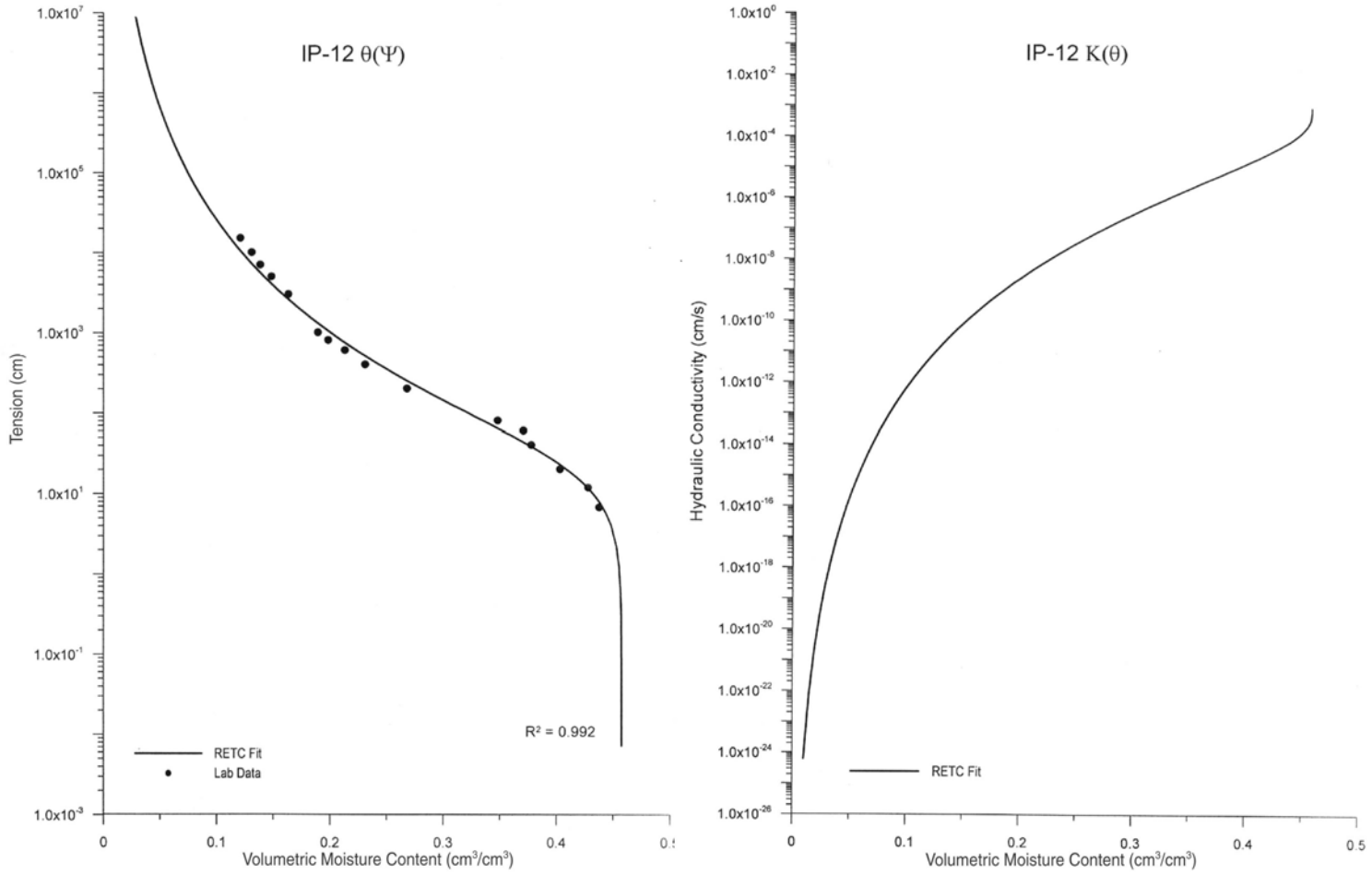

Figure 5-13 RETC Code Simulation of θ(Ψ) and K(θ) Hydraulic Properties for IP-12

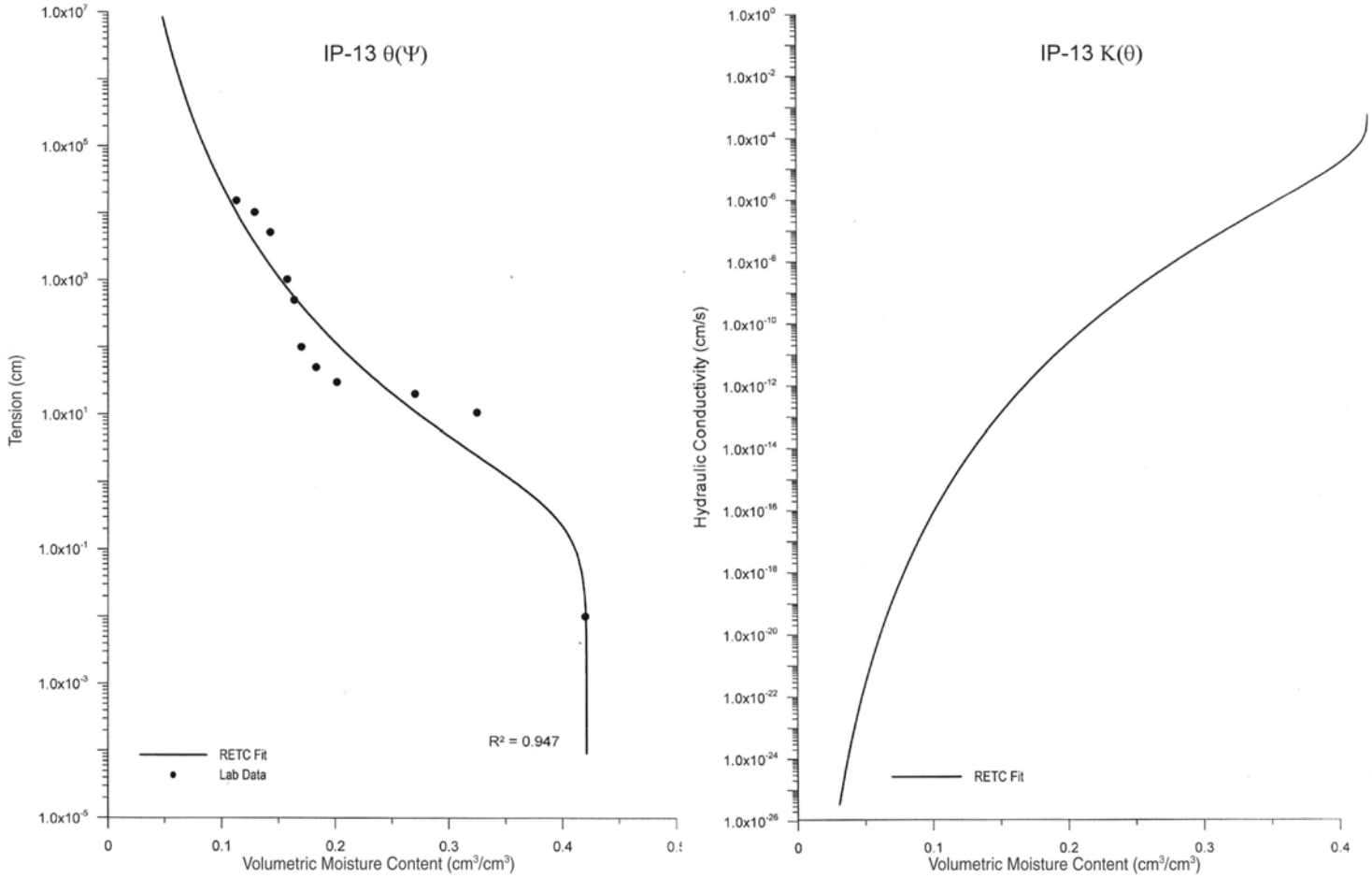

Figure 5-14 RETC Code Simulation of θ(Ψ) and K(θ) Hydraulic Properties for IP-13

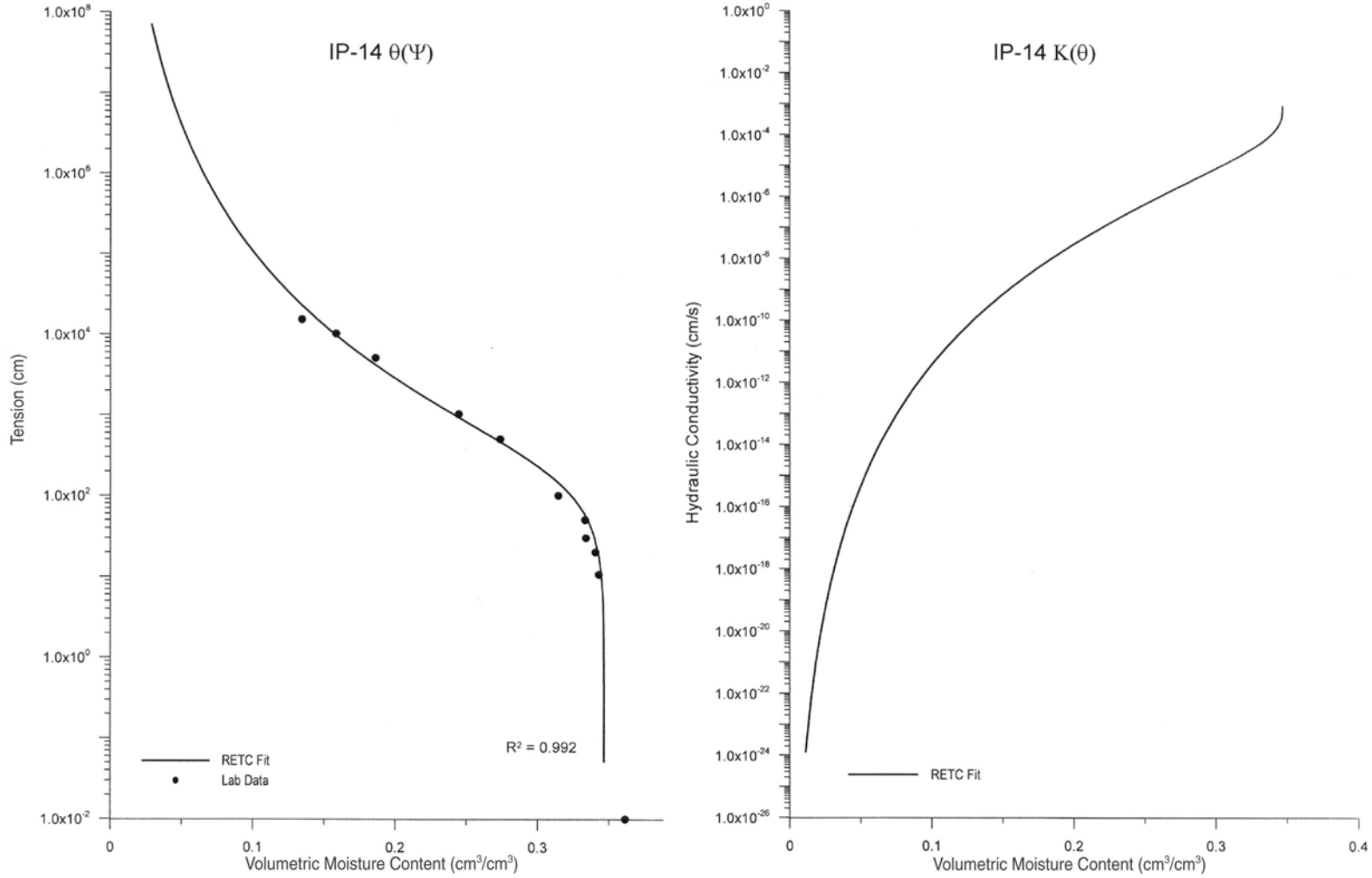

Figure 5-15 RETC Code Simulation of θ(Ψ) and K(θ) Hydraulic Properties for IP-14

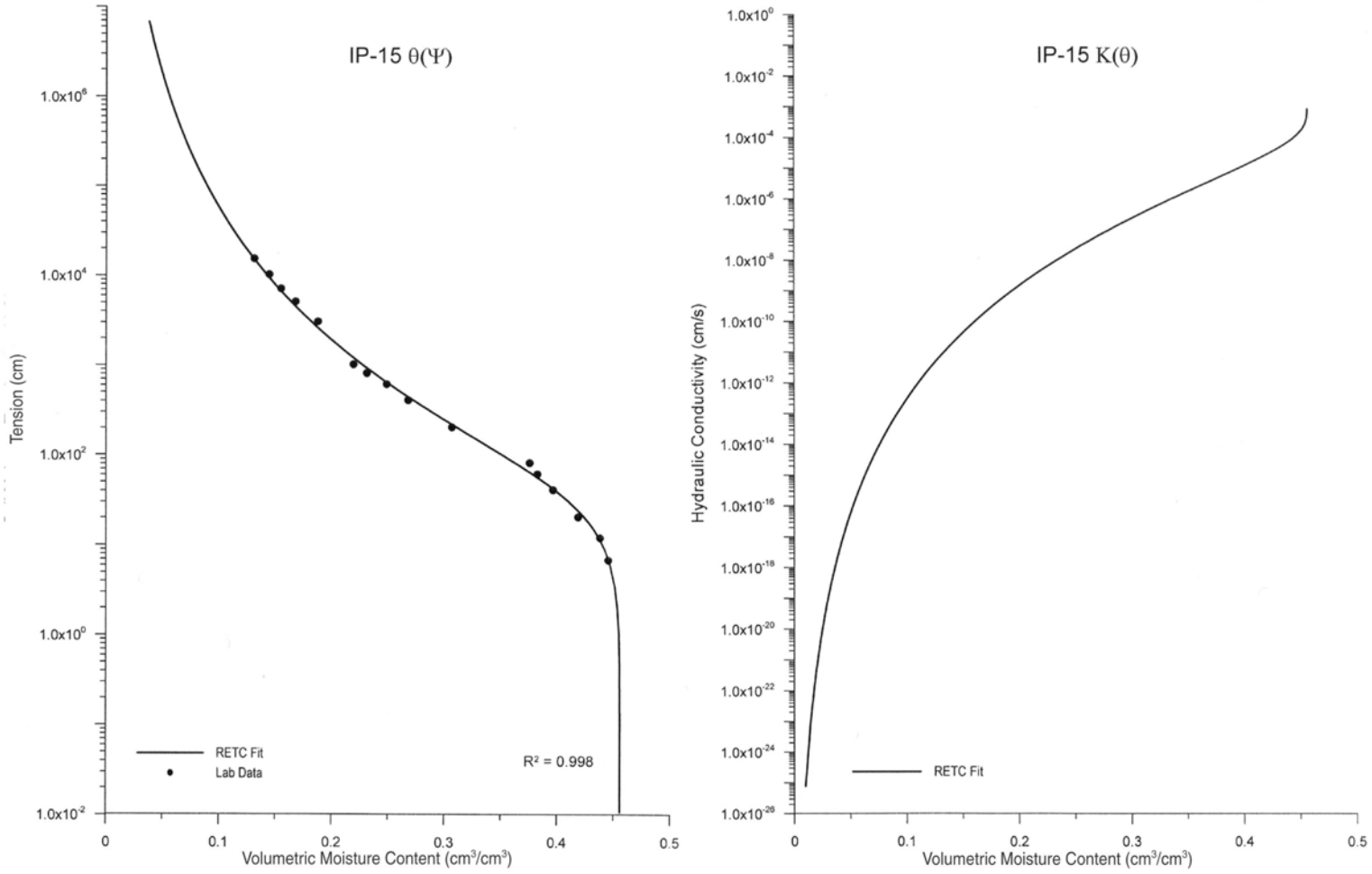

Figure 5-16 RETC Code Simulation of θ(Ψ) and K(θ) Hydraulic Properties for IP-15

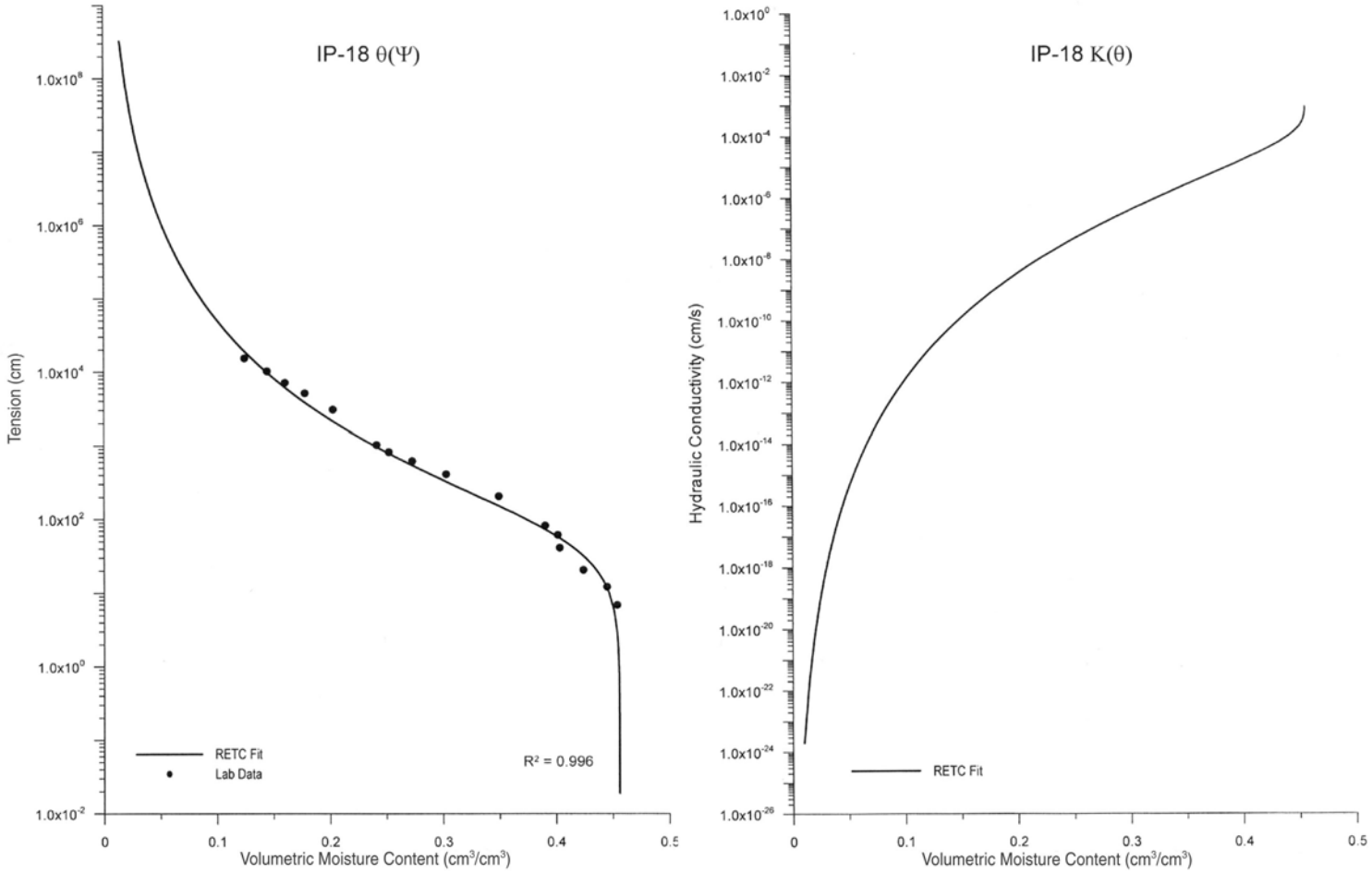

Figure 5-17 RETC Code Simulation of θ(Ψ) and K(θ) Hydraulic Properties for IP-18

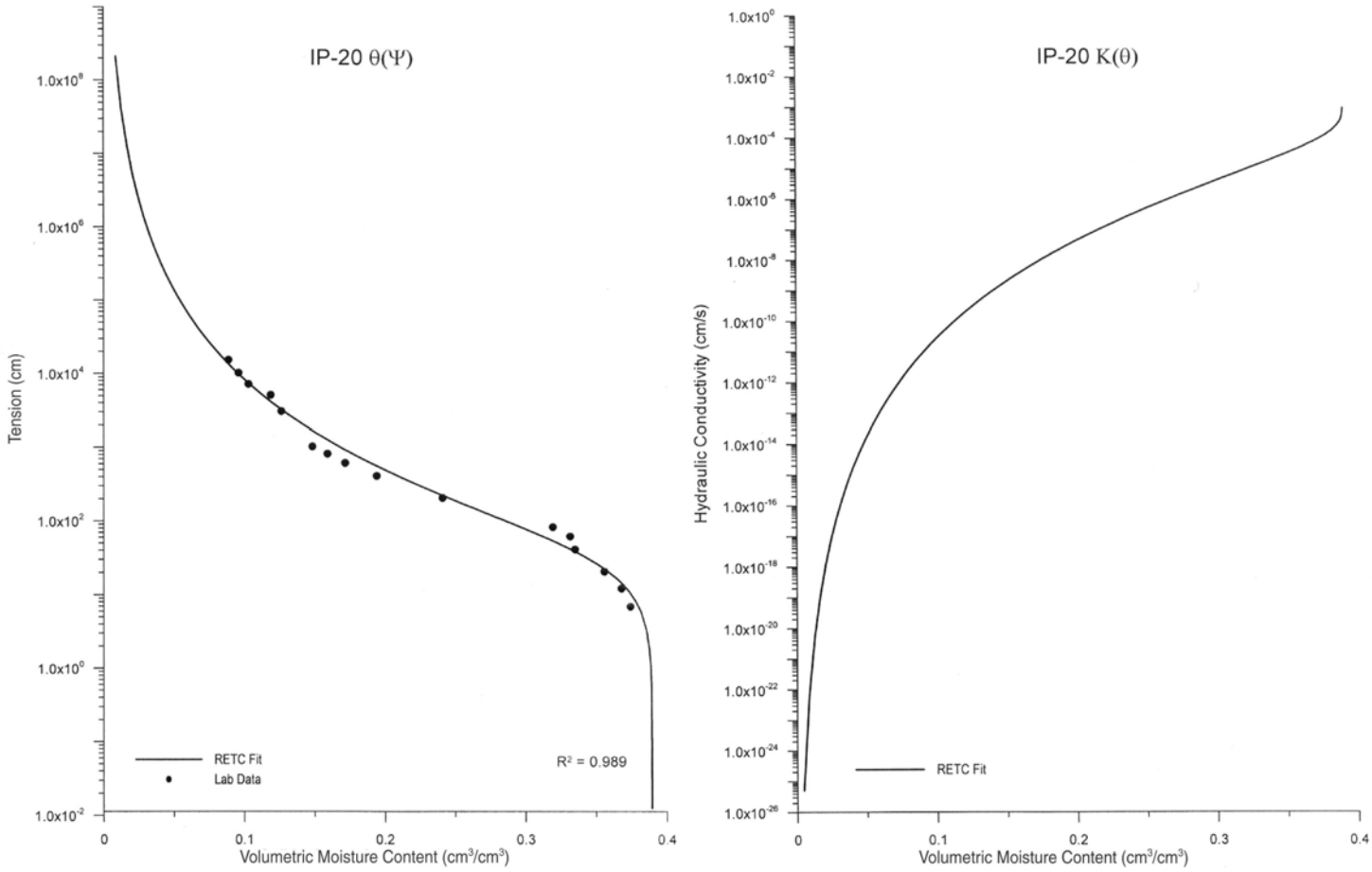

Figure 5-18 RETC Code Simulation of θ(Ψ) and K(θ) Hydraulic Properties for IP-20

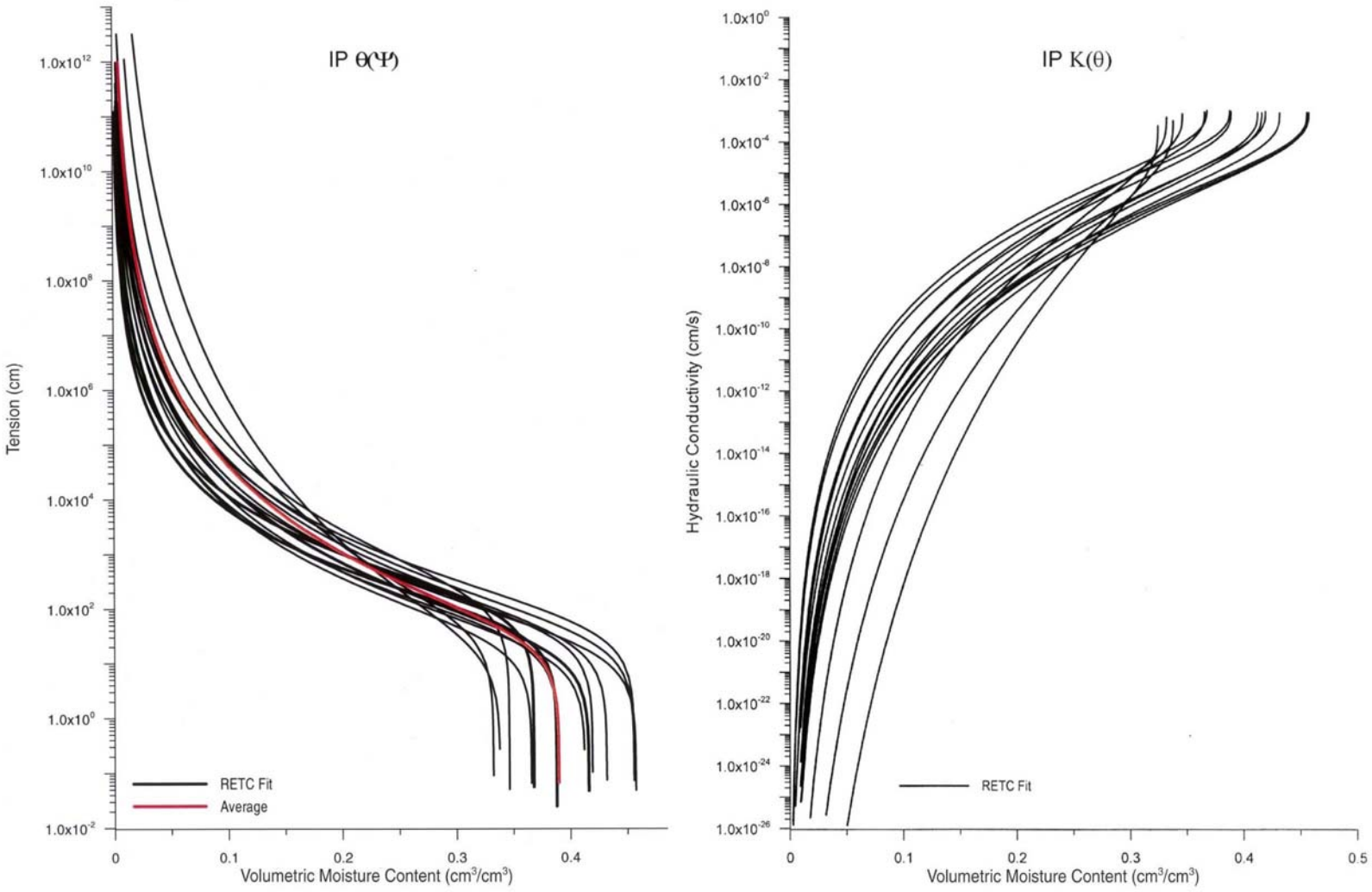

Figure 5-19 RETC Code Prediction of the Hydraulic Conductivity Function Based on θ(Ψ) Data

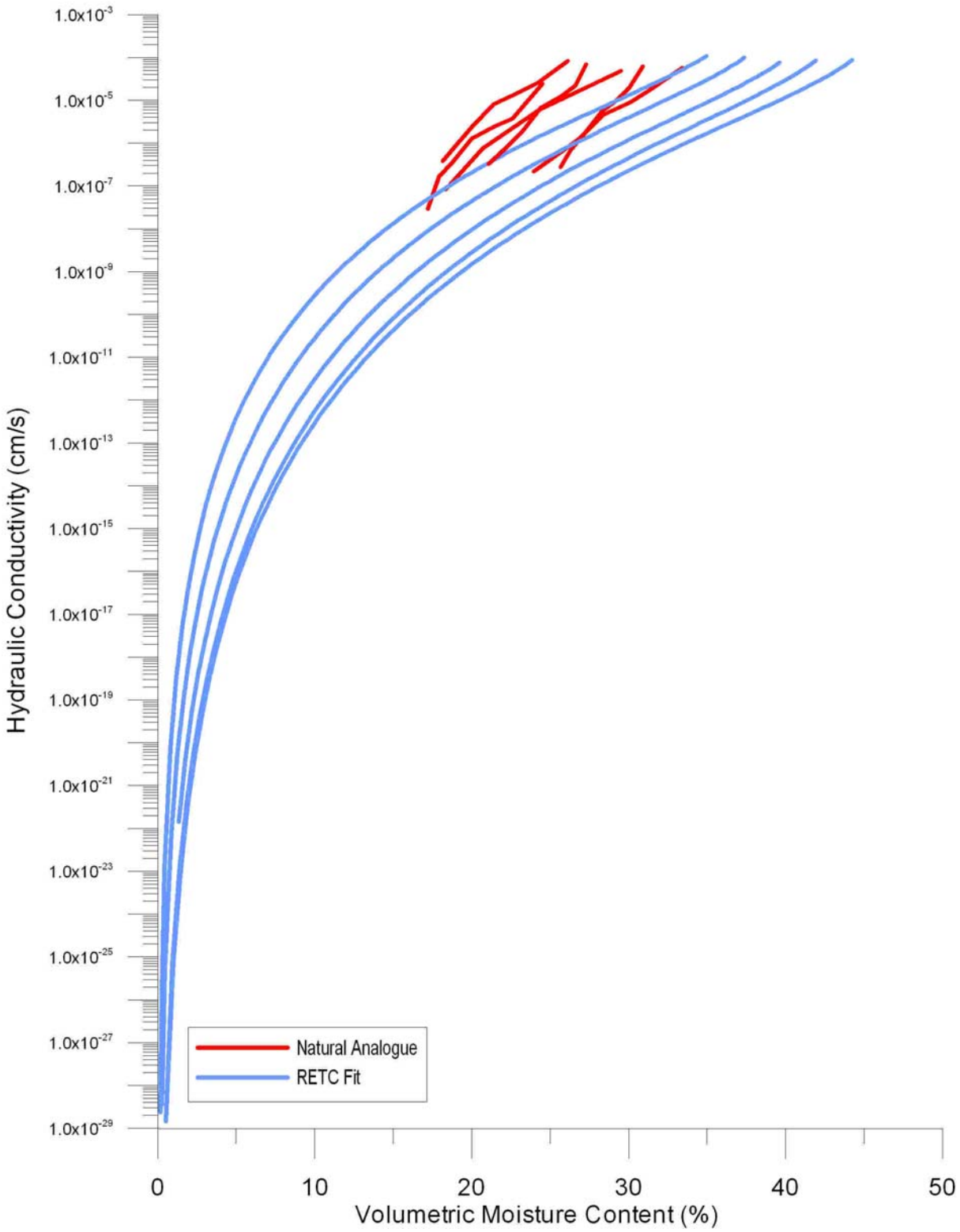

Figure 5-20 Comparison of K(θ) Obtained from the IP Test and K(θ) Obtained from RETC

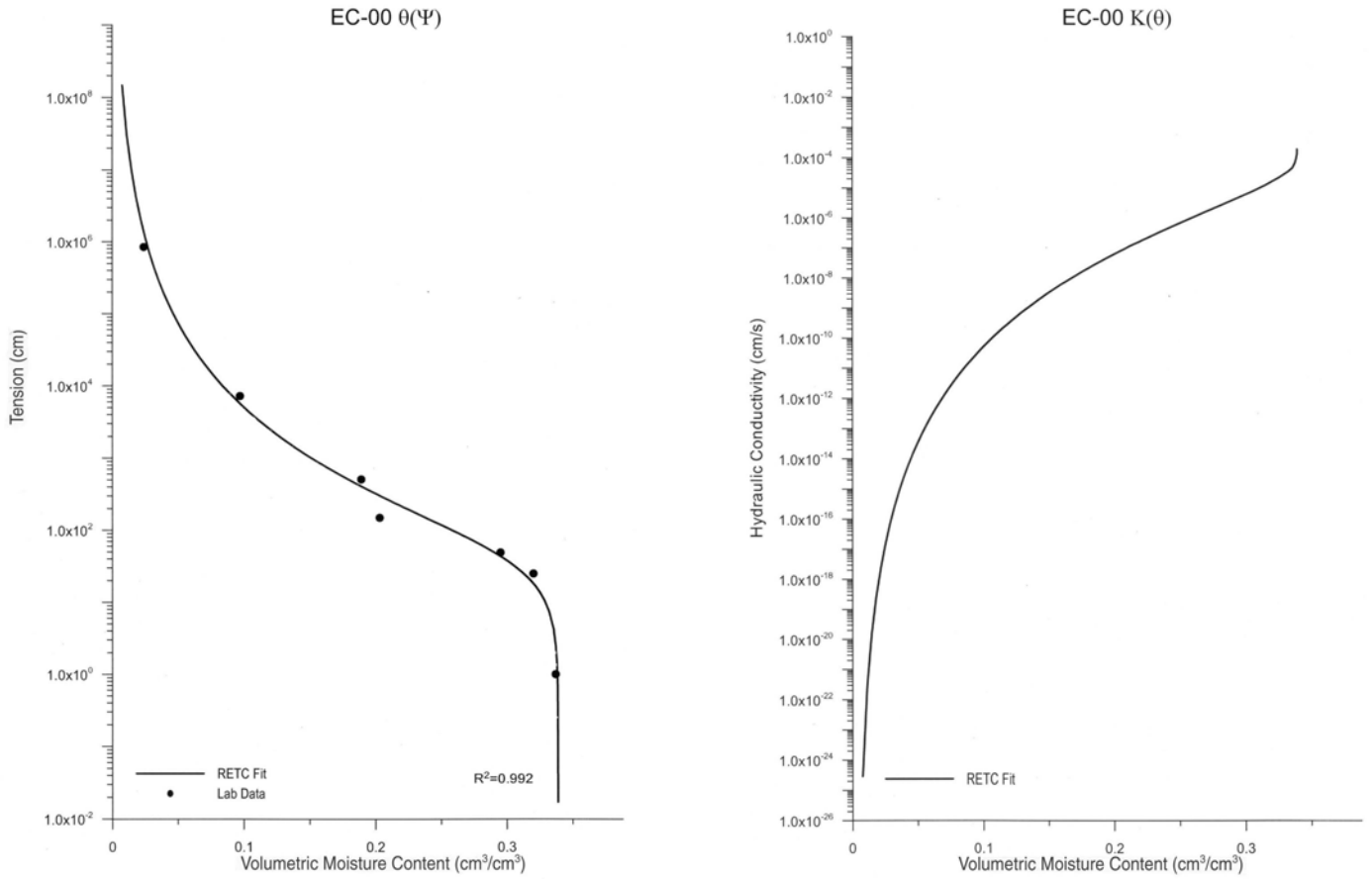

Figure 5-21 RETC Code Simulation of θ(Ψ) and K(θ) Hydraulic Properties for EC-00

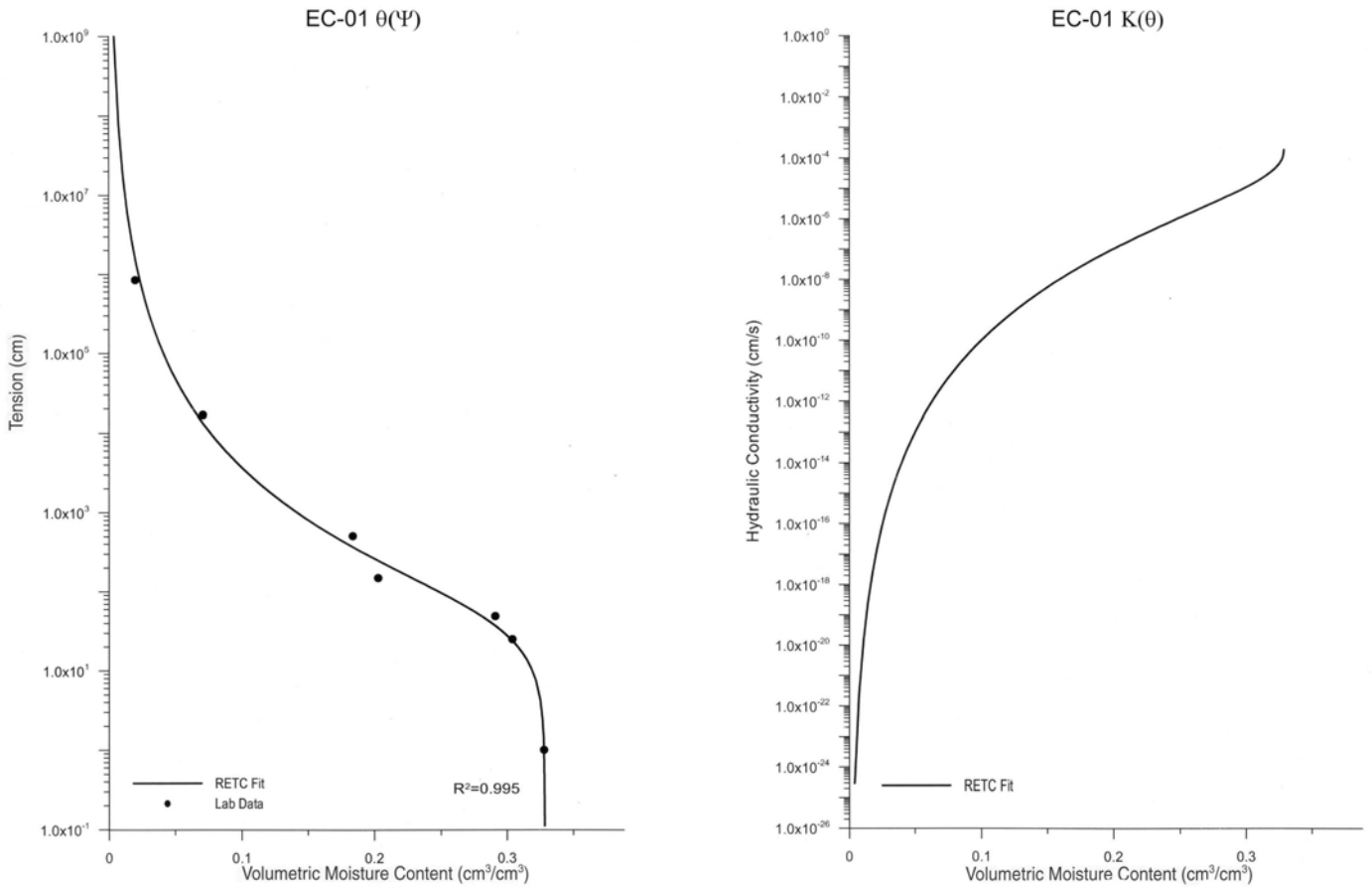

Figure 5-22 RETC Code Simulation of θ(Ψ) and K(θ) Hydraulic Properties for EC-01

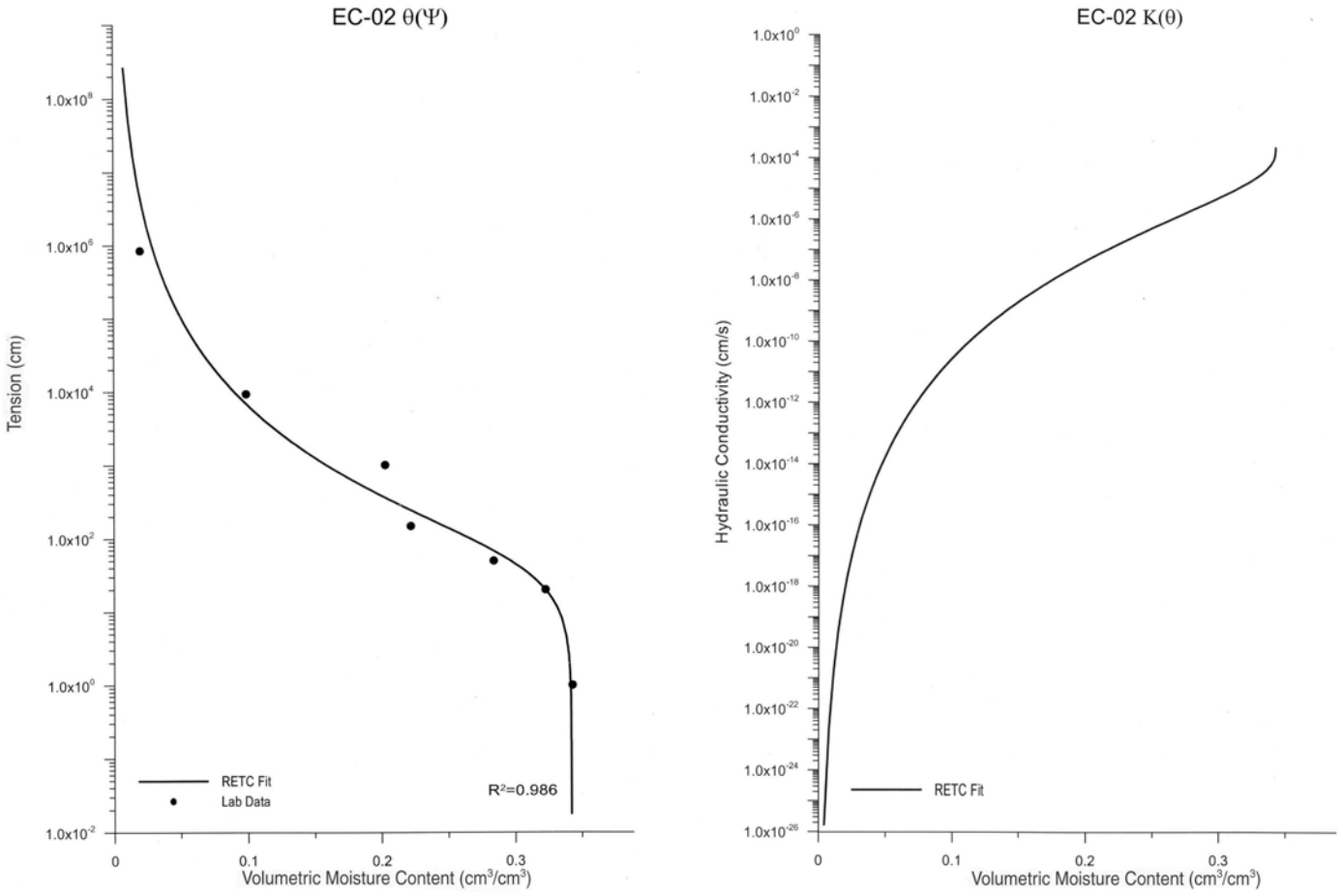

Figure 5-23 RETC Code Simulation of θ(Ψ) and K(θ) Hydraulic Properties for EC-02

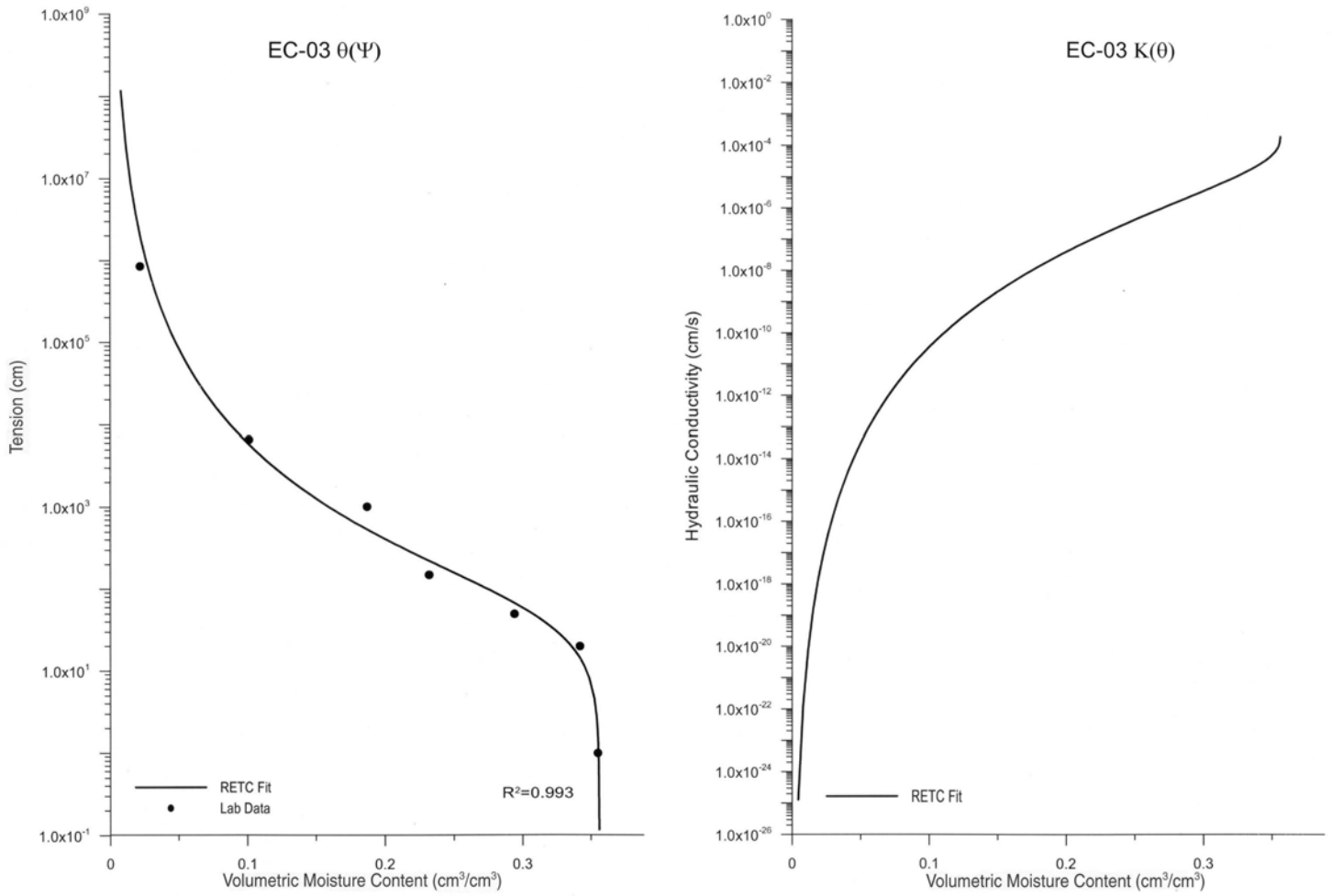

Figure 5-24 RETC Code Simulation of θ(Ψ) and K(θ) Hydraulic Properties for EC-03

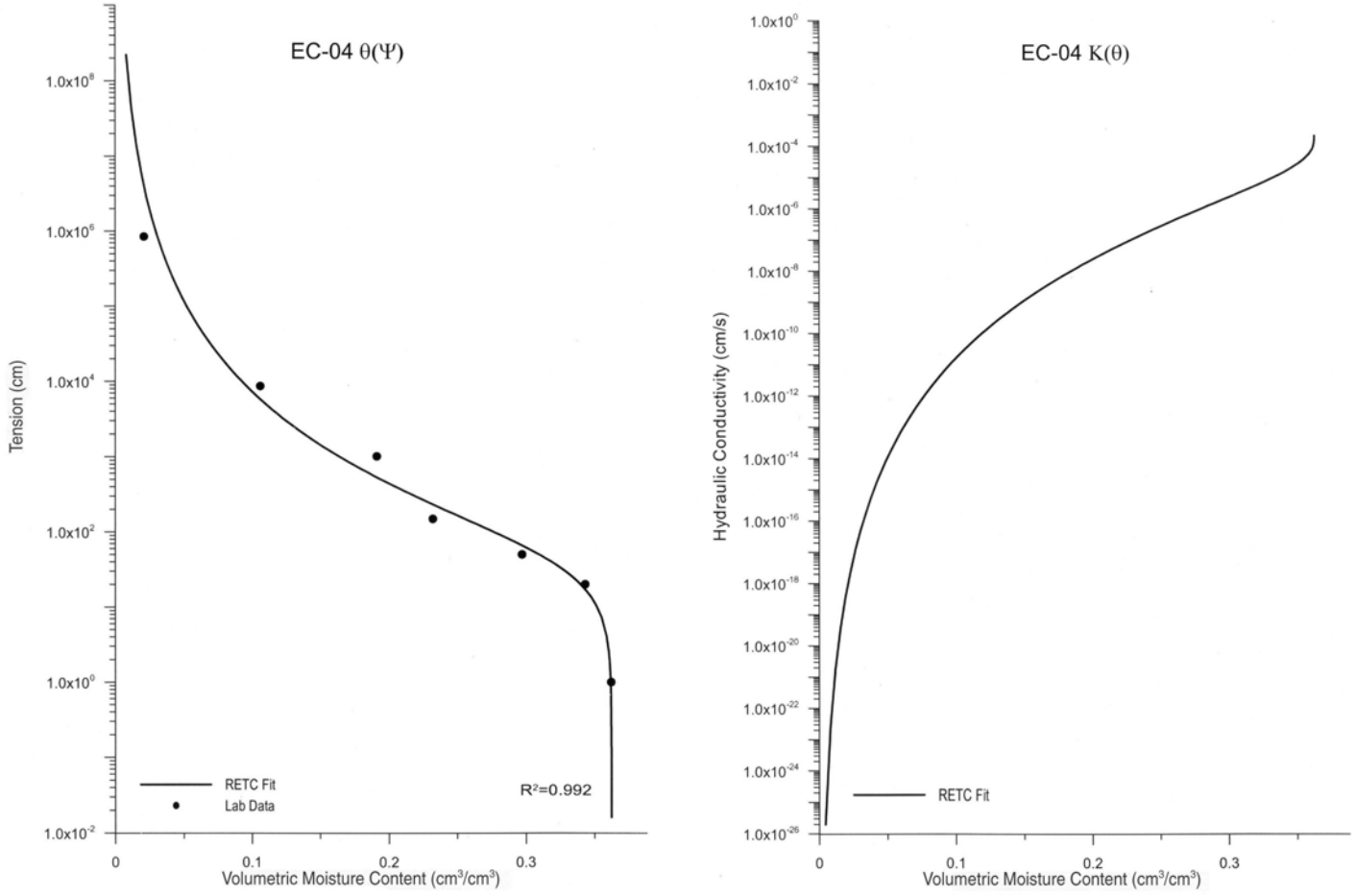

Figure 5-25 RETC Code Simulation of θ(Ψ) and K(θ) Hydraulic Properties for EC-04

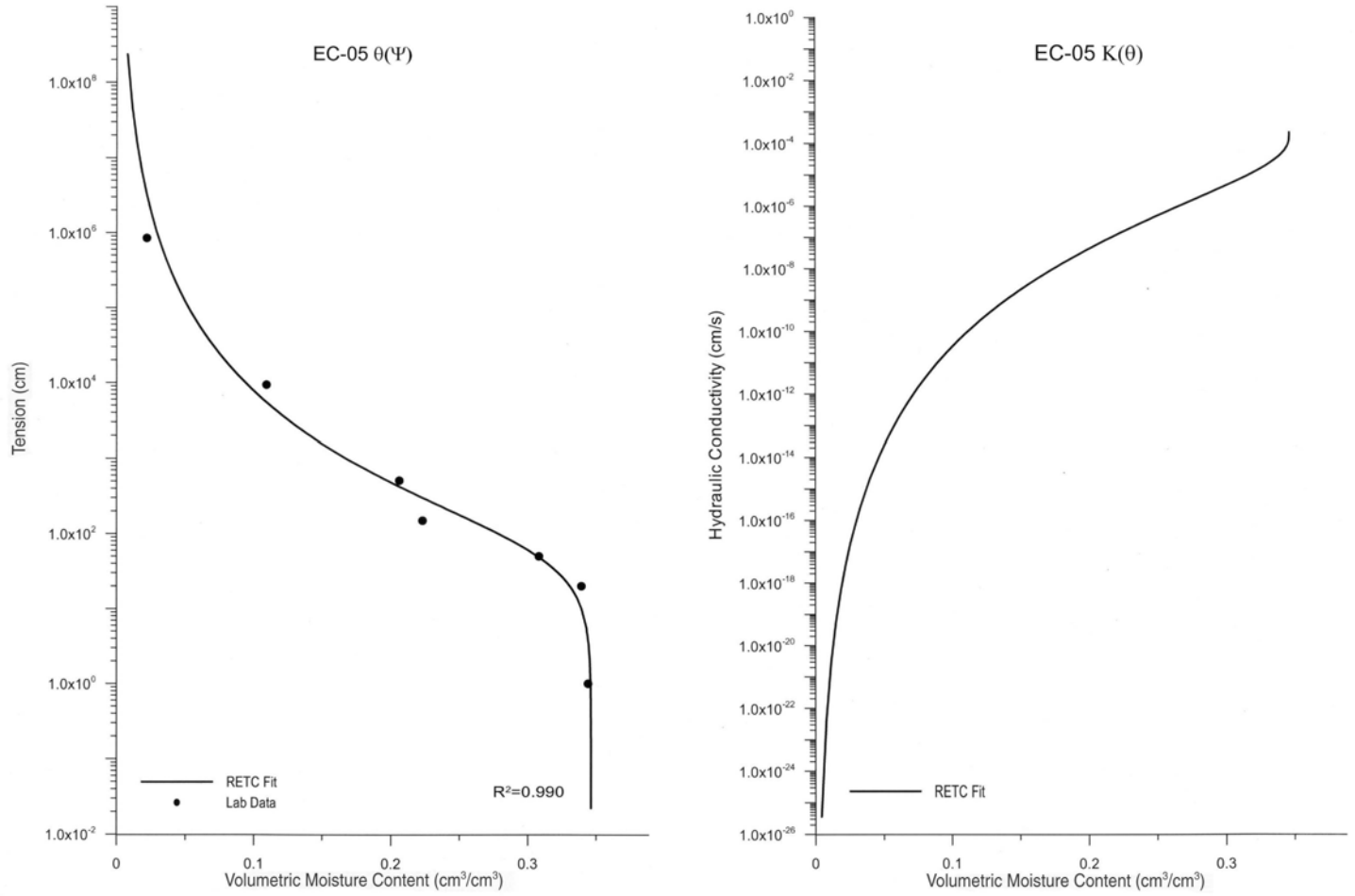

Figure 5-26 RETC Code Simulation of θ(Ψ) and K(θ) Hydraulic Properties for EC-05

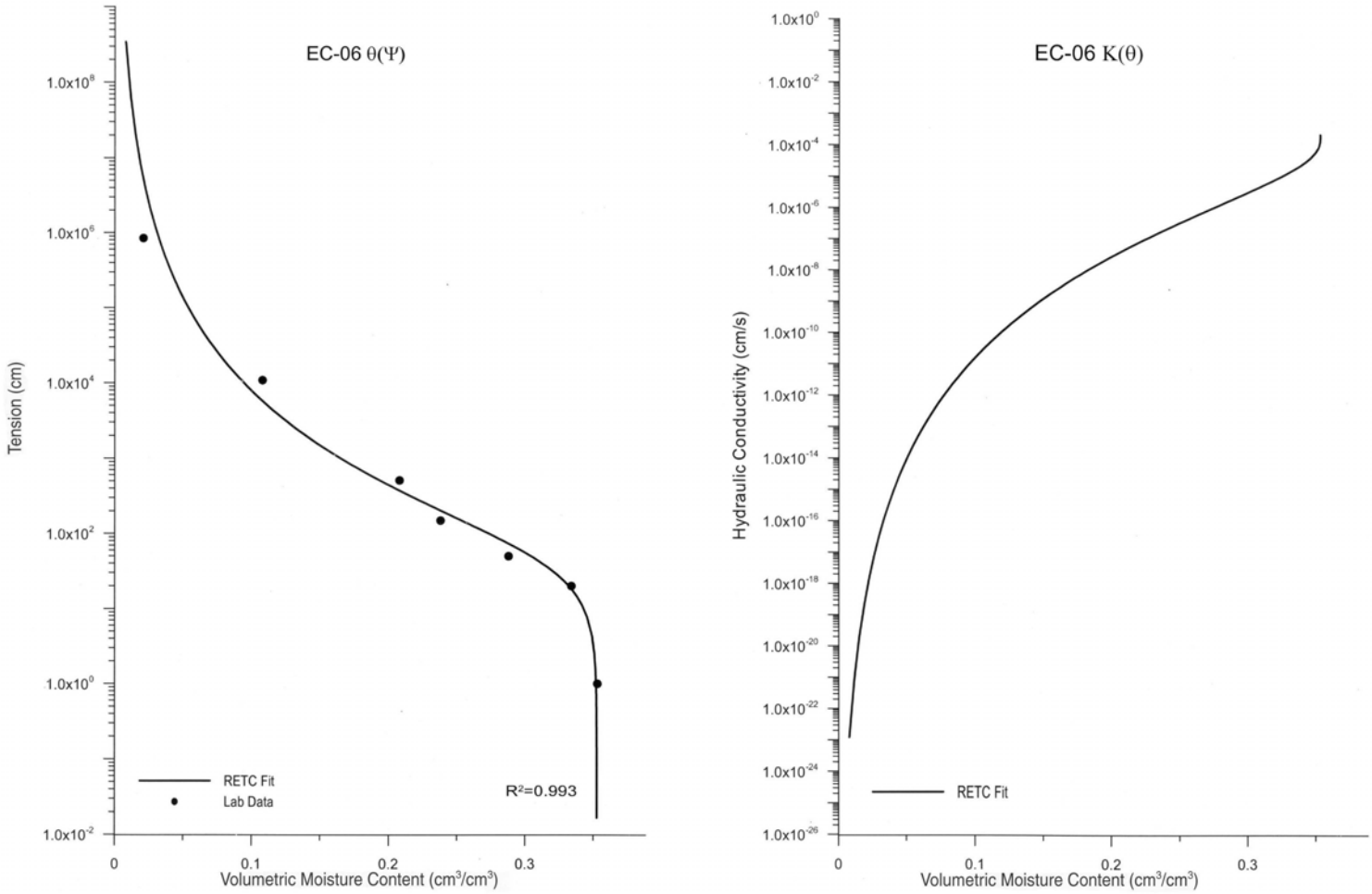

Figure 5-27 RETC Code Simulation of θ(Ψ) and K(θ) Hydraulic Properties for EC-06

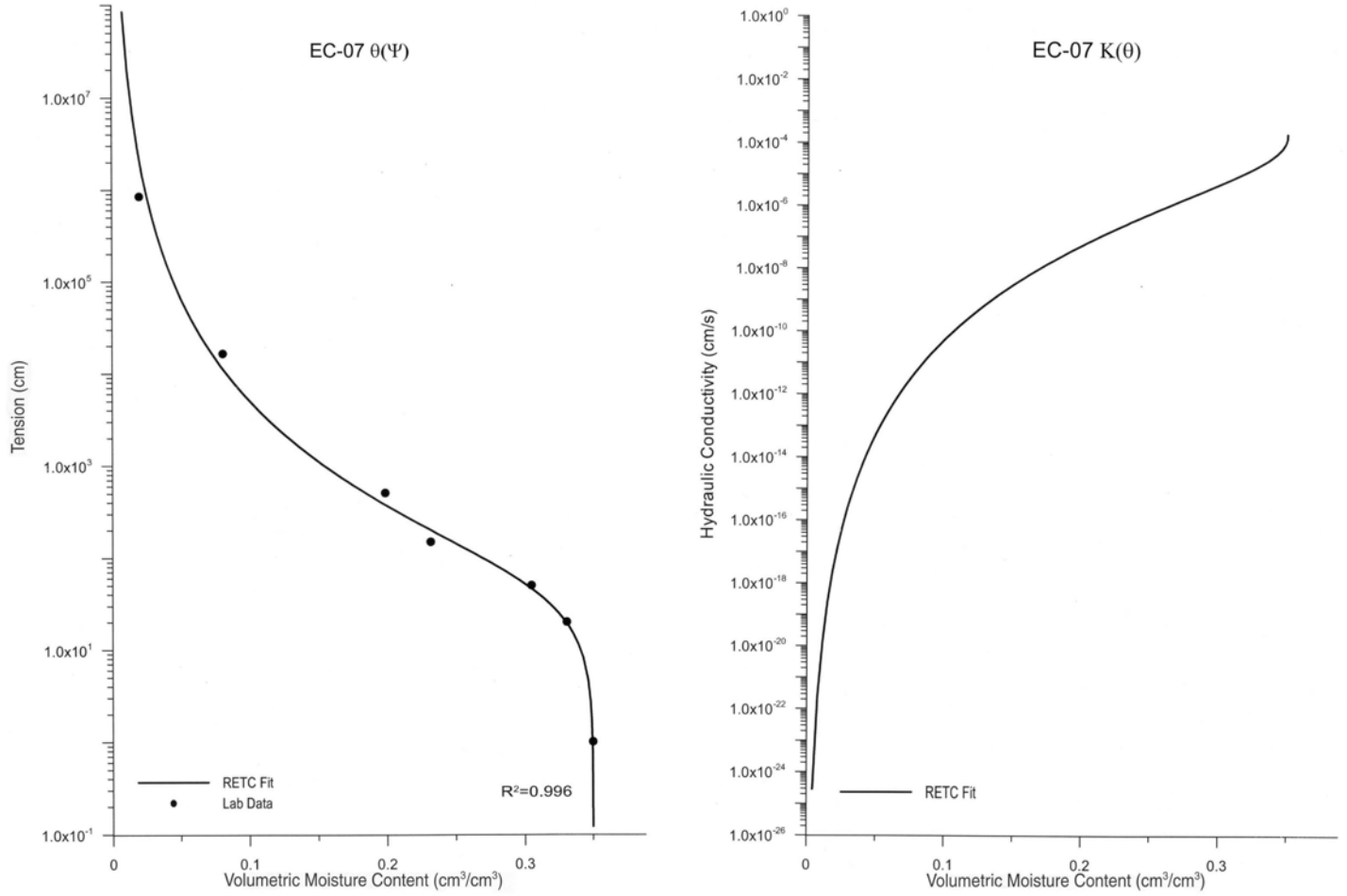

Figure 5-28 RETC Code Simulation of θ(Ψ) and K(θ) Hydraulic Properties for EC-07

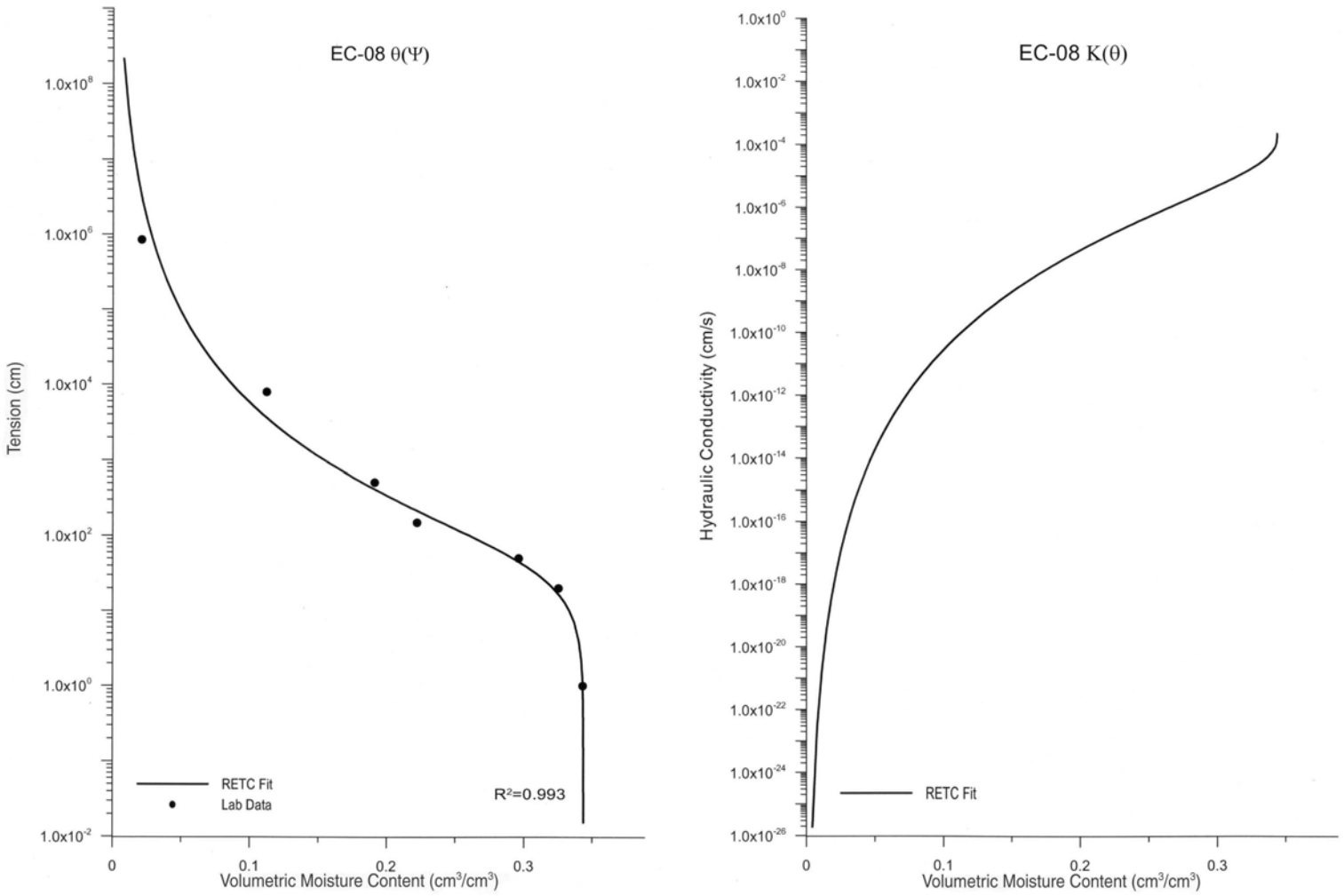

Figure 5-29 RETC Code Simulation of θ(Ψ) and K(θ) Hydraulic Properties for EC-08

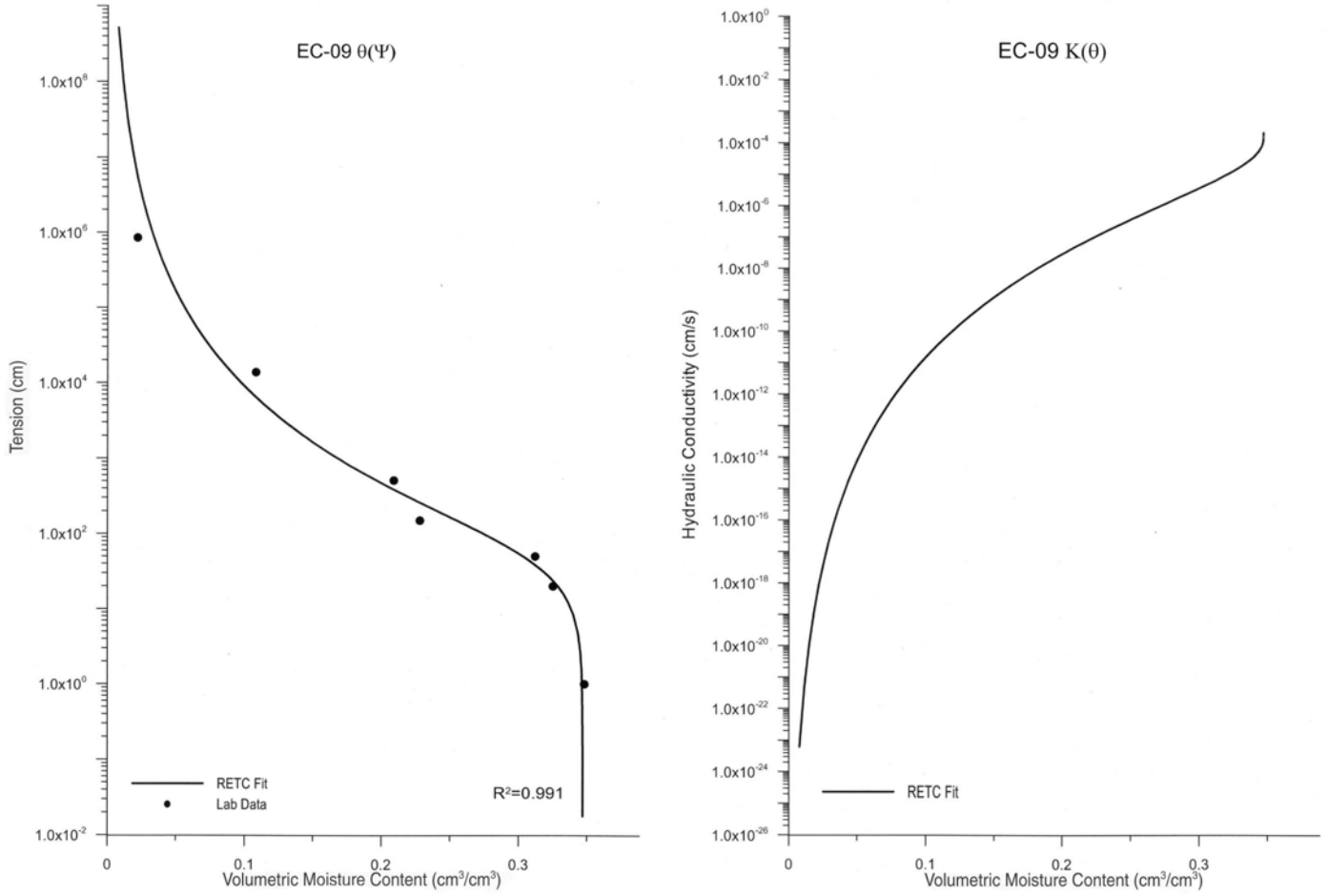

Figure 5-30 RETC Code Simulation of θ(Ψ) and K(θ) Hydraulic Properties for EC-09

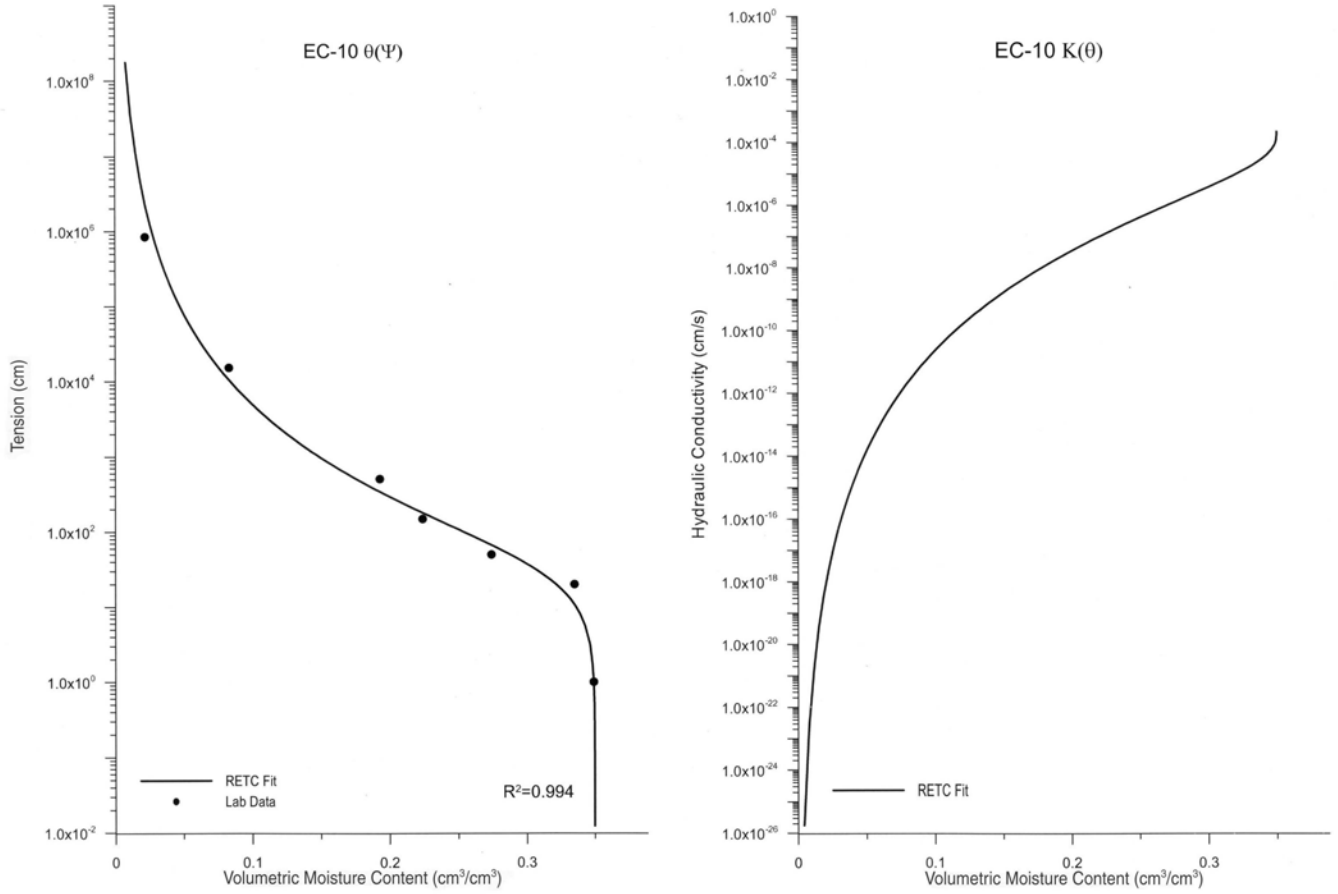

Figure 5-31 RETC Code Simulation of θ(Ψ) and K(θ) Hydraulic Properties for EC-10

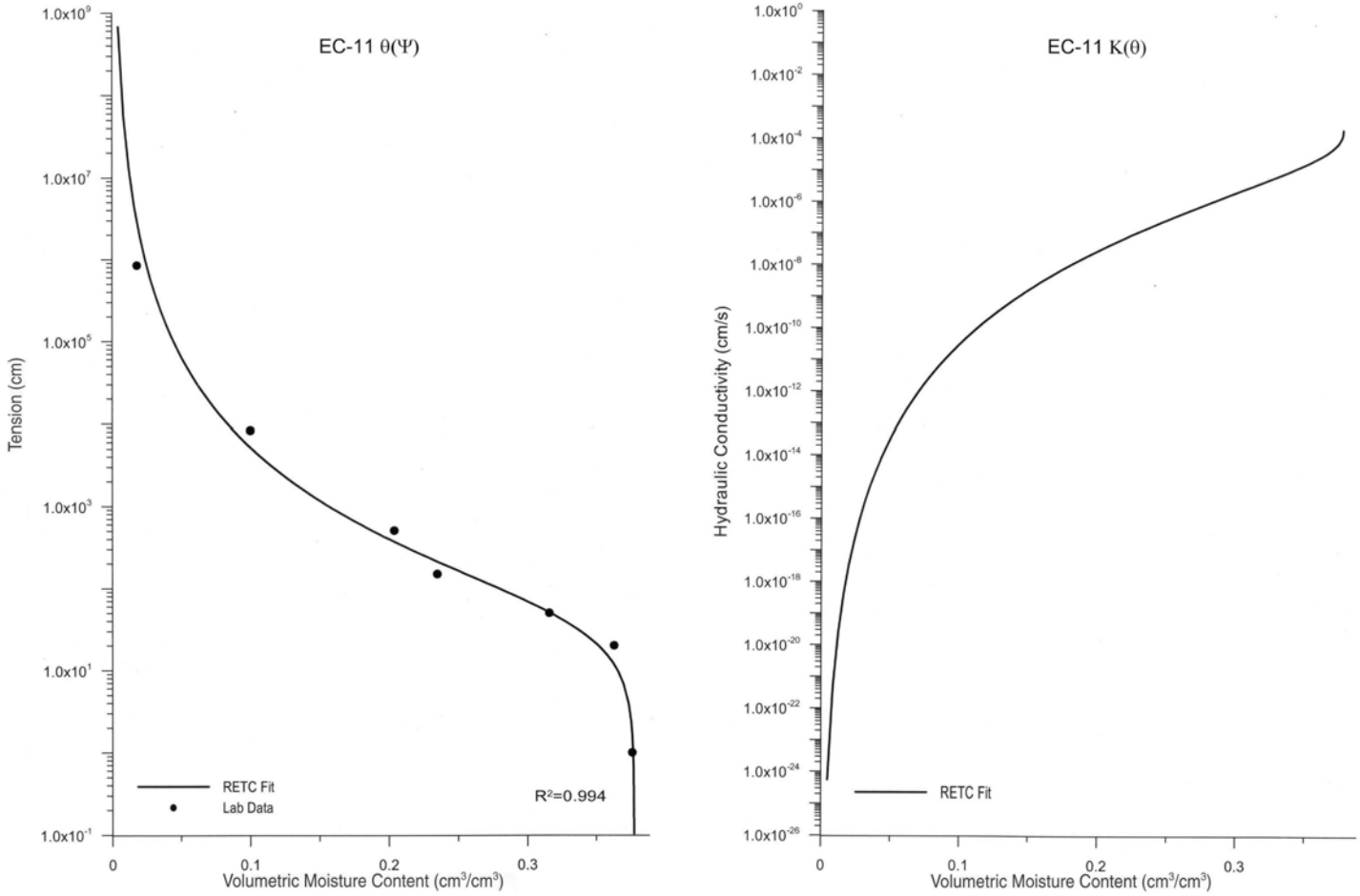

Figure 5-32 RETC Code Simulation of θ(Ψ) and K(θ) Hydraulic Properties for EC-11

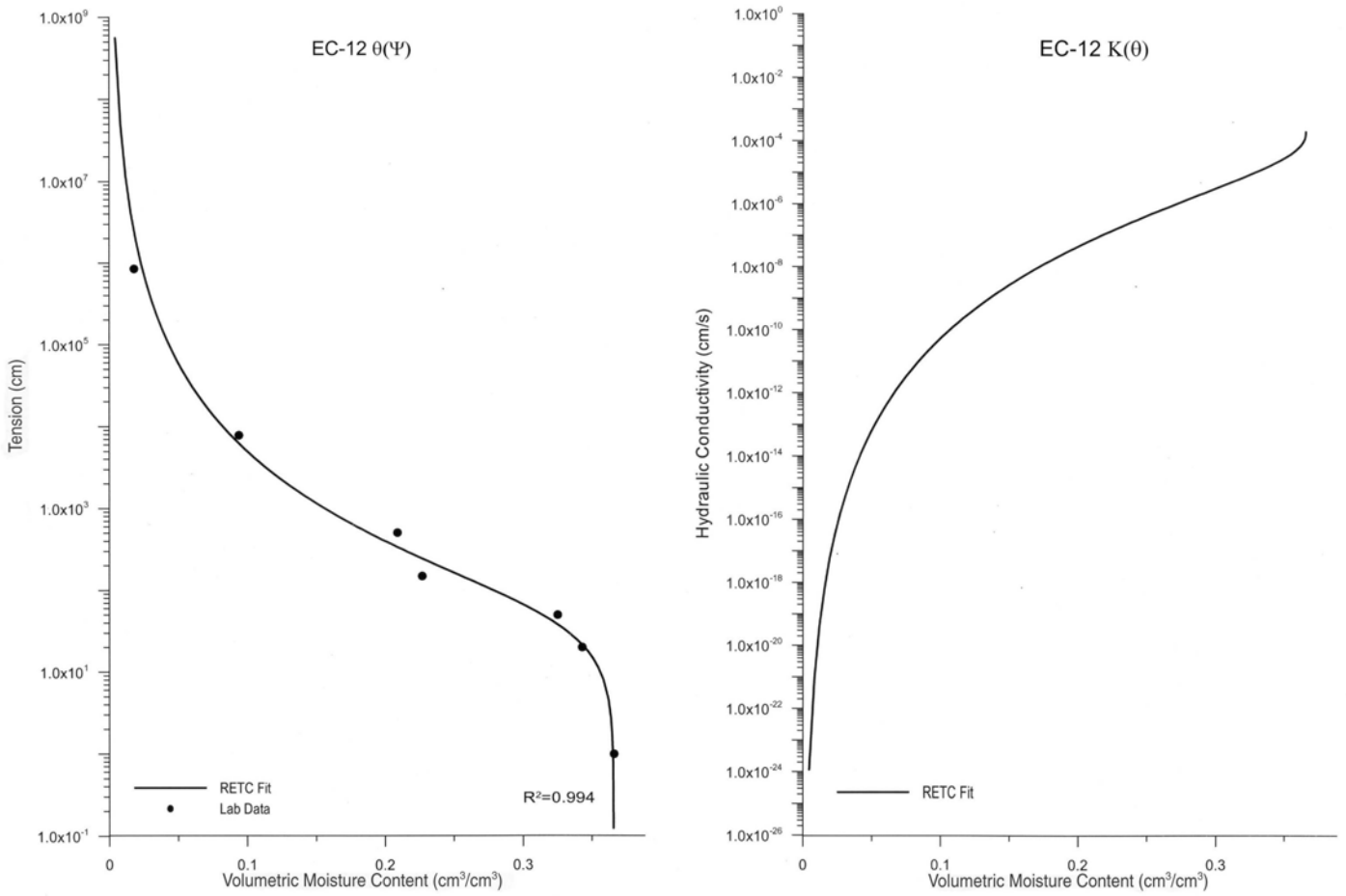

Figure 5-33 RETC Code Simulation of θ(Ψ) and K(θ) Hydraulic Properties for EC-12

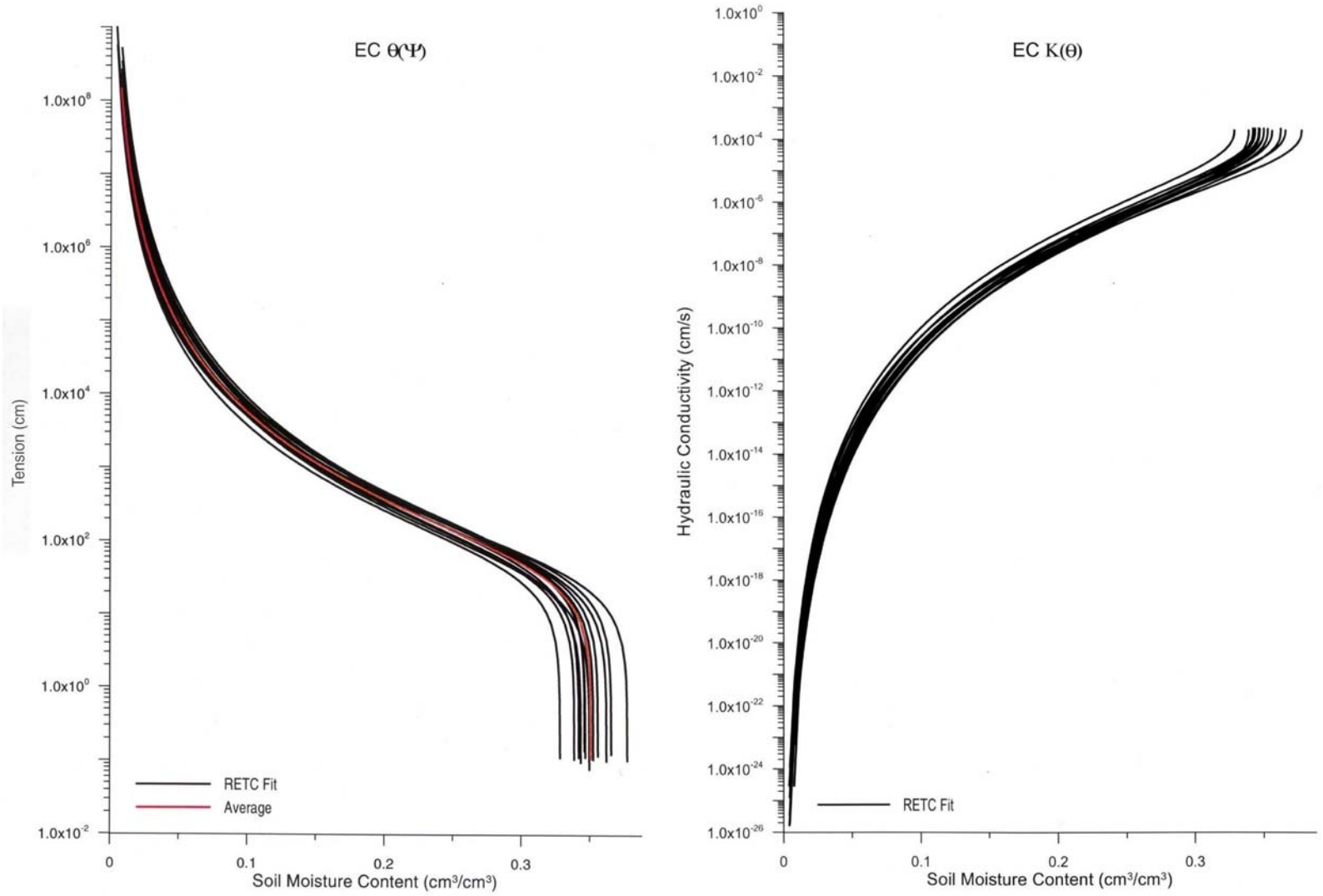

Figure 5-34 RETC Code Prediction of the Hydraulic Conductivity Function Based on θ(Ψ) Data

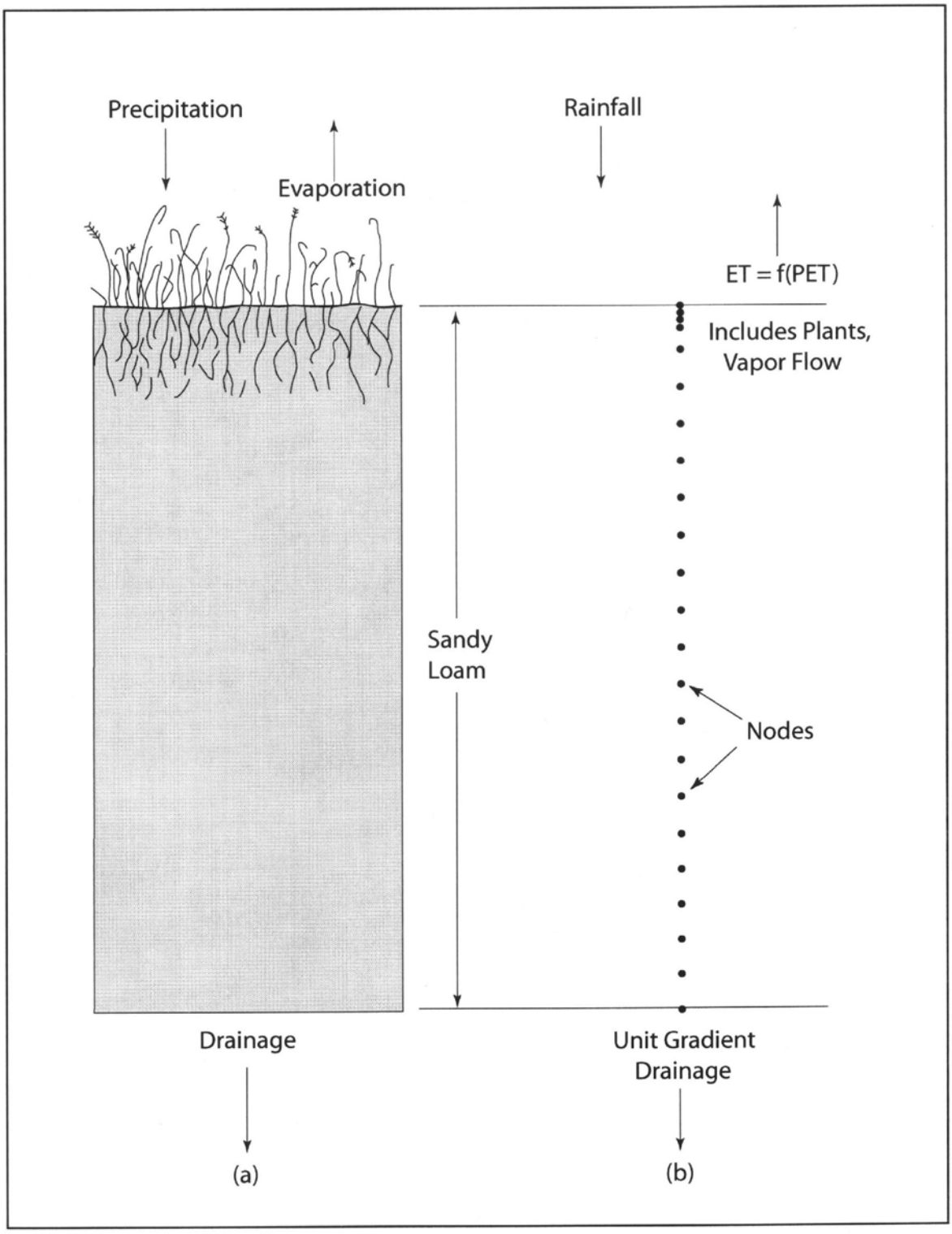

Figure 6-1 Example Problem Formulation:
(a) Site Description, (b) Model Representation

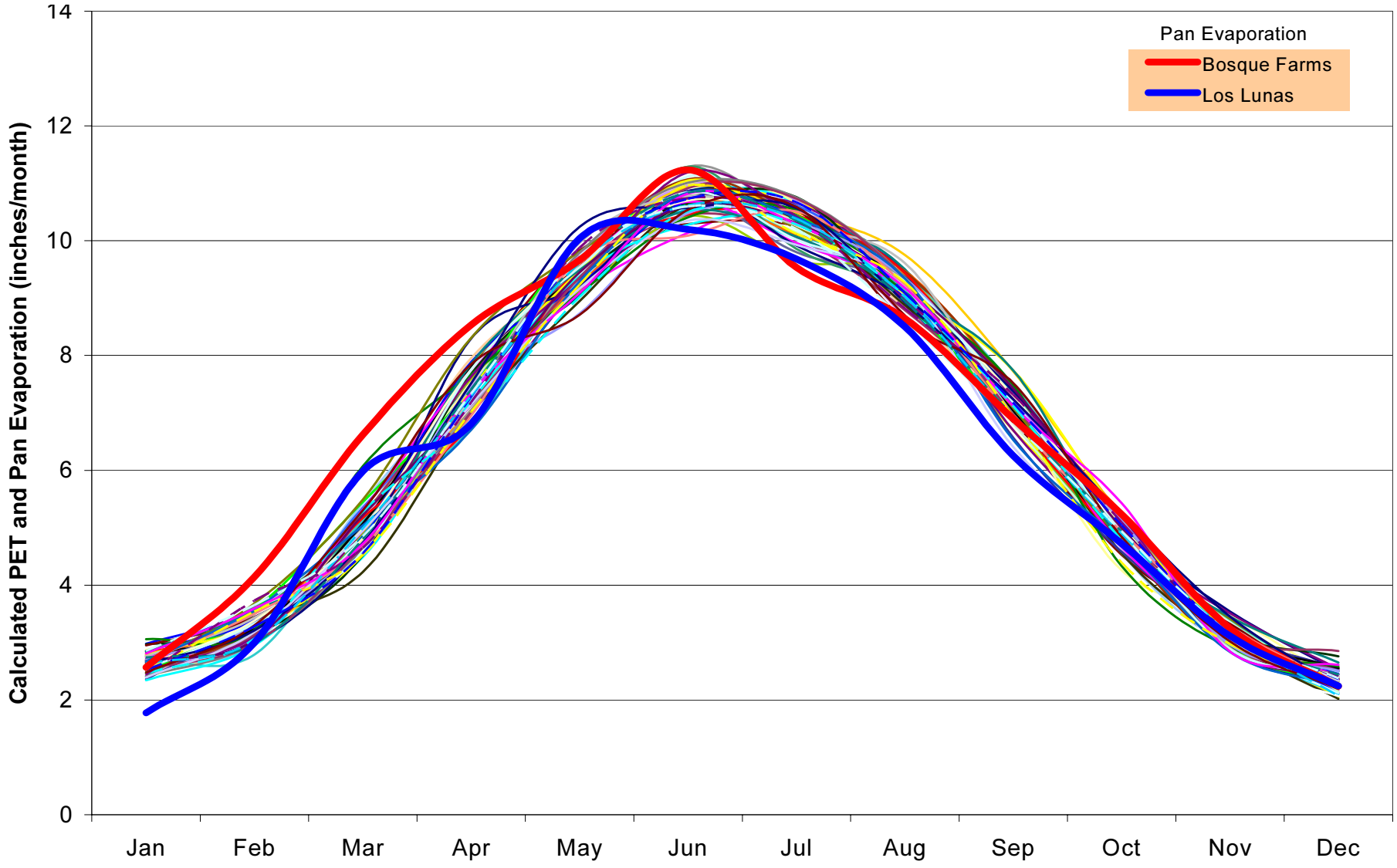

Figure 6-2 HELP-Derived PET for the Years 1932 Through 1996 (fine lines) with Average Monthly Pan Evaporation for Bosque Farms and Los Lunas, New Mexico (thick lines)

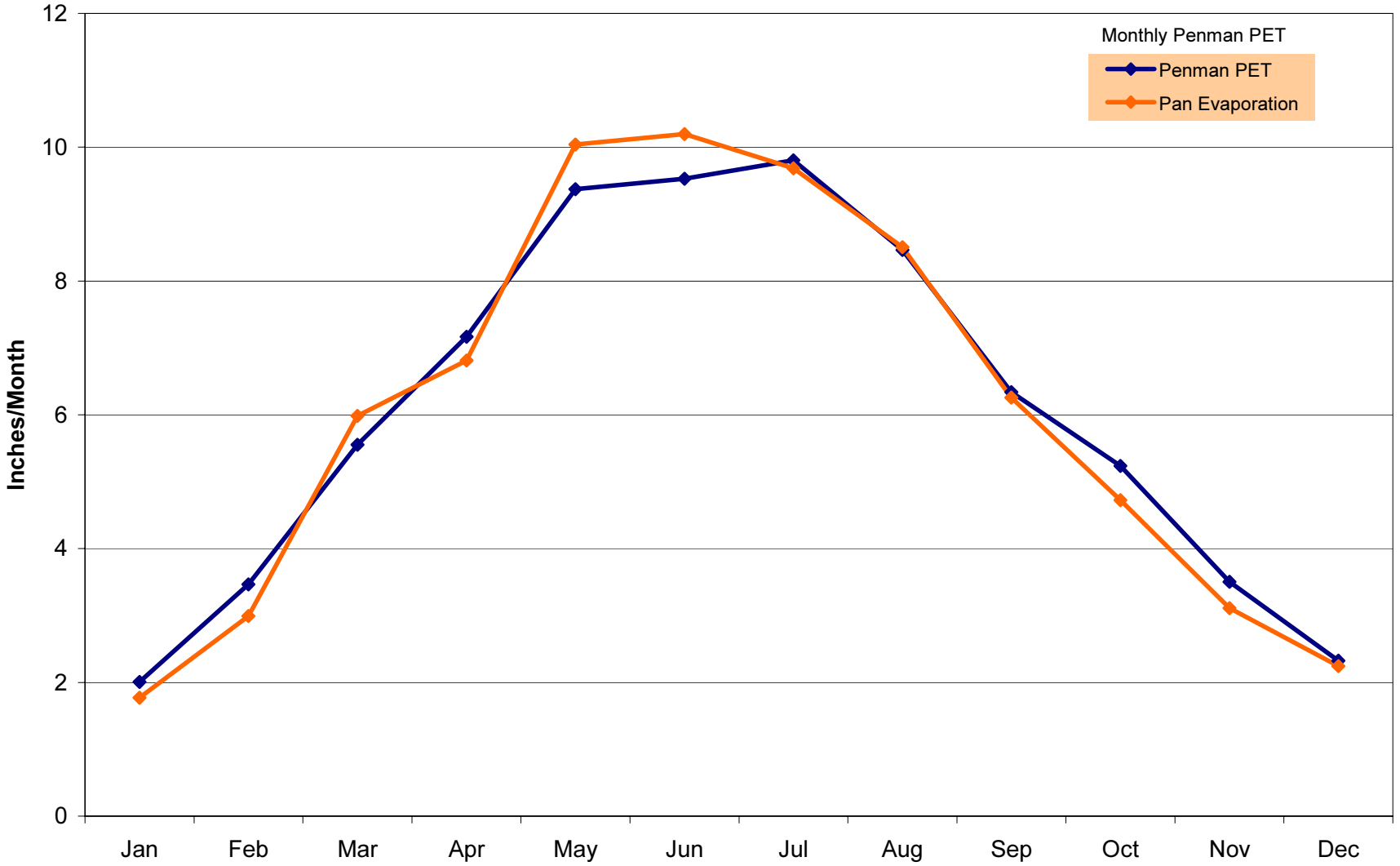

Figure 6-3 Comparison of Pan Evaporation and Penman PET for Los Lunas, New Mexico (Sammis et al. 1977)

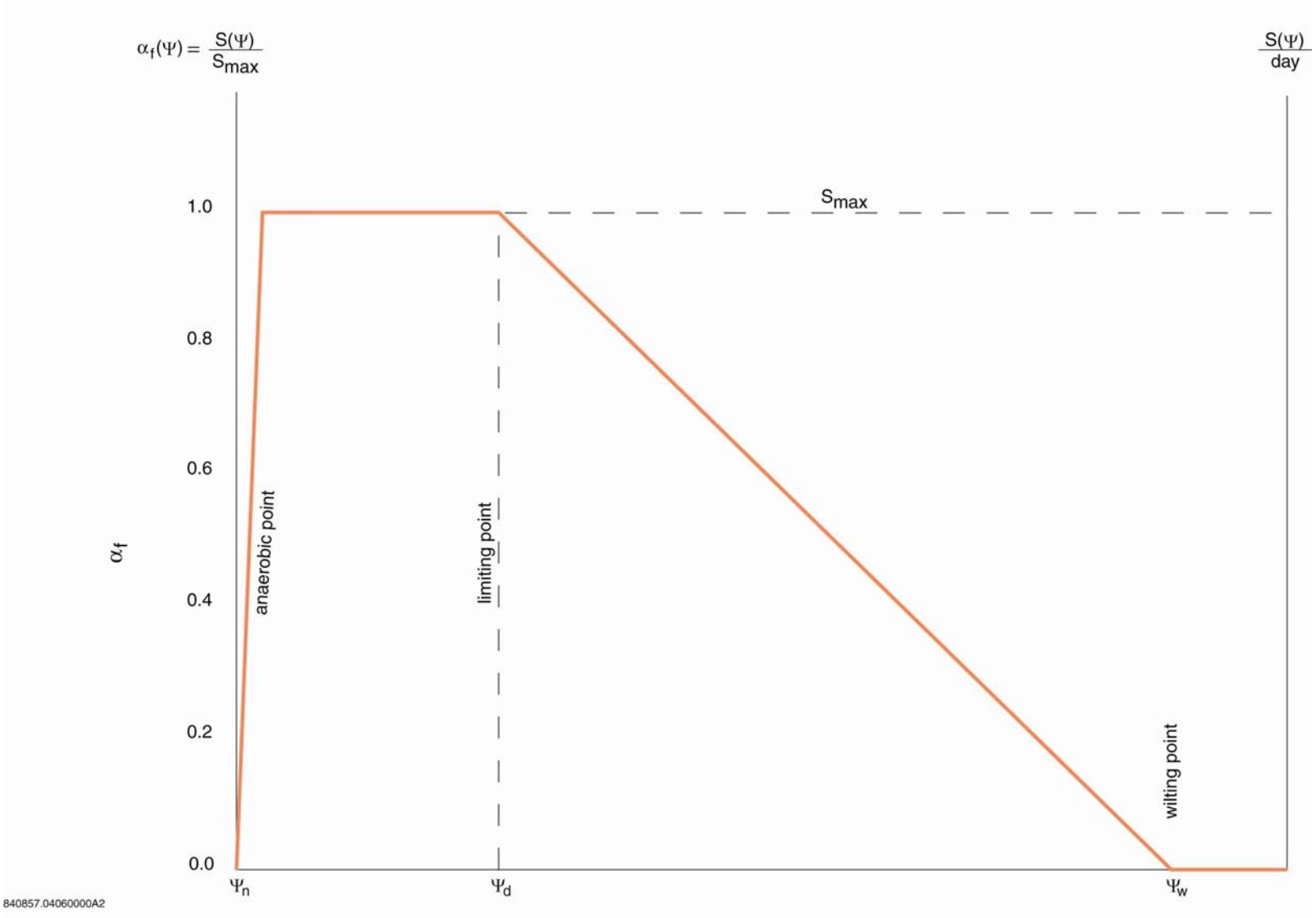

Figure 6-4 Sink Term Reduction Factor α_f as a Function of Suction Head Ψ (Feddes et al. 1978, Fayer 2000)

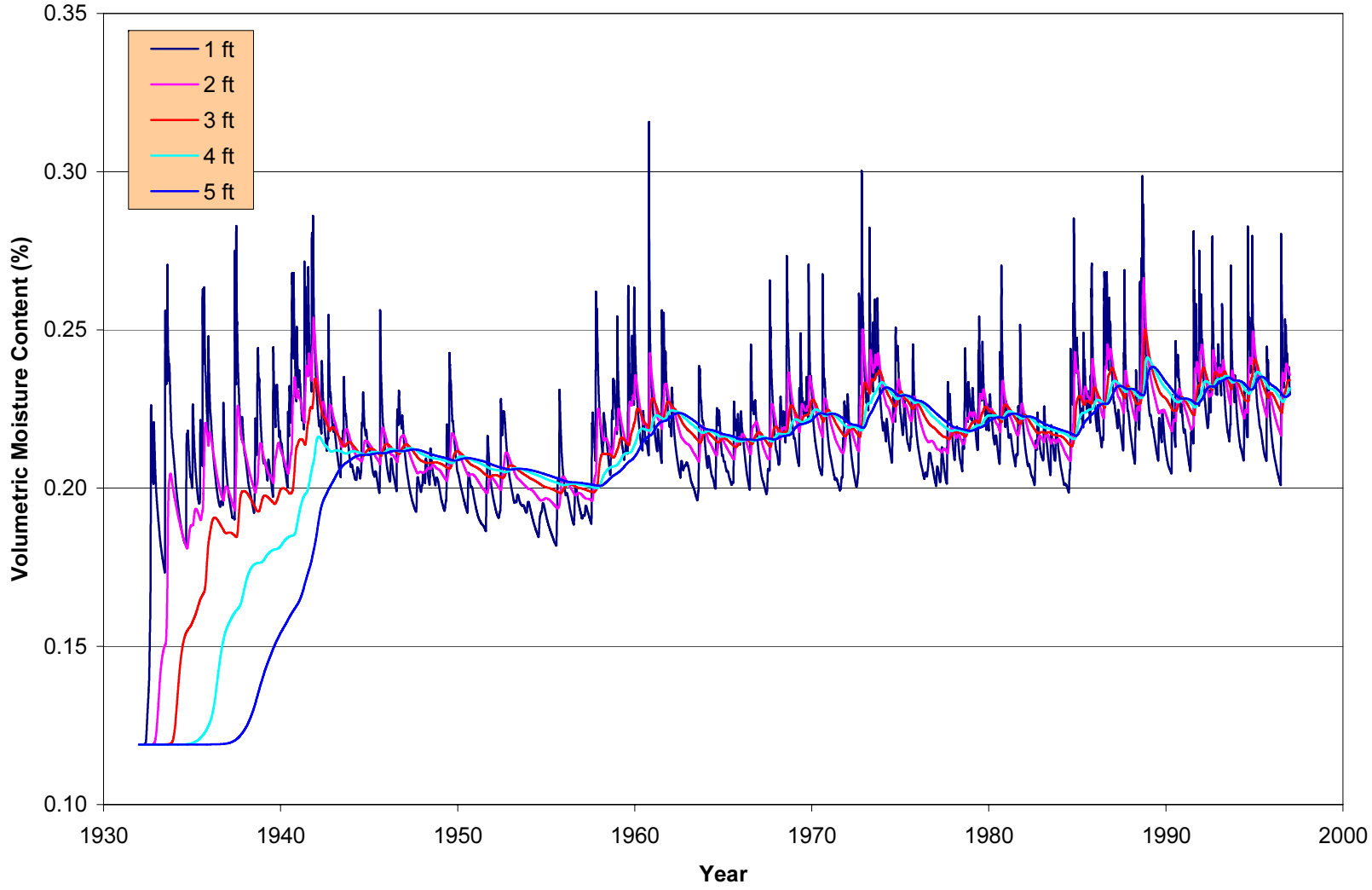

Figure 7-1 Natural Analogue without Vegetation, Volumetric Moisture Content—Historical Precipitation

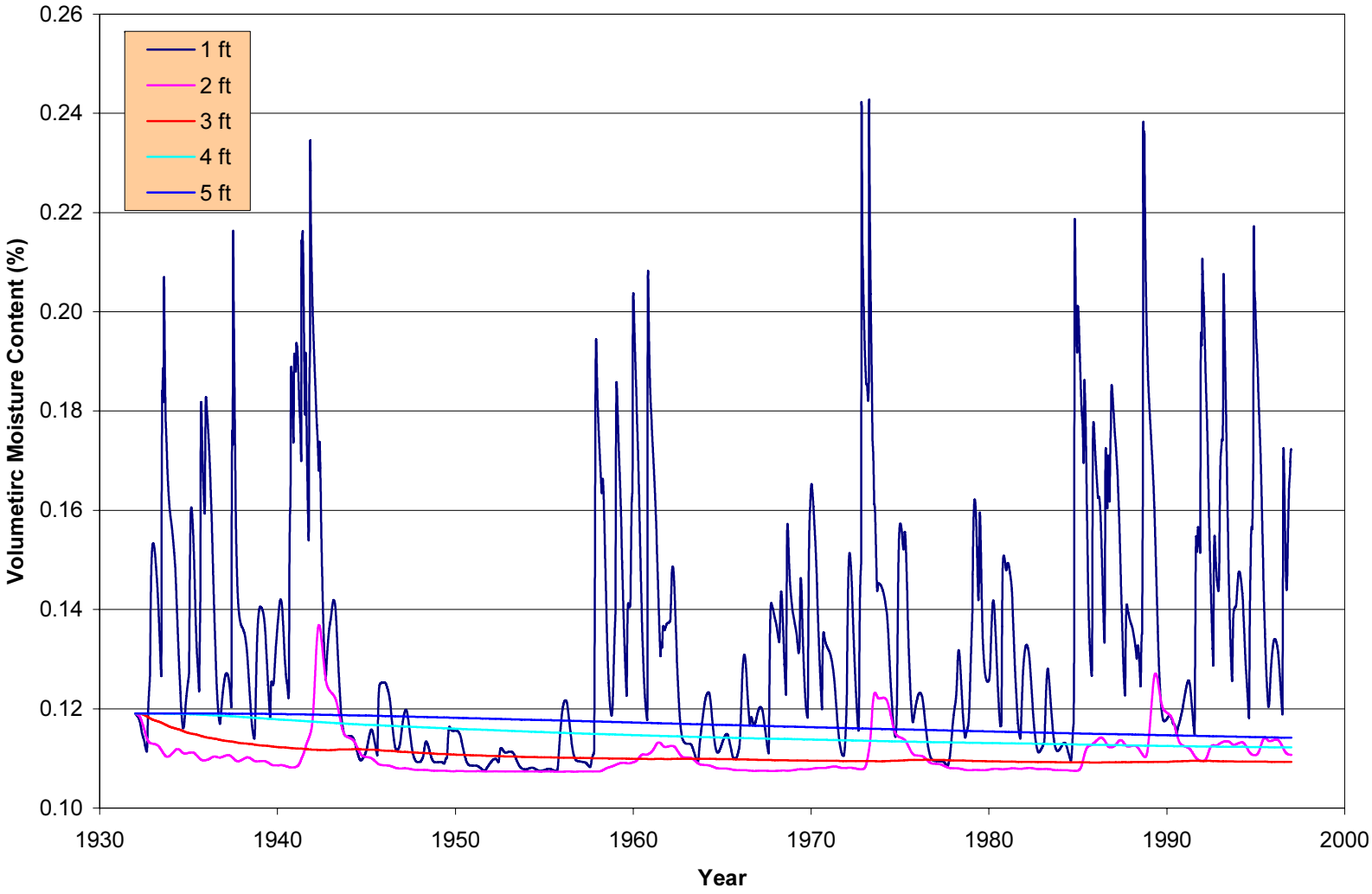

Figure 7-2 Natural Analogue with Vegetation, Volumetric Moisture Content—Historical Precipitation

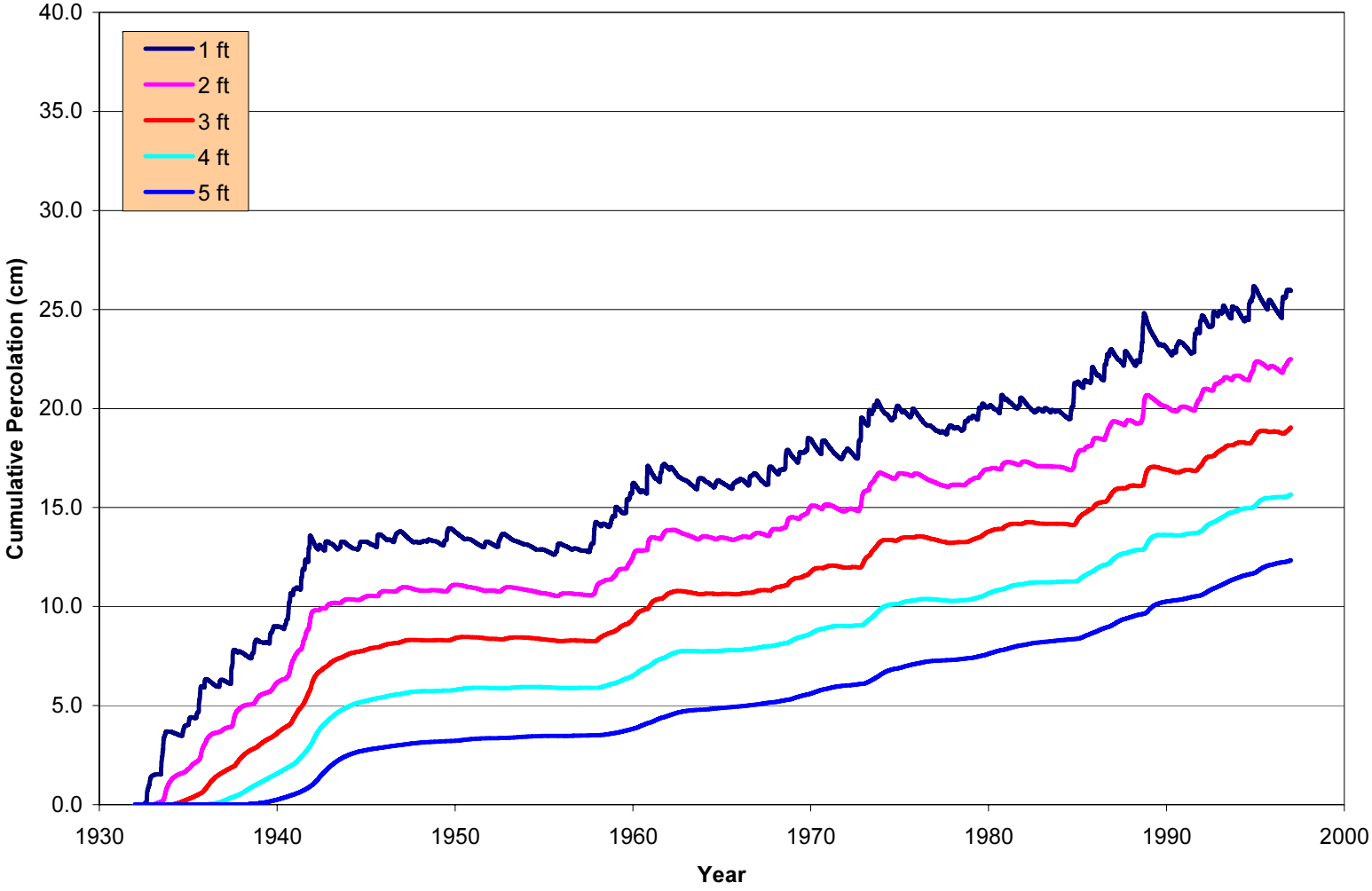

Figure 7-3 Natural Analogue without Vegetation, Cumulative Percolation—Historical Precipitation

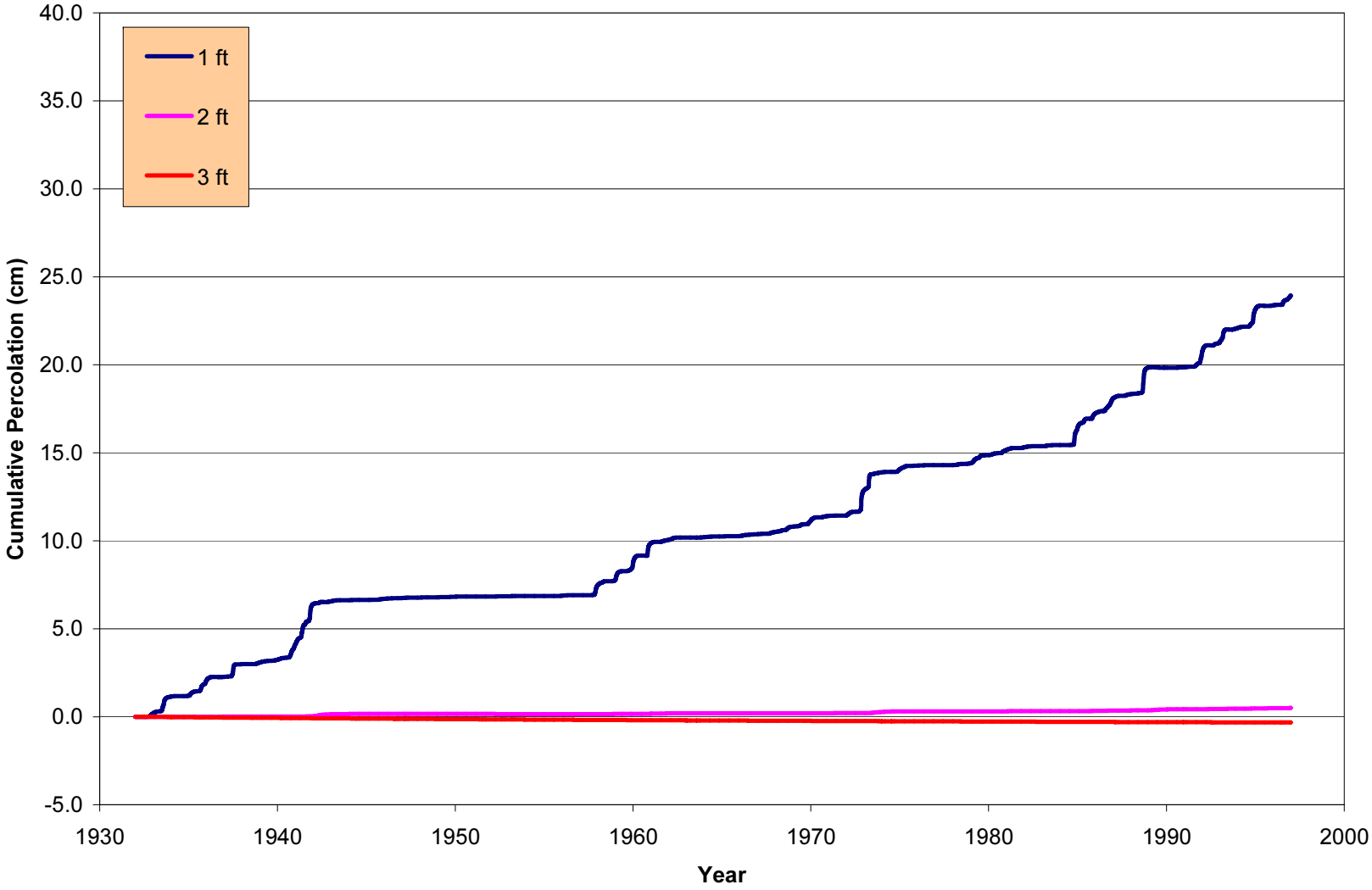

Figure 7-4 Natural Analogue with Vegetation, Cumulative Percolation—Historical Precipitation

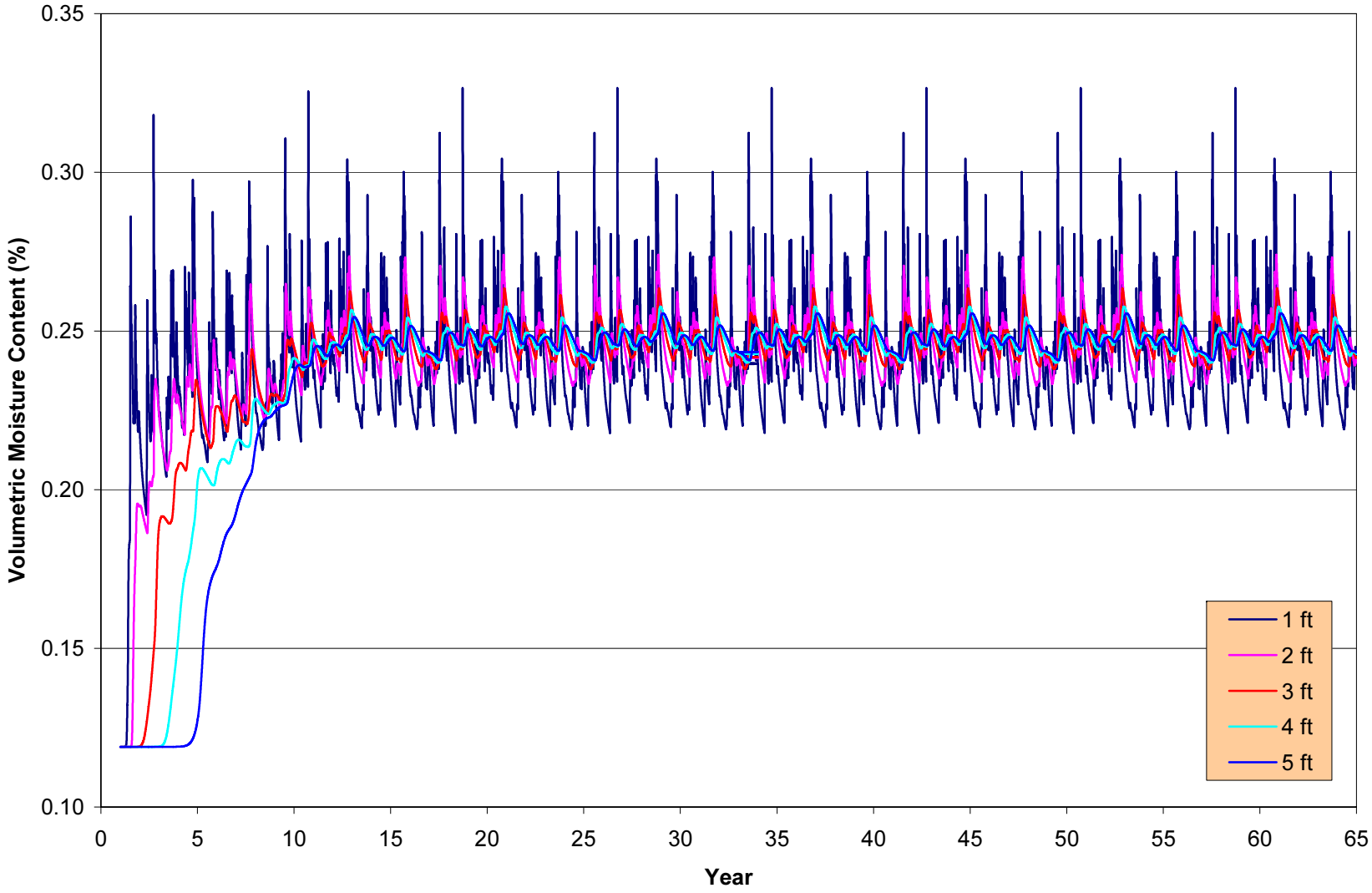

Figure 7-5 Natural Analogue without Vegetation, Volumetric Moisture Content—Maximum Precipitation

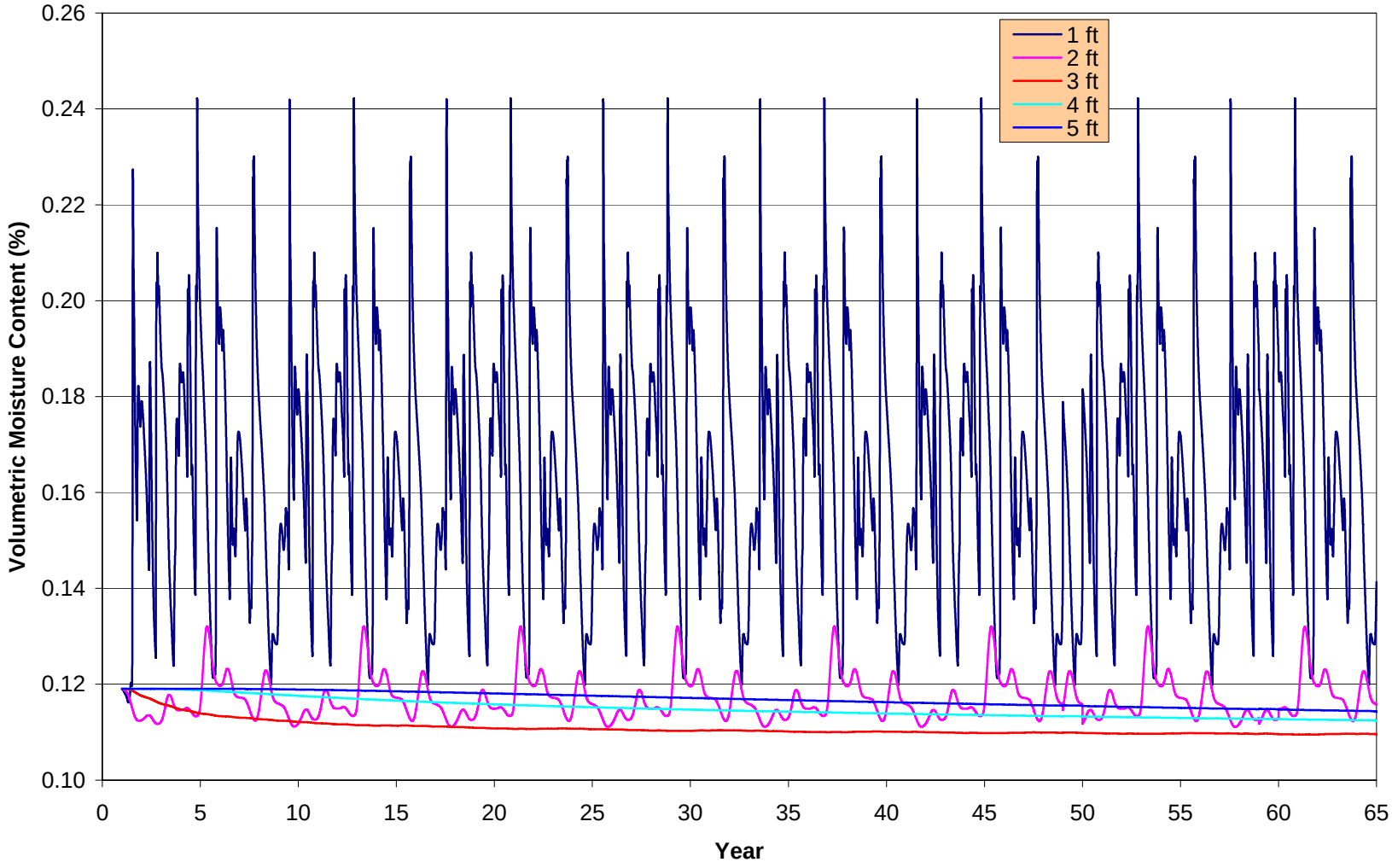

Figure 7-6 Natural Analogue with Vegetation, Volumetric Moisture Content—Maximum Precipitation

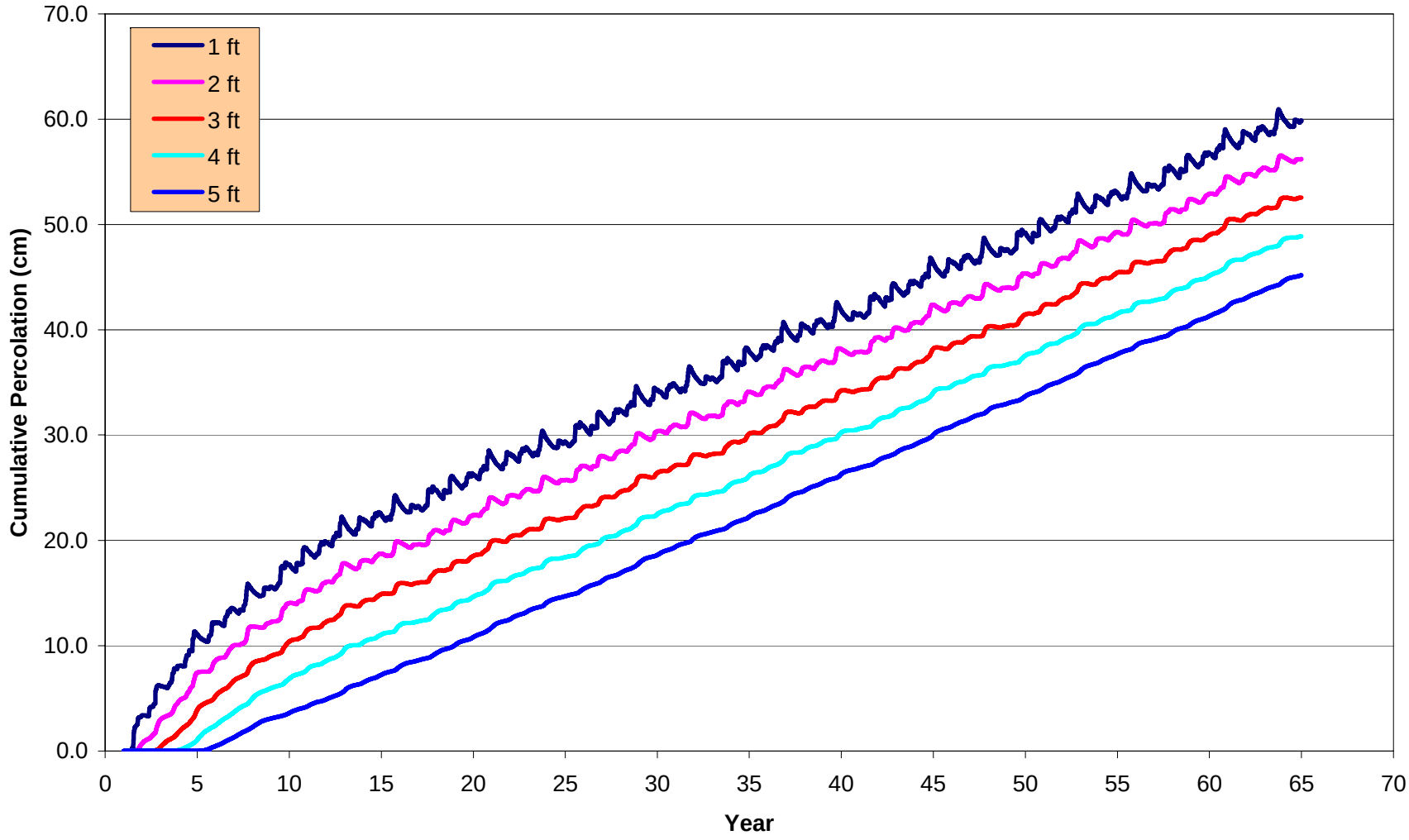

Figure 7-7 Natural Analogue without Vegetation, Cumulative Percolation—Maximum Precipitation

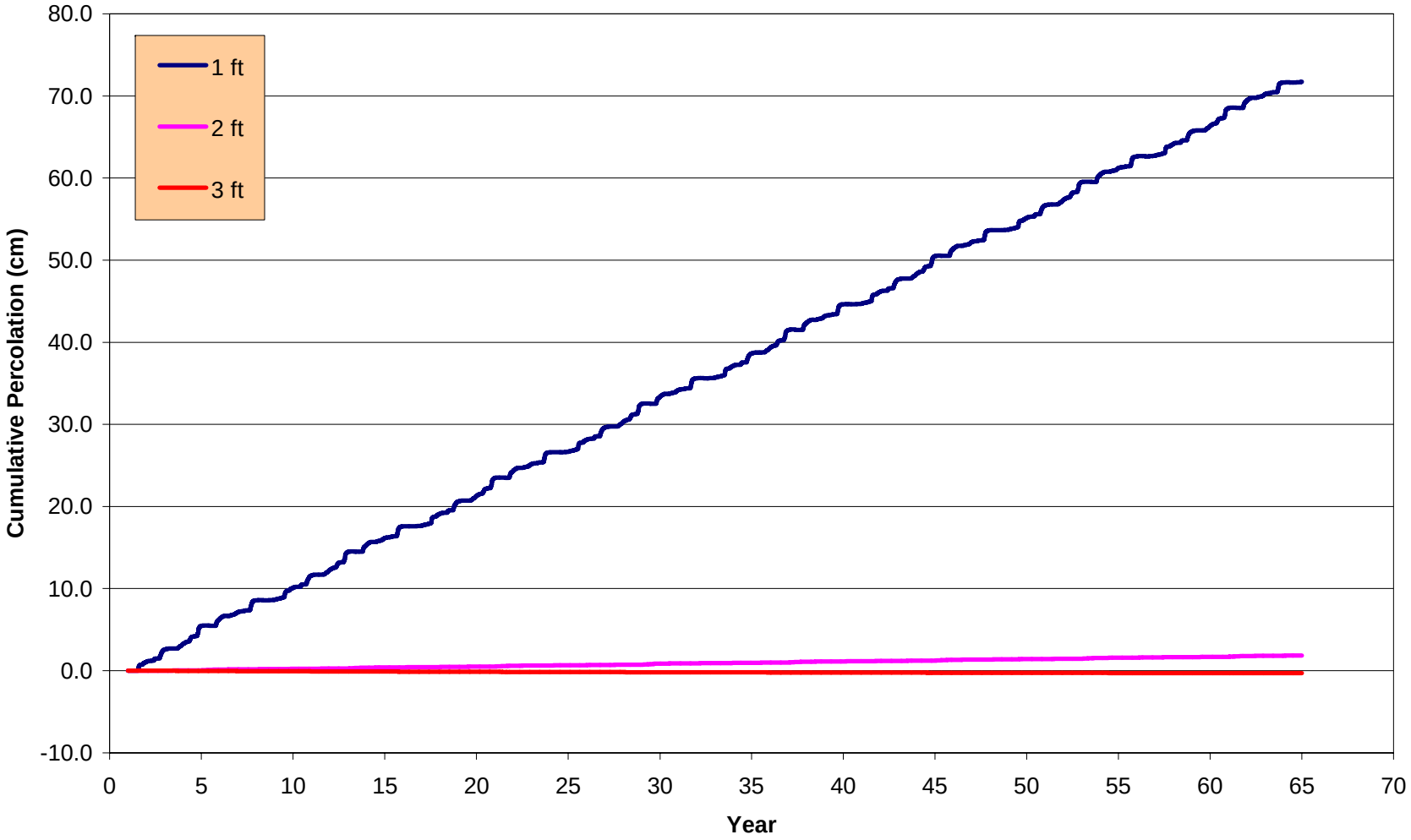

Figure 7-8 Natural Analogue with Vegetation, Cumulative Percolation—Maximum Precipitation

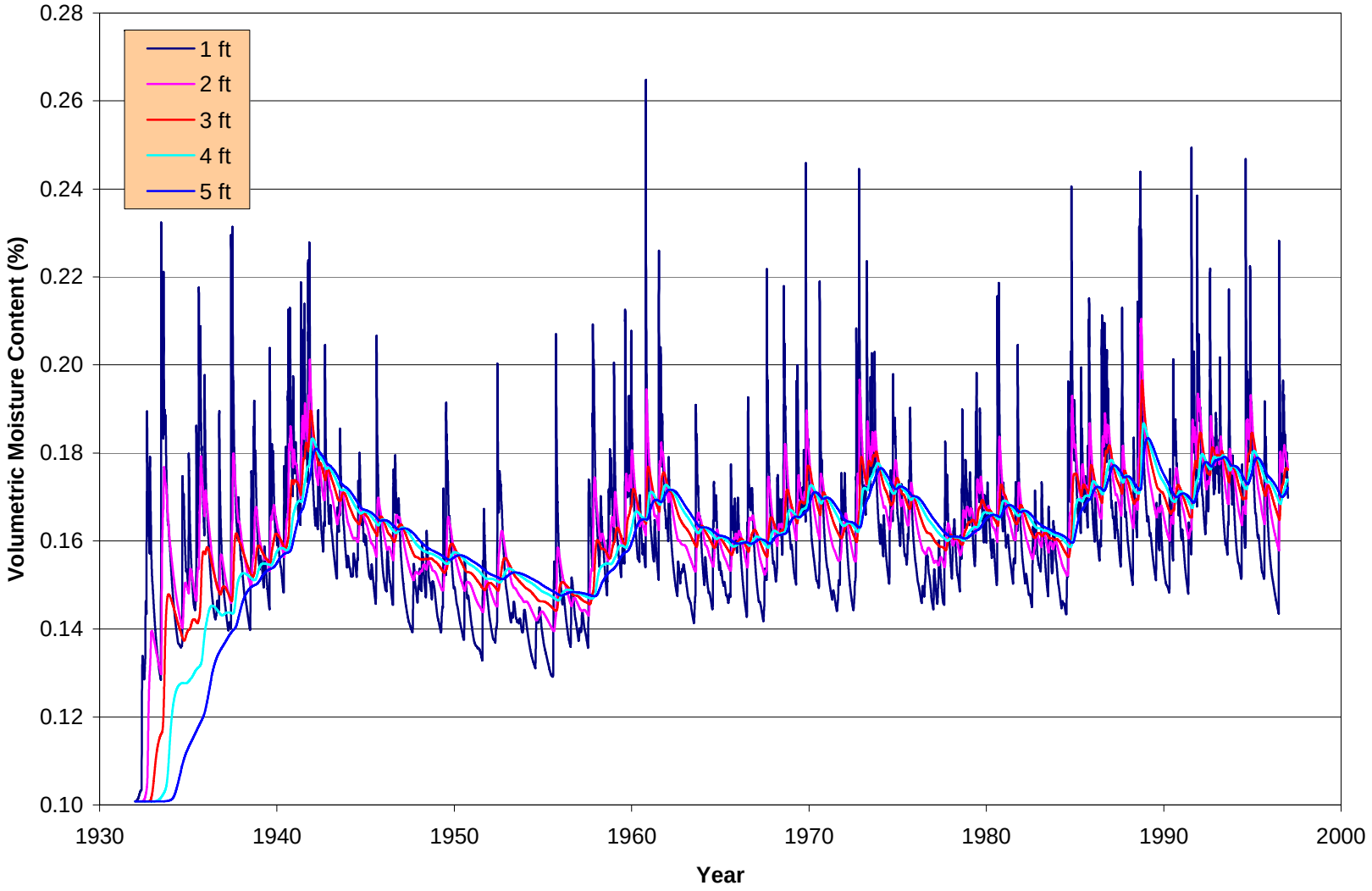

Figure 7-9 Engineered Cover without Vegetation, Volumetric Moisture Content—Historical Precipitation

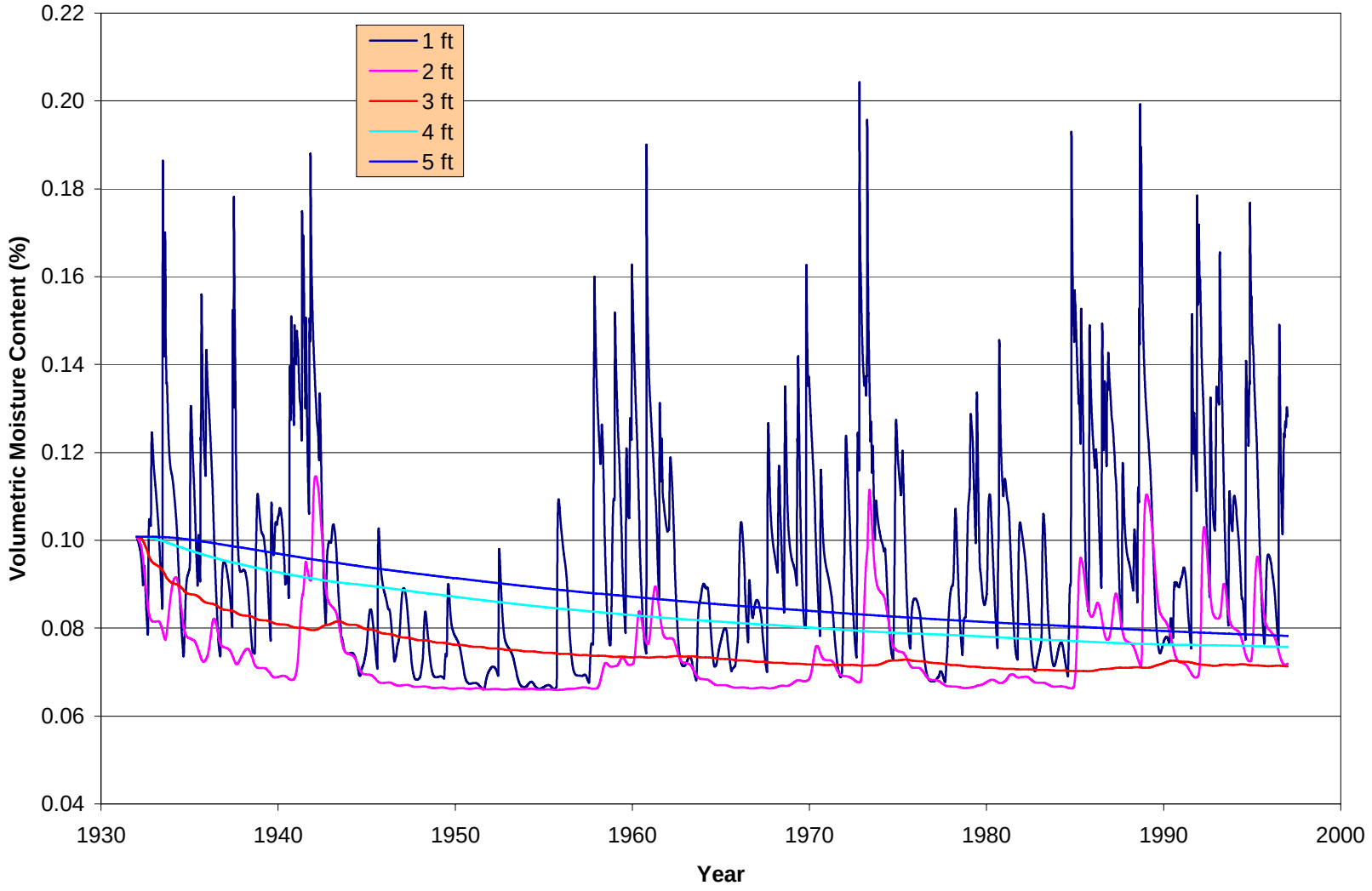

Figure 7-10 Engineered Cover with Vegetation, Volumetric Moisture Content—Historical Precipitation

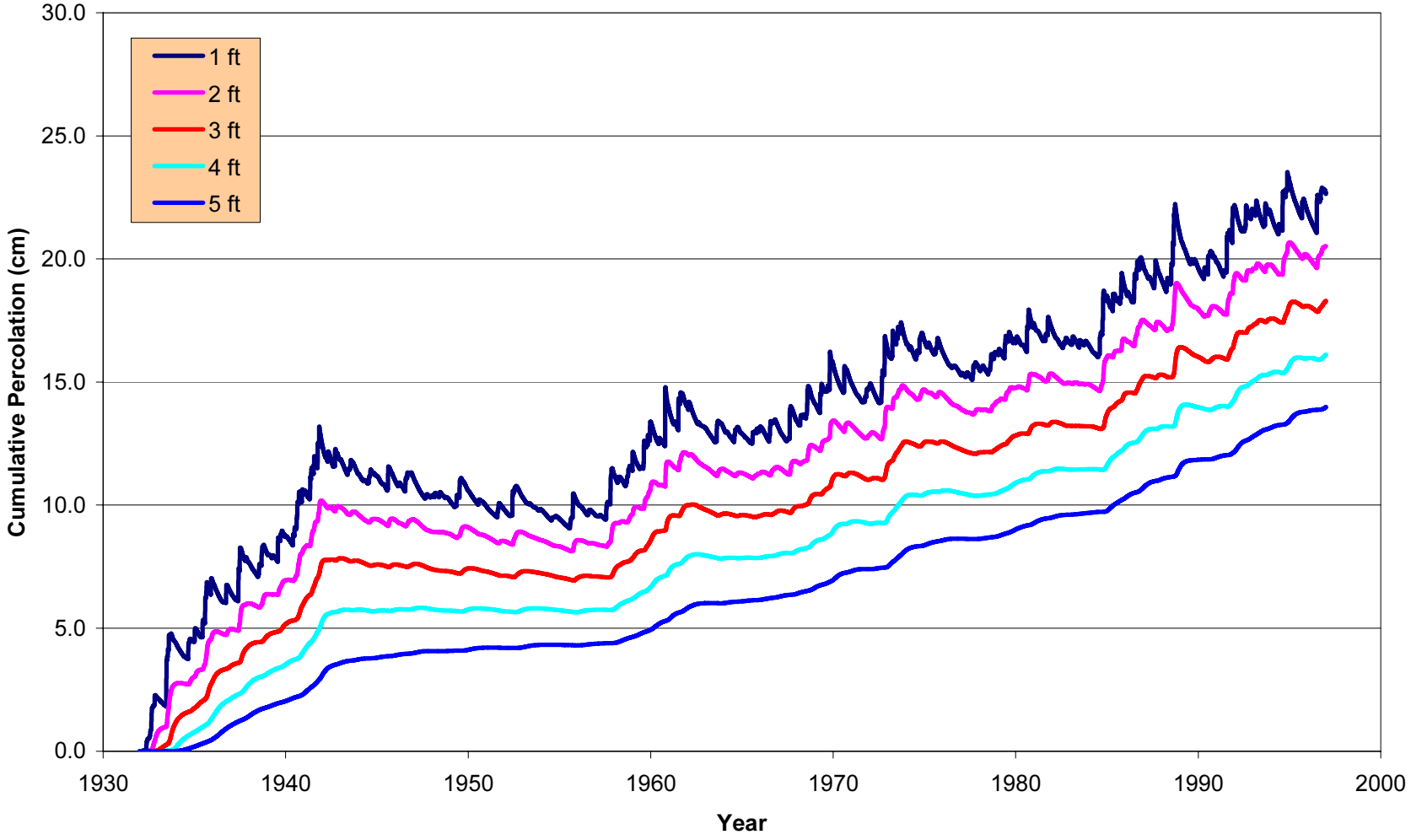

Figure 7-11 Engineered Cover without Vegetation, Cumulative Percolation—Historical Precipitation

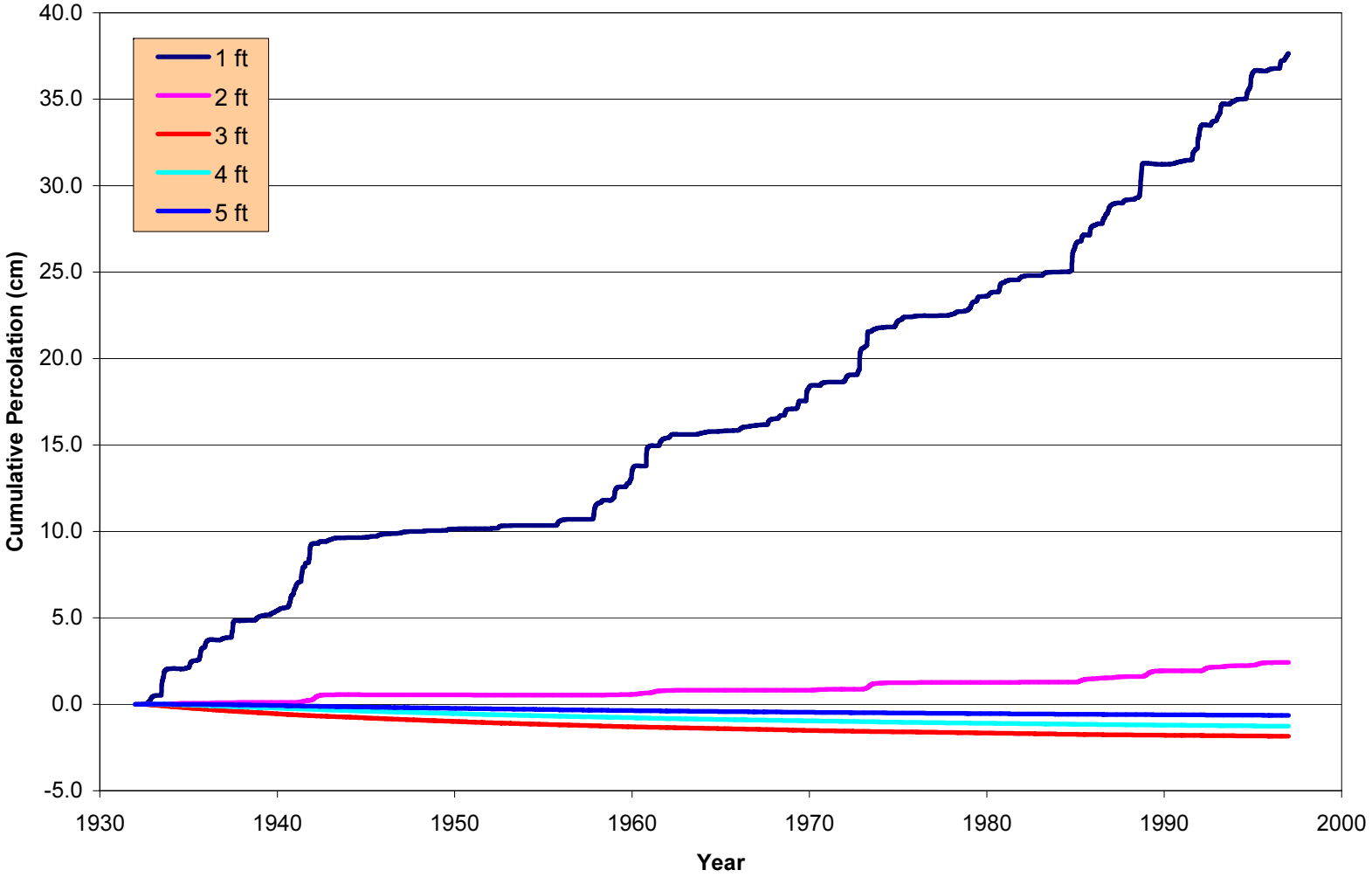

Figure 7-12 Engineered Cover with Vegetation, Cumulative Percolation—Historical Precipitation

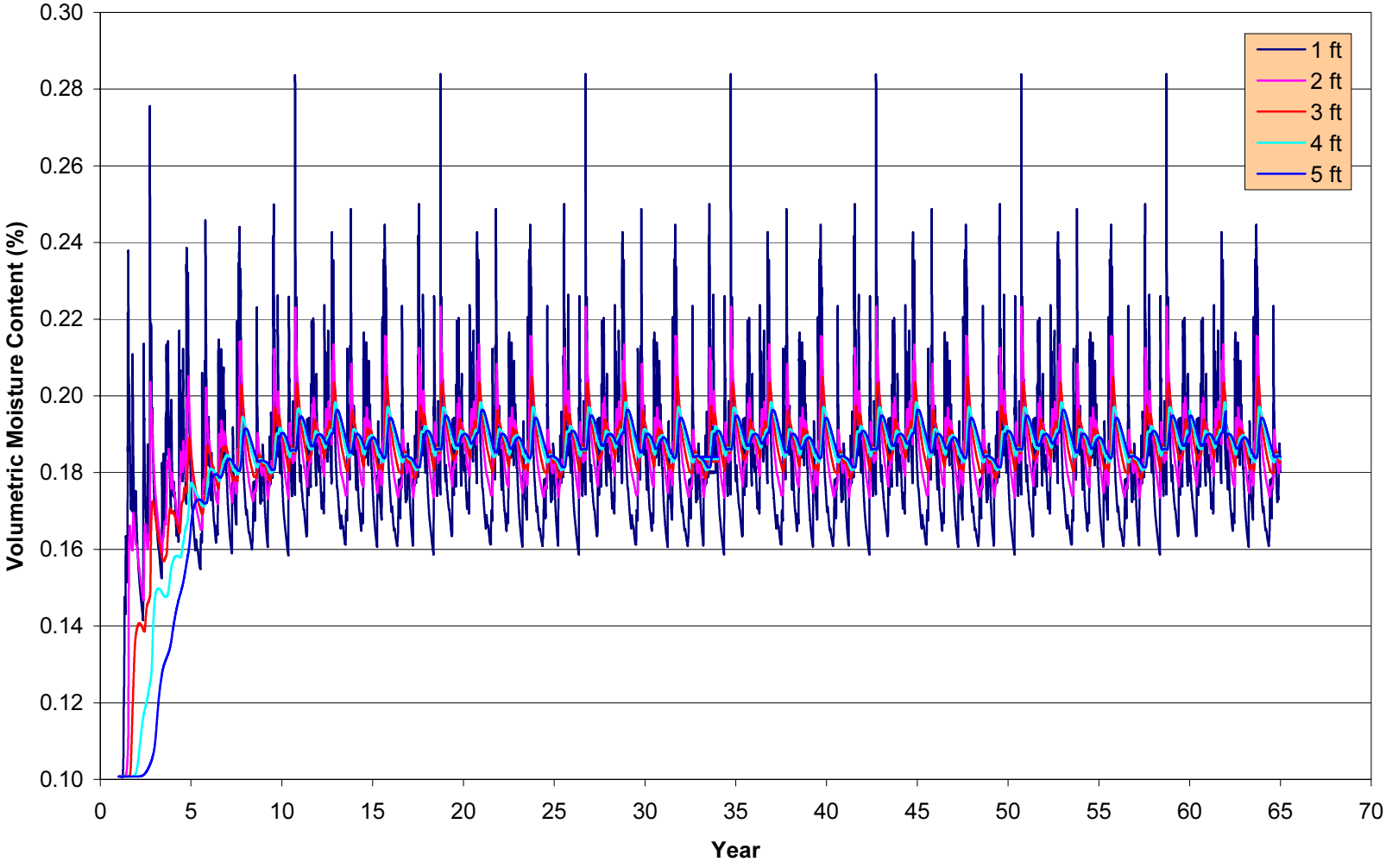

Figure 7-13 Engineered Cover without Vegetation, Volumetric Moisture Content—Maximum Precipitation

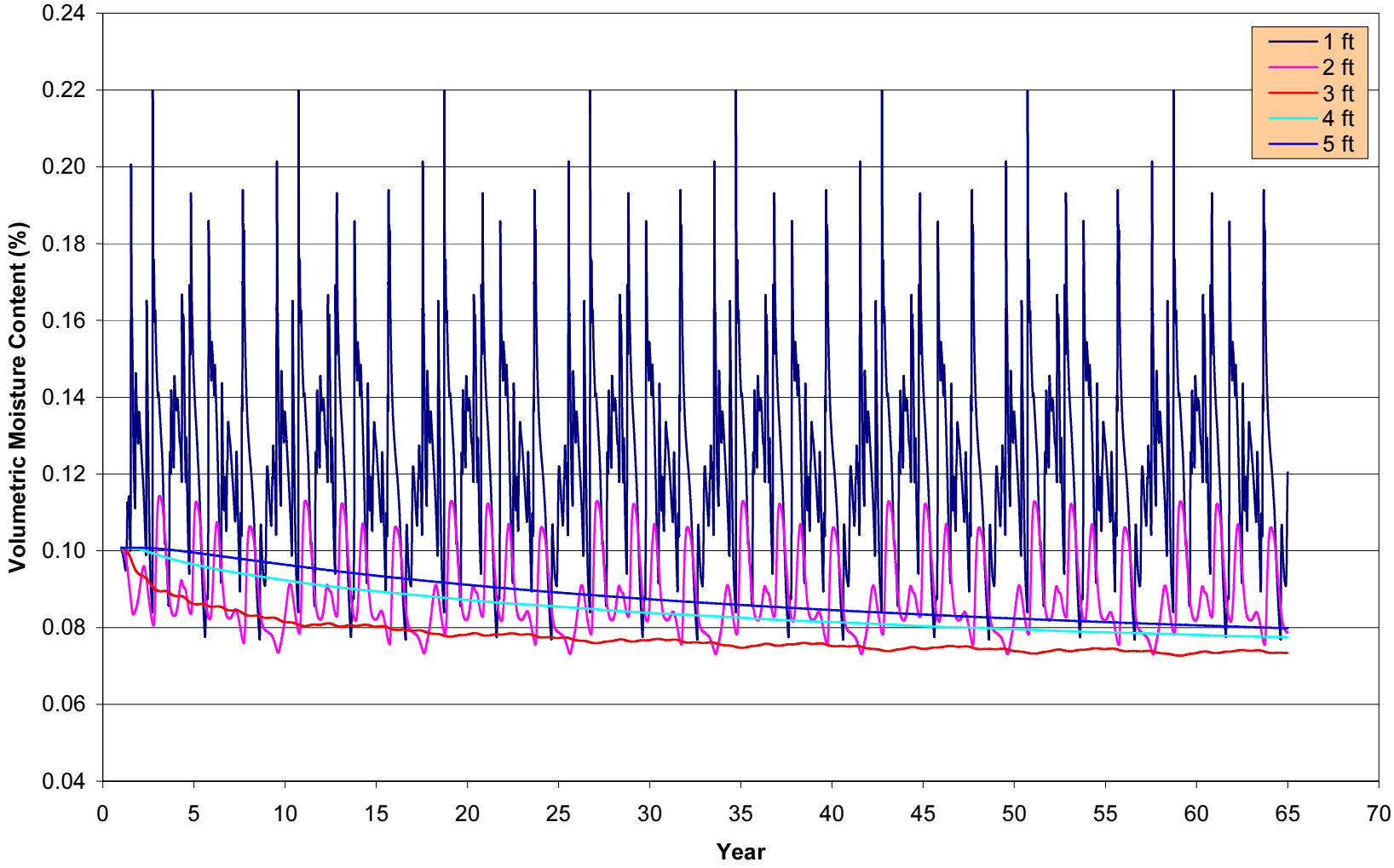

Figure 7-14 Engineered Cover with Vegetation, Volumetric Moisture Content—Maximum Precipitation

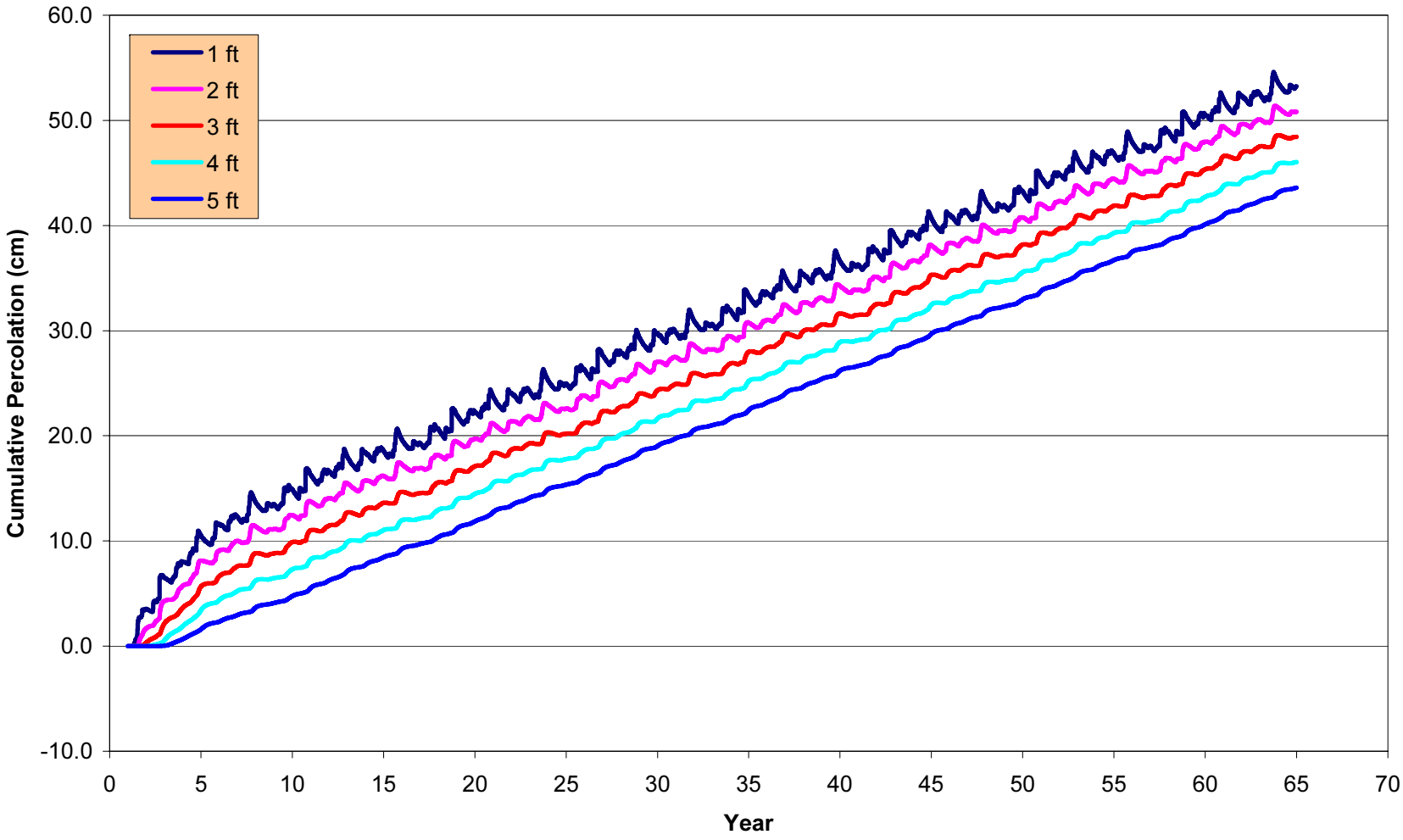

Figure 7-15 Engineered Cover without Vegetation, Cumulative Percolation—Maximum Precipitation

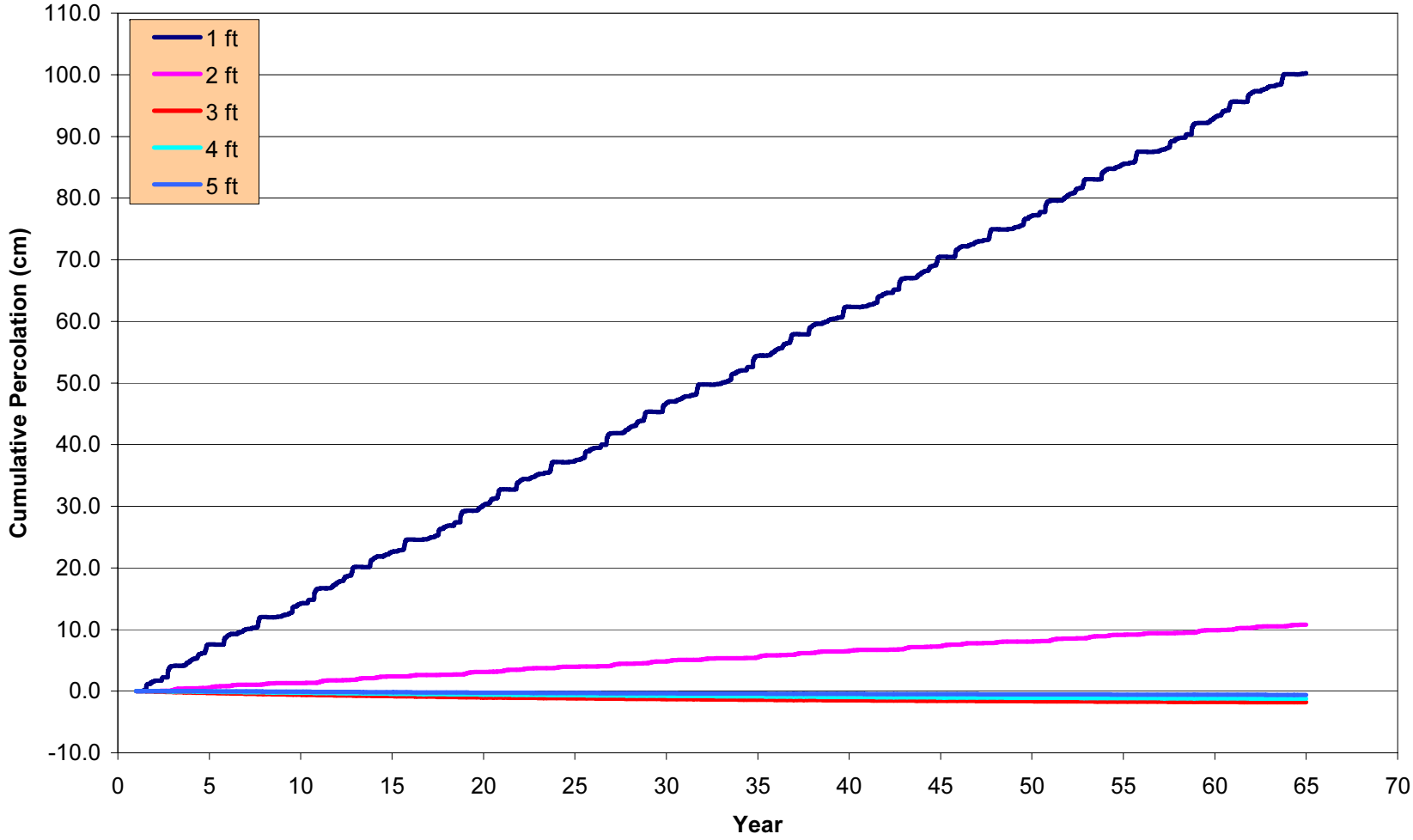

Figure 7-16 Engineered Cover with Vegetation, Cumulative Percolation—Maximum Precipitation

TABLES

Table 3-1
Soil Moisture Analyses for Trenches 1 through 5

Trench	Depth (cm)	Gravimetric Moisture (%)	Volumetric Moisture (%)
1	0–8	7.04	9.81
1	8–15	4.57	6.37
1	15–23	4.44	6.19
1	23–30	4.51	6.29
1	30–38	4.00	5.58
1	38–46	4.12	5.74
1	46–53	3.80	5.30
1	53–61	5.79	8.07
1	61–69	4.94	6.88
1	69–76	4.73	6.60
1	76–84	4.60	6.42
1	84–91	5.01	6.99
2	0–8	5.86	8.17
2	8–15	5.64	7.86
2	15–23	4.28	5.97
2	23–30	4.92	6.86
2	30–38	4.05	5.64
2	38–46	4.22	5.88
2	46–53	4.19	5.84
2	53–61	6.24	8.69
2	61–69	5.54	7.73
2	69–76	5.01	6.98
2	76–84	4.59	6.39
2	84–91	4.76	6.64
2	91–99	4.48	6.24
2	99–107	4.19	5.84
3	0–8	6.35	8.85
3	8–15	13.39	18.66
3	15–23	14.46	20.15
3	23–30	12.35	17.22
3	30–38	11.40	15.89
3	38–46	9.01	12.56
3	46–53	5.85	8.15
3	53–61	5.49	7.65
3	107	6.54	9.12
3	147	7.49	10.44
4	0–8	4.32	6.02
4	8–15	14.44	20.13
4	15–23	6.24	8.7
4	23–30	11.06	15.42
4	30–38	8.97	12.50

Refer to footnotes at end of table.

Table 3-1 (Concluded)

Trench	Depth (cm)	Gravimetric Moisture (%)	Volumetric Moisture (%)
4	38–46	7.09	9.88
4	46–53	5.54	7.72
4	53–61	5.82	8.11
4	91	11.45	15.96
4	132	5.46	7.61
4	152	9.57	13.34
5	0–8	6.92	9.65
5	8–15	16.13	22.48
5	15–23	12.14	16.92
5	23–30	10.45	14.57
5	30–38	7.82	10.90
5	38–46	7.76	10.82
5	46–53	7.22	10.07
5	53–61	6.88	9.59
5	61–69	6.03	8.40
5	69–76	5.49	7.65
5	91	4.32	6.02
5	122	5.14	7.17
Average	–	6.85	9.55

cm Centimeter(s)
– Not applicable

Table 3-2
Grain-size Distribution, Maximum Dry Density, Optimum Moisture Content, Atterberg Limits, and Soil Classification

Trench	Depth (cm)	Grain-size Analysis (Weight % Passing) U.S. Standard Sieve Numbers				Standard Proctor			Atterberg Limits		Soil Classification (USCS)
		#10	#40	#100	#200	Maximum Dry Density (Mg/m^3)	Maximum Dry Density (lb/ft^3)	Optimum Moisture Content (%)	LL	PI	
1	0–15	100	98	50	16	1.78	111.4	11.4	NV	NP	SM
1	15–30	99	98	66	35	1.86	116.4	13.3	NV	NP	SM
1	30–61	97	93	56	24	1.86	116.2	11.2	NV	NP	SM
1	61–81	96	90	56	25	1.73	108.3	10.4	NV	NP	SM
1	81–112	96	90	73	41	1.73	108.2	15.1	24	5	SC-SM
1	112–127	97	92	73	32	1.86	116.0	11.2	22	4	SC-SM
2	0–15	98	95	72	29	1.85	115.2	12.1	NV	NP	SM
2	15–30	98	94	67	34	1.93	120.7	11.4	25	9	SC
2	30–46	96	91	66	32	1.91	119.4	11.7	24	6	SC-SM
2	46–91	94	88	61	28	1.84	115.0	10.0	NV	NP	SM
3	0–15	99	96	73	39	1.85	115.2	13.6	28	10	SC
3	15–30	98	94	66	34	1.86	116.1	13.1	24	5	SC-SM
3	30–46	94	88	51	22	1.88	117.4	11.9	NV	NP	SM
3	46–107	99	94	64	29	1.90	118.4	10.7	NV	NP	SM
3	107–147	98	94	64	28	1.81	113.2	13.2	NV	NP	SM
4	0–15	98	92	61	21	1.84	114.6	11.3	NV	NP	SM
4	15–28	98	94	67	29	1.93	120.2	12.5	NV	NP	SM
4	28–38	96	92	66	31	1.83	114.0	12.8	NV	NP	SM
4	38–91	97	91	68	38	1.69	105.8	12.7	NV	NP	SM
4	91–132	98	95	69	30	1.83	114.4	14.2	NV	NP	SM
4	132–152	98	96	70	30	1.77	110.7	11.1	NV	NP	SM

Refer to footnotes at end of table.

Table 3-2 (Concluded)

Trench	Depth (cm)	Grain-size Analysis (Weight % Passing) U.S. Standard Sieve Numbers				Standard Proctor			Atterberg Limits		Soil Classification (USCS)
		#10	#40	#100	#200	Maximum Dry Density (Mg/m^3)	Maximum Dry Density (lb/ft^3)	Optimum Moisture Content (%)	LL	PI	
Trench Composite Soil Sample 1	0–61	95	89	82	58	1.70	106.1	9.7	NV	NP	ML
Trench Composite Soil Sample 2	61–152	95	87	56	25	1.66	103.7	10.2	NV	NP	SM

ASTM American Society for Testing and Materials
cm Centimeter(s)
lb/ft^3 Pound(s) per cubic foot (feet)
LL Liquid Limit
Mg/m^3 Megagram(s) per cubic meter
ML Very fine sand and silt
NP Non-plastic
NV Could not be determined in accordance with ASTM-D4318
PI Plasticity Index
SC Clayey sand
SM Silty sand
USCS Unified Soil Classification System

Table 3-3
Soil Profile Description from Persaud and Wierenga (1982)

Horizon	Depth (cm)	Description
B21t	0-28	Yellowish red (5YR5/8) loamy fine sand, yellowish red (5YR4/6) moist; weak, coarse prismatic structure; hard, friable, slightly sticky and slightly plastic; few thin discontinuous clay films on ped faces; clear wavy boundary.
B22tca	28-46	Reddish yellow (7.5YR6/6) loamy find sand, yellowish red (5YR5/8) moist; weak coarse prismatic structure; very hard, firm slightly sticky and non-plastic; few thin discontinuous clay films on ped faces; violently effervescent with disseminated lime; clear wavy boundary.
B3ca	46-66	Reddish yellow (7.5YR7/6) loamy fine sand, light brown (7.5YR6/4) moist; weak coarse subangular blocky structure; slightly hard, firm, slightly sticky and non-plastic; violently effervescent with disseminated lime; clear wavy boundary.
B21tcab	66-97	Pink (7.5YR8/4) loamy fine sand, light brown (7.5YR6/4) moist; weak coarse subangular blocky structure; hard, firm, slightly sticky and non-plastic; few thin discontinuous clay films on ped faces; violently effervescent with disseminated lime, clear wavy boundary.
B22tcab	97-157	Pink (7.5YR7/4) very fine sandy loam, light brown (7.5YR6/4) moist; weak coarse prismatic structure; hard, firm, slightly sticky and non-plastic; violently effervescent with disseminated lime; five percent gravel; clear wavy boundary.
B3cab	157-180	Pink (7.5YR7/4) very fine sandy loam, brown (7.5YR5/4) moist; weak coarse prismatic structure; slightly hard, firm, slightly sticky and non-plastic; violently effervescent with disseminated lime; clear wavy boundary.
C1	180-201	Light brown (7.5YR6/4) loamy fine sand, brown (7.5YR5/4) moist; massive; soft, friable, non-sticky and non-plastic; violently effervescent with disseminated lime and common medium irregular soft masses of lime; clear wavy boundary.

Refer to footnotes at end of table.

Table 3-3 (Continued)

Horizon	Depth (cm)	Description
IIC2	201-211	Light brown (7.5YR6/4) loamy fine sand, brown (7.5YR5/4) moist; massive; soft, friable, non-sticky and non-plastic; violent effervescent with disseminated lime and common medium irregular soft masses of lime and lime on the gravel; 10 percent gravel; clear wavy boundary.
IIIC3	211-226	Brown (7.5YR6/4) loamy fine sand, brown (7.5YR5/4) moist; massive; soft, very friable, non-sticky and non-plastic; violently effervescent with disseminated carbonates; five percent gravel; clear wavy boundary.
IIIC4ca	226-251	Pink (7.5YR7/4) very fine sandy loam, brown (7.5YR5/4) moist; weak coarse prismatic structure grading to massive; slightly hard, friable, slightly sticky and non-plastic; violently effervescent with disseminated carbonates; few gravels; clear wavy boundary.
IVB21tcab	251-297	Pink (7.5YR7/4) fine sandy loam, brown (7.5YR5/4) moist; weak coarse prismatic structure; hard, firm, sticky and slightly plastic; violently effervescent with disseminated carbonates and common medium irregular soft masses of lime; clear wavy boundary.
IVB22tcab	297-330	Light brown (7.5YR6/4) very fine sandy loam, brown (7.5YR5/4) moist; weak coarse subangular blocky structure; slightly hard, friable, slightly sticky and non-plastic; violently effervescent with disseminated lime; clear wavy boundary.
Vcca	330-348	Light brown (7.5YR6/4) very fine sandy loam, brown (7.5YR5/4) moist; massive; slightly hard, friable, slightly sticky and non-plastic; violently effervescent with disseminated lime; clear wavy boundary.
VICca	348-384	Pink (7.5YR7/4) very fine sandy loam, dark brown to brown (7.5YR4/4) moist, massive; slightly hard to hard, friable, slightly sticky and non-plastic; violently effervescent with disseminated lime; 10 percent gravel; clear wavy boundary.
VIICca	384-432	Pink (7.5YR7/4) loam, dark brown to brown (7.5YR4/4) moist; massive; slightly hard, friable, sticky and slightly plastic; violently effervescent with disseminated lime; clear wavy boundary.

Refer to footnotes at end of table.

Table 3-3 (Continued)

Horizon	Depth (cm)	Description
VIIICca	432-467	Light brown (7.5YR6/4) very fine sandy loam, brown (7.5YR5/4) moist; massive; slightly hard; friable, slightly sticky and non-plastic; violently effervescent with disseminated lime; clear wavy boundary.
IXCca	467-493	Reddish yellow (5YR6/6) loamy fine sand, yellowish red (5YR5/6) moist; massive; hard, friable, slightly sticky and non-plastic; violently effervescent with disseminated lime; less than five percent gravel; clear wavy boundary.
Xcxa	493-549	Reddish yellow (5YR6/6) fine sand, strong brown (7.5YR5/6) moist; massive; slightly hard, very friable, non-sticky and non-plastic; violently effervescent with disseminated lime; clear wavy boundary.
XICca	549-592	Pinkish white (5YR8/2) loamy fine sand, pink (7.5YR7/4) moist; massive; hard, friable, slightly sticky, non-plastic; violently effervescent with disseminated lime; stone line at the surface of the horizon; clear wavy boundary.
XIICca	592-643	Light reddish brown (5YR6/4) loamy fine sand, light brown (7.5YR6/4) moist; massive; hard, very friable, slightly sticky and non-plastic; violently effervescent with disseminated lime; clear wavy boundary.
XIIICca	643-683	Light reddish brown (5YR6/4) fine sand, light brown (7.5YR6/4) moist; massive; slightly hard, very friable, non-sticky and non-plastic; violently effervescent with disseminated lime; clear wavy boundary.
XIVCca	683-716	Light reddish brown (5YR6/4) fine sand, brown (7.5YR5/4) moist; massive; slightly hard, very friable, non-sticky and non-plastic; violently effervescent with disseminated lime; less than five percent gravel; abrupt wavy boundary.
XVCca	716-767	Pink (5YR7/4) very gravelly fine sand, light reddish brown (5YR6/4) moist; massive; hard, very friable, non-sticky and non-plastic; violently effervescent with disseminated lime and with lime on the gravel; approximately 60 percent gravel and 10 percent cobbles; clear wavy boundary.
XVICca	767-808	Light reddish brown (5YR6/4) very gravelly coarse sand, brown (7.5YR5/4) moist; massive; hard, very friable, non-sticky and non-plastic; violently effervescent with disseminated lime and with lime on the gravel; approximately 50 percent gravel; abrupt wavy boundary.

Refer to footnotes at end of table.

Table 3-3 (Concluded)

Horizon	Depth (cm)	Description
XVIICca	808-881	Reddish yellow (5YR6/6) loamy fine sand, strong brown (7.5YR5/6) moist; massive; slightly hard, very friable, non-sticky and non-plastic; violently effervescent with disseminated lime; clear wavy boundary.
XVIIICca	880 +	Pinkish white (7.5YR8/2) fine sand, light brown (7.5YR6/4) moist; massive; very hard, friable, slightly sticky and non-plastic; violently effervescent with disseminated lime.

cm Centimeter(s)

Table 3-4
Geochemical Properties and Textural Parameters for Soil Samples from Persaud and Wierenga (1982)

Depth (cm)	Electrical Conductivity (mmhos/ cm)	pH	$CaCO_3$ (%)	Organic Matter (%)	CEC (meq/100g)	Sand (%)	Silt (%)	Clay (%)
0-28	3.45	8.27	.5	0.20	6.51	82.58	8.95	8.47
28-46	15.53	7.86	3.9	0.20	8.18	83.28	7.13	9.59
46-66	13.79	7.76	5.5	0.10	7.27	85.90	6.17	7.93
66-97	19.70	7.63	11.3	0.27	5.76	86.69	8.43	4.88
97-157	27.81	7.48	21.4	0.07	7.36	76.28	14.15	9.57
157-180	9.26	7.95	17.1	0.07	6.52	69.49	25.05	5.46
180-201	6.37	7.99	8.8	0.00	6.67	85.52	8.16	6.32
201-211	4.60	8.25	8.3	0.00	5.88	86.97	9.91	3.12
211-226	4.31	8.17	6.3	0.00	6.80	84.23	9.57	6.20
226-251	5.43	7.93	10.8	0.00	9.15	75.19	14.59	10.22
251-297	6.34	7.96	16.8	0.00	10.10	76.75	9.22	14.03
297-330	5.47	7.99	10.9	0.07	9.17	62.42	26.65	10.93
330-348	3.46	8.10	8.3	0.00	7.41	70.39	23.18	6.43
348-384	4.31	8.04	8.6	0.03	7.66	71.14	19.28	9.58
384-432	5.78	7.94	11.8	0.00	10.93	49.58	40.99	9.43
432-467	5.43	7.93	9.1	0.03	7.57	59.22	27.16	13.62
467-493	3.31	8.08	4.2	0.00	7.88	86.06	4.20	9.74
493-549	1.91	8.31	4.4	0.00	5.34	91.51	2.17	6.32

Refer to footnotes at end of table.

Table 3-4 (Concluded)

Depth (cm)	Electrical Conductivity (mmhos/ cm)	pH	CaCO3 (%)	Organic Matter (%)	CEC (meq/100g)	Sand (%)	Silt (%)	Clay (%)
549-592	3.81	8.02	18.9	0.00	4.24	85.20	12.18	2.62
592-643	3.71	8.00	7.9	0.00	5.31	85.11	6.31	8.58
643-683	2.84	8.13	5.3	0.00	4.35	91.95	2.39	5.66
683-716	1.96	8.45	3.5	0.00	2.83	92.56	3.22	4.22
716-767	2.28	8.20	7.4	0.00	3.59	91.47	3.97	4.56
767-808	1.27	8.18	9.9	0.00	3.38	89.51	5.67	4.82
808-881	1.35	8.36	3.5	0.03	5.60	86.93	4.92	8.15
881 +	1.74	8.33	6.5	0.03	3.68	92.91	1.98	5.11

$CaCO_3$	Calcium carbonate
CEC	Cation exchange capacity
cm	Centimeter(s)
g	Gram(s)
meq	Milliequivalents
mmhos/cm	Millimhos per centimeter

Table 3-5
Root Biomass from RLD-1 and RLD-2

RLD-1			RLD-2			RLD-1 + RLD-2	
Soil Depth (cm)	Root Biomass (g/m^2)	Percent Biomass	Soil Depth (cm)	Root Biomass (g/m^2)	Percent Biomass	Average Percent Biomass	Cumulative Average Percent Biomass
0–10	186.4	38.99	0–10	168	40.39	39.69	39.69
10–20	82.4	17.24	10–20	92	22.12	19.68	59.37
20–30	61.8	12.93	20–30	62	14.91	13.92	73.29
30–40	47.6	9.96	30–40	42	10.10	10.03	83.32
40–50	33.2	6.94	40–50	22	5.29	6.12	89.44
50–60	25.6	5.36	50–60	12	2.89	4.13	93.56
60–70	17.6	3.68	60–70	9	2.16	2.92	96.48
70–80	12.7	2.66	70–80	4	0.96	1.81	98.29
80–90	5.7	1.19	80–90	3	0.72	0.96	99.25
90–100	5.1	1.07	90–100	2	0.48	0.78	100.0
Total	478.1	100	–	416	100	–	–

cm Centimeter(s)
g/m^2 Gram(s) per square meter
– Not applicable

Table 3-6
Root Biomass, Root Length Density, and Root Density Function for RLD-1

Depth Interval (cm)	Root Biomass (g/m^2)	Normalized Biomass	Root Length Density (cm roots/cm soil)	Root Density Function for Depth of 80 cm (cm^{-1})
0–10	186.4	0.3989	0.3906	0.0391
10–20	82.4	0.1763	0.2055	0.0206
20–30	61.8	0.1322	0.1192	0.0119
30–40	47.6	0.1019	0.0790	0.0079
40–50	33.2	0.0710	0.0603	0.0060
50–60	25.6	0.0548	0.0516	0.0052
60–70	17.6	0.0377	0.0475	0.0048
70–80	12.7	0.0272	0.0456	0.0046
Total	467.3	1.0000	9.9946	–

cm Centimeter(s)
g/m^2 Gram(s) per square meter
– Not applicable

Table 3-7
Root Biomass, Root Length Density, and Root Density Function for RLD-2

Depth Interval (cm)	Root Biomass (g/m^2)	Normalized Biomass	Root Length Density (cm roots/cm soil)	Root Density Function for Depth of 80 cm (cm^{-1})
0–10	168	0.4088	0.4259	0.0426
10–20	92	0.2238	0.2422	0.0242
20–30	62	0.1509	0.1389	0.0139
30–40	42	0.1022	0.0808	0.0081
40–50	22	0.0535	0.0482	0.0048
50–60	12	0.0292	0.0299	0.0030
60–70	9	0.0219	0.0195	0.0020
70–80	4	0.0097	0.0137	0.0014
Total	411	1.0000	9.9924	–

cm Centimeter(s)
g/m^2 Gram(s) per square meter
– Not applicable

Table 3-8
Growing Season and Leaf Area Index for TA-3

Julian Day	Leaf Area Index		Julian Day	Leaf Area Index	
	Historical Precipitation	Maximum Precipitation		Historical Precipitation	Maximum Precipitation
1	0	0	205	0.784	1.176
2	0.04	0.06	215	0.8	1.2
60	0.096	0.144	225	0.8	1.2
90	0.128	0.192	245	0.784	1.176
100	0.16	0.24	260	0.64	0.96
120	0.32	0.48	270	0.56	0.84
130	0.384	0.576	285	0.4	0.6
150	0.4	0.6	300	0.16	0.24
160	0.416	0.624	364	0.04	0.06
180	0.48	0.72	365	0	0

TA-3 Technical Area 3

Table 3-9
Foliar Coverage Based on Linear Transects

Common Name	Percent Coverage	Percent of Total Foliar Coverage
Perennial		
Black Grama	13.8	61.59
Threadleaf Snakeweed	2.5	10.99
Galleta Grass	1.2	5.25
Spike Dropseed	1.2	5.12
Sand Sagebrush	0.2	0.94
Ring Muhly	0.2	0.86
Gray Globemallow	0.04	0.19
Puncturevine	0.03	0.15
Small Soapweed	0.03	0.12
Tulip Pricklypear	0.02	0.09
Perennial Total	**19.2**	
Annual		
Deertongue	2.03	9.00
Prickly Russian Thistle	0.73	3.24
Sonoran Sandmat	0.27	1.19
Hairy Grama	0.11	0.51
False Buffalo Grass	0.11	0.47
Wild Buckwheat	0.06	0.25
Wooly Plantain	0.002	0.009
Annual Total	**3.3**	
Total Foliar Coverage	**22.5**	**99.97**

Table 3-10
Foliar Coverage Based on Digital Photography

Surface Plot	Foliar Coverage (%)
DP-1	27.1
DP-2	25.6
DP-3	30.6
DP-4	27.2
DP-5	19.9
Average	**26.1**

Table 4-1
Calculation of Center Neutron Probe Water Flux

Z		Time	Q	dH/dz (min)	dH/dz (max)	*K* (max)	*K* (min)
(cm)	(ft)	(day)	(cm/day)	(cm/cm)	(cm/cm)	(cm/day)	(cm/day)
30	1	1	1.05	0.5	1.78	2.100	0.590
30	1	2	0.20	0.62	1.76	0.319	0.113
30	1	4	0.15	0.68	1.7	0.216	0.086
30	1	8	0.08	0.73	1.62	0.111	0.050
30	1	16	0.03	0.8	1.63	0.032	0.015
30	1	32	0.01	0.95	1.55	0.014	0.009
30	1	64	0.00	0.92	1.3	0.003	0.002
61	2	1	2.10	0.5	1.78	4.200	1.180
61	2	2	0.61	0.62	1.76	0.987	0.348
61	2	4	0.36	0.68	1.7	0.525	0.210
61	2	8	0.19	0.73	1.62	0.263	0.119
61	2	16	0.05	0.8	1.63	0.065	0.032
61	2	32	0.03	0.95	1.55	0.032	0.020
61	2	64	0.01	0.92	1.3	0.008	0.005
91	3	1	2.48	0.5	1.78	4.950	1.390
91	3	2	0.90	0.62	1.76	1.456	0.513
91	3	4	0.53	0.68	1.7	0.772	0.309
91	3	8	0.29	0.73	1.62	0.395	0.178
91	3	16	0.08	0.8	1.63	0.106	0.052
91	3	32	0.05	0.95	1.55	0.051	0.031
91	3	64	0.02	0.92	1.3	0.020	0.014
122	4	1	2.64	0.5	1.78	5.280	1.483
122	4	2	1.01	0.62	1.76	1.621	0.571
122	4	4	0.61	0.68	1.7	0.900	0.360
122	4	8	0.35	0.73	1.62	0.481	0.217
122	4	16	0.11	0.8	1.63	0.144	0.070
122	4	32	0.06	0.95	1.55	0.060	0.037
122	4	64	0.02	0.92	1.3	0.025	0.018
152	5	1	2.93	0.5	1.78	5.868	1.648
152	5	2	1.16	0.62	1.76	1.877	0.661
152	5	4	0.74	0.68	1.7	1.085	0.434
152	5	8	0.42	0.73	1.62	0.575	0.259
152	5	16	0.14	0.8	1.63	0.172	0.084
152	5	32	0.08	0.95	1.55	0.080	0.049

Refer to footnotes at end of table.

Table 4-1 (Concluded)

Z		Time (day)	Q (cm/day)	dH/dz (min) (cm/cm)	dH/dz (max) (cm/cm)	*K* (max) (cm/day)	*K* (min) (cm/day)
(cm)	(ft)						
152	5	64	0.03	0.92	1.3	0.029	0.020
183	6	1	3.53	0.5	1.78	7.068	1.985
183	6	2	1.36	0.62	1.76	2.187	0.770
183	6	4	0.89	0.68	1.7	1.310	0.524
183	6	8	0.51	0.73	1.62	0.695	0.313
183	6	16	0.17	0.8	1.63	0.207	0.101
183	6	32	0.09	0.95	1.55	0.093	0.057
183	6	64	0.03	0.92	1.3	0.034	0.024

cm Centimeter(s)
dH/dz Hydraulic gradient
ft Foot (feet)
K Unsaturated hydraulic conductivity
max Maximum
min Minimum
Q Water flow rate (flux)
z Depth

Table 4-2
Calculation of Southeast Neutron Probe Water Flux

Z		Time	Q	dH/dz (min)	dH/dz (max)	*K* (max)	*K* (min)
(cm)	(ft)	(day)	(cm/day)	(cm/cm)	(cm/cm)	(cm/day)	(cm/day)
30	1	1	0.75	0.5	1.78	1.500	0.421
30	1	2	0.17	0.62	1.76	0.271	0.095
30	1	4	0.12	0.68	1.7	0.181	0.072
30	1	8	0.08	0.73	1.62	0.107	0.048
30	1	16	0.03	0.8	1.63	0.041	0.020
30	1	32	0.01	0.95	1.55	0.008	0.005
30	1	64	0.00	0.92	1.3	0.003	0.002
61	2	1	2.14	0.5	1.78	4.278	1.202
61	2	2	0.47	0.62	1.76	0.765	0.269
61	2	4	0.29	0.68	1.7	0.428	0.171
61	2	8	0.17	0.73	1.62	0.238	0.107
61	2	16	0.06	0.8	1.63	0.077	0.038
61	2	32	0.02	0.95	1.55	0.020	0.012
61	2	64	0.01	0.92	1.3	0.007	0.005
91	3	1	3.08	0.5	1.78	6.162	1.731
91	3	2	0.72	0.62	1.76	1.161	0.409
91	3	4	0.49	0.68	1.7	0.724	0.289
91	3	8	0.30	0.73	1.62	0.408	0.184
91	3	16	0.11	0.8	1.63	0.138	0.068
91	3	32	0.04	0.95	1.55	0.040	0.025
91	3	64	0.02	0.92	1.3	0.018	0.013
122	4	1	3.37	0.5	1.78	6.744	1.894
122	4	2	0.81	0.62	1.76	1.301	0.458
122	4	4	0.56	0.68	1.7	0.829	0.332
122	4	8	0.35	0.73	1.62	0.480	0.216
122	4	16	0.14	0.8	1.63	0.177	0.087
122	4	32	0.06	0.95	1.55	0.059	0.036
122	4	64	0.02	0.92	1.3	0.026	0.018
152	5	1	3.62	0.5	1.78	7.230	2.031
152	5	2	0.91	0.62	1.76	1.475	0.520
152	5	4	0.65	0.68	1.7	0.949	0.379
152	5	8	0.41	0.73	1.62	0.558	0.251
152	5	16	0.17	0.8	1.63	0.214	0.105
152	5	32	0.07	0.95	1.55	0.075	0.046
152	5	64	0.03	0.92	1.3	0.034	0.024

Refer to footnotes at end of table.

Table 4-2 (Concluded)

Z		Time	Q	dH/dz (min)	dH/dz (max)	*K* (max)	*K* (min)
(cm)	(ft)	(day)	(cm/day)	(cm/cm)	(cm/cm)	(cm/day)	(cm/day)
183	6	1	4.37	0.5	1.78	8.730	2.452
183	6	2	1.16	0.62	1.76	1.872	0.659
183	6	4	0.82	0.68	1.7	1.212	0.485
183	6	8	0.51	0.73	1.62	0.698	0.315
183	6	16	0.20	0.8	1.63	0.254	0.125
183	6	32	0.08	0.95	1.55	0.088	0.054
183	6	64	0.04	0.92	1.3	0.043	0.030

cm Centimeter(s)
dH/dz Hydraulic gradient
ft Foot (feet)
K Unsaturated hydraulic conductivity
max Maximum
min Minimum
Q Water flow rate (flux)
z Depth

Table 4-3
Slope Determination for $K(\theta)$

Day	Equation	r^2
1 Lower Segment	0.5x + 96	0.987
1 Upper Segment	1.78x – 69	0.998
2 Lower Segment	0.62x + 107	0.998
2 Upper Segment	1.76x – 49	0.993
4 Lower Segment	0.68x + 121	0.998
4 Upper Segment	1.7x – 22	0.995
8 Lower Segment	0.73x + 137	0.999
8 Upper Segment	1.62x + 17	0.992
16 Lower Segment	0.8x + 156	0.999
16 Upper Segment	1.63x + 40	0.980
32 Lower Segment	0.95x + 176	0.995
32 Upper Segment	1.55x + 82	0.980
64 Lower Segment	0.92x + 213	0.987
64 Upper Segment	1.3x + 148	0.998

$K(\theta)$ Hydraulic conductivity
r^2 Correlation coefficient
x Soil depth

Table 4-4
Engineered Cover Soil Characteristics

Lift Number	Lift Interval (ft)	Reading Depth (ft)	Volumetric Moisture (%)	Dry Bulk Density (Mg/m^3)	Dry Bulk Density (lb/ft^3)	Wet Bulk Density (Mg/m^3)	Wet Bulk Density (lb/ft^3)
Subgrade	6.5–6.0	6.5	10.4	1.64	102.2	1.81	112.7
Subgrade	6.5–6.0	6.5	10.2	1.70	106.2	1.86	116.4
Subgrade	6.5–6.0	6.25	10.3	1.68	104.9	1.85	115.2
Subgrade	6.5–6.0	6	11.1	1.66	103.8	1.84	114.9
1	6.0–5.5	5.75	10.9	1.70	106.0	1.87	116.8
1	6.0–5.5	5.75	9.7	1.67	104.3	1.83	114.1
1	6.0–5.5	5.75	9.3	1.63	101.5	1.78	110.8
1	6.0–5.5	5.75	7.4	1.62	101.1	1.74	108.5
1	6.0–5.5	5.75	8.9	1.66	103.6	1.80	112.6
2	5.5–5.0	5.25	10.9	1.70	106.2	1.88	117.1
2	5.5–5.0	5.25	8.8	1.75	109.5	1.90	118.3
2	5.5–5.0	5.25	10.3	1.73	108.3	1.90	118.7
3	5.0–4.5	4.75	9.0	1.73	108.0	1.88	117.3
3	5.0–4.5	4.75	8.3	1.76	110.1	1.90	118.5
3	5.0–4.5	4.75	9.6	1.69	105.3	1.84	114.9
3	5.0–4.5	4.75	8.6	1.74	108.6	1.88	117.2
3	5.0–4.5	4.75	8.0	1.68	105.1	1.81	113.1
4	4.5–4.0	4.25	11.3	1.81	113.2	2.00	124.6
4	4.5–4.0	4.25	8.0	1.68	105.0	1.81	113.0
4	4.5–4.0	4.25	9.4	1.69	105.6	1.84	115.0
4	4.5–4.0	4.25	8.8	1.70	105.9	1.84	114.7
5	4.0–3.5	3.75	9.1	1.82	113.3	1.96	122.4
5	4.0–3.5	3.75	9.8	1.77	110.5	1.93	120.3
5	4.0–3.5	3.75	7.7	1.68	104.9	1.80	112.6
5	4.0–3.5	3.75	9.4	1.74	108.9	1.90	118.3
5	4.0–3.5	3.75	10.3	1.77	110.7	1.94	121.0
6	3.5–3.0	3.25	10.3	1.71	107.0	1.88	117.2
6	3.5–3.0	3.25	11.8	1.73	108.3	1.93	120.2
6	3.5–3.0	3.25	8.6	1.59	99.5	1.73	108.1
6	3.5–3.0	3.25	9.1	1.69	105.7	1.84	114.8
6	3.5–3.0	3.25	9.8	1.70	106.0	1.86	115.9
7	3.0–2.5	2.75	11.9	1.84	114.8	2.03	126.7
7	3.0–2.5	2.75	10.8	1.75	109.5	1.93	120.4
7	3.0–2.5	2.75	12.5	1.75	109.0	1.95	121.6
7	3.0–2.5	2.75	12.8	1.80	112.1	2.00	124.9
7	3.0–2.5	2.75	11.9	1.75	109.0	1.94	120.9
8	2.5–2.0	2.25	12.0	1.67	104.3	1.86	116.3
8	2.5–2.0	2.25	11.2	1.78	110.8	1.95	122.0

Refer to footnotes at end of table.

Table 4-4 (Concluded)

Lift Number	Lift Interval (ft)	Reading Depth (ft)	Volumetric Moisture (%)	Dry Bulk Density (Mg/m^3)	Dry Bulk Density (lb/ft^3)	Wet Bulk Density (Mg/m^3)	Wet Bulk Density (lb/ft^3)
8	2.5–2.0	2.25	12.3	1.81	113.2	2.01	125.5
8	2.5–2.0	2.25	11.5	1.76	109.8	1.94	121.2
8	2.5–2.0	2.25	10.4	1.76	109.6	1.92	120.1
9	2.0–1.5	1.75	10.9	1.80	112.1	1.97	122.9
9	2.0–1.5	1.75	10.5	1.60	99.9	1.77	110.4
9	2.0–1.5	1.75	9.7	1.70	106.3	1.86	115.9
9	2.0–1.5	1.75	10.5	1.68	104.8	1.85	115.3
9	2.0–1.5	1.75	14.0	1.74	108.7	1.97	122.7
10	1.5–1.0	1.25	8.0	1.58	98.9	1.71	106.9
10	1.5–1.0	1.25	7.9	1.65	103.1	1.78	110.9
10	1.5–1.0	1.25	9.2	1.73	108.3	1.88	117.6
10	1.5–1.0	1.25	9.7	1.67	104.0	1.82	113.7
10	1.5–1.0	1.25	9.5	1.70	106.2	1.85	115.6
11	1.0–0.5	0.75	9.3	1.72	107.4	1.87	116.7
11	1.0–0.5	0.75	8.6	1.70	106.1	1.84	114.6
11	1.0–0.5	0.75	8.9	1.69	105.3	1.83	114.2
11	1.0–0.5	0.75	9.2	1.70	106.0	1.85	115.2
11	1.0–0.5	0.75	8.2	1.71	106.5	1.84	114.8
12	0.5–0.0	0.25	8.2	1.69	105.7	1.82	113.9
12	0.5–0.0	0.25	10.3	1.78	111.1	1.94	121.4
12	0.5–0.0	0.25	9.3	1.73	108.0	1.88	117.2
12	0.5–0.0	0.25	10.1	1.75	109.4	1.91	119.5
12	0.5–0.0	0.25	11.3	1.68	104.6	1.86	115.8
Topsoil	+0.75	–	–	–	–	–	–
Average	–	–	9.9	1.71	106.9	1.87	116.9

ft Foot (feet)
lb/ft^3 Pound(s) per cubic foot
Mg/m^3 Megagram(s) per cubic meter
– Not applicable

Table 5-1
Natural Analogue Soil Core Characteristics

Sample Number	Sample Depth (cm)	Sample Length (cm)	Sample Diameter (cm)	Sample Condition	Porosity (%)	Bulk Density (g/cm^3)	Saturated Hydraulic Conductivity (cm/s)
IP-00	0–15	4	5	Remolded	40.8	1.57	3.29×10^{-4}
IP-01	23–30	3	5	Remolded	35.8	1.70	9.18×10^{-5}
IP-02	33–38	3	5	Undisturbed	36.7	1.68	1.27×10^{-4}
IP-03	38–53	3	5	Undisturbed	37.7	1.65	2.81×10^{-4}
IP-04	64–69	3	5	Undisturbed	35.8	1.70	2.74×10^{-4}
IP-05	69–84	4	5	Remolded	41.9	1.54	1.26×10^{-4}
IP-06	84–89	3	5	Undisturbed	30.2	1.85	1.67×10^{-5}
IP-07	94–99	3	5	Undisturbed	33.2	1.77	7.06×10^{-7}
IP-08	99–114	3	5	Remolded	41.1	1.56	6.71×10^{-5}
IP-09	130–145	3	5	Undisturbed	30.2	1.85	1.66×10^{-6}
IP-10	145–150	3	5	Undisturbed	37.0	1.67	3.16×10^{-6}
IP-11	157–160	3	5	Undisturbed	37.4	1.66	1.67×10^{-5}
IP-12	160–175	3	5	Remolded	39.2	1.61	3.66×10^{-5}
IP-13	178–180	3	5	Undisturbed	44.2	1.48	3.24×10^{-4}
IP-14	185–191	3	5	Undisturbed	44.5	1.47	3.19×10^{-5}
IP-15	201–206	4	5	Remolded	41.1	1.56	3.38×10^{-5}
IP-16	206–216	–	–	No sample	–	–	–
IP-17	216–221	–	–	No sample	–	–	–
IP-18	221–236	4	5	Remolded	42.6	1.52	2.04×10^{-5}
IP-19	244–254	–	–	No sample	–	–	–
IP-20	254–269	4	5	Remolded	38.9	1.62	1.08×10^{-4}
Average		–	–	–	38.2	1.64	4.01×10^{-5}

cm Centimeter(s)
cm/s Centimeter(s) per second
g/cm^3 Gram(s) per cubic centimeter
IP Instantaneous profile
– Not applicable

Table 5-2
Engineered Cover Soil Core Characteristics

Sample Number	Sample Depth (cm)	Sample Length (cm)	Sample Diameter (cm)	Sample Condition	Porosity (%)	Bulk Density (g/cm^3)	Saturated Hydraulic Conductivity (cm/s)
EC-00	0–8	8	5	Remolded	37.4	1.66	9.0×10^{-5}
EC-01	8–20	13	5	Remolded	37.3	1.66	4.8×10^{-5}
EC-02	20–36	15	5	Remolded	37.3	1.66	8.2×10^{-5}
EC-03	36–51	15	5	Remolded	37.6	1.65	1.4×10^{-4}
EC-04	51–66	15	5	Remolded	37.5	1.66	1.2×10^{-4}
EC-05	66–81	15	5	Remolded	36.9	1.67	1.6×10^{-4}
EC-06	81–94	13	5	Remolded	37.5	1.66	1.7×10^{-4}
EC-07	94–107	13	5	Remolded	37.0	1.67	1.3×10^{-4}
EC-08	107–122	15	5	Remolded	36.7	1.68	6.9×10^{-5}
EC-09	122–140	18	5	Remolded	36.9	1.67	9.2×10^{-5}
EC-10	140–152	13	5	Remolded	37.4	1.66	1.4×10^{-4}
EC-11	152–168	15	5	Remolded	37.0	1.67	3.1×10^{-4}
EC-12	168–183	15	5	Remolded	37.3	1.66	9.0×10^{-5}
Average		–	–	–	37.2	1.66	1.1×10^{-4}

cm Centimeter(s)
cm/s Centimeter(s) per second
EC Engineered Cover
g/cm^3 Gram(s) per cubic centimeter
– Not applicable

Table 5-3
Natural Analogue RETC-Derived Parameters from Laboratory-Observed θ(Ψ) Data

Sample	WCr (%)	WCs (%)	α (cm^{-1})	n (-)	m (-)	ℓ (-)	K_S, RETC (cm/s)	r^2 (-)
IP-00	0.001	0.368	0.0076	1.29	=1-1/n	0.5	9.81×10^{-4}	0.993
IP-01	0.001	0.388	0.0171	1.29	=1-1/n	0.5	9.79×10^{-4}	0.994
IP-02	0.001	0.432	0.0284	1.21	=1-1/n	0.5	8.04×10^{-4}	0.992
IP-03	0.001	0.416	0.0451	1.21	=1-1/n	0.5	8.21×10^{-4}	0.992
IP-04	0.001	0.413	0.0538	1.22	=1-1/n	0.5	8.47×10^{-4}	0.984
IP-05	0.001	0.366	0.0341	1.24	=1-1/n	0.5	8.81×10^{-4}	0.994
IP-06	0.001	0.338	0.0583	1.11	=1-1/n	0.5	4.61×10^{-4}	0.986
IP-07	0.001	0.353	0.7419[a]	1.06	=1-1/n	0.5	1.72×10^{-4}	0.970
IP-08	0.001	0.419	0.0217	1.24	=1-1/n	0.5	8.86×10^{-4}	0.993
IP-09	0.001	0.324	0.0593	1.09	=1-1/n	0.5	3.22×10^{-4}	0.986
IP-10	0.001	0.337	0.0217	1.15	=1-1/n	0.5	5.99×10^{-4}	0.988
IP-11	0.001	0.348	0.3798[a]	1.14	=1-1/n	0.5	5.88×10^{-4}	0.934
IP-12	0.001	0.458	0.0442	1.22	=1-1/n	0.5	8.36×10^{-4}	0.992
IP-13	0.001	0.420	1.1656[a]	1.14	=1-1/n	0.5	5.63×10^{-4}	0.947
IP-14	0.001	0.346	0.0059	1.19	=1-1/n	0.5	7.71×10^{-4}	0.992
IP-15	0.001	0.456	0.0290	1.21	=1-1/n	0.5	8.05×10^{-4}	0.998
IP-18	0.001	0.448	0.0135	1.23	=1-1/n	0.5	8.53×10^{-4}	0.996
IP-20	0.001	0.385	0.0231	1.27	=1-1/n	0.5	9.09×10^{-4}	0.989
Average		0.390	0.0309	1.19	0.16	0.5	7.27×10^{-4}	0.984

[a]RETC could not fit a reasonable value.

α	Air entry parameter
cm	Centimeter(s)
cm/s	Centimeter(s) per second
IP	Instantaneous profile
K_s	Saturated hydraulic conductivity
ℓ	Mualem numerical parameter
m	van Genuchten curve-fitting parameter
n	van Genuchten curve-fitting parameter
RETC	Retention curve
r^2	Statistical curve-fitting parameter
WCr	Residual water content
WCs	Saturated water content
(-)	Unitless

Table 5-4
Engineered Cover RETC-Derived Parameters from Laboratory-Measured θ(Ψ) Data

Sample	WCr (%)	WCs (%)	α (cm^{-1})	*n* (-)	*m* (-)	ℓ (-)	K_S, RETC (cm/s)	r^2 (-)
EC-00	0.001	0.338	0.022	1.26	=1-1/n	0.5	2.89×10^{-4}	0.992
EC-01	0.001	0.328	0.022	1.27	=1-1/n	0.5	2.89×10^{-4}	0.995
EC-02	0.001	0.342	0.021	1.25	=1-1/n	0.5	2.89×10^{-4}	0.986
EC-03	0.001	0.356	0.020	1.27	=1-1/n	0.5	2.89×10^{-4}	0.993
EC-04	0.001	0.362	0.023	1.25	=1-1/n	0.5	2.89×10^{-4}	0.992
EC-05	0.001	0.346	0.017	1.26	=1-1/n	0.5	2.89×10^{-4}	0.990
EC-06	0.001	0.332	0.022	1.25	=1-1/n	0.5	2.89×10^{-4}	0.993
EC-07	0.001	0.350	0.020	1.27	=1-1/n	0.5	2.89×10^{-4}	0.996
EC-08	0.001	0.343	0.024	1.25	=1-1/n	0.5	2.89×10^{-4}	0.993
EC-09	0.001	0.346	0.020	1.24	=1-1/n	0.5	2.89×10^{-4}	0.991
EC-10	0.001	0.349	0.030	1.25	=1-1/n	0.5	2.89×10^{-4}	0.994
EC-11	0.001	0.377	0.024	1.28	=1-1/n	0.5	2.89×10^{-4}	0.994
EC-12	0.001	0.367	0.020	1.28	=1-1/n	0.5	2.89×10^{-4}	0.994
Average		0.350	0.022	1.26	=1-1/n	0.5	2.89×10^{-4}	0.993

α	Air entry parameter
cm	Centimeter(s)
cm/s	Centimeter(s) per second
EC	Engineered Cover
K_s	Saturated hydraulic conductivity
ℓ	Mualem numerical parameter
m	van Genuchten curve-fitting parameter
n	van Genuchten curve-fitting parameter
RETC	Retention curve
r^2	Statistical curve-fitting parameter
WCr	Residual water content
WCs	Saturated water content
(-)	Unitless

Table 6-1
UNSAT-H Code Input Parameters

Parameter	Natural Analogue		Engineered Cover		Source
	Input value	Unit(s)	Input value	Unit(s)	
Initial Head	17,200	cm	5620	cm	RETC Code
θ_s	0.39	Percent	0.35	Percent	RETC Code
θ_r	0.001	Percent	0.001	Percent	RETC Code
α	0.0309	cm^{-1}	0.022	cm^{-1}	RETC Code
n	1.19	(-)	1.26	(-)	RETC Code
ℓ	0.5	(-)	0.5	(-)	[a]
K_s	4.05×10^{-4}	cm/s	3.46×10^{-4}	cm/s	Field
Root Depth	80	cm	80	cm	Field
LAI Historical Precipitation	0.8 max	(-)	0.8 max	(-)	[b, c, d]
LAI Maximum Precipitation	1.2 max		1.2 max		
Growing Season	2–364	Julian Day	2–364	Julian Day	[b, c, d]
PBA	81	Percent	81	Percent	Field
RLD coefficient *a*	0.5090	(-)	0.5090	(-)	Field
RLD coefficient *b*	-0.0630	(-)	-0.0630	(-)	Field
RLD coefficient *c*	0.0262	(-)	0.0262	(-)	Field
Ψ_w	30,000	cm	30,000	cm	[e, f, g]
Ψ_d	3000	cm	3000	cm	[h, i]
Ψ_n	30	cm	30	cm	[h, i]
PET coefficient *a*	0	(-)	0	(-)	[j]
PET coefficient *b*	0.52	(-)	0.52	(-)	[j]
PET coefficient *c*	0.5	(-)	0.5	(-)	[j]
PET lower limit *d*	0.0	(-)	0.0	(-)	[j]
PET upper limit *e*	3.7	(-)	3.7	(-)	[j]

[a]Maulem (1976)
[b]NMED (1998)
[c]Scurlock et al. (2001)
[d]Munk (2004)
[e]HDR Engineering (2000)
[f]ITRC (2003)
[g]Hillel (1998)
[h]Fayer (2000)
[i]Feddes et al. (1978)
[j]Ritchie and Burnett (1971)

α Air entry parameter
θ_r Residual moisture content
θ_s Saturated moisture content
cm Centimeter(s)
cm/s Centimeter(s) per second
ITRC Interstate Technology and Regulatory Council
K_s Saturated hydraulic conductivity
ℓ Mualem numerical parameter
LAI Leaf area index
max Maximum
n van Genuchten curve-fitting parameter
NMED New Mexico Environment Department
PBA Percent bare area
PET Potential evapotranspiration
RETC Retention curve
RLD Root length density
UNSAT-H Unsaturated Water and Heat Flow
Ψ_w Wilting point
Ψ_d Limiting point
Ψ_n Anaerobic point
(-) Unitless

Table 7-1
Percolation—Natural Analogue without Vegetation

Depth		Cumulative Percolation (cm)		Net Annual Percolation (mm/yr)		Average Flux (cm/s)	
(cm)	(ft)	Historical[a]	Maximum[b]	Historical[a]	Maximum[b]	Historical[a]	Maximum[b]
30	1	25.93	59.86	3.99	9.35	1.27×10^{-8}	2.97×10^{-8}
61	2	22.50	56.21	3.46	8.78	1.10×10^{-8}	2.79×10^{-8}
91	3	19.04	52.57	2.93	8.21	9.29×10^{-9}	2.60×10^{-8}
122	4	15.66	48.89	2.41	7.64	7.64×10^{-9}	2.42×10^{-8}
152	5	12.34	45.19	1.90	7.06	6.02×10^{-9}	2.24×10^{-8}

[a]65-year historical rainfall record
[b]64-year maximum rainfall record
cm Centimeter(s)
cm/s Centimeter(s) per second
ft Foot (feet)
mm/yr Millimeter(s) per year

Table 7-2
Percolation—Natural Analogue with Vegetation

Depth		Cumulative Percolation (cm)		Net Annual Percolation (mm/yr)		Average Flux (cm/s)	
(cm)	(ft)	Historical[a]	Maximum[b]	Historical[a]	Maximum[b]	Historical[a]	Maximum[b]
30	1	23.94	71.41	3.68	11.16	1.17×10^{-8}	3.53×10^{-8}
61	2	0.50	2.09	0.08	0.33	2.44×10^{-10}	1.04×10^{-9}
91	3	-0.33	-0.32	-0.05	-0.05	-1.61×10^{-10}	-1.59×10^{-10}
122	4	-0.20	-0.20	-0.03	-0.03	-9.76×10^{-10}	-9.91×10^{-11}
152	5	-0.09	-0.09	-0.01	-0.01	-4.39×10^{-11}	-4.46×10^{-11}

[a]65-year historical rainfall record
[b]64-year maximum rainfall record
cm Centimeter(s)
cm/s Centimeter(s) per second
ft Foot (feet)
mm/yr Millimeter(s) per year

Table 7-3
Percolation—Engineered Cover without Vegetation

Depth		Cumulative Percolation (cm)		Net Annual Percolation (mm/yr)		Average Flux (cm/s)	
(cm)	(ft)	Historical[a]	Maximum[b]	Historical[a]	Maximum[b]	Historical[a]	Maximum[b]
30	1	22.64	53.23	3.48	8.32	1.10×10^{-8}	2.64×10^{-8}
61	2	20.52	50.83	3.16	7.94	1.00×10^{-8}	2.52×10^{-8}
91	3	18.29	48.44	2.81	7.57	8.92×10^{-9}	2.40×10^{-8}
122	4	16.11	46.04	2.48	7.19	7.86×10^{-9}	2.28×10^{-8}
152	5	13.98	43.60	2.15	6.81	6.82×10^{-9}	2.16×10^{-8}

[a]65-year historical rainfall record
[b]64-year maximum rainfall record
cm Centimeter(s)
cm/s Centimeter(s) per second
ft Foot (feet)
mm/yr Millimeter(s) per year

Table 7-4
Percolation—Engineered Cover with Vegetation

Depth		Cumulative Percolation (cm)		Net Annual Percolation (mm/yr)		Average Flux (cm/s)	
(cm)	(ft)	Historical[a]	Maximum[b]	Historical[a]	Maximum[b]	Historical[a]	Maximum[b]
30	1	37.66	100.26	5.79	15.67	1.84×10^{-8}	4.97×10^{-8}
61	2	2.42	10.77	0.37	1.68	1.18×10^{-9}	5.34×10^{-9}
91	3	-1.85	-1.80	-0.28	-0.28	-9.03×10^{-10}	-8.92×10^{-10}
122	4	-1.27	-1.20	-0.20	-0.19	-6.20×10^{-10}	-5.95×10^{-10}
152	5	-0.64	-0.61	-0.10	-0.09	-3.12×10^{-10}	-3.02×10^{-10}

[a]65-year historical rainfall record
[b]64-year maximum rainfall record
cm Centimeter(s)
cm/s Centimeter(s) per second
ft Foot (feet)
mm/yr Millimeter(s) per year

DISTRIBUTION:

6	0750	J.L. Peace, 6116
1	1089	T.J. Goering, 6135
1	0651	ISS Records Center, 9612
1	9018	Central Technical Files, 8945-1
2	0899	Technical Library, 9616
1		K. Wahi